72-14,838

DAVIS, Wendell Alan, 1941-
DESIGN AND ANALYSIS OF A PARAMETRIC
LOWER SIDEBAND UPCONVERTER.

The University of Michigan, Ph.D., 1971
Engineering, electrical

University Microfilms, A XEROX Company, Ann Arbor, Michigan

THIS DISSERTATION HAS BEEN MICROFILMED EXACTLY AS RECEIVED

DESIGN AND ANALYSIS OF A PARAMETRIC LOWER SIDEBAND UPCONVERTER

by
Wendell Alan Davis

A dissertation submitted in partial fulfillment
of the requirements for the degree of
Doctor of Philosophy
(Electrical Engineering)
in The University of Michigan
1971

Doctoral Committee:

Associate Professor Peter J. Khan, Chairman
Professor Thomas W. Butler, Jr.
Associate Professor Walter R. Curtice
Professor Dale M. Grimes
Professor Albert E. Heins

PLEASE NOTE:

Some pages have indistinct print. Filmed as received.

University Microfilms, A Xerox Education Company

ACKNOWLEDGEMENTS

The author wishes to express his gratitude to the members of his doctoral committee for their helpful comments and in particular to his chairman, Professor Peter J. Khan, for his technical guidance throughout the course of the investigation. The help from the staff of Cooley Electronics Laboratory is greatly appreciated, particularly that of Miss Olive Lockwood, Mrs. Mickey Cohn, Mrs. Kathy Bartlett, and Mrs. Ann Fulmer for typing and putting in final form the manuscript. Finally the author appreciates the support supplied by the U. S. Army Electronics Command.

TABLE OF CONTENTS

	Page
ACKNOWLEDGEMENTS	ii
LIST OF TABLES	vii
LIST OF ILLUSTRATIONS	ix
LIST OF SYMBOLS	xvii
LIST OF APPENDICES	xxvi
ABSTRACT	xxvii
CHAPTER I: INTRODUCTION	1
1.1 Background	1
1.2 Literature Review	3
1.3 Topics of Investigation	5
CHAPTER II: COAXIAL MICROWAVE BAND-PASS FILTERS	7
2.1 Introduction	7
2.2 Review of Filter Theory	8
2.2.1 Derivation of the Lumped-Element Low-Pass Prototype Circuit	8
2.2.2 Band-pass Filter Networks	9
2.2.3 Immittance Inverters	10
2.2.4 Microwave Realization	13
2.3 Distributed Impedance and Admittance Inverter Design	17
2.3.1 Coaxial Impedance Inverter Design	18
2.3.2 Coaxial Admittance Inverter Design	22
2.4 Theoretical Results of the Distributed Design Method	23
2.4.1 Band-pass Filters Using K Inverters	23
2.4.2 Filter Using K and J Inverters	30
2.4.3 Impedance Transformer	30
2.5 Effect of Discontinuity Capacitance	32
2.6 Numerical Example and Experimental Results	40
2.7 Discussion	46
2.7.1 Filter Limitations Imposed by Choice of Bandwidth	46
2.7.2 Bandwidth Discrepancy	46
2.7.3 Low-frequency Characteristics	47
2.7.4 Effect of Filter Parameter Variations	49
2.8 Conclusions	49

TABLE OF CONTENTS (Cont.)

	Page
CHAPTER III: DESIGN THEORY FOR THE LOWER SIDEBAND UPCONVERTER	51
3.1 Introduction	51
3.2 Review of Existing LSUC Design Theory	51
3.2.1 Method of Harmonic Balance	52
3.2.2 Elastance Coefficients	55
3.2.3 Gain Relationship for the LSUC	56
3.2.4 Bandwidth and Gain-Bandwidth Product	60
3.2.5 Noise Figure Relationship for the LSUC	61
3.2.6 Origin of Shot Noise	66
3.2.7 Summary of Existing Design Theory	67
3.3 Effects of Upper Sideband Reactance on the LSUC	68
3.3.1 Effects of X_{33} on Gain	68
3.3.2 Effects of X_{33} on Gain Sensitivity	74
3.3.3 Effects of X_{33} on Gain-Bandwidth Product	78
3.3.4 Effects of X_{33} on Noise Figure	80
3.3.5 Conclusions on the Effects of X_{33}	82
3.4 Numerical Comparison of Three Possible LSUC Circuits	85
3.4.1 Diode Model and Desired Circuit Parameters	87
3.4.2 Gain for the Ideal Circuit with Unpackaged and Packaged Diode	88
3.4.3 Comparison of Three Circuit Designs Using Ideal Impedance Transformers	91
3.4.4 Effect of Signal Circuit Length	98
3.4.5 Effect of Diode Parasitic Inductance	98
3.4.6 Effect of Shunt-Stub Tuners	102
3.4.7 Conclusions on the Use of the Three LSUC Configurations	102
3.5 LSUC Design with Coaxial Band-pass Impedance Matching Circuits	103
3.5.1 General Design Procedure for the Three LSUC Circuits	104
3.5.1.1 Pump Circuit	104
3.5.1.2 Lower Sideband Circuit	106
3.5.1.3 Signal Circuit	107
3.5.2 Special Design Considerations for LSUC1	109
3.5.3 Special Design Considerations for LSUC2	109
3.5.3.1 LSUC2 with the Low-pass Signal Matching Circuit	111
3.5.3.2 LSUC2 with the Band-pass Signal Matching Circuit	111
3.5.4 Special Design Considerations for LSUC3	119
3.6 Conclusions	121
CHAPTER IV: EXPERIMENTAL EVALUATION OF THE LOWER SIDEBAND UPCONVERTER	125
4.1 Introduction	125
4.2 Diode Measurement	125
4.2.1 Diode Measurement Review	125
4.2.1.1 Method 1	127
4.2.1.2 Method 2	128
4.2.1.3 Method 3	129
4.2.1.4 Conclusions on the Three Methods	132
4.2.2 Experimental Diode Measurement Results	133
4.3 External Microwave Circuit Measurements	137
4.3.1 Band-pass Transformers	137
4.3.2 The Tee Junction	141

TABLE OF CONTENTS (Cont.)

	Page
4.4 The Experimental LSUC Circuits	145
4.4.1 Gain	147
4.4.2 Bandwidth	147
4.4.3 Noise Figure	150
4.4.3.1 Circuit Losses	158
4.4.3.2 Incorrect Value of Diode Bulk Resistance	158
4.4.3.3 Noisy Pump Source	160
4.4.3.4 Pump Heating of Diode	162
4.4.3.5 Shot Noise	162
4.5 Conclusions	167
CHAPTER V: DIFFUSION ADMITTANCE	168
5.1 Introduction	168
5.2 Literature Review	169
5.3 Varactor Diode Model	173
5.3.1 Depletion Layer Capacitance	173
5.3.2 Diffusion Admittance	174
5.3.3 Alternate Formulation	178
5.3.4 Numerical Calculations of the Diffusion Admittance	180
5.3.5 Varactor Diode Model with both Diffusion and Depletion Admittance	189
5.3.6 Comparison with Experimental Work	193
5.4 Effects of Diffusion Admittance on a LSUC	194
5.4.1 Large Signal Analysis of the Diffusion Admittance in a LSUC	196
5.4.1.1 Incommensurate Frequencies in the LSUC	196
5.4.1.2 Phase of the Lower Sideband Voltage	197
5.4.1.3 Numerical Calculation of LSUC Currents	199
5.4.2 Small Signal Analysis of the LSUC	200
5.4.3 The LSUC with the Total Varactor Diode Model	209
5.5 Conclusions	218
CHAPTER VI: CONCLUSIONS AND SUGGESTION FOR FUTURE RESEARCH	219
6.1 Introduction	219
6.2 Summary of Original Contributions	219
6.2.1 Distributed Design of Coaxial Filters	219
6.2.2 Discontinuity Capacitance Compensation	219
6.2.3 Effect of Higher Order Sidebands in the LSUC	220
6.2.4 A Noniterative Design Algorithm for a LSUC	220
6.2.5 Verification of Noise Figure Dependence on Gain	220
6.2.6 Application of Diffusion Admittance to a LSUC	220
6.2.7 Modified Bessel Functions	221
6.3 Suggestions for Future Research	221
6.3.1 Stripline Filters	221
6.3.2 A LSUC Made in Stripline	221
6.3.3 Double Sideband Operation	221
6.3.4 The Coaxial Tee Junction	221
6.3.5 Measurement of Diffusion Admittance	222
6.3.6 A LSUC with a Step Recovery Diode	222
6.4 Conclusion	223

TABLE OF CONTENTS (Cont.)

	Page
APPENDICES	224
REFERENCES	268

LIST OF TABLES

Table		Page
2.1	Disk parameters for three pole filters	27
2.2	Disk parameters for five pole band-pass filters	27
2.3	Filter parameters for three pole Chebyshev and maximally flat filters where discontinuity capacitance has been neglected and all disk diameters are 0.502 in.	28
2.4	Band-pass filter using K and J inverters	31
2.5	Disk parameters for band-pass impedance transformer using three disks	36
2.6	Experimental design parameters of the filter shown in Figs. 2.27 and 2.28	42
3.1	Values of X_{33} where the gain and noise figure extrema occur	85
3.2	Distances in cm between the diode and lower sideband (LSB) or pump filters. The * values are not true minima as the slope in these cases is monotonically increasing	94
3.3	Gain-bandwidth product when $S_1/S_0 = 0.35$	103
3.4	Gain and bandwidth of the LSUC2 using coaxial band-pass filters in all three ports	119
3.5	Design parameters for the LSUC when the diode is in the lower sideband port	121
4.1	References for measuring diode parameters	132
4.2	Noise figure of the LSUC	158
5.1	Variation of the minimum loss with doping profiles	189
5.2	Exact calculation of the current desnities	201
5.3	Current densities caused only by nonlinear depletion capacitance when normalized to give the same pump current $\|J_0\|$ as the diffusion current	202
5.4	Small signal method for calculating the current densities	203

LIST OF TABLES (Cont.)

Table		Page
5. 5	Susceptance values in mhos needed to tune the diffusion susceptance of the diode when it is biased at 0. 7 V	208
D. 1	Laplace asymptotic method for calculating the current densities	267

LIST OF ILLUSTRATIONS

Figure		Page
2. 1	Low-pass prototype circuit with shunt capacitor adjacent to source	10
2. 2	Low-pass prototype circuit with series inductor adjacent to source	10
2. 3	Band-pass prototype with shunt resonator adjacent to the generator	11
2. 4	Band-pass prototype with series resonator adjacent to the generator. The element values are given by the same formulas given in Fig. 2. 3	11
2. 5	Definition of an ideal K inverter and J interter	12
2. 6	Lumped band-pass impedance matching network using K inverters	12
2. 7	Lumped band-pass impedance matching network using J inverters	12
2. 8	Generalized impedance matching networks using K inverters	14
2. 9	Generalized impedance matching networks using J inverters	14
2. 10	Alternate K and J inverters	16
2. 11	Lumped-element K inverter realization	16
2. 12	Lumped-element J inverter realization	16
2. 13	(a) Disk impedance inverter, and (b) bisected impedance inverter	19
2. 14	(a) Coaxial admittance inverter, and (b) bisected admittance inverter	22
2. 15	A schematic diagram of a coaxial band-pass filter with Teflon dielectric around the center two disks	24
2. 16	Theoretical comparison between the lumped and distributed design for filters with bandwidth of (a) 1 percent, (b) 5 percent, and (c) 10 percent. The impedance of the 10 percent filter is shown in (d)	25

LIST OF ILLUSTRATIONS (Cont.)

Figure		Page
2.17	Theoretical comparison between the lumped and distributed design for 5 pole filters with bandwidth of (a) 5 percent and (b) 10 percent	26
2.18	10 percent bandwidth band-pass filter with 0.5 dB ripple	29
2.19	10 percent bandwidth, three pole, band-pass, maximally flat filter	29
2.20	Band-pass filter with alternate K and J inverters	32
2.21	Filters using alternate K and J inverters separated by quarter wavelength lines with bandwidth of (a) 20 percent, and (b) 40 percent	33
2.22	Theoretical comparison between the lumped and distributed design for 50:1 impedance transformers with bandwidth of (a) 1 percent, (b) 5 percent, (c) 10 percent, and (d) 20 percent	34
2.23	Theoretical comparison of the impedance between the lumped and distributed design of the 10 percent bandwidth 50:1 impedance transformer	35
2.24	(a) Length of transmission line representing disk, and (b) length of transmission line representing disk with discontinuity capacitance	39
2.25	π equivalent circuit for a transmission line where $X_b = Z_o \sin(\beta\ell)$ and $B_a = Y_o \tan(\beta\ell/2)$	39
2.26	A 1 percent bandwidth band-pass filter for the ideal case when there is no discontinuity capacitance (. . .), when the filter is compensated for discontinuity capacitance by method 1 (— -), method 2 (---), and method 3 (—). The ideal case and the compensation by method 3 merge at the left side	41
2.27	A 1 percent bandwidth band-pass filter designed by the lumped method (— -), by the distributed method (---), by the distributed method with discontinuity capacitance accommodated by method 3 (—), and experimental results of the solid line filter (xxx). The ideal case when there is no discontinuity capacitance (---) and the case where method 3 is used (—) merge for the lower frequencies	43
2.28	A 10 percent band-pass filter designed by the distributed method where discontinuity capacitance is accommodated by method 2 with experimental results (×). The insert is a portion of the characteristic drawn on an expanded scale.	44
2.29	Photograph of 1 percent band-pass filter	45

LIST OF ILLUSTRATIONS (Cont.)

Figure		Page
2.30	Low-frequency response of band-pass filter with center frequency of 8.5 GHz for bandwidth of (a) 1 percent, (b) 10 percent, (c) 20 percent, and (d) 10 percent bandwidth with modified diameters	48
3.1	Noise equivalent circuit	63
3.2	Transformed noise equivalent circuit	63
3.3	Equivalent circuit of LSUC where X_c is the circuit reactance and X_{33} is finite	70
3.4	The impedances induced into the signal circuit by the finite value of X_{33}	72
3.5	Midband transducer power gain when $S_2/S_0 = 0.044$	76
3.6	The transducer power gain when $S_2 = 0$	77
3.7	The gain-bandwidth product $(G^{\frac{1}{2}}w)$ when $S_2/S_0 = 0.044$ where the dashed curve corresponds to the expanded X_{33} scale	79
3.8	The noise figure when $S_2/S_0 = 0.044$ where the dashed curve corresponds to the expanded X_{33} scale	83
3.9	The actual noise measure of the LSUC when $S_2/S_0 = 0.044$	84
3.10	Drawings of LSUC1, LSUC2, and LSUC3 together with the corresponding schematics of the circuits are shown in (a), (b), and (c) respectively. d_0, d_1, and d_2 are the distances between the diode and the corresponding impedance transformers respectively. Z_s, Z_p, and Z_{p-s} are the impedances of the signal, pump, and lower sideband ports as seen by the diode	86
3.11	Package varactor diode model	88
3.12	LSUC transducer power gain with out-of-band circuits completely isolated and the diode has no parasitic elements	89
3.13	Variation of gain-bandwidth product $(G^{\frac{1}{2}}w)$ with pumping level when out-of-band circuits are completely isolated and there are no diode parasitics ———, and Robinson's gain-bandwidth formula - - - -	90

LIST OF ILLUSTRATIONS (Cont.)

Figure		Page
3.14	LSUC transducer power gain with out-of-band circuits completely isolated where the diode parasitic elements are as follows: L = 2 nH and $S_p = 2.856\ 10^{12}\ F^{-1}$ — — — —, L = 1 nH and $S_p = 1.428\ 10^{12}\ F^{-1}$ — — — —, L = 1 nH and $S_p = 2.856\ 10^{12}\ F^{-1}$ -----	92
3.15	LSUC gain-bandwidth product ($G^{\frac{1}{2}}w$) with out-of-band circuits completely isolated from one another where the diode parasitic elements are as follows: L = 2 nH and $S_p = 1.428\ 10^{12}\ F^{-1}$ ——, L = 2 nH and $S_p = 2.856\ 10^{12}\ F^{-1}$ — — — —, L = 1 nH and $S_p = 2.856\ 10^{12}\ F^{-1}$ -----	93
3.16	Transducer power gain for the three LSUC circuits when ideal impedance matching circuits and the 5 x 5 matrix approximation are used	96
3.17	Noise figure for the three LSUC circuits when ideal impedance matching circuits and the 5 x 5 matrix approximation are used	97
3.18	Variation of gain-bandwidth product ($G^{\frac{1}{2}}w$) versus pumping level with signal circuit distance as a parameter, using ideal impedance matching circuits, the 5 x 5 matrix approximation, and standard diode inductance of 2 nH	99
3.19	Variation of gain bandwidth product ($G^{\frac{1}{2}}w$) versus pumping level with signal circuit distance as a parameter, using ideal impedance matching circuits, the 5 x 5 matrix approximation, and a diode package inductance of 0.2203 nH	100
3.20	Variation of gain-bandwidth product ($G^{\frac{1}{2}}w$) with diode package inductance for LSUC1, using the 5 x 5 matrix approximation and a signal port distance of $\lambda_s/4$	101
3.21	Pump circuit without (a) and with (b) ideal transformer	106
3.22	Circuit model used to design the signal circuit	108
3.23	Gain of LSUC when all filters in parallel with one another	110
3.24	LSUC1 circuit using a semilumped low-pass signal circuit	112
3.25	Gain of LSUC using coaxial filters with diode in center conductor	113
3.26	LSUC1 circuit using a distributed band-pass signal circuit	114

LIST OF ILLUSTRATIONS (Cont.)

Figure		Page
3. 27	LSUC transducer power gain using the coaxial microwave filters when the diode model has the following elements: R_S = 1 ohm, L = 2 nH, C_p = 0. 7 pF, S_0 = 6. 28 10^{11} F^{-1}, and S_1/S_0 = 0. 35	115
3. 28	LSUC transducer power gain using the coaxial microwave filters when the diode model has the following elements: R_S = 1 ohm, L = 2 nH, C_p = 0. 5 pF, S_0 = 6. 28 10^{11} F^{-1}, and S_1/S_0 = 0. 35	116
3. 29	LSUC transducer power gain using the coaxial microwave filters when the diode model has the following elements: R_S = 1 ohm, L = 1. 428 nH, C_p = 0. 7 pF, S_0 = 6. 28 10^{11} F^{-1}, and S_1/S_0 = 0. 35	117
3. 30	LSUC noise figure using the coaxial microwave filters when the diode model has the following elements: R_S = 1 ohm, L = 2 nH, C_p = 0. 7 pF, S_0 = 6. 28 10^{11} F^{-1}, and S_1/S_0 = 0. 35	118
3. 31	LSUC3 using coaxial disk band-pass impedance transformers	122
3. 32	LSUC transducer power gain using coaxial microwave filters when the diode is mounted in the lower sideband port. The diode model elements are R_S = 1. 41 ohm, L = 1. 834 nH, C_p = 0. 1633 pF, S_0 = 1. 0456 10^{12} F^{-1}, and S_1/S_0 = 0. 35	123
4. 1	(a) The varactor diode equivalent circuit and (b) the modified simple equivalent circuit	127
4. 2	Distributed diode model	134
4. 3	Houlding's varactor diode model	134
4. 4	Diode measurement mount with (a) the varactor diode and (b) the short-circuit reference plane	135
4. 5	The measured diode impedance data points are designated by o and the selected points obtained from analysis of the resulting diode model are designated by ×	136
4. 6	Diode measurement circuit	137
4. 7	Comparison of the reactance for the measured diode · · · and the diode model o o o	138
4. 8	Impedance of the signal frequency transformer	139

LIST OF ILLUSTRATIONS (Cont.)

Figure		Page
4.9	Impedance of the lower sideband frequency transformer	140
4.10	The impedance of the coaxial tee circuit as seen from (a) the leg port, and (b) the arm port	142
4.11	The impedance as a function of frequency in GHz of a 7 mm coaxial tee junction as seen from the leg Z_a, ----, and the impedance as seen from the arm Z_b, ——, when the other two ports are terminated with 50 ohms	143
4.12	(a) The coaxial tee junction and (b) the equivalent circuit of the tee junction at the reference plane	144
4.13	Schematic diagram of the experimental LSUC2 including the final experimental dimensions. The transmission line is standard 14 mm 50 ohm coaxial line and the cross-hatched sections are Teflon	146
4.14	Photograph of the LUSC	148
4.15	Photograph of the LSUC when in operation	148
4.16	Experimental power gain of LSUC3 when the midband gain is 30 dB (Δ), 25 dB (o), 20 dB (□), 15 dB (◇), 10 dB (+), and 5 dB (×)	149
4.17	Theoretical gain curves for LSUC3 when the circuit is modified because of physical requirements	151
4.18	Comparison of theoretical and experimental gain-bandwidth product	152
4.19	Noise figure measuring circuit	153
4.20	Photographs of the noise figure measuring circuit	154
4.21	Noise figure of LSUC2	156
4.22	Noise figure of LSUC3	157
4.23	Theoretical noise figure for LSUC3	159
4.24	Thermal plus shot noise figure of a LSUC at $290^{\circ}K$ when the diode is at $290^{\circ}K$ and $300^{\circ}K$. The dashed curves have slopes 10 and 15 times larger than the noise figure curve	163
4.25	Noise figure of a LSUC as a function of bias voltage when the gain and pump power is constant	165

LIST OF ILLUSTRATIONS (Cont.)

Figure		Page
4. 26	Varactor diode dc current-voltage characteristics with no RF power (o), with 71 mW RF (□), and with 0. 71 W (×). The applied RF is 9. 5 GHz, and the diode is series mounted in a terminated 14 mm coaxial line	166
4. 27	Mount for measuring diode current-voltage characteristic under pumped conditions	167
5. 1	Normalized diffusion admittance when $\gamma = 1/2$, $\tau_p = 10^{-7}$ sec, and $W/L_p = 0.1$	182
5. 2	Normalized diffusion admittance when $\gamma = 1/3$, $\tau_p = 10^{-7}$ sec, and $W/L_p = 0.1$	182
5. 3	Normalized diffusion admittance when $\gamma = 1/5$, $\tau_p = 10^{-7}$ sec, and $W/L_p = 0.1$	183
5. 4	Normalized diffusion admittance when $\gamma = 1/3$, $\tau_p = 10^{-7}$ sec, and $W/L_p = 0.01$	183
5. 5	Normalized diffusion admittance when $\gamma = 1/2$, $\tau_p = 10^{-5}$ sec, and $W/L_p = 0.1$	184
5. 6	Normalized diffusion admittance when $\gamma = 1/3$, $\tau_p = 10^{-5}$ sec, and $W/L_p = 0.1$	184
5. 7	Normalized diffusion admittance when $\gamma = 1/2$, $\tau_p = 10^{-10}$ sec, and $W/L_p = 0.1$	185
5. 8	Relative loss of an abrupt and graded junction diode under forward bias conditons	187
5. 9	Relative loss of diffusion admittance with doping profile $N(x) = ax^3$	188
5. 10	Total varactor model of diode wafer	190
5. 11	The depletion and diffusion susceptance when the minority carrier lifetime is chosen to minimize loss in the graded junction diode, i. e., $\tau = 1.84 \times 10^{-10}$ sec	191
5. 12	The impedance of the total varactor model when the minority carrier lifetime is chosen to minimize loss in the graded junction diode	192
5. 13	The total diode susceptance for $\tau = 10^{-7}$ sec and $\tau = 1.84 \times 10^{-10}$ sec (minimum loss) when the bulk series resistance $R_s = 1$ ohm	195
5. 14	LSUC circuit model for the diffusion admittance	197

LIST OF ILLUSTRATIONS (Cont.)

Figure		Page
5.15	A comparison of the sideband currents generated by the nonlinear diffusion admittance and the nonlinear depletion capacitance when $V_1 = 0.01$ V and $V_2 = -0.1$ V.	203
5.16	Maximum gain as function of bias voltage with pump voltage = 0.1 V when the optimum lifetime is used for both doping profiles. In each case $\phi_V = 0.9$ V, $S_1 = 2.20 \times 10^{11}$ F^{-1}, $W/L = 0.1$, and $p_n(W) = 10^{10}$ cm^{-3}	212
5.17	Noise figure as a function of bias voltage with pump voltage = 0.1 V when the optimum lifetime is used for both doping profiles. In each case $\phi_V = 0.9$ V, $S_1 = 2.20 \times 10^{11}$ F^{-1}, $W/L = 0.1$, and $p_n(W) = 10^{10}$ cm^{-3}	213
5.18	Maximum gain as a fucntion of pump voltage at zero bias voltage when the optimum lifetime is used for both doping profiles. In each case $\phi_V = 0.9$ V, $S_1 = 2.20 \times 10^{11}$ F^{-1}, and $p_n(W) = 10^{10}$ cm^{-3}	214
5.19	Noise figure as a function of pump voltage at zero bias voltage when the optimum lifetime is used for both doping profiles. In each case $\phi_V = 0.9$ V, $S_1 = 2.20 \times 10^{11}$ F^{-1}, $W/L = 0.1$, and $p_n(W) = 10^{10}$ cm^{-3}	215
5.20	Experimental gain of a LSUC as a function of bias voltage on the varactor	217

LIST OF SYMBOLS

Symbol	Meaning	Defined By Or First Used In
A	Diode area	(5.22)
$\overline{A}$	Voltage-current transmission matrix parameter	Sec. 2.2.1
A_{k+m}	Terms used in recurrence relation	(C.2)
a	Parameter in diode doping concentration profile	(3.9)
$\overline{a}$	Inner radius of coaxial line	(2.36)
a_v	$= V_0/(V_b - \phi_v)$	(5.41)
a_k	Coefficients in infinite power series	(C.1)
a_r	Resistance slope	Sec. 3.2.3
a_x	Reactance slope	Sec. 3.2.3
B	Susceptance	(2.9)
$\overline{B}$	Voltage-current transmission matrix parameter	Sec. 2.2.1
B_p	Hole diffusion susceptance	Sec. 5.2
B_w	Bandwidth	(3.22)
B_{ij}	Admittance matrix susceptance for coaxial tee junction	Sec. 4.4.3
$\tilde{b}$	Susceptance slope parameter	(2.9)
b	Exponent for diode profile power law	(3.9)
b_k	Polynomial coefficient	(C.3)
$\overline{b}$	Outer radius of coaxial line	(2.36)
b'	$= (b+1)/2$	Sec. 5.3.2
b''	$= (b-1)/2$	Sec. 5.3.2
$\overline{C}$	Voltage-current transmission matrix parameter	Sec. 2.2.1
C_b	Zero bias varactor junction capacitance	(5.6)

LIST OF SYMBOLS (Cont.)

Symbol	Meaning	Defined By Or First Used In
C_d	Discontinuity capacitance	(2.36)
C_f	Diode fringing capacitance	Fig. 4.1
C_j	Diode junction capacitance	Fig. 4.1
C_ℓ	Band-pass filter capacitance	Fig. 2.3
C_p	Diode package capacitance	Sec. 3.4.1
C_{ij}	Admittance matrix capacitance for coaxial tee junction	Sec. 4.4.3
$C_{r,i}$	Filter capacitance	(2.7)
c	Velocity of light in a vacuum	Sec. 2.6
$\overline{D}$	Voltage-current transmission matrix parameter	Sec. 2.2.1
D_p, D_n	Diffusion constant for holes, electrons	(5.5)
d	Transmission line length	(2.32)
d'	$= (\omega - \omega_o)/\omega_o$	Sec. 2.7.2
d_w	Distance between waveguide adapter and last disk	Fig. 3.31
E	Electric field	(5.12)
E'	Filter parameter	(2.32)
F	Noise figure	Sec. 4.4.3
$\overline{F}$	Average noise figure	(4.9)
F'	Filter parameter	(2.35)
F_i	Noise figure of stage i	Sec. 4.4.3
F_m	Noise figure at output frequency ω_m	Sec. 3.2.5
F_{AM}	Additional AM upconverter noise from pump source	Sec. 4.4.3.3
F_{FM}	Additional FM upconverter noise from pump source	Sec. 4.4.3.3
f_a	Diode series resonant frequency	Sec. 4.2.1.3
f_b	Diode parallel resonant frequency	Sec. 4.2.1.3
f_c	Diode cutoff frequency	Sec. 4.2.1.3
f_f	Fundamental frequency	Sec. 5.4.1.1

LIST OF SYMBOLS (Cont.)

Symbol	Meaning	Defined By Or First Used In
f_s, f_p, f_{p-s}	Signal, pump, and lower sideband frequency	
G_j	Conductance shunting diode junction capacitance	Fig. 4.1
G_g	LSUC generator conductance	Sec. 5.4.2
G_ℓ	LSUC load conductance	Sec. 5.4.2
G_{mn}	Transducer power gain with input at ω_n and output at ω_m	(3.11)
G_0	Midband transducer power gain	(4.11)
GBW	Voltage gain-bandwidth product	(3.21)
g_i	Lumped low-pass prototype circuit values	Fig. 2.1
g'_0, g'_{mc}, g'_{ms}	dc, cosine, and sine Fourier components of $e^{\alpha V}$	Sec. 5.3.2
g_p, g_n	Hole, electron generation term	(5.9), (5.10)
H_ℓ	Coefficient of Fourier expansion of depletion layer capacitance	(5.40)
h(x)	Function of x	(D.1)
$I_n(x)$	Modified Bessel Function	
i_0	dc diode current	(3.22)
i_k	Current component at ω_k	(3.8)
i_s	Diode reverse saturation current	Sec. 3.2.5
$<i^2>$	Mean, square, fluctuation noise current	(3.22)
J, $J_{i,i+1}$	Admittance inverter	Fig. 2.5
J	Current density	Sec. 5.3.2
J_p, J_n	Current density due to holes, electrons	(5.7), (5.8)
J_{mc}, J_{ms}	dc, cosine, and sine Fourier components of J(t)	(5.20), (5.21)
J_{p-s}	Current density at lower sideband frequency	Sec. 5.4.1.2
J_{ss}	Small signal current density	Sec. 5.2
K, $K_{i,i+1}$	Impedance inverter	Fig. 2.5
K_q	$= Q_{11}Q_{21}$	(3.15)
$K_n(z)$	Modified Bessel Function	Sec. 5.3.2
k	Boltzmann's constant	(3.22)

LIST OF SYMBOLS (Cont.)

Symbol	Meaning	Defined By Or First Used In
L	Diode lead inductance	Sec. 3.4.1
L_2	Attenuation of second stage	Sec. 4.4.3
L_{33}	Admittance matrix inductance for coaxial tee junction	Sec. 4.3.2
L_ℓ	Band-pass filter inductance	Fig. 2.3
L_p, L_n	Diode hole, electron diffusion length	(5.5)
$L_{r,i}$	Filter inductance	(2.7)
LSUC	Lower sideband upconverter	Sec. 1.1
L_T	Transforming inductance of diode package	Fig. 4.3
ℓ	Transmission line length	Fig. 2.13
M	Noise measure	Sec. 3.3.4
M_a, M_b, etc.	arbitrary constants	
m_k	Subscript for currents, voltages, etc.	(5.27)
m_s	$= S_1/S_0 = -C_1/C_0$	(5.37)
$N(x)$	Diode impurity concentration on the n side	(3.9)
N_d, N_a	Diode donor, acceptor density	(5.11)
n	Minority electron density	Sec. 5.2
n'	Transformer turns ratio	Sec. 3.5
$\tilde{n}$	Parameter in exponent of Shockley diode equation	Sec. 5.3.4
n_p	Equilibrium minority electron density	Sec. 5.2
$\mathcal{O}(x)$	Order symbol	(4.11)
P	Power	Sec. 3.5.1.1
P_{mn}	Power at frequency $mf_p + nf_s$	(3.1)
P_{LR}	Transducer power loss ratio	Sec. 2.2.1
p	Minority hole density	Sec. 5.2
p_n	Equilibrium minority hole density	Sec. 5.2
p_0, p_{mc}, p_{ms}	dc, cosine, and sine Fourier components of hole density	Sec. 5.3.2
Q	Charge	(5.3)

LIST OF SYMBOLS (Cont.)

Symbol	Meaning	Defined By Or First Used In
$\bar{Q}$	Normalized charge on varactor	Sec. 5.2
Q_A	Resonated circuit Q	Sec. 2.4.3
Q_B	Charge on varactor at $V = V_B$	Sec. 5.2
Q_c	Circuit quality factor	Sec. 4.2.1.2
Q_ϕ	Charge on varactor at $V = \phi_v$	Sec. 5.2
Q_{ij}	Varactor dynamic quality factor	(3.12)
q	Electronic charge $= +1.602 \times 10^{-19}$ coul.	(3.22)
q_b	dc bias charge	(5.3)
q_p	Charge at pump frequency	Sec. 3.2.1
q_s	Charge at signal frequency	Sec. 3.2.1
q_s'	Signal plus sideband charge	Sec. 3.2.1
q_t	Total charge	(3.3)
q_u	Charge at $f_p + f_s$	(5.3)
R	Resistance	Sec. 2.2.1
R_g	Generator resistance	Sec. 2.2.1
R_{gn}	LSUC generator resistance at ω_n	(3.11)
R_ℓ, $R_{\ell m}$	LSUC load resistance at ω_m	(3.11)
R_x	Diode noise resistance	Sec. 3.2.5
R_{er}	Equivalent noise resistance at ω_r	Sec. 3.2.5
R_{ind}	Resistance induced into the pump circuit	(3.41)
R_s	Diode spreading resistance	Sec. 3.2.3
R_s'	Diode input resistance at signal frequency	(3.44)
RPA	Reflection parametric amplifier	Sec. 1.1
r	Ratio of lower sideband to signal frequencies	(3.17)
$\bar{r}$	Radius of coaxial disk	(2.36)
r_c	Critical r	(3.30)
r_{opt}	Optimum r	(3.31)

LIST OF SYMBOLS (Cont.)

Symbol	Meaning	Defined By Or First Used In
$S(t)$	Diode elastance	(3.3)
S_b	Zero bias elastance	(3.10)
S_L	Load SWR	(4.4)
S_m	Measured SWR	(4.4)
S_{max}	Maximum SWR	(4.4)
S_n	Fourier component of diode elastance	(3.3)
S_p	Diode package elastance	Sec. 3.4.1
T	Absolute temperature	(3.22)
T_a	Ambient temperature	Sec. 3.2.5
T_d	Diode temperature	Sec. 3.2.5
T_n	Chebyshev polynomial of first kind	(2.3)
T_n^*	Shifted Chebyshev polynomial of first kind	Appendix C
t	Time	(3.5)
USUC	Upper sideband upconverter	Sec. 1.1
U_j	Partial sum	(C.13)
u	Function of x	Sec. 5.3.2
u_n	Polynomial of degree n	(C.3)
$V(t)$	Voltage	(3.10)
$\overline{V}$	Normalized voltage on varactor	Sec. 5.2
V_B	Diode breakdown voltage	Sec. 5.2
V_b	dc bias voltage	Sec. 5.2
V_k	Voltage at ω_k	(3.6)
v_p	Pump voltage	Sec. 3.2.1
v_s'	Signal plus sideband voltages	Sec. 3.2.1
v_t	Total voltage	Sec. 3.2.1
W	Diode depletion layer width	Sec. 5.3.2
w	Fractional bandwidth	Sec. 2.2.2

LIST OF SYMBOLS (Cont.)

Symbol	Meaning	Defined By Or First Used In
w_k	Weight function	(C.16)
X	Reactance	Sec. 2.2.1
X_{ij}	Reactance matrix element	(3.8)
x	Distance variable	(3.9)
$\bar{x}$	$= \xi x$	(Sec. 5.3.2
x_g	Normalized generator resistance	(3.14)
x_s	Normalized effective generator noise resistance	(3.24)
Y_c, Y_o	Characteristic admittance	(Sec. 2.3.2 or Fig. 2.14)
Y_I	Image admittance	Sec. 2.3.2
Y_{mn}	Admittance matrix element	(3.11)
y_I	Normalized image admittance	Sec. 2.3.2
y_ℓ	Normalized load resistance	(3.15)
y_o	Normalized characteristic admittance	Sec. 2.3.2
y_s	Normalized effective load noise resistance	Sec. 3.2.5
Z_c, Z_o	Characteristic impedance	Fig. 2.13
Z_d	Diode impedance	Sec. 3.5.1.3
Z_I	Image impedance	(2.22)
Z_i	Impedance of the lower sideband circuit at ω_{20} required to make $Z_{22} = R_\ell + R_s$	Sec. 3.4.3
Z_k	Iteration characteristic impedances	(2.41)
Z_{kk}	Circuit impedance at frequency ω_k as seen by the diode	Sec. 3.2.1
Z_s, Z_p, Z_{p-s}	LSUC circuit impedances at signal, pump, and lower sideband frequencies	Fig. 3.10
Z_t	Impedance of the signal circuit at ω_{10} required to make $Z_{11} = R_g + R_s$	Sec. 3.4.3
Z_v	Impedance	Sec. 3.2.3
Z_{v0}	Impedance Z_v at ω_{10}	Sec. 3.2.3
z	Complex variable	Appendix C

LIST OF SYMBOLS (Cont.)

Symbol	Meaning	Defined By Or First Used In
z_I	Normalized image impedance	(2.24)
z_o	Normalized characteristic impedance	(2.21)
z_r	= 1/z	Appendix C
α	= q/kT	Sec. 5.2
$\bar{\alpha}$	Coaxial disk parameter	(2.36)
α_m	Diffusion admittance parameter	(5.19)
α_w	Parameter used in gain-bandwidth expression	(3.20)
α_w'	Modified parameter used in gain-bandwidth expression	(3.42)
β	Wave number	(3.20)
β_m	Diffusion admittance parameter	(5.19)
Γ	Voltage reflection coefficient	Sec. 2.2.1
$\Gamma(x)$	Gamma function	(5.40)
γ	Doping Profile parameter	(3.10)
δ	Decrement	Sec. 2.4.3
δ_{ij}	Kronecker Delta function	Sec. 5.4.2
ϵ	Permittivity	Sec. 5.3.5
ϵ_e	Error term	(C.4)
ϵ_o	Free space permittivity	(2.36)
θ	Electrical distance	(2.23)
θ_p	Electrical distance between diode and pump filter	(3.42)
θ_s	Electrical distance between diode and signal filter	(3.43)
κ	Constant coefficient	(5.42)
λ	Wavelength	Sec. 3.4.4
μ_p, μ_n	Hole, electron mobility	(5.7), (5.8)
ν	Order of Bessel function (not necessarily integer)	Appendix C
ξ	$= (1 + jm\omega\tau_p)/L_p^2$	(5.15)
ρ	Charge density	(5.12)

LIST OF SYMBOLS (Cont.)

Symbol	Meaning	Defined By Or First Used In
σ_k	$= \left.\frac{d^k S}{dQ^k}\right\|_{Q_0}$	(3.37)
τ	Parameter in Lanzco's tau method	(C.4)
$\overline{\tau}$	Coaxial disk parameter	(2.36)
τ_p, τ_n	Hole, electron minority carrier lifetime	(5.5)
υ	Pass-band tolerance	(2.2)
ϕ	Electrical length	Fig. 2.12
ϕ_v	Built-in potential	(3.10)
χ	Reactance slope parameter	(2.8)
Ψ	Range parameter	Appendix C
ψ	Electrical phase angle	(5.3)
ω	Radian frequency	Sec. 2.2.1
ω'	Low-pass frequency variable	Sec. 2.2.2
ω_c	Filter cutoff radian frequency	Sec. 2.2.1
ω_c'	Normalized filter cutoff radian frequency	Sec. 2.2.2
ω_f	Fundamental radian frequency	(5.28)
ω_k	Radian frequency for $k = 0, 1, 2 \ldots$	(3.7)
ω_o	Filter center radian frequency	Sec. 2.2.2
ω_0	Pump radian frequency	(5.23)
ω_p, ω_s	Pump, signal radian frequency	(3.1)

LIST OF APPENDICES

		Page
APPENDIX A:	PROGRAM LISTINGS	224
APPENDIX B:	DETERMINATION OF PARAMETRIC CONVERTER CIRCUIT IMPEDANCES	246
APPENDIX C:	CALCULATION OF $K_\nu(z)$ BESSEL FUNCTIONS WITH COMPLEX ARGUMENT	255
APPENDIX D:	LAPLACE ASYMPTOTIC METHOD OF INTEGRATION	265

ABSTRACT

This report describes a method for synthesizing a parametric lower sideband upconverter (LSUC) in coaxial line and reports an analysis of a forward biased varactor diode as it would be used in a LSUC. In most analyses of parametric devices the circuit is assumed to consist of either ideal filters (total transmission for in-band frequencies and total rejection for out-of-band frequencies) or lumped-element filters. However, experimentally a LSUC requires the use of microwave circuit elements that are neither lumped nor ideal.

The LSUC described here consists of a silicon varactor diode mounted close to the intersection of a coaxial tee junction where each port separately carries the signal, pump, and lower sideband power. These three frequencies are isolated from one another by making use of some nonideal properties of the coaxial tee junction and by using coaxial filters, which also serve an impedance matching function. The available theory for design of coaxial band-pass filters was found inadequate so an improved synthesis technique was developed to design filters with center frequencies from 1 to 20 GHz and bandwidths from 1 to 20 percent of the center frequency. This theory was then applied to the noniterative design and construction of a LSUC which exhibited 20 dB of power gain.

As for the varactor diode itself, it has been known that increased capacitance variation can be obtained if the diode is forward biased for at least part of the pump cycle. This additional capacitance comes from diffusion effects. The theory for diffusion admittance is reviewed and extended to apply to the LSUC. An optimum forward bias level for maximum gain is found both theoretically and experimentally, and beyond this optimum bias, the LSUC performance rapidly deteriorates.

CHAPTER I

INTRODUCTION

1.1 Background

In recent years much effort has been concentrated on the development of microwave receivers in response to increased activity in satellite communication, manned space flight, telemetry, radar, and radio astronomy. There are several low-noise microwave amplifiers available today, each having its own advantages and disadvantages; among these, listed in order of decreasing noise figure, are the traveling-wave tube, transistor, tunnel diode, parametric amplifier, and maser.

Modern, ultra-low noise, traveling wave tube amplifiers are available today with a noise temperature as low as $400^{\circ}K$ at 1 GHz, although most amplifiers of this kind are much noisier. At this same frequency noise temperatures range between $400^{\circ}K$ and $800^{\circ}K$ for transistor amplifiers, between $300^{\circ}K$ and $400^{\circ}K$ for tunnel diode amplifiers, between $80^{\circ}K$ and $180^{\circ}K$ for uncooled parametric amplifiers, between $40^{\circ}K$ and $65^{\circ}K$ for parametric amplifiers cooled to $77^{\circ}K$, between $10^{\circ}K$ and $30^{\circ}K$ for parametric amplifiers cooled to $20^{\circ}K$, and between $5^{\circ}K$ and $10^{\circ}K$ for masers (Ref. 1).

In applications where an ultra-low noise preamplifier is required, the choice is generally limited to either the parametric amplifier or the maser. The maser today offers the ultimate in low-noise temperature, although a cooled parametric amplifier has been built with a system noise temperature of $12.5^{\circ}K$ at 4 GHz, a value which is competitive with the maser at this frequency (Ref. 2). The maser has the advantages of not requiring a bias voltage and of being unaffected by changes in pump amplitude and frequency. However, usually the maser must be cooled to $4^{\circ}K$ for successful operation while the parametric amplifier may be operated at room temperature. Furthermore, the maser is very temperature-sensitive, has a long recovery time when overloaded (on the order of microseconds as compared to nanoseconds for the parametric amplifier), and has a narrower bandwidth than the parametric amplifier.

This thesis is concerned with the study of parametric devices. The parametric principle, which forms the basis for these devices, can be stated as follows: under certain circumstances, the energy of an oscillating system can be increased by supplying to the system energy the frequency of which differs from the oscillation frequency. The term "parametric" comes from the need to vary a system parameter to obtain gain. This principle was discovered over a century ago; Faraday (1831), Melde (1859), and Lord Rayleigh (1883-1896) all published calculations and observations on the principle as applied to mechanical systems.

The most common form of electronic parametric device is the reflection parametric amplifier (RPA). In this device a high-power, high-frequency pump signal is reactively mixed with the incoming low-frequency signal. The resulting lower sideband signal is supported in a resonant circuit while the upper sideband signal is rejected. The lower sideband frequency mixes again with the pump frequency, providing an additional component to the low-frequency signal. The double reactive mixing process introduces a 180^{o} phase shift between the incoming and outgoing signal frequency, with the result that the device appears as a negative resistance.

The upper sideband upconverter (USUC) suppresses the lower sideband and takes the output at the upper sideband frequency. The upconverter is a positive resistance device in which the power gain for the ideal lossless reactance is limited to the ratio of the output to the input frequencies (Manley-Rowe gain).

The lower sideband upconverter (LSUC) suppresses the upper sideband signal and provides an output at the lower sideband frequency. The LSUC, like the RPA, is a negative resistance device; however, the gain of this amplifier includes a component due to the ratio of the output frequency to the input frequency.

Within the family of parametric devices, a comparison between the widely used RPA and the LSUC shows the following differences:

(1) Although the noise figures for both devices are identical at infinite gain, they differ for finite gain: the noise figure increases with gain in the RPA, but decreases with gain in the LSUC.

(2) For gain below a threshold value, the gain sensitivity to pump amplitude variations is lower in the LSUC, since only part of its gain is derived from

the negative resistance. Above this gain value the RPA exhibits greater stability (Ref. 3, pp. 214-215).

(3) The gain bandwidth product is larger for the LSUC than for the RPA, by a factor approximately equal to the square root of the output to input frequency ratio.

(4) For optimum performance, the RPA requires a circulator at the input port while the LSUC requires an isolator; this provides an advantage to the LSUC since a circulator generally has higher insertion loss than an isolator.

(5) The input and output of the RPA are at the same frequency, whereas the output of the LSUC is at a higher frequency. This is usually not a serious drawback since in both cases the signal must be downconverted, and the mixer loss and noise figure are independent of the frequency ratio.

The aim of this thesis is to extend and develop further the design theory for the lower sideband upconverter, and to facilitate exploitation of the relative advantages of the LSUC, which have been enumerated above.

1.2 Literature Review

Capacitive parametric amplifiers have been used successfully only since the advent of high-Q varactor diodes. The investigation into the properties of solid-state diodes necessary for parametric amplification can be considered to have been initiated in the mid-1940's by workers at General Electric, together with Torrey at the MIT Radiation Laboratory. They discovered that certain welded-contact mixer diodes exhibited negative IF conductance and gain, although noise figure was found to be higher than for other mixer diodes. The primary cause for this phenomenon was found to be the variable barrier capacitance of the diode (Ref. 4, Chapter 13). In 1948 A. van der Ziel (Ref. 5) derived relationships for the gain and impedances in terms of the conversion transconductance between the input and output, and thus generalized Torrey's work by giving a more unified treatment of the variable capacitance amplifier. In 1956 Manley and Rowe (Ref. 6) published their now famous work in which they derived the general power-frequency relationships for a nonlinear reactance. Practical application of this theory was dependent upon the development of a low-loss variable-capacitance diode (or varactor). Work on

this began at Bell Telephone Laboratories in 1954 and the successful results were published in 1959 (Ref. 7).

The advent of low-loss varactor diodes motivated researchers to improve the theory and design of parametric amplifiers; many of the papers of that period are reviewed by Mumford (Ref. 8). Notable among these is the paper by Rowe (Ref. 9) who used the small-signal assumption and the method of harmonic balance to obtain expressions for gain, bandwidth, terminal admittances, and gain sensitivity to change in pump-power or terminal conductance for the RPA, the USUC, and the LSUC. Later Kurokawa and Uenohara (Ref. 10) derived design relations for achieving maximum gain (for the USUC) or minimum-noise figure for these parametric devices; this work was extended by Khan (Ref. 11) by eliminating the high-gain assumption which they had used. This extended theory has been found useful in the design of a LSUC and is discussed in more detail in Chapter III. Although historically the LSUC has not been as widely used as the other parametric devices, its special characteristics were found to be essential in a preamplifier designed for Project Echo (Ref. 12). The results reported in many of the later papers have recently been published in book form (Refs. 13, 14), providing an excellent introduction to the subject.

Although much fundamental work has been carried out, parametric device theory remains in an incomplete form. Several deficiencies in the theory hinder designers in their attempts to apply these results directly to the synthesis or analysis of a parametric device. These inadequacies include the following.

(1) The pumped varactor diode is represented by a sinusoidal time-varying elastance (or capacitance), while in a physical circuit it produces many harmonic components of the time-varying elastance.

(2) The circuit is assumed either to short-circuit the higher order harmonic voltages or to open-circuit the higher order harmonic currents, so that there remains power flow at only two frequencies: that of the signal and that of either the upper sideband or the lower sideband. However, the impedance at a third frequency (such as the unwanted sideband) may drastically alter the performance of the device under study.

(3) The average varactor elastance (or capacitance) is assumed to be resonated by a single-tuned lumped circuit. However, in a physical microwave circuit the diode is tuned by a complex combination of lumped and distributed circuit elements resulting from the diode parasitic elements and the microwave transmission line.

(4) Because of the small-signal assumption, the pump circuit elements are usually assumed to be completely isolated from the rest of the circuit. Physically the pump port must be considered part of the total circuit.

(5) There is no adequate representation of the circuit behavior of a pumped forward-biased varactor in a parametric device.

These assumptions have been made to describe, to a first approximation, the observed parametric effects; however, their effect has been to oversimplify the analysis to such an extent that application of the existing theory to the design of a parametric device must usually be supplemented by empirical tuning adjustments and circuit modifications.

1.3 Topics of Investigation

The primary goals of this study are to refine the analysis, and to develop further the design theory for the varactor LSUC. With the aid of the studies reported by Oliver (Ref. 15), the effect of elastance harmonics, and hence higher order harmonic voltages and currents, may be included in the analysis. With an accurate synthesis technique and an accurate representation of the microwave circuit, the circuit environment in which the diode is embedded may be analyzed. Furthermore, by incorporating the diffusion admittance in the diode model, the effects of forward-biasing the diode in a LSUC can be found. The following chapters of this thesis describe how the goals of this study are achieved.

In the course of the work, it was found necessary to design and build microwave impedance transformers in coaxial line, so that the required impedance transformation would be obtained as close to the diode as possible. Although much fundamental study has been carried out on microwave filters in the past, the existing theory had to be extended to achieve reasonable correlation between theory and experiment. It is now possible to design coaxial band-pass filters and impedance transformers with little or no experimental adjustment by use of the theory presented in Chapter II.

In Chapter III a detailed review of existing LSUC design theory is presented. This is followed by an extension to include the effect of the impedance at the upper sideband frequency, and a discussion of the effect of various circuits on the gain-bandwidth product of the LSUC. The chapter culminates with a realizable design of a microwave LSUC for which the experimental results are given in Chapter IV.

Many varactor parametric amplifiers operate best when they are biased so that the diode is in the forward-conduction region during part of the pump cycle. This permits larger susceptance variation, which in turn may improve the gain stability and decrease the minimum noise figure. When the diode is forward-biased, the principal contribution to the capacitance is the diffusion susceptance. The theory for the diffusion admittance as it applies to a LSUC is outlined and extended in Chapter V.

Finally, Chapter VI provides conclusions and recommendations for future work.

CHAPTER II

COAXIAL MICROWAVE BAND-PASS FILTERS

2.1 Introduction

The design of a microwave lower sideband upconverter (LSUC) requires band-pass impedance transformers, to prevent unwanted frequencies from propagating in the signal, lower sideband, and pump ports, and to present to the diode the correct design impedance. Since the behavior of these impedance transformers has such a crucial effect on the operation of a LSUC, a detailed investigation of microwave filter design has been undertaken, and is reported here. Most of the theory developed here applies to filters terminated at both ends with loads equal to the characteristic impedance of the line; however it is shown how this theory may be modified for the design of impedance transformers in which the terminations are unequal.

At low frequencies a very general and complete filter synthesis technique has been developed, utilizing lumped inductors and capacitors as the basic building blocks. However, filter synthesis is much more complicated at microwave frequencies since distributed-parameter elements must be used. Although these distributed elements often have a complex frequency dependence, the lumped techniques developed for low frequencies provide an invaluable guide to microwave filter synthesis.

The following discussion presents the necessary equations for the design of band-pass filters in coaxial line. In Section 2.2, the conventional lumped-element filter synthesis theory is reviewed briefly; a lumped low-pass prototype circuit is developed, is transformed into a band-pass circuit, and is reformulated in terms of lengths of transmission line and impedance inverters. A new method of designing these impedance inverters is presented in Section 2.3 and is shown, in Section 2.4, to yield improved filter characteristics. Since a typical inverter utilizing a coaxial disk introduces discontinuity capacitance, the design must be modified to accommodate this reactance; three methods of so doing are reviewed in Section 2.5. A detailed procedure,

together with some experimental results, is presented in Section 2.6. Section 2.7 follows with a discussion of the properties and limitations of this kind of filter, while Section 2.8 contains some concluding remarks.

2.2 Review of Filter Theory

Two basic approaches may be used in designing a microwave filter: synthesis based on a direct transmission-line or waveguide formulation, or modification of lumped-constant filter theory. The latter approach has been more successful, and has been used here to design coaxial band-pass filters. In the following sections are found a review of lumped filter synthesis (Sections 2.2.1 and 2.2.2), a description of immittance inverters (Section 2.2.3), and an indication of how this theory is applied to a microwave structure (Section 2.2.4).

2.2.1 Derivation of the Lumped-Element Low-Pass Prototype Circuit. The lumped-element filter synthesis technique is based upon derivation of the parameters of a network having a prescribed value of transducer power loss ratio P_{LR}, which is defined by

$$P_{LR} = \frac{\text{available power to the network}}{\text{power delivered to the load}} .$$

For a lossless network with an input impedance $Z = R + jX$ and a source impedance R_g,

$$P_{LR} = \frac{1}{1 - |\Gamma|^2}$$

where Γ is the voltage reflection coefficient at the input given by

$$\Gamma = \frac{R + jX - R_g}{R + jX + R_g} .$$

Substituting for Γ, it is readily shown that

$$P_{LR} = 1 + \frac{(R - R_g)^2 + X^2}{4R R_g} . \qquad (2.1)$$

For a low-pass maximally flat or Butterworth filter

$$P_{LR} = 1 + \upsilon^2(\omega/\omega_c)^{2n}, \tag{2.2}$$

and for a low-pass equal-ripple or Chebyshev filter

$$P_{LR} = 1 + \upsilon^2 T_n^2(\omega/\omega_c) \tag{2.3}$$

where ω_c is the cutoff frequency, and υ^2 is the pass-band tolerence. T_n is the Chebyshev polynomial of degree n, defined by

$$T_n(\omega/\omega_c) = \cos\left[n \operatorname{Arccos}(\omega/\omega_c)\right] \quad \text{for} \quad \left|\frac{\omega}{\omega_c}\right| \leq 1$$

$$= \cosh\left[n \operatorname{arccosh}(\omega/\omega_c)\right] \quad \text{for} \quad \left|\frac{\omega}{\omega_c}\right| \geq 1.$$

The polynomial T_n oscillates between ± 1 for $|\omega/\omega_c| \leq 1$ and equals one at the band-edge $|\omega/\omega_c| = 1$.

To synthesize a Chebyshev filter, the two P_{LR} expressions (2.1) and (2.3) are equated. This defines a load impedance in terms of the Chebyshev polynomial. The resulting polynomial can be realized as either one of the two dual prototype lumped ladder networks shown in Figs. 2.1 and 2.2. Although explicit expressions exist for the g_k values of these filters for both the Butterworth and Chebyshev forms, tabulated values are readily available (e.g. Ref. 16) and are used in the filter designs studied here.

2.2.2 Band-pass Filter Networks. In building a lower sideband upconverter, band-pass impedance matching circuits are used rather than low-pass networks, because they provide the necessary filtering action and are easier to build at microwave frequencies.

A band-pass filter is easily derived from the low-pass prototype by use of the low-pass to band-pass frequency mapping:

$$\frac{\omega'}{\omega'_c} = \frac{1}{w}\left(\frac{\omega}{\omega_o} - \frac{\omega_o}{\omega}\right).$$

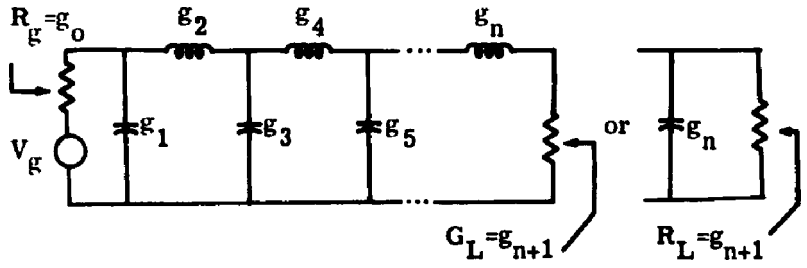


Fig. 2.1 Low-pass prototype circuit with shunt capacitor adjacent to source

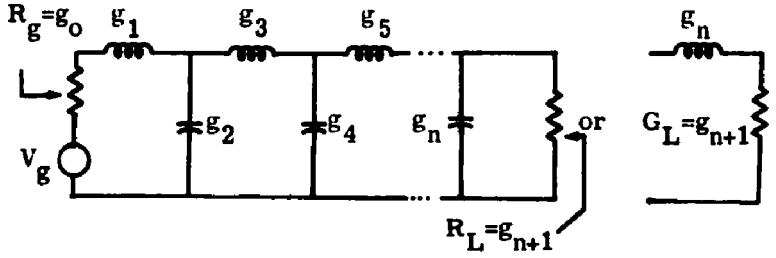
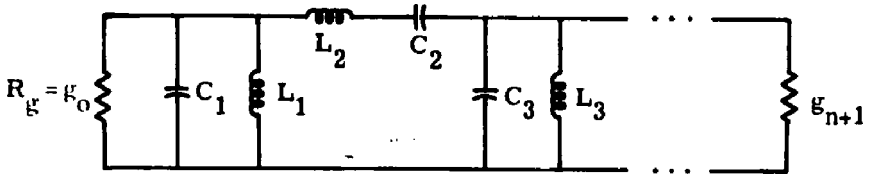


Fig. 2.2 Low-pass prototype circuit with series inductor adjacent to source

The low-pass frequency variable is ω' and the band-pass frequency variable is ω. The bandwidth of the band-pass filter is $\omega_2 - \omega_1$ and the center frequency is ω_o, such that $\omega_o^2 = \omega_1\omega_2$: $w = \frac{\omega_2 - \omega_1}{\omega_o}$. This mapping transforms shunt capacitors into parallel resonant circuits and series inductors into series resonant circuits, both of which are resonant at ω_o. The circuits of Figs. 2.1 and 2.2 are transformed into the band-pass circuits of Figs. 2.3 and 2.4. The steps are carried out in greater detail in several references, (e.g. Ref. 17, pp. 356-362).

2.2.3 Immittance Inverters. Microwave low-pass filters can be constructed more conveniently if they can be built entirely from either capacitive or inductive elements. Similarly microwave band-pass filters can be constructed more conveniently if they can be built entirely from either series or shunt resonant circuits. This can be done by using impedance (or K) inverters or admittance (or J) inverters. Ideal



$$C_\ell = \frac{g_\ell \omega'_c}{\omega_0 w} \qquad L_\ell = \frac{w}{\omega_0 \omega'_c g_\ell} \qquad \text{(Shunt Reactances)}$$

$$C_\ell = \frac{w}{\omega_0 \omega'_c g_\ell} \qquad L_\ell = \frac{g_\ell \omega'_c}{\omega_0 w} \qquad \text{(Series Reactances)}$$

Fig. 2.3 Band-pass prototype with shunt resonator adjacent to the generator

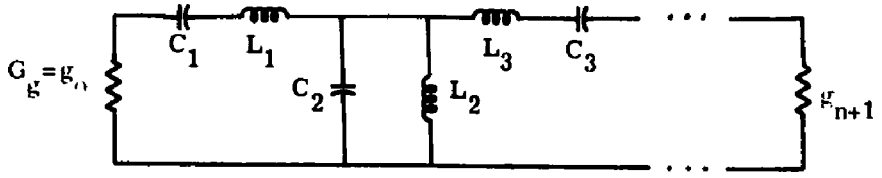


Fig. 2.4 Band-pass prototype with series resonator adjacent to the generator. The element values are given by the same formulas given in Fig. 2.3

immittance inverters are defined in Fig. 2.5. One obvious example of a K inverter is a quarter-wavelength transmission line.

The lumped-element band-pass filters shown in Figs. 2.2 and 2.3 are equivalent to the circuits shown in Figs. 2.6 and 2.7, where series resonant circuits are separated by K inverters or shunt resonant circuits are separated by J inverters. Referring to Figs. 2.3 and 2.6, the values of $L_{r,i}$, $C_{r,i}$ and $K_{i,i+1}$ are found by equating a section of the filter in Fig. 2.3 to the same section in Fig. 2.6. This calculation (Ref. 18, pp. 415-422, Ref. 19, pp. 9-15) gives the following results:

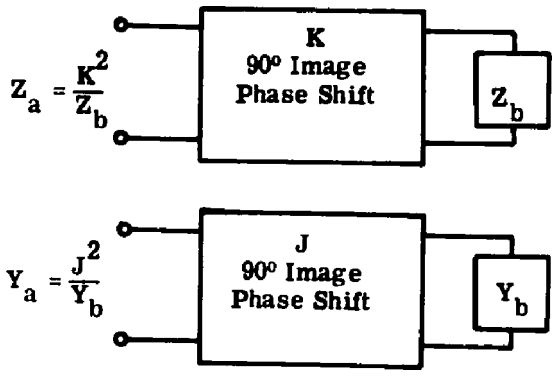


Fig. 2.5 Definition of an ideal K inverter and J inverter

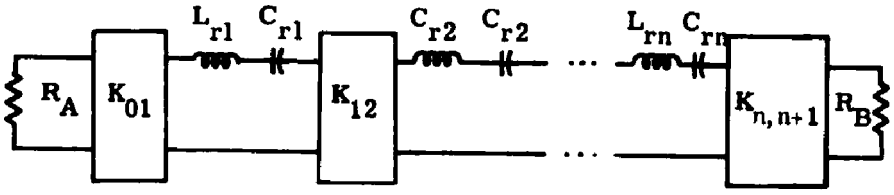


Fig. 2.6 Lumped band-pass impedance matching network using K inverters

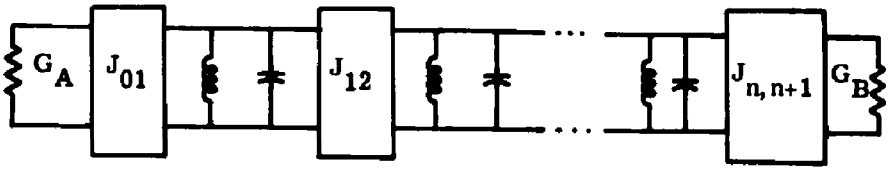


Fig. 2.7 Lumped band-pass impedance matching network using J inverters

$$K_{i,i+1} = \frac{\omega_o w}{\omega_c'} \sqrt{\frac{L_{r,i}(L_{r,i+1})}{g_i g_{i+1}}} \qquad i = 1,2,\ldots n-1 \qquad (2.4)$$

$$K_{0,1} = \sqrt{\frac{\omega_o w L_{r,1} R_A}{\omega_c' g_0 g_1}} \qquad (2.5)$$

$$K_{n,n+1} = \sqrt{\frac{\omega_o w L_{r,n} R_B}{\omega_c' g_n g_{n+1}}} \qquad (2.6)$$

$$L_{r,i} C_{r,i} = L_i C_i = \omega_o^{-2} \quad . \qquad (2.7)$$

Similar expressions hold for the admittance inverters.

2.2.4 Microwave Realization. Although the parameters for circuit of Fig. 2.6 can be found explicitly, two problems still remain for realization of the filter in a microwave structure: (1) how are the series resonant circuits made, and (2) how are the K inverters realized. Before resolving the first question, it is convenient to generalize the expressions for the K's and corresponding J's to make them more compatible with distributed elements.

A series LC circuit, or more generally a series resonator which has zero reactance at ω_o, can be described in terms of its resonant frequency ω_o and a reactance slope parameter χ.

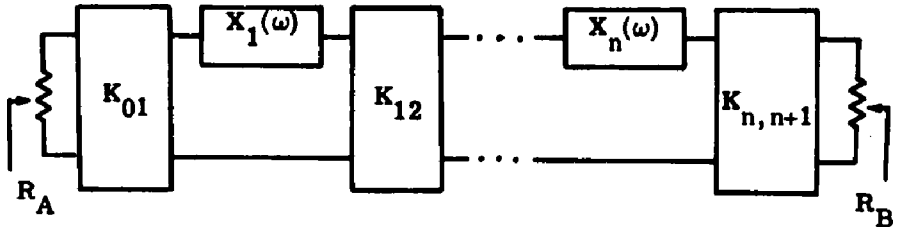
$$\chi = \frac{\omega_o}{2} \frac{dX}{d\omega}\bigg|_{\omega_o} \tag{2.8}$$

A shunt resonator, in which the susceptance is zero at ω_o, can be described in terms of its resonant frequency and a susceptance slope parameter $\tilde{b}$.

$$\tilde{b} = \frac{\omega_o}{2} \frac{dB}{d\omega}\bigg|_{\omega_o} \tag{2.9}$$

For a series LC circuit $\chi = \omega_o L$, and for a shunt LC circuit $\tilde{b} = \omega_o C$. Thus the Q values for a circuit with resistance R in series with a series resonator or a conductance G in parallel with a shunt resonator are $Q_c = \chi/R$ and $Q_c = \tilde{b}/G$ respectively. The K and J values in terms of these slope parameters are given in Figs. 2.8 and 2.9, which should be used rather than Figs. 2.6 and 2.7 for distributed circuit design.

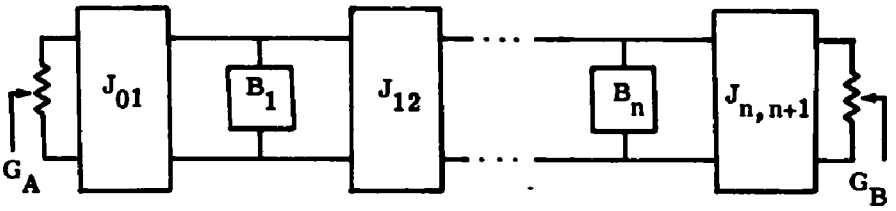
The series resonant circuits $X_i(\omega)$, shown in Fig. 2.9 can be realized as half-wavelength transmission lines. Thus the choice of $L_{r,i}$ in the previous section is equivalent to the choice of characteristic impedance of the half-wavelength line. Often all the X_i can be made to have the same characteristic impedance of 50 ohms. In this case the



$$K_{01} = \sqrt{\frac{R_A w \chi_1}{g_0 g_1 \omega_c'}} \qquad K_{j,j+1} = \frac{w}{\omega_c'}\sqrt{\frac{\chi_j \chi_{j+1}}{g_j g_{j+1}}} \qquad K_{n,n+1} = \sqrt{\frac{R_B w \chi_n}{\omega_c' g_n g_{n+1}}}$$

$$j = 1, \ldots, n-1$$

Fig. 2.8 Generalized impedance matching networks using K inverters



$$J_{01} = \sqrt{\frac{G_A b_1 w}{g_0 g_1 \omega_c'}} \qquad J_{j,j+1} = \frac{w}{\omega_c'}\sqrt{\frac{b_j b_{j+1}}{g_j g_{j+1}}} \qquad J_{n,n+1} = \sqrt{\frac{G_B b_n w}{\omega_c' g_n g_{n+1}}}$$

$$j = 1, \ldots, n-1$$

Fig. 2.9 Generalized impedance matching networks using J inverters

reactance slope parameter is obtained from the transmission line equation in the following manner. The reactance of a transmission line of electrical length ϕ and characteristic impedance Z_c terminated in a load R_L is given by

$$X = Z_c \frac{\left(Z_c^2 - R_L^2\right) \tan \phi}{Z_c^2 + R_L^2 \tan^2 \phi} \quad . \tag{2.10}$$

The slope parameter is readily obtained by differentiation of X, and for a transmission line resonant at $\phi = \pi$

$$\chi = \frac{Z_c \pi}{2} \left(\frac{Z_c^2 - R_L^2}{Z_c^2} \right) \quad . \tag{2.11}$$

Inversion networks often present a very small resistance in shunt with the series resonator so that $R_L / Z_c << 1$. In this case

$$\chi \cong \frac{Z_c \pi}{2} \tag{2.12}$$

and in similar fashion

$$\tilde{b} \cong \frac{Y_c \pi}{2} \quad . \tag{2.13}$$

When wavelengths are too long to feasibly permit spacing inverters of one kind every half wavelength, K and J inverters can be placed alternately every quarter wavelength as in Fig. 2.10. The only difference between the values here and those in Figs. 2.8 and 2.9 is a difference in slope parameter. For a quarter wavelength line $\chi = \pi Z_c / 4$ and $\tilde{b} = \pi Y_c / 4$.

The series resonant circuits can be realized in a microwave structure by a half wavelength transmission line with a reactance slope parameter of $\pi Z_c / 2$. The second question needing clarification is how the K inverters are realized. One inverter already mentioned is a quarter-wavelength line. Much broader bandwidth may be achieved using the K inverters shown in Fig. 2.11 or the J inverters shown in Fig. 2.12.

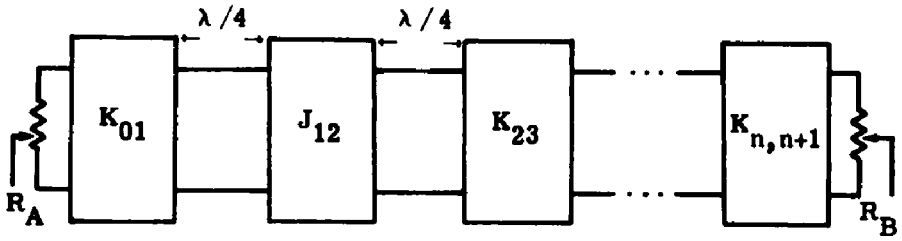


Fig. 2.10 Alternate K and J inverters

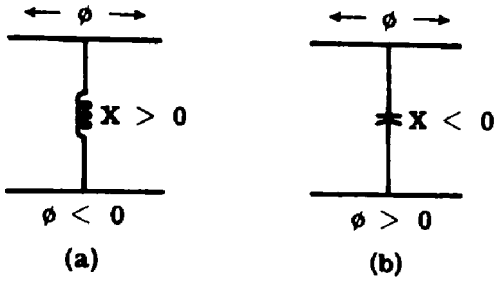


Fig. 2.11 Lumped-element K inverter realization

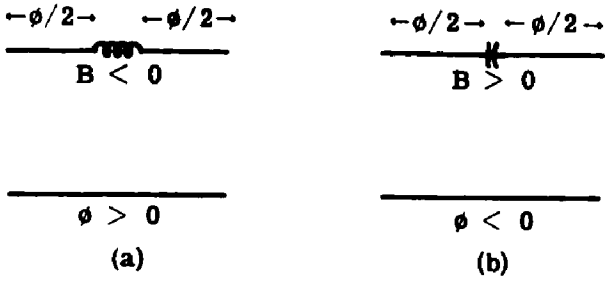


Fig. 2.12 Lumped-element J inverter realization

In Fig. 2.11(a) and 2.12(b) the negative line length must be absorbed by available line length between inverters. The value of K for the inverters of Fig. 2.11 is

$$K = Z_c \tan \theta/2 \tag{2.14}$$

where

$$\theta = - \text{Arctan}\,(2X/Z_c) \tag{2.15}$$

$$X/Z_c = \frac{K/Z_c}{1 - (K/Z_c)^2} \tag{2.16}$$

The value of J for the inverters in Fig. 2.12 is

$$J = Y_c \tan \theta/2 \tag{2.17}$$

where

$$\theta = - \text{Arctan}\, 2B/Y_c \tag{2.18}$$

$$B/Y_c = \frac{J/Y_c}{1 - (J/Y_c)^2} \tag{2.19}$$

Thus when K or J is calculated by the equations in Figs. 2.8 or 2.9, θ and the reactance or susceptance can be found. The derivation of these formulas may be found in Cohn's work (Ref. 20) and is not reproduced here. A more general set of relations based on Fig. 2.11(b) derived later for a distributed element in an inverter, gives the above results when specialized to a lumped capacitor.

2.3 Distributed Impedance and Admittance Inverter Design

Microwave filter design has been greatly facilitated by the development of direct-coupled filter design techniques by Cohn (Ref. 20) described in the previous sections. Details have been published for a wide variety of microwave structures which provide immittance inverter realization over a range of frequencies in coaxial line, strip line, and waveguide (Ref. 18). In many cases these structures consist of a uniform section of transmission line loaded with a lumped reactive element. In particular, series

capacitances and shunt inductances were used by Cohn (Ref. 20) to fabricate immittance inverters in strip line and waveguide respectively.

Coaxial-line filter design utilizing this method, has been based upon use of a short section of low-Z_o line to approximate a lumped shunt capacitance or a short section of high-Z_o line to approximate a lumped series inductance (Ref. 21). Such elements are more easily obtained than lumped series capacitances or shunt inductances and are readily used in the design of coaxial-line immittance inverters. In addition the shunt capacitance which is realized by a low-Z_o line (disk) has been found to offer an important advantage for the coaxial line filter in that there is no dc path between the center conductor and the outer conductor.

The lumped-element approximation to a short section of low-Z_o or high-Z_o line is shown here to yield significant error in the design of band-pass filters having bandwidths $\leq$ 10 percent of the center frequency, and this error increases as the bandwidth is reduced. A more accurate immittance inverter realization technique is presented here, taking account of both the distributed line lengths and the reactive elements resulting from the discontinuity associated with the change in characteristic impedance. The accuracy of this technique has been ascertained through numerical analysis and experimental evaluation of filters having bandwidths as low as 1 percent.

2.3.1 Coaxial Impedance Inverter Design. A band-pass filter using impedance inverters requires that the parameter K, which determines the value of each impedance inverter, be specified. A network designed to realize such an impedance inverter must have an image impedance Z_I equal to K and an image phase θ which is some multiple of $\pm \pi/2$ (Ref. 20).

Consider the coaxial impedance inverter shown in Fig. 2.13(a), consisting of a short length ℓ of line of low characteristic impedance Z_o, together with two lengths $\phi/2$ of line with characteristic impedance, Z_c. The image parameters may be determined using the half-section shown in Fig. 2.13(b).

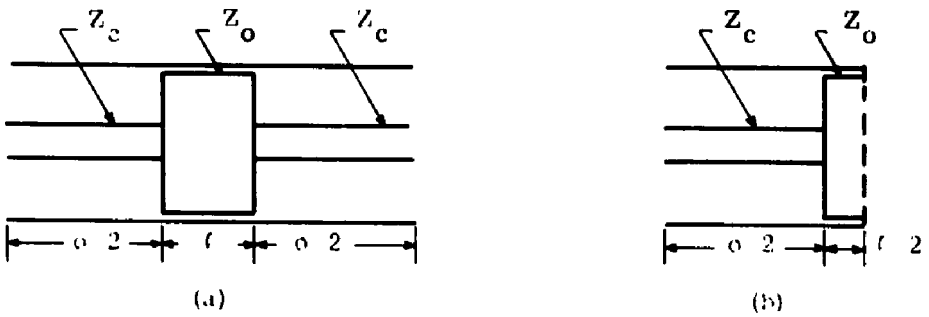


Fig. 2.13 (a) Disk impedance inverter, and (b) bisected impedance inverter

The general transmission circuit matrix (i.e., $\bar{A}\bar{B}\bar{C}\bar{D}$ matrix) may be written for a lossless line of length ℓ, characteristic impedance Z_o, and wave number β, in the form:

$$\begin{bmatrix} \cos \beta\ell & j Z_o \sin \beta\ell \\ \frac{j}{Z_o} \sin \beta\ell & \cos \beta\ell \end{bmatrix} \tag{2.20}$$

The transmission circuit matrix for the half-section of Fig. 2.13b is readily found to be

$$\begin{bmatrix} \bar{A} & \bar{B} \\ \bar{C} & \bar{D} \end{bmatrix} = \begin{bmatrix} \left(\cos \frac{\beta\ell}{2} \cos \frac{\phi}{2} - \frac{1}{z_o} \sin \frac{\beta\ell}{2} \sin \frac{\phi}{2}\right) & j Z_o \left(\cos \frac{\phi}{2} \sin \frac{\beta\ell}{2} + \frac{1}{z_o} \cos \frac{\beta\ell}{2} \sin \frac{\phi}{2}\right) \\ j Y_c \left(\sin \frac{\phi}{2} \cos \frac{\beta\ell}{2} + \frac{1}{z_o} \cos \frac{\phi}{2} \sin \frac{\beta\ell}{2}\right) & \left(\cos \frac{\beta\ell}{2} \cos \frac{\phi}{2} - z_o \sin \frac{\beta\ell}{2} \sin \frac{\phi}{2}\right) \end{bmatrix} \tag{2.21}$$

where $z_o = Z_o / Z_c$ and $Y_c = 1/Z_c$. The image parameters Z_I and θ are given by (Ref. 16, p. 53)

$$Z_I = \left(\frac{\bar{A}\bar{B}}{\bar{C}\bar{D}}\right)^{\frac{1}{2}} \tag{2.22}$$

and

$$j \tan \frac{\theta}{2} = \left(\frac{\bar{B}\bar{C}}{\bar{A}\bar{D}}\right)^{\frac{1}{2}} \tag{2.23}$$

where $\frac{\theta}{2}$ is used because the inverter has been bisected. The conditions stated in (2.22) and (2.23) will be used to solve for the unknowns ℓ and ϕ when K and θ are known. From (2.21),

$$\frac{\bar{A}}{\bar{C}} = \frac{z_o \cot \frac{\beta\ell}{2} - \tan \frac{\phi}{2}}{j Y_c(z_o \cot \frac{\beta\ell}{2} \tan \frac{\phi}{2} + 1)}$$

$$= - j Z_c \tan \left[- \frac{\phi}{2} + \text{Arctan} (z_o \cot \frac{\beta\ell}{2}) \right]$$

and

$$\frac{\bar{B}}{\bar{D}} = \frac{j Z_c(z_o \tan \frac{\beta\ell}{2} + \tan \frac{\phi}{2})}{1 - z_o \tan \frac{\beta\ell}{2} \tan \frac{\phi}{2}}$$

$$= j Z_c \tan \left[\frac{\phi}{2} + \text{Arctan}(z_o \tan \frac{\beta\ell}{2}) \right]$$

so the image impedance is given by:

$$z_I^2 = \tan \left[\frac{\phi}{2} + \text{Arctan}(z_o \tan \frac{\beta\ell}{2}) \right] \tan \left[- \frac{\phi}{2} + \text{Arctan}(z_o \cot \frac{\beta\ell}{2}) \right] \tag{2.24}$$

where $z_I = Z_I / Z_c$.

Using the impedance inverter requirement that $\theta = \pi/2$, together with the circuit reciprocity requirement, $\bar{A}\bar{D} - \bar{B}\bar{C} = 1$, (2.23) may be written as

$$2 \bar{A} \bar{D} = 1 \tag{2.25}$$

which yields upon substitution from (2.21),

$$2(\cos^2\frac{\beta\ell}{2}\cos^2\frac{\theta}{2} + \sin^2\frac{\beta\ell}{2}\sin^2\frac{\theta}{2}) - 2(z_o + \frac{1}{z_o})\sin\frac{\beta\ell}{2}\cos\frac{\beta\ell}{2}\sin\frac{\theta}{2}\cos\frac{\theta}{2} = 1 .$$

Using the double angle trigonometric identities, this can be reduced to

$$\tan\beta\ell\tan\theta = \frac{2z_o}{1 + z_o^2} \quad . \tag{2.26}$$

Equations(2.24) and (2.26) provide a set of equations in the unknown lengths ℓ and θ in terms of Z_I and Z_o. An expression for θ can be obtained from (2.26).

$$\theta = \text{Arctan}\left[\left(\frac{z_o}{1 + z_o^2}\right)\left(\cot\frac{\beta\ell}{2} - \tan\frac{\beta\ell}{2}\right)\right] \tag{2.27}$$

$$= \text{Arctan}(z_o\cot\frac{\beta\ell}{2}) - \text{Arctan}(z_o\tan\frac{\beta\ell}{2}) \tag{2.28}$$

Thus the image impedance can be written as:

$$z_I = \tan\left[\frac{\theta}{2} + \text{Arctan}(z_o\tan\frac{\beta\ell}{2})\right]$$

$$= \frac{\tan\frac{\theta}{2} + z_o\tan\frac{\beta\ell}{2}}{1 - z_o\tan\frac{\theta}{2}\tan\frac{\beta\ell}{2}} \tag{2.29}$$

which when solved for $\frac{\theta}{2}$ yields

$$\tan\frac{\theta}{2} = \frac{z_I - z_o\tan\frac{\beta\ell}{2}}{1 + z_o z_I\tan\frac{\beta\ell}{2}} \quad . \tag{2.30}$$

Elimination of $\tan\frac{\theta}{2}$ between (2.27) and (2.30) yields a quartic which can be written in the following factored form:

$$\left(\tan^2\frac{\beta\ell}{2} + \frac{1}{z_o^2}\right)\left(\tan^2\frac{\beta\ell}{2} - 2E'\tan\frac{\beta\ell}{2} + 1\right) = 0 \tag{2.31}$$

where

$$E' = \left(\frac{z_I}{1 - z_I^2}\right)\left(\frac{z_o}{1 - z_o^2}\right)^{-1} \qquad (2.32)$$

The solution to this equation gives the following real values for $\tan \frac{\beta\ell}{2}$:

$$\tan \frac{\beta\ell}{2} = E' \pm (E'^2 - 1)^{\frac{1}{2}}$$

which also may be written as

$$\tan \beta\ell = \mp (E'^2 - 1)^{-\frac{1}{2}} \qquad (2.33)$$

From this expression the value of $\tan \phi$ may readily be obtained using (2.26). Although two solutions are given in (2.33), the one with the lower sign has given better results. If the upper sign is used the impedance at the center frequency is correct but the pass-band ripple and the band edges are seriously distorted.

Comparison of the above results with that of Cohn (Ref. 20) shows that when $\beta\ell << 1$, (2.27) is equivalent to his expression for K. The equations derived here do not take account of the discontinuity capacitance associated with the abrupt change in center conductor diameter. Design modification to accommodate this effect is discussed in Section 2.5.

2.3.2 Coaxial Admittance Inverter Design. A suitable coaxial admittance inverter is of the form shown in Fig. 2.14, consisting of a short length ℓ of line of characteristic admittance Y_o together with two lengths $\frac{\phi}{2}$ of Y_c line.

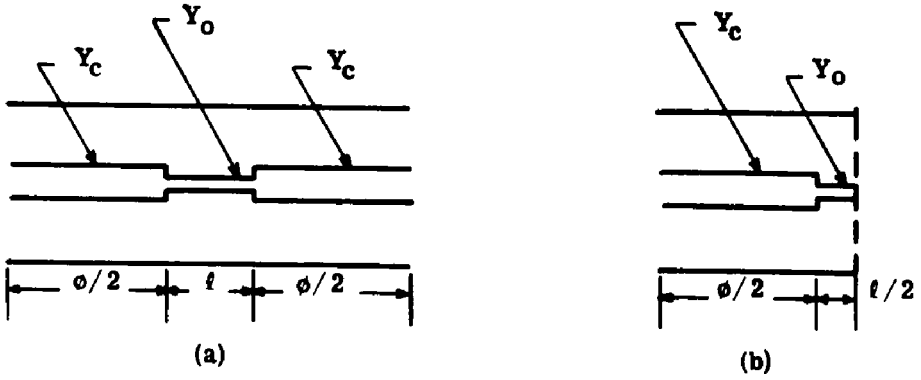


Fig. 2.14 (a) Coaxial admittance inverter, and (b) bisected admittance inverter

Derivation of expressions for ℓ and o in terms of the admittance inverter parameter Y_I follow the same procedure as used for the impedance inverter above. Imposing the inverter requirement $\theta = \frac{\pi}{2}$ there result two analogous equations for ℓ and o:

$$\tan o = \frac{2y_o}{1 + y_o^2} \cot \beta\ell \tag{2.34}$$

$$\tan \beta\ell = \mp (F'^2 - 1)^{-\frac{1}{2}} \tag{2.35}$$

where

$$F' = \left(\frac{y_I}{1 - y_I^2}\right)\left(\frac{y_o}{1 - y_o^2}\right)^{-1}$$

$$y_I = Y_I / Y_c$$

and

$$y_o = Y_o / Y_c \quad .$$

Other forms of the immittance inverter used by Cohn (Ref. 20) include a shunt inductance or a series capacitance together with a length of transmission line. These structures are not as readily analyzed on a distributed basis.

2.4 Theoretical Results of the Distributed Design Method

A new method for designing impedance inverters was derived in the previous section. In this section this method is compared with the lumped design method, and the distributed design is shown to be superior in (1) band-pass filters using K inverters, (2) band-pass filters using alternately K and J inverters, and (3) impedance transformers using K inverters. In the following theoretical curves, the effect of discontinuity capacitance has been neglected. However when a coaxial filter or impedance transformer is built, the design must be modified to account for the discontinuity capacitance as discussed below in Section 2.5.

2.4.1 Band-pass Filters Using K Inverters. Several curves were derived for various band-pass filters of the form shown in Fig. 2.15 centered at 8.5 GHz with

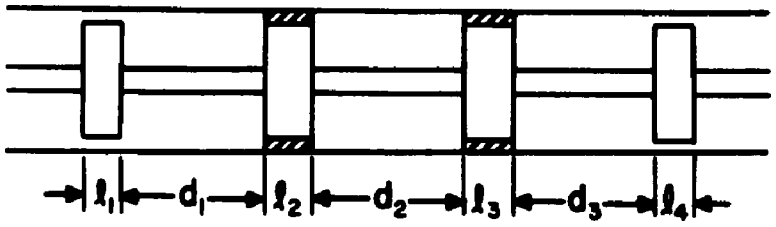


Fig. 2.15 A schematic diagram of a coaxial band-pass filter with Teflon dielectric around the center two disks

different fractional bandwidths, for the purpose of comparing the distributed design described in the previous section with the lumped design. The following filters were based on a Chebyshev low-pass prototype circuit with 0.1 dB ripple. The design was carried out using 50-ohm coaxial line with an outer conductor diameter of 0.5625 in. and a center conductor diameter of 0.24425 in. In the theoretical curves which follow, the effect of discontinuity capacitance has been neglected. For a three pole Chebyshev filter Fig. 2.16 shows that there is considerable improvement in using the distributed design. The distributed design filters are all centered at the design frequency although the bandwidth is narrower than the design bandwidth. The maximum ripple in the passband is smaller for the distributed case although it is still larger than the design ripple of 0.1 dB ($|\Gamma|^2 = 0.023$).

The design data for these curves are shown in Table 2.1. Since each band-pass filter is symmetrical, the first two disks are identical with the last two; consequently only the values for the first two are given.

Five percent and a 10 percent bandwidth 5-pole Chebyshev filters were designed using the distributed design technique. The resulting curves are shown in Fig. 2.17. The same improvements over the lumped design are evident for the five-ripple case. A comparison of the five-ripple case and the three-ripple case for the distributed design shows that the maximum ripple is higher for the five-ripple case.

The design parameters for the filters are shown in Table 2.2. Since the filters are symmetrical, the first three disks are identical to the last three.

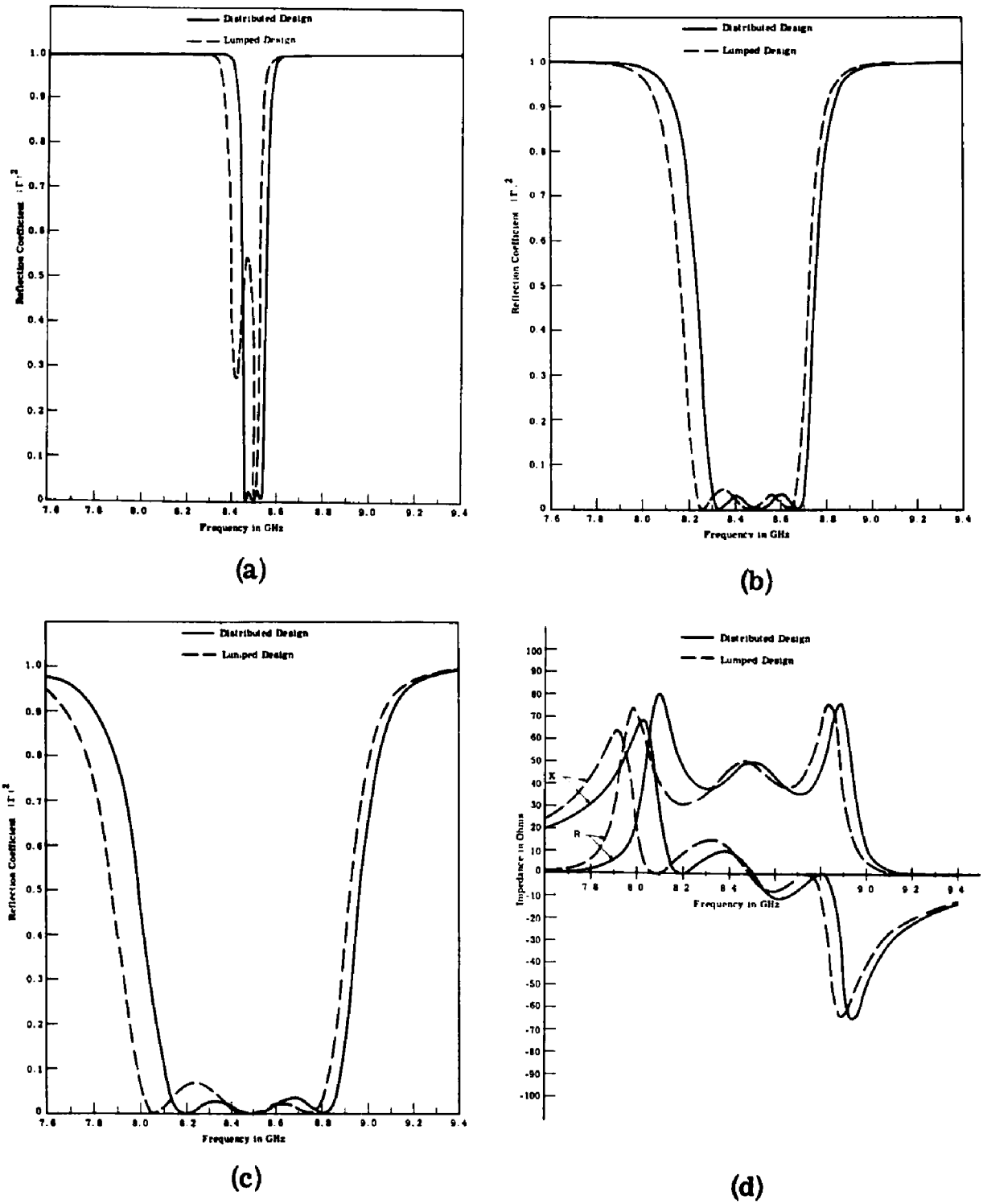


Fig. 2.16 Theoretical comparison between the lumped and distributed design for filters with bandwidth of (a) 1 percent, (b) 5 percent, and (c) 10 percent. The impedance of the 10 percent filter is shown in (d).

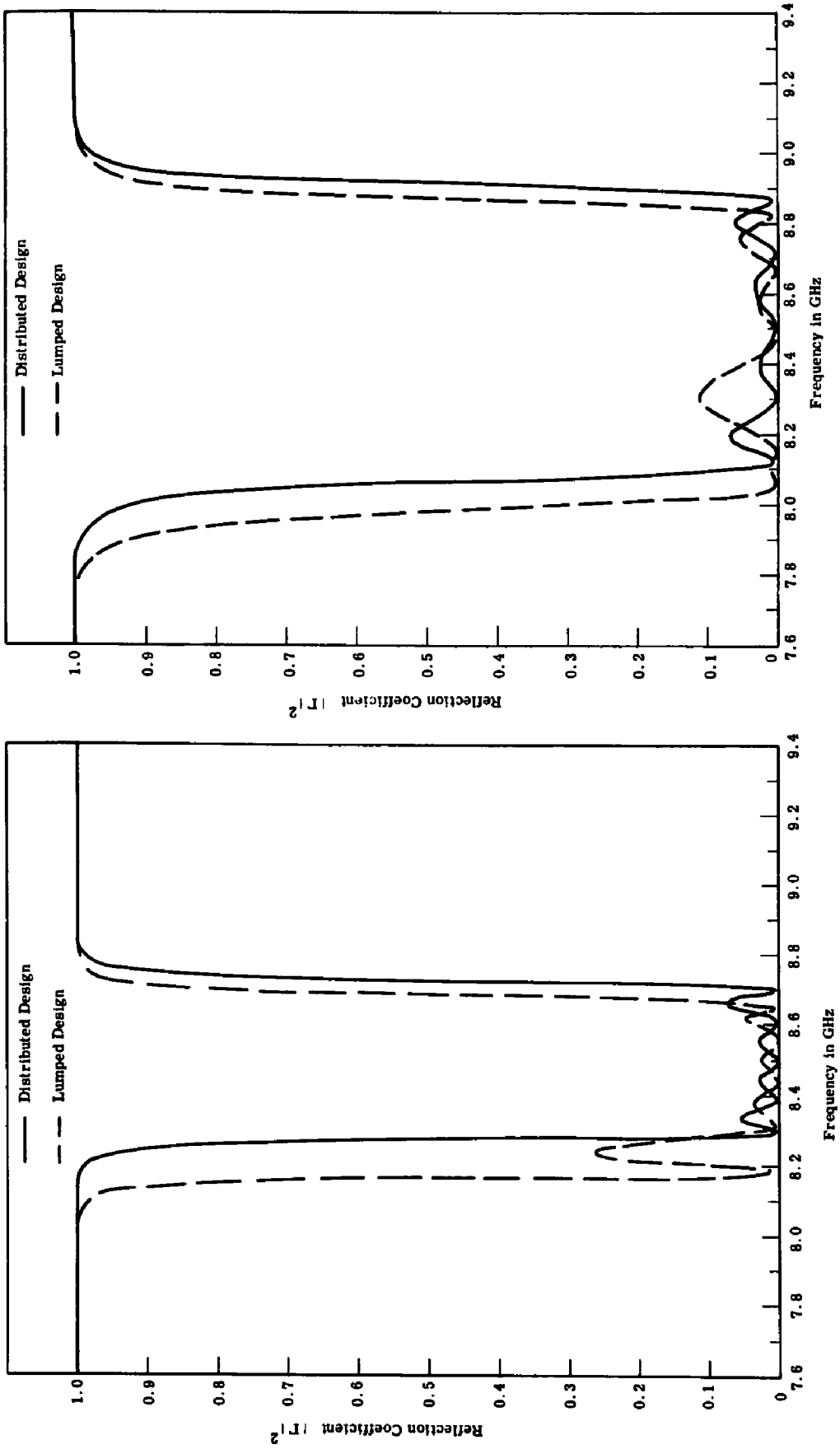


Fig. 2.17 Theoretical comparison between the lumped and distributed design for 5 pole filters with bandwidth of (a) 5 percent and (b) 10 percent

Lumped or Distributed	Bandwidth w	K_{01}	K_{12}	Disk Diameter D_1 in.	Disk Diameter D_2 in.	ℓ_1 cm	ℓ_2 cm	ϕ_1 rad.	ϕ_2 rad.
L	1%	6.1701	0.72194	0.502	0.554	0.3011	0.3496	0.24556	0.02888
D	1%	"	"	"	"	0.3471	0.4302	0.15534	0.01330
L	5%	13.7969	3.6097	0.502	0.532	0.1263	0.2547	0.53847	0.14414
D	5%	"	"	"	"	0.1298	0.2777	0.50663	0.10963
L	10%	19.5117	7.2193	0.502	0.502	0.0820	0.2559	0.74412	0.28679
D	10%	"	"	"	"	0.0833	0.2816	0.72378	0.21529

Table 2. 1. Disk parameters for three pole filters

Lumped or Distributed	Bandwidth w	K_{01}	K_{12}	K_{23}	D_1 in.	D_2 in.	D_3 in.
L	5%	13.0849	3.1316	2.3863	0.502	0.532	0.532
D	5%	"	"	"	"	"	"
L	10%	18.5049	6.2632	4.7726	0.502	0.502	0.532
D	10%	"	"	"	"	"	"

Lumped or Distributed	Bandwidth w	ℓ_1 cm	ℓ_2 cm	ℓ_3 cm	ϕ_1 radian	ϕ_2 radian	ϕ_3 radian
L	5%	0.1343	0.2940	0.3864	0.51192	0.12510	0.09538
D	5%	0.1384	0.3328	0.5462	0.47793	0.82929	0.01747
L	10%	0.0880	0.2965	0.1919	0.70893	0.24923	0.19033
D	10%	0.0896	0.3399	0.2009	0.68706	0.16114	0.16587

Table 2. 2 Disk parameters for five pole band-pass filters

Tables 2.1 and 2.2 show that the difference in disk lengths between the lumped and distributed case is not large. As would be expected, the difference in the phase angles o between the two cases is greatest when the disk length is large. The different disk diameters used in Tables 2.1 and 2.2 were the result of increasing the diameter to make $E' \rightarrow 1$ in (2.33).

The above filter design examples were all designed from tables which specified 0.1 dB ripple in the passband. Filters with other ripple factors as well as maximally flat filters may be designed by simply using the g values (Ref. 16, pp. 98-102) appropriate to these criteria. A 10 percent bandwidth Chebyshev filter with 0.5 dB ripple and a maximally flat filter were successfully designed. The design parameters are shown in Table 2.3, and the resulting characteristics are shown in Figs. 2.18 and 2.19.

	$g_1=g_3$	g_2	$K_{01}=K_{34}$	$K_{12}=K_{23}$	$\phi_1=\phi_4$ Radians	$\phi_2=\phi_3$ Radians	Disk Length cm	
							$\ell_1=\ell_4$	$\ell_2=\ell_3$
0.5 dB ripple	1.5963	1.0967	15.685	5.935	0.5510	0.1401	0.2308	0.3671
Maximally Flat	1.0000	2.0000	19.817	5.554	0.7134	0.1124	0.1685	0.4075

Table 2.3. Filter parameters for three pole Chebyshev and maximally flat filters where discontinuity capacitance has been neglected and all disk diameters are 0.502 in.

For a 10 percent bandwidth when the center frequency is 8.500 GHz the lower and upper band-edges should be 8.075 and 8.925 GHz respectively. For the Chebyshev filter, the band-edge is defined at the 0.5 dB level ($|\Gamma|^2 = 0.109$) where the lower and upper frequencies are 8.16 and 8.89 GHz respectively. For the maximally flat case, the band-edge is defined at the 3 dB point ($|\Gamma|^2 = 0.5$). Here the lower and upper band-edge frequencies are 8.15 and 8.89 GHz respectively. Thus in both cases the bandwidth of the resulting filter is approximately 8.5 percent which is slightly narrower than what was sought. As in the other examples the ripple for the Chebyshev filter exceeded the design ripple slightly. As would be expected the band-edges of the maximally flat filter were not as steep as those for the Chebyshev filter.

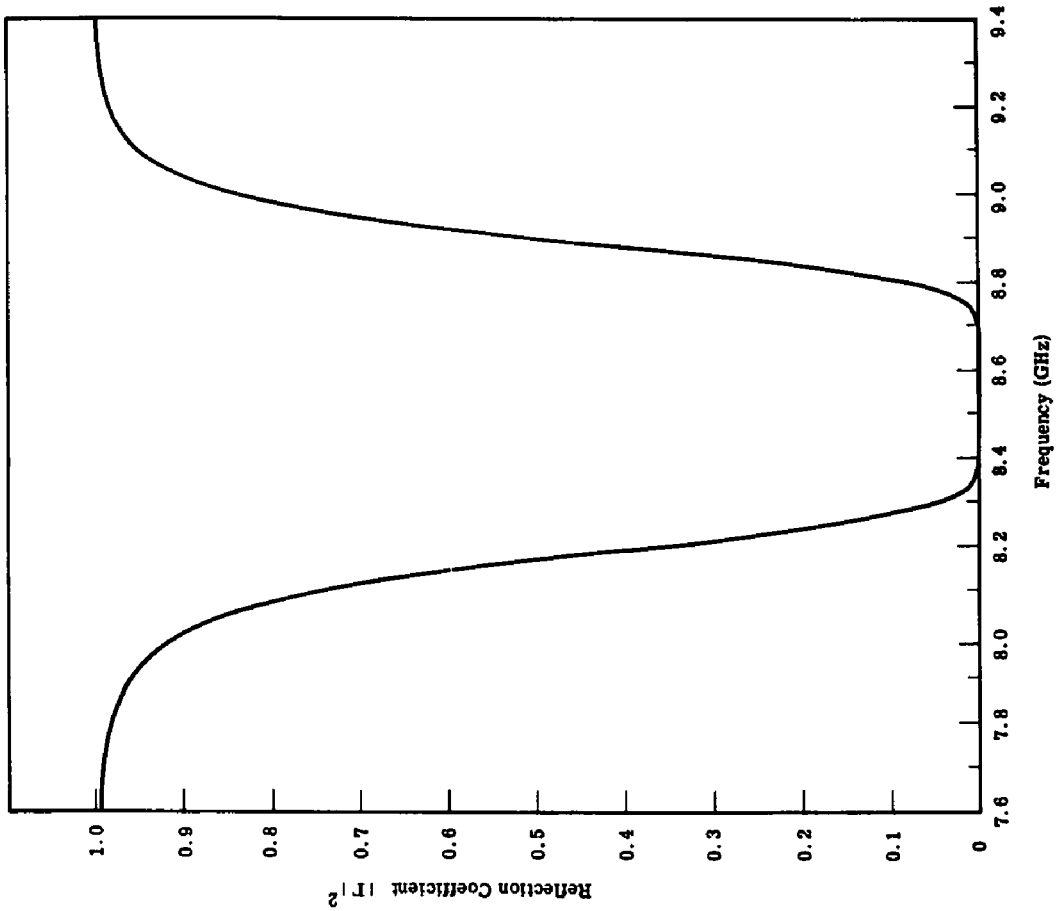


Fig. 2.18. 10 percent bandwidth band-pass filter with 0.5 dB ripple

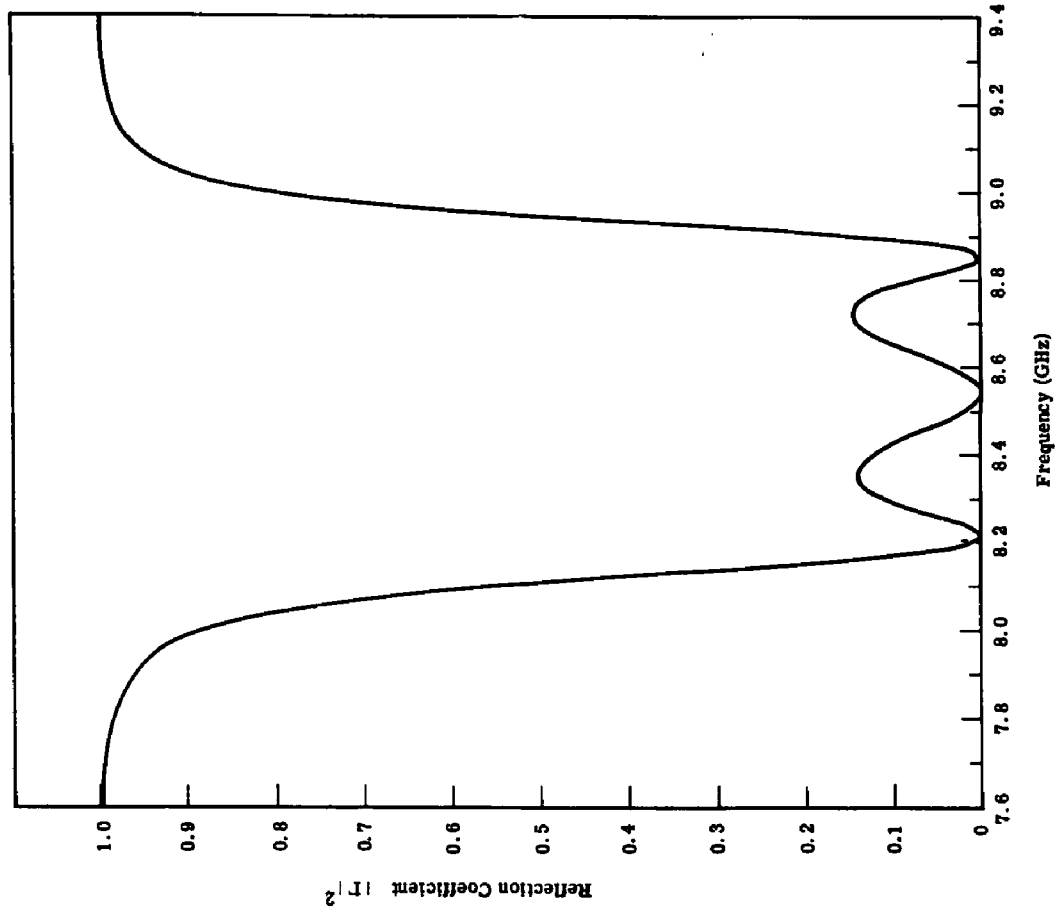


Fig. 2.19. 10 percent bandwidth, three pole, band-pass, maximally flat filter

The distributed design procedure applies to any type of filter where the g values are known although it may be limited by practical considerations such as disk size and discontinuity capacitance.

2.4.2 Filter Using K and J Inverters. The possibility of designing a band-pass filter with center frequency of 1 GHz was investigated. The primary problem is that the wavelength at this frequency (30cm) is inconveniently long. To make the filter more compact, a filter consisting of alternate K and J inverters shown in Fig. 2.20 was designed. Here the inverters are separated by a quarter-wavelength line rather than a half-wavelength line so the filter length is reduced by about one half.

The J inverter can be either a series inductance or a series capacitance. For a series inductance J inverter, however, the diameter of the inductive wire would be impractically thin. Therefore a semi-lumped capacitance was used for the J inverter.

Since the inverters are separated by a quarter-wavelength of line, the reactance slope parameter of the transmission line is half of that used previously. This means that filters can be built with approximately twice the fractional bandwidth. The lumped procedure and the distributed procedure were used to design filters with fractional bandwidths of 0.20 (Fig. 2.21a) and 0.40 (Fig. 2.21b). The design parameters for these four filters are shown in Table 2.4.

The filter characteristics again show that by using the distributed design procedure an improvement is obtained, although the difference becomes less significant at the broader bandwidths. The lower frequency end of the passband was disappointing, but this is probably due to the asymmetrical structure of the filter. This filter has a transfer impedance pole at dc in contrast with the filter with no series capacitances. The attenuation thus remains high from the lower end of the passband all the way down to dc.

2.4.3 Impedance Transformer. The distributed design approach was used to design an impedance transformer operating between 50 ohms and a complex load whose real part was 1 ohm. The load was resonated with an appropriate reactance so that the resonated Q was Q_A. The load was assumed to have a Q_A such that the decrement δ was the same for all design bandwidths.

Distributed or Lumped	w	K_{01}	J_{12}	K_{23}	J_{34}	ρ_1 rad	ρ_2 rad	ρ_3 rad	ρ_4 rad	ℓ_1 cm	C_2 pF	ℓ_3 cm	C_4 pF	$Diam_1$ in.	$Diam_3$ in.
D	0.2	19.512	0.002888	7.219	0.007805	0.72378	-0.28679	0.21529	-0.74412	0.7085	0.4694	2.3939	1.4653	0.502	0.502
L	0.2	19.512	0.002888	7.219	0.007805	0.74412	-0.28679	0.28679	-0.74412	0.6967	0.4694	2.1750	1.4653	0.502	0.502
D	0.4	27.594	0.005775	14.439	0.01104	0.99685	-0.56225	0.53214	-1.00856	0.4089	1 0028	1.0443	2.5260	0.502	0.502
L	0.4	27.594	0.005775	14.439	0.01104	1.00856	-0.56225	0.56225	-1.00856	0.4042	1 0028	1.0180	2.5260	0.502	0.502

Table 2.4 Band-pass filter using K and J inverters

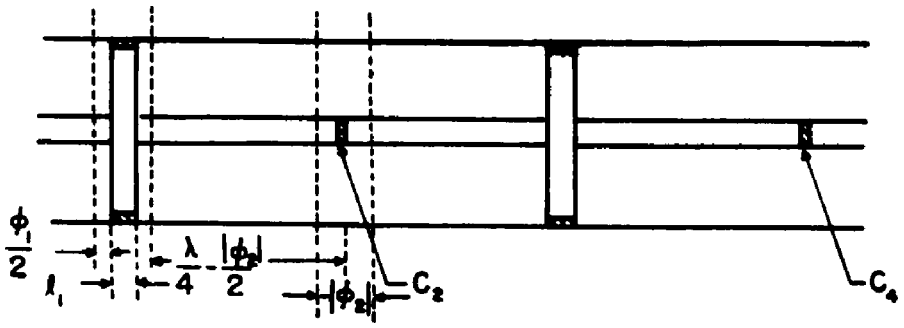


Fig. 2.20 Band-pass filter with alternate K and J inverters

$$\delta = \frac{1}{wQ_A} = \frac{1}{17.5} = 0.0571$$

In this case the complex load acts as the first series resonator; the first K inverter is K_{12}, which is given by

$$K_{12} = \frac{1}{\omega_c'} \sqrt{\frac{wR_A\chi_2}{g_1 g_2 \delta}},$$

The low-pass prototype g values can be obtained from a graph (Ref. 16, p. 128), and the values for K can be determined from the above expression and the formulas found in Fig. 2.8. For a n-pole low-pass prototype circuit, only n K inverters are needed for the matching network whereas (n + 1) K inverters are needed for a 50-ohm to 50-ohm filter.

The responses of the 50:1 impedance transformers are shown in Fig. 2.22 for various bandwidths and the impedance in Fig. 2.23 for the 10 percent transformer. Again the passband was centered around f_o for the distributed design case. The distributed design transformers generally had a flatter passband and a slightly narrower bandwidth than the design goal. Table 2.5 summarizes the design data for these curves.

2.5 Effect of Discontinuity Capacitance

Discontinuities associated with an abrupt change in characteristic impedance of a coaxial transmission line result in the excitation of higher-order modes in addition to

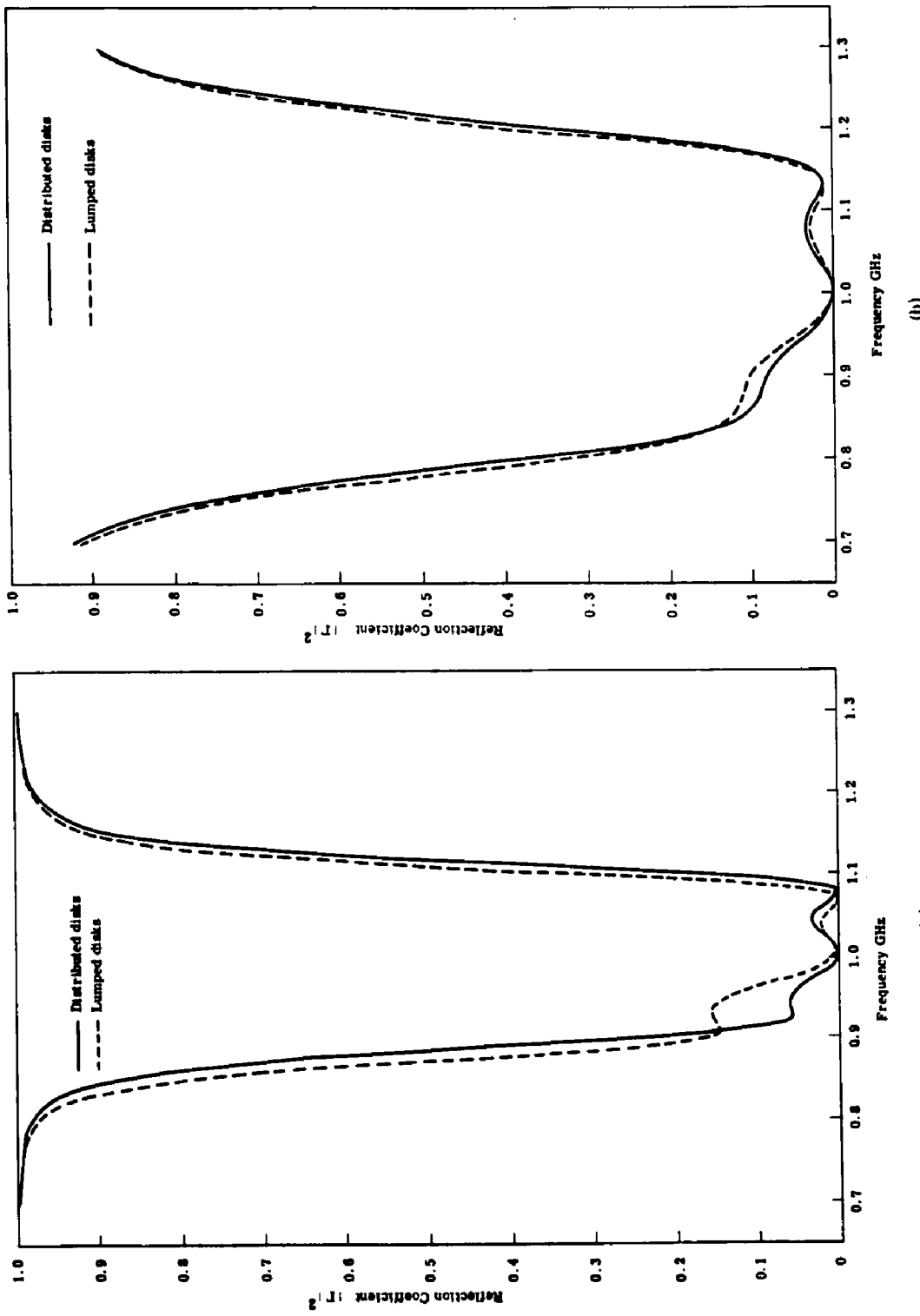


Fig. 2.21 Filters using alternate K and J inverters separated by quarter wavelength lines with bandwidth of (a) 20 percent, and (b) 40 percent

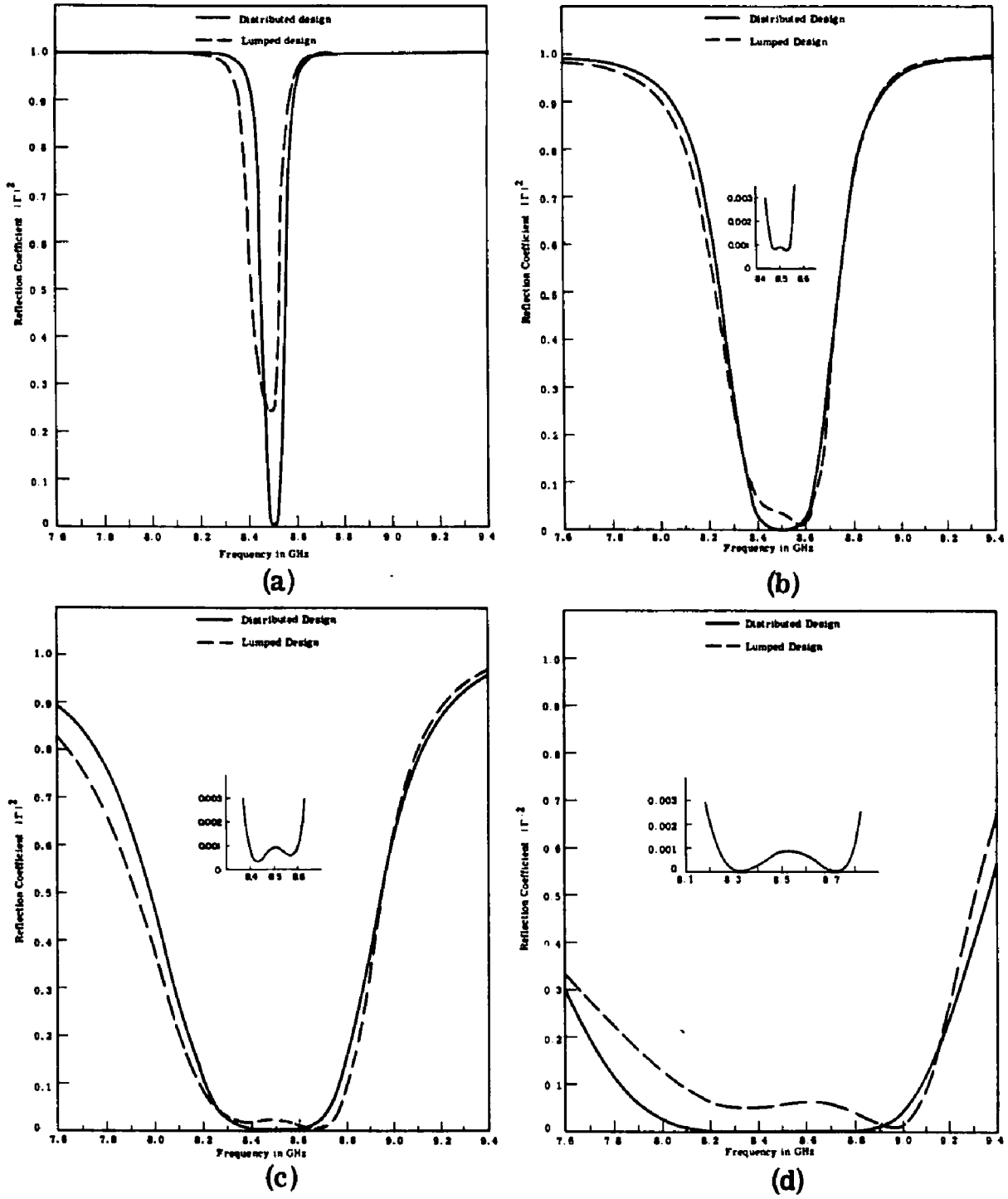


Fig. 2.22 Theoretical comparison between the lumped and distributed design for 50:1 impedance transformers with bandwidth of (a) 1 percent, (b) 5 percent, (c) 10 percent, and (d) 20 percent

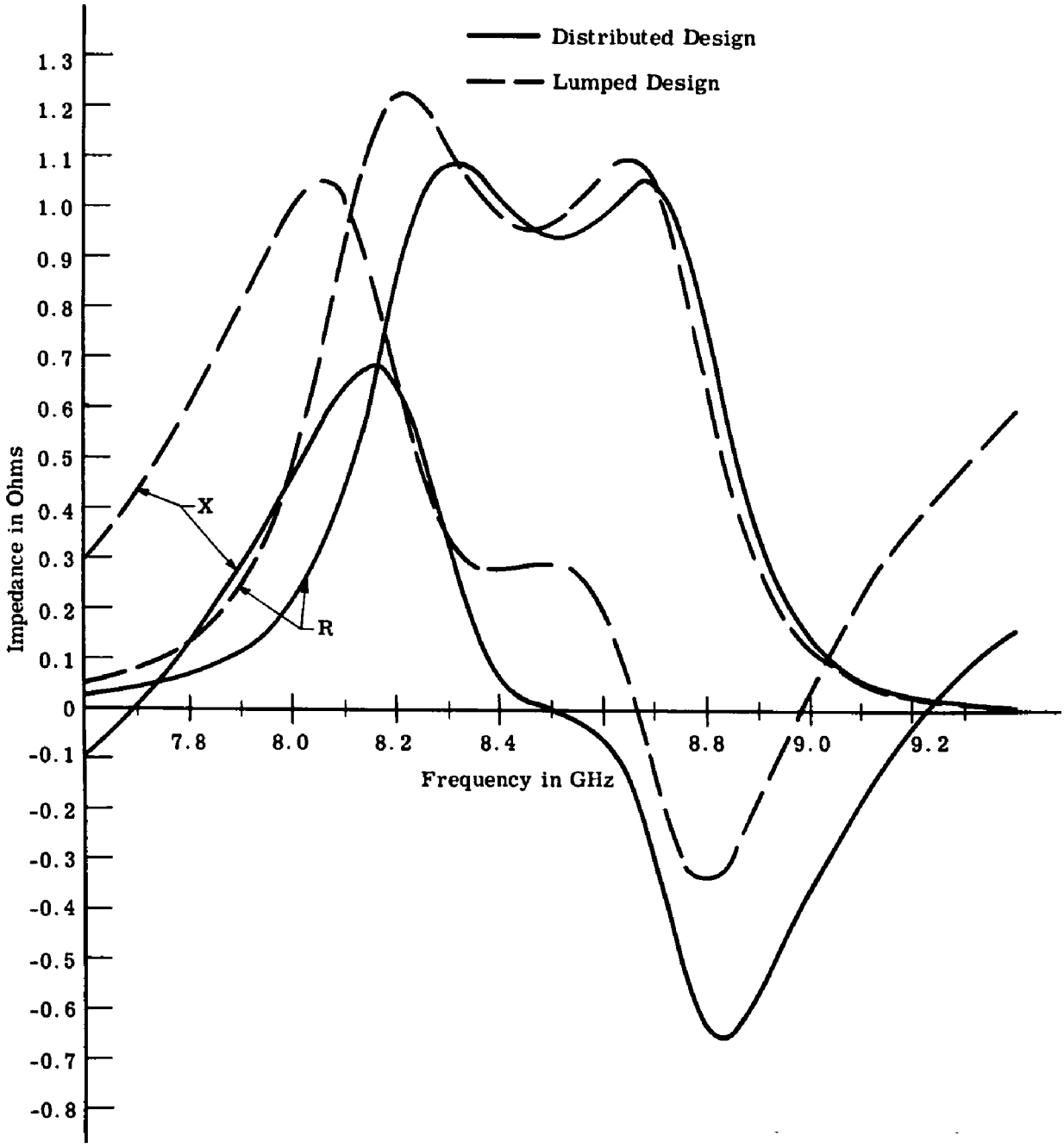


Fig. 2.23 Theoretical comparison of the impedance between the lumped and distributed design of the 10 percent bandwidth 50:1 impedance transformer

Lumped or Distributed	Bandwidth w				Disk Diameters								
		K_{12}	K_{23}	K_{34}	D_1 in.	D_2 in.	D_3 in.	ℓ_1 cm	ℓ_2 cm	ℓ_3 cm	ϕ_1 rad.	ϕ_2 rad.	ϕ_3 rad.
L	1%	0.7338	0.6973	6.5221	0.554	0.554	0.502	0.3439	0.3620	0.2843	0.02935	0.02789	0.25942
D	1%	"	"	"	"	"	"	0.4183	0.4591	0.3215	0.01431	0.01100	0.17667
L	5%	1.6409	3.4864	14.5839	0.542	0.532	0.502	0.3747	0.2638	0.1184	0.06561	0.13923	0.56761
D	5%	"	"	"	"	"	"	0.4963	0.2899	0.1214	0.02006	0.10307	0.53787
L	10%	2.3206	6.9727	20.6247	0.542	0.502	0.502	0.2647	0.2653	0.0759	0.0276	0.27712	0.78246
D	10%	"	"	"	"	"	"	0.2906	0.2944	0.0771	0.06861	0.20206	0.76366
L	20%	3.2818	13.9454	26.1678	0.532	0.502	0.502	0.2804	0.1248	0.0427	0.13108	0.54399	1.05618
D	20%	"	"	"	"	"	"	0.3129	0.1282	0.0432	0.09173	0.51256	1.04568

Table 2. 5 Disk parameters for band-pass impedance transformer using three disks

the TEM mode. These higher-order modes are generally evanescent and thus contribute energy storage elements to the equivalent circuit of the transmission line. The discontinuities considered here give rise to electric energy storage which is modeled by capacitive elements in shunt with the transmission line.

The low-frequency capacitance associated with a discontinuity remote from any other discontinuities may be determined by reference to the work of Whinnery et. al. (Refs. 22, 23) and Somlo (Ref. 24). The results of Somlo are particularly useful in filter design, since he has fitted an equation to the curves of discontinuity capacitance, C_d, as a function of line dimensions. For the case where the discontinuity occurs on the inner conductor, his expression gives

$$C_d = 2\bar{b}\epsilon_o \left[\frac{\bar{\alpha}^2 + 1}{\bar{\alpha}} \ln \frac{1 + \bar{\alpha}}{1 - \bar{\alpha}} - 2\ln \frac{4\bar{\alpha}}{1 - \bar{\alpha}^2} \right] \qquad (2.36)$$

$$+ 0.111\ (1 - \bar{\alpha})\ (\bar{\tau} - 1)\ 2\pi\bar{b}\ 10^{-12} \text{ Farads}$$

where

$\bar{b}$ = outer conductor radius, meters

$\bar{a}$ = inner conductor radius, meters

$\bar{r}$ = disk radius, meters

$\bar{\alpha} = (\bar{b} - \bar{r})/(\bar{b} - \bar{a})$

$\bar{\tau} = \bar{b}/\bar{a}$.

The maximum error resulting from use of this expression is stated to be $\pm$ 0.03 (2πb) pF in the ranges $0.01 \leq \bar{\alpha} \leq 1.0$ and $1.0 \leq \bar{\tau} \leq 6.0$.

The capacitance value obtained by use of (2.36) must be modified for the effects of frequency. At high frequencies the transverse dimensions of the coaxial line are of magnitude comparable to a wavelength, resulting in a transverse resonance effect. This series resonance in the shunt circuit may conveniently be accommodated by use of a frequency correction factor M' which modifies C_d. Although it is not possible to present a universally valid correction factor, sufficiently accurate values are obtainable by use of the curves of Somlo (Ref. 24). The discontinuity capacitance value C'_d to be used in the filter design is thus given by

$$C'_d = M' C_d .$$

The filter disk dimensions determined in Section 2.3 above must now be modified to take account of C'_d, such that there is equivalence between the circuits shown in Figs. 2.24(a) and 2.24(b). Three methods are in common use for determining this equivalence. The first two methods retain the value Z_o for the terminated line and use a modified line length ℓ'; the third method uses a modified value Z'_o in addition to changing the disk length ℓ to a different value ℓ'.

Method 1 is due to Cohn (Ref. 25). The transmission line is replaced by a π equivalent circuit of the form shown in Fig. 2.25. The impedance $Z'_o = Z_o$ while ℓ' is chosen such that

$$Y_o \tan \frac{\beta\ell}{2} = Y_o \tan \frac{\beta\ell'}{2} + \omega C'_d$$

or

$$\ell' = \frac{2}{\beta} \text{Arctan}(\tan \frac{\beta\ell}{2} - Z_o \omega C'_d). \qquad (2.38)$$

Method 2 is due to Matthaei (Ref. 26). It follows that of Cohn with the additional assumption that the tangent functions may be replaced by their arguments, since ℓ and ℓ' are small.

$$\ell' = \ell - 2Z_o C'_d \frac{\omega}{\beta} \qquad (2.39)$$

The principal inaccuracy with these two methods is that they take no account of the change in the value of X_b, which occurs when ℓ is altered; this deficiency is avoided in the third method.

Method 3 is due to Levy and Rozzi (Ref. 27). The transmission matrices of the two structures shown in Fig. 2.24 are equated, yielding two equations in the two unknowns Z'_o and ℓ'. A difficulty arises in the solution of these equations, since the C'_d in Fig. 2.24(b) has been computed for the original value Z_o, whereas the actual value of the discontinuity capacitance is determined by the revised disk size. Consequently recourse must be made to an iterative procedure to obtain an accurate solution. If ℓ_0,

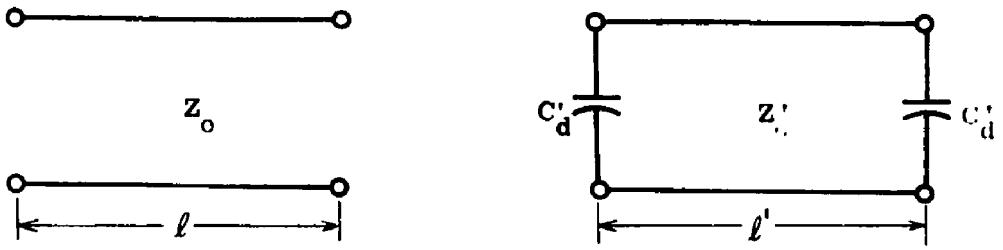


Fig. 2.24. (a) Length of transmission line representing disk, and (b) length of transmission line representing disk with discontinuity capacitance

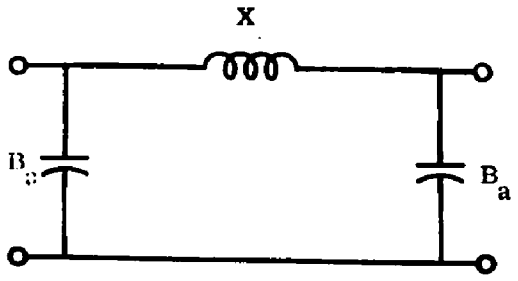


Fig. 2.25. π equivalent circuit for a transmission line where $X_b = Z_o \sin(\beta\ell)$ and $B_a = Y_o \tan(\beta\ell/2)$

Z_0, and $C_0 = C'_d$ are the length, characteristic impedance, and discontinuity capacitance for the original disk, then the new length and characteristic impedance are found by reapplication of Levy and Rozzi's formulas:

$$\cos(\beta\ell_{k+1}) = \cos(\beta\ell_k) + \omega(C_k - C_{k-1})\, Z_k \sin(\beta\ell_k) \tag{2.40}$$

$$Z_{k+1} = Z_k \frac{\sin(\beta\ell_k)}{\sin(\beta\ell_{k+1})} \tag{2.41}$$

where $k = 0, 1, 2, \ldots$ and $C_{-1} = 0$. Experience has shown that between three and eleven iterations are required to obtain a solution in which the discontinuity capacitance change between successive iterations is less than 1 percent.

One sees from methods 1 and 2 that ℓ must be sufficiently large and C'_d sufficiently small that $\ell' > 0$. A similar restriction holds for method 3 since the magnitude of the right hand side of (2.40) must be less than 1. This implies the discontinuity

susceptance must be smaller than the susceptance of the transmission line equivalent circuit:

$$B_a > \omega C'_d \quad . \tag{2.42}$$

Equation (2.42) imposes a more severe computational restriction than the limitations imposed by either methods 1 or 2. In practice, method 3 is not applicable for the broader bandwidth filters where the disk lengths can become rather short and the right side of (2.40) becomes larger than 1. For the 1 percent bandwidth filter the relative accuracy of these various methods of accommodating the discontinuity capacitance is illustrated in Fig. 2.26. On the basis of such comparisons the third method was selected for the narrow band filters; the less accurate methods 1 and 2 are used for the broader bandwidth filters.

2.6 Numerical Example and Experimental Results

The band-pass filter design consists of a series of impedance inverters each separated by a half wavelength line. A step by step design procedure for a filter is outlined here using the distributed design technique.

1.) A low-pass prototype filter with the desired characteristics is chosen. From this a value of $K = Z_I$ is found from Fig. 2.8 using a reactance slope parameter of $\frac{\pi Z_c}{2}$ for the half wavelength line.

2.) An arbitrary diameter is chosen for the disk. The larger the disk diameter, the shorter its length.

3.) The disk characteristic impedance Z_o is found.

4.) The value for E' is found from (2.32).

5.) A test is made to insure $E' > 1$. If $E' < 1$, the disk diameter is too small, and a larger diameter must be chosen.

6.) The disk length is found from (2.33).

7.) The length of line ϕ on either side of the disk is found from (2.30).

8.) The discontinuity capacitance is found from (2.36).

9.) Finally the disk dimensions are modified in accordance with one of the three methods of Section 2.5.

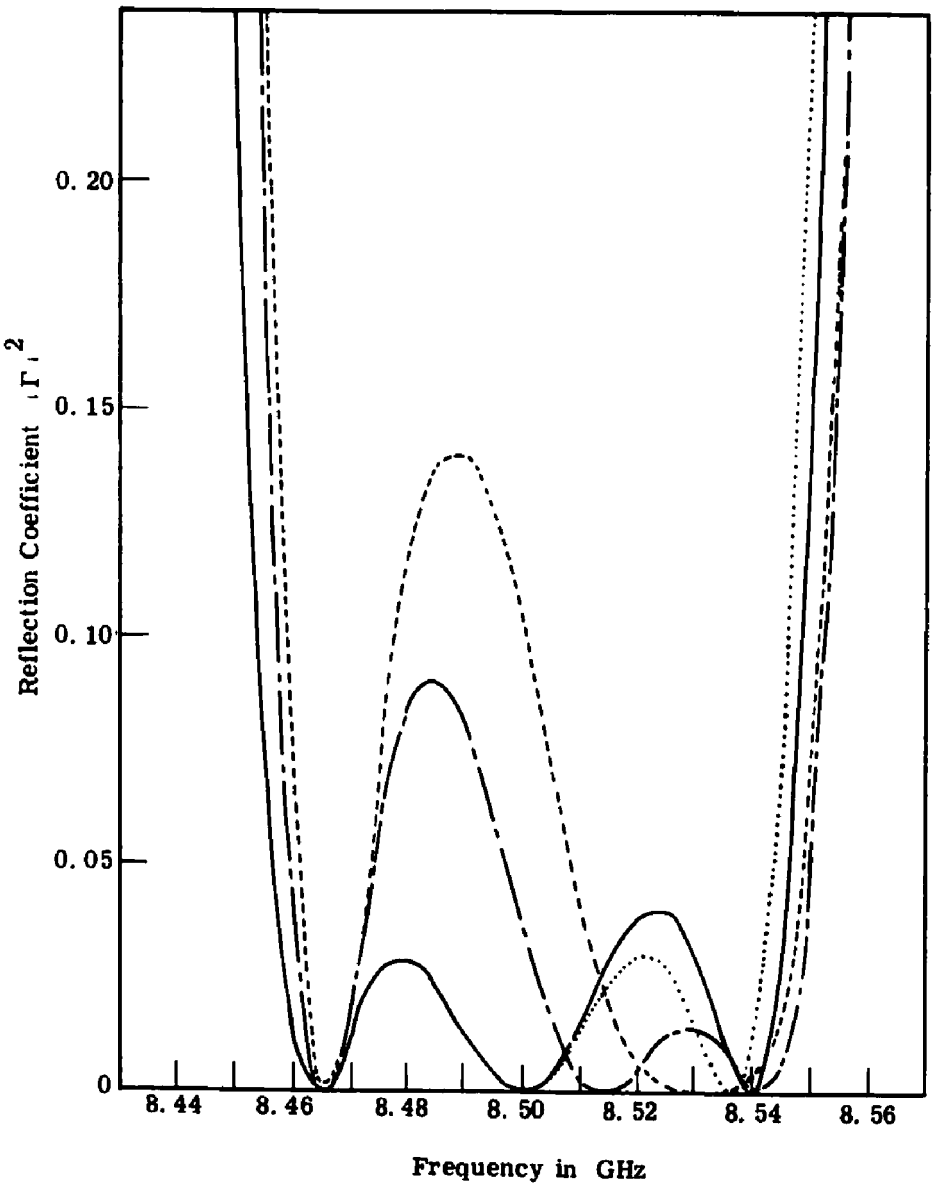


Fig. 2.26. A 1 percent bandwidth band-pass filter for the ideal case when there is no discontinuity capacitance (. . .), when the filter is compensated for discontinuity capacitance by method 1 (— -), method 2 (---), and method 3 (—). The ideal case and the compensation by method 3 merge at the left side

This algorithm was used in computer program A listed in Appendix A which designs and analyzes these filters.

As an example of the application of the design procedure, consider the design of a three pole Chebyshev filter with a center frequency of 8.50 GHz, fractional bandwidth w = 0.10, and pass-band ripple of 0.1 dB. The prototype elements, which may be found in various references (e.g. Ref. 16), for this case are $g_0 = 1.0000$, $g_1 = 1.0315$, $g_2 = 1.4740$, $g_3 = 1.0315$, and $g_4 = 1.0000$. The filter is to be constructed in

standard 14 mm 50-ohm coaxial line, and each disk will be surrounded by Teflon material with a relative dielectric constant of 2.03 (Ref. 28). Step 1 shows that $Z_I = 19.5117$ for the first impedance inverter. A disk diameter of 1.275 cm is assumed, giving a characteristic impedance of 9.68 ohms. Step 4 shows $E' = 2.28 > 1$ so the disk diameter is large enough. Since $\beta = \omega(2.03)^{\frac{1}{2}}/c$, (2.33) gives the disk length as 0.0833 cm. Step 7 indicates that the length of transmission line on each side of the disk is 0.3619 radians. Since the network is symmetrical, the first and second disks are identical to the fourth and third disks respectively.

The design must now be modified to accommodate the effect of discontinuity capacitance. This capacitance has a value of 0.3306 pF for one side of the first disk. Method 2 is sufficiently accurate for this case, so the new disk length is found from (2.39) to be 0.03698 cm, giving a 50 percent reduction in disk length. The modified lengths of the remaining three disks may be found similarly.

The above theory was experimentally verified with both 10 percent and 1 percent bandwidth filters. The preceding design procedure was used, with the exception that no Teflon material was used around the outer two disks, in order to make ℓ' longer. Fig. 2.15 shows a schematic and Table 2.6 gives the final design parameters for these two filters. Figs. 2.27 and 2.28 show the experimental data obtained from slotted line measurements compared with calculations which accounted for the discontinuity capacitance. Method 2 was used for the 10 percent filter and method 3 for the 1 percent filter. The minimum insertion loss for the 1 percent filter was 2.1 dB at center frequency. A photograph of the 1 percent filter is shown in Fig. 2.29. Using this design procedure, several filters have been built with good results in 7 mm coaxial line, having center frequencies in the 14 - 20 GHz range, with bandwidths around 5 percent.

Fractional Bandwidth w	$\phi_1=\phi_4$ radians	$\phi_2=\phi_3$ radians	$\ell_1=\ell_4$ cm	$\ell_2=\ell_3$ cm	Disk Diameters		$d_1=d_3$ cm	d_2 cm
					$D_1=D_4$ inches	$D_2=D_3$ inches		
0.10	0.7019	0.2153	0.03698	0.21501	0.502	0.502	2.0209	1.8843
0.01	0.2067	0.0133	0.21681	0.40795	0.532	0.554	1.8252	1.7710

Table 2.6 Experimental design parameters of the filter shown in Figs. 2.27 and 2.28

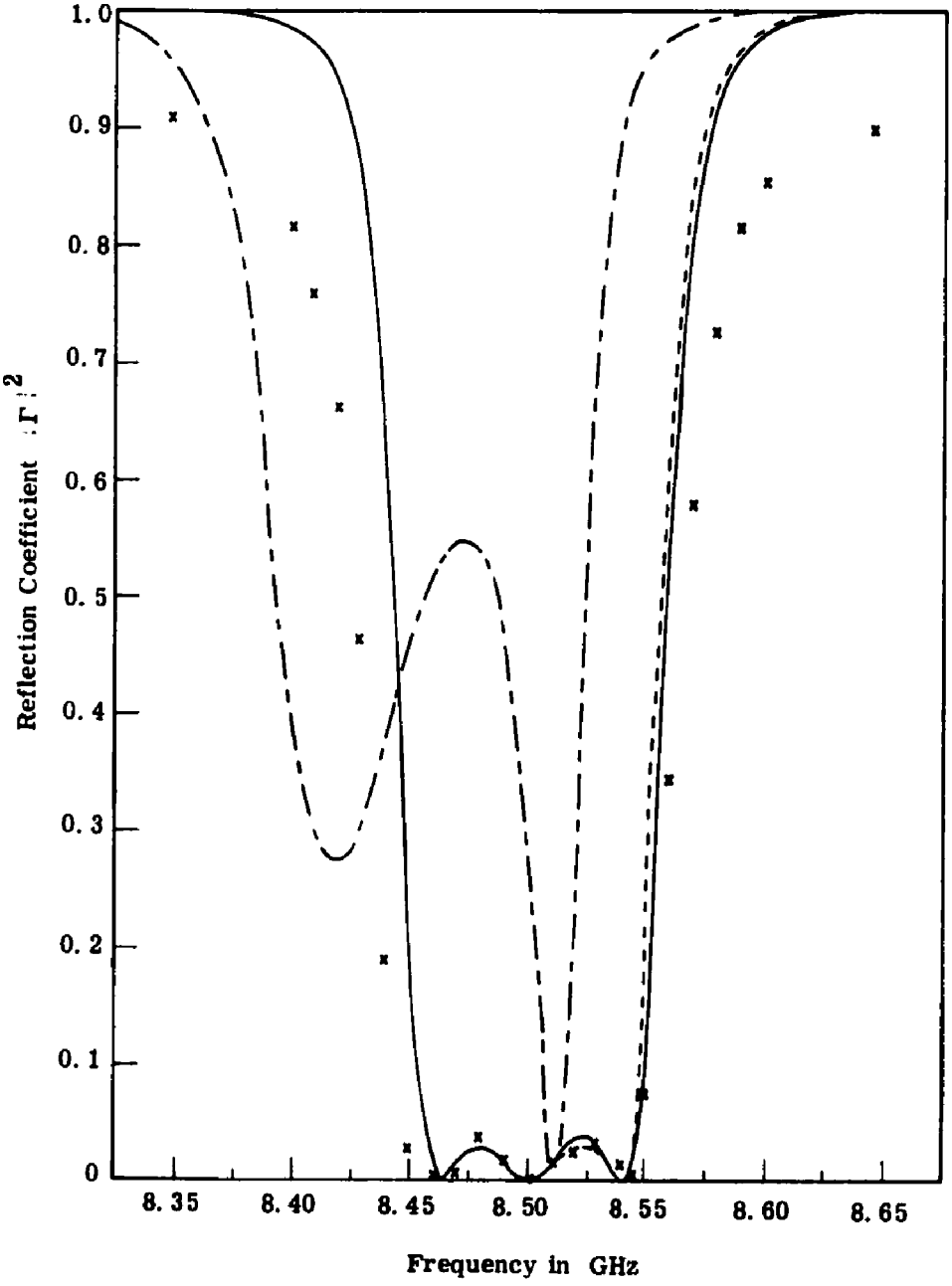


Fig. 2.27. A 1 percent bandwidth band-pass filter designed by the lumped method (— -), by the distributed method (---), by the distributed method with discontinuity capacitance accommodated by method 3 (——), and experimental results of the solid line filter (xxx). The ideal case when there is no discontinuity capacitance (---) and the case where method 3 is used (——) merge for the lower frequencies

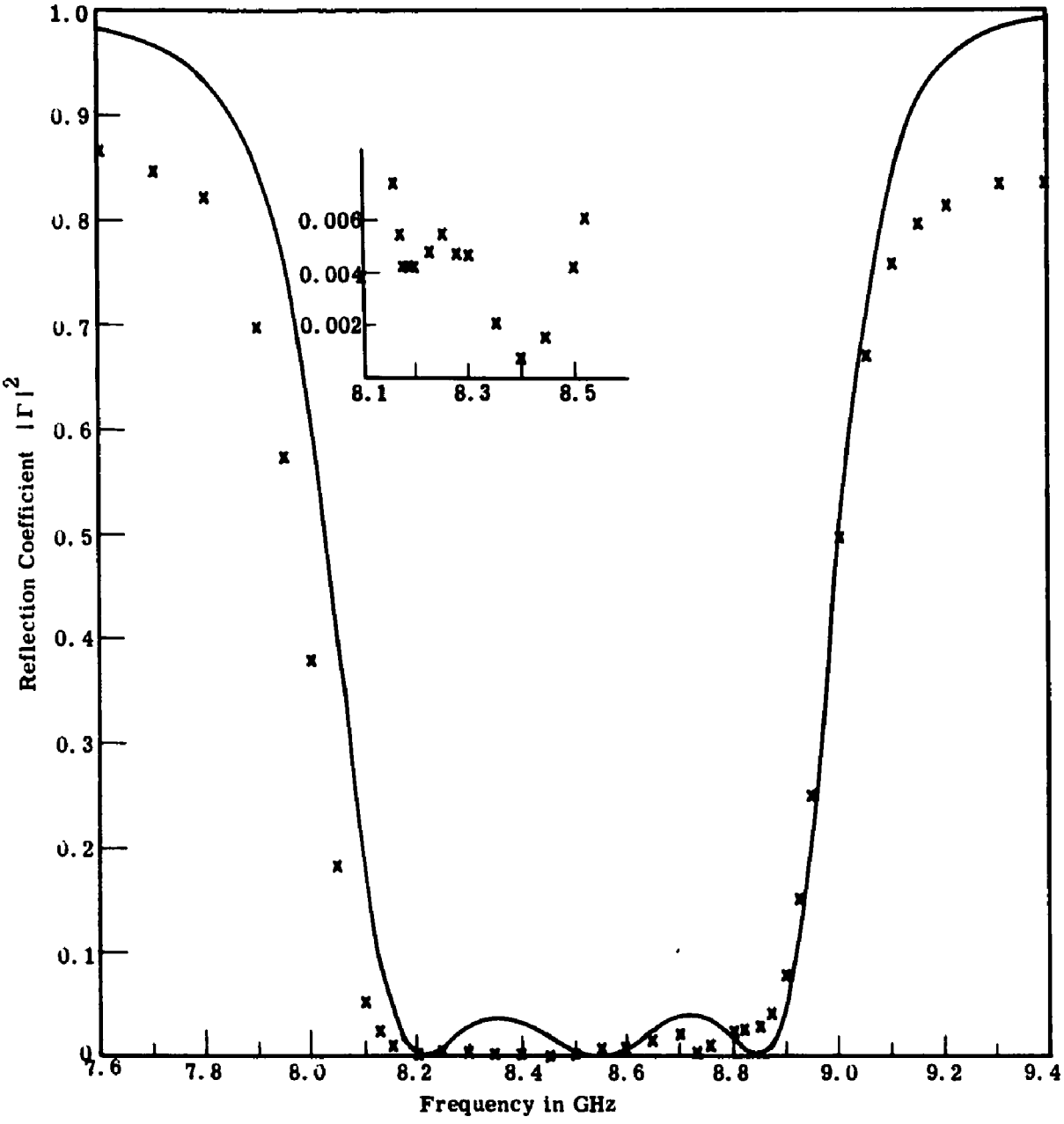


Fig. 2.28. A 10 percent band-pass filter designed by the distributed method where discontinuity capacitance is accommodated by method 2 with experimental results (×). The insert is a portion of the characteristic drawn on an expanded scale.

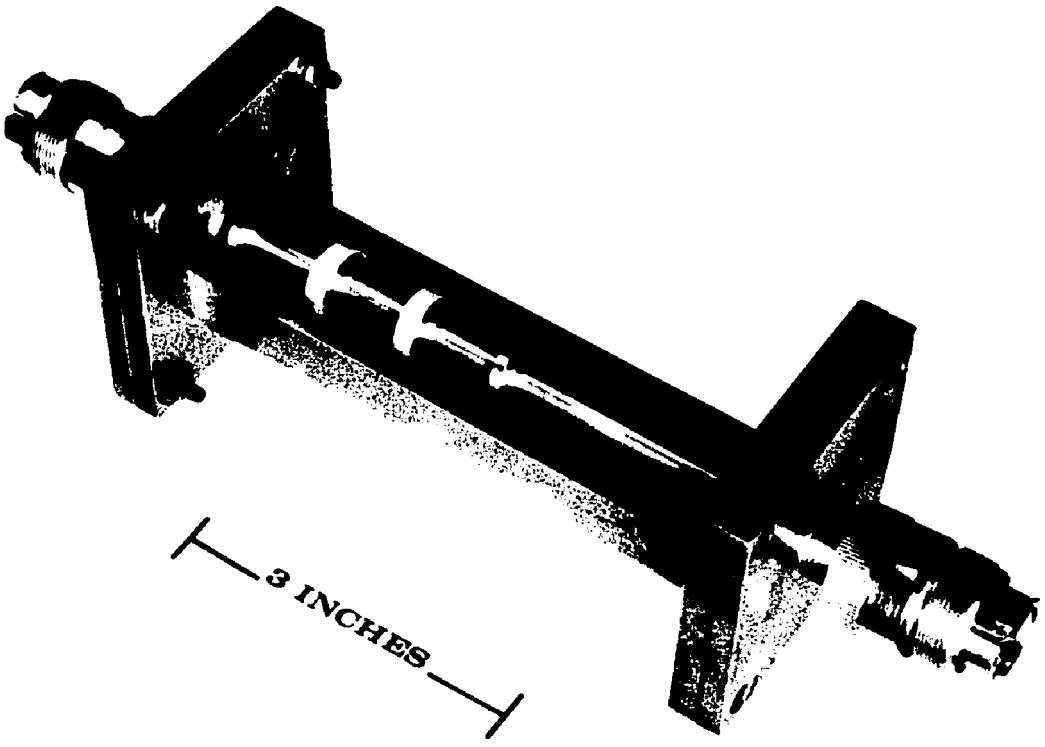


Fig 2.29. Photograph of the 1 percent bandwidth band-pass filter

2.7 Discussion

2.7.1 Filter Limitations Imposed by Choice of Bandwidth. The filter design is limited to a maximum of approximately 20 percent bandwidth, for beyond this value disks of reasonable diameter are of such small length ℓ that the modified disk length $\ell' < 0$. The filter is limited to a minimum bandwidth (somewhat less than 1 percent) by the requirement that $E' > 1$, i.e., the disk length must be shorter than a quarter wavelength. As the desired bandwidth decreases this inequality can be satisfied by increasing the disk diameter; consequently, the minimum bandwidth is restricted by the physical requirement that the difference between the disk diameter and outer conductor diameter not exceed the limits imposed by manufacturing tolerances.

The lumped design approach places no a priori limitation on disk diameters, while the distributed design approach requires $E' > 1$, setting a lower limit on the disk size. When filters designed by the lumped approach use diameters below this boundary, the resulting filters fail to give even reasonably acceptable characteristics. When the disk diameters are above this boundary the distributed design method continues to give superior filter characteristics as the graphs have shown.

2.7.2 Bandwidth Discrepancy. The computed bandwidth of the filter obtained from numerical calculation, does not agree exactly with the design bandwidth. The calculated bandwidth is approximately 1 percent for the 1 percent filter design, 4 percent for the 5 percent filter design, 8.5 percent for the 10 percent filter design, and 14.5 percent for the 20 percent filter design. Young (Ref. 16, pp. 564-566) listed two causes for bandwidth contraction with the direct coupled cavity filter designed using a quarter-wave transformer prototype. They are (1) electrical separation between reference planes shrinks as frequency increases and (2) the electrical lengths (his ψ' and ψ'') associated with the reactive discontinuity also shrink with increasing frequency.

A similar argument can be used here, with reference to the impedance inverters and their associated angles ϕ. Consider a shorted length of transmission line of reactance X_t, which is half-wave resonant at frequency ω_o, and a series LC circuit of reactance X_c, which is also resonant at ω_o. If the two circuits have equal values for the reactance slope parameter at resonance, the ratio X_t/X_c at a general frequency ω will be given by

$$\frac{X_t}{X_c} = \left(1 + \frac{d'}{2 + d'}\right)\left[1 + 1/3(\pi d')^2 + 2/15(\pi d')^4 \ldots\right] \qquad \text{for } |d'| < 1/2$$

where

$$d' = \frac{\omega - \omega_o}{\omega_o}$$

and a series expansion has been used for the tangent function. Thus $X_t > X_c$, and the ratio increases rapidly with increase in $|d'|$. Consequently the equivalence between the distributed-circuit filter and its lumped-element prototype might be expected to break down as the filter bandwidth is increased.

2.7.3 Low-frequency Characteristics. Since the filter structure discussed here is quite similar to the popular low-pass coaxial filter, it is expected that power transmission through the filter will occur at some lower frequency. Figures 2.30(a) and 2.30(b) show theoretical and experimental plots for the 1 percent and 10 percent bandwidth filters and Fig. 2.30(c) shows the low-frequency response for a 20 percent bandwidth filter. All of these filters were designed to have a passband at 8.5 GHz. The low-pass 3 dB point is 0.750 GHz for the 1 percent filter, 3.02 GHz for the 10 percent filter, and 3.95 GHz for the 20 percent filter. Furthermore, as the fractional bandwidth increases, the low-frequency passband increases and the low-frequency response looks more like a low-pass filter.

These low-frequency characteristics will be seen to be of major importance in the design of a LSUC. However actually controlling these characteristics seems to be limited to the choice of design bandwidth. If the fractional bandwidth of the filter is specified, the only degree of freedom left is the choice of disk diameter. If the disk diameters are made smaller, and hence the disks made longer, some change in the low-frequency response can be made as indicated in Fig. 2.30(d). Although the low-pass 3 dB point is at a lower frequency when the disk diameters are smaller, the choice of disk diameters does not seem to have sufficient influence to make it a design parameter for the low-frequency characteristic. Figures 2.30(a), 2.30(b), and 2.30(c) show that for a given passband ripple and a fixed number of impedance inverters, the bandwidth exerts the major influence on the low-frequency response.

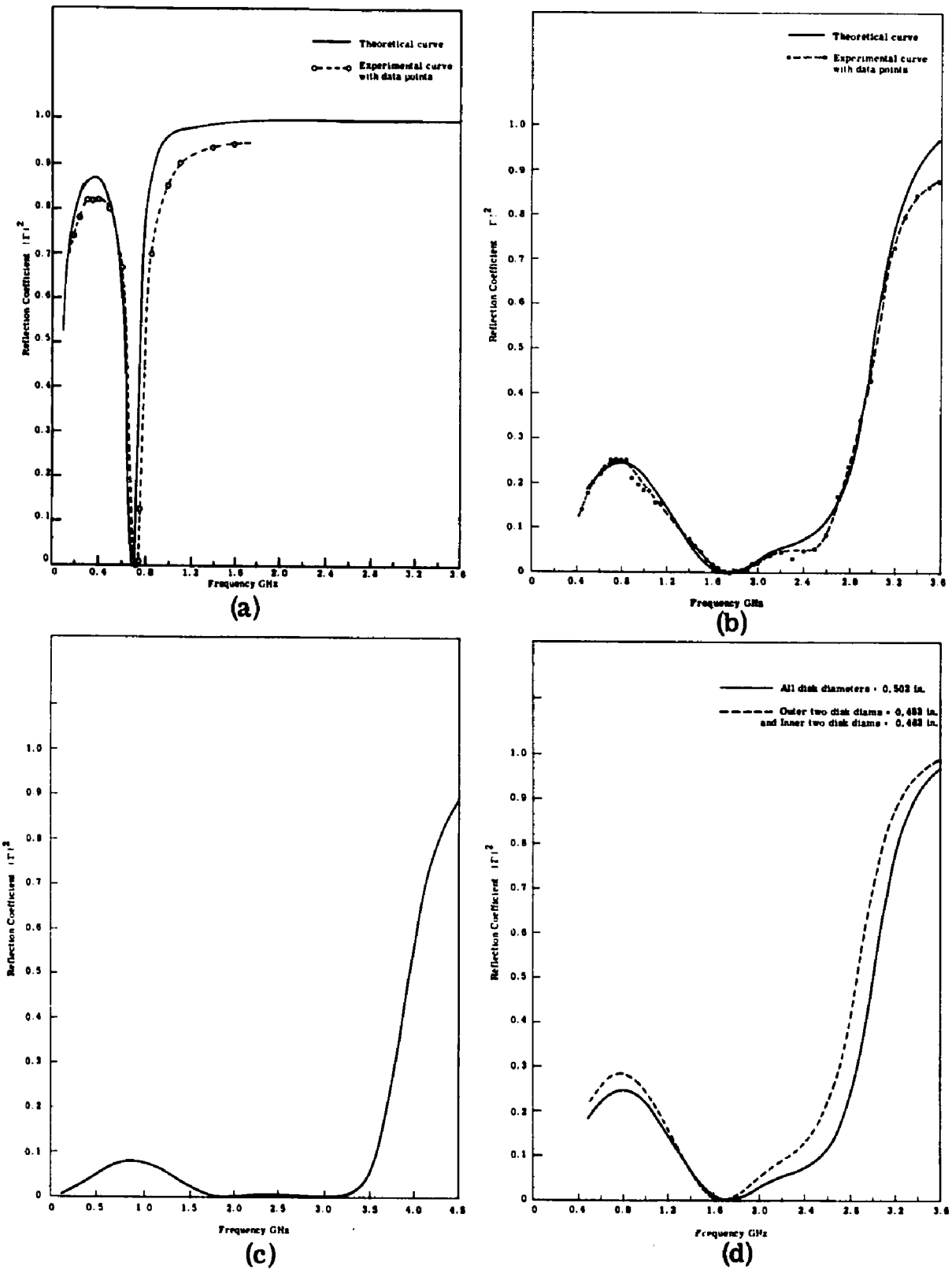


Fig. 2.30 Low-frequency response of band-pass filter with center frequency of 8.5 GHz for bandwidth of (a) 1 percent, (b) 10 percent, (c) 20 percent, and (d) 10 percent bandwidth with modified diameters

2.7.4 Effect of Filter Parameter Variations. Some knowledge of the mechanical tolerances is helpful in constructing a filter. When numerical calculations were made on a 10 percent bandwidth filter with all four disks shortened by 0.02 cm the center frequency increased approximately 50 MHz, the high frequency ripple decreased from $|\Gamma|^2 = 0.04$ to 0, and the low frequency ripple increased from $|\Gamma|^2 = 0.04$ to 0.05. Lengthening all 4 disks by 0.02 cm decreased the center frequency approximately 50 MHz, increased the high frequency ripple to $|\Gamma|^2 = 0.12$ and decreased slightly the low frequency ripple. In other words, lengthening and shortening the disk had the opposite effects. If the distances between disks are shortened 0.04 cm, the center frequency increases only 20 MHz, which is less than was expected. Increasing or decreasing the disk diameter has a similar effect on the filter characteristic as increasing or decreasing the disk length. Thus the filter is relatively insensitive to errors in the distance between disks but moderately sensitive to errors in disk size, especially for a narrow-band filter where the ratio of disk to outer conductor diameters is only slightly less than one.

The effect of using incorrect values for dielectric constant and discontinuity capacitance was studied. If the dielectric constant ϵ_r of the material surrounding the center two disks of the 1 percent bandwidth filter is reduced by 26 percent, from 2.03 to 1.50, the filter bandwidth increases to 1.26 percent. Also when the filter response was computed using values for discontinuity capacitance which were 10 percent to high, the center frequency of the original 1 percent bandwidth filter decreased approximately 2 MHz and the bandwidth increased by only 2.3 percent of its original value.

Narrow-band filters generally have higher pass-band losses than wider filters. A lossy-line analysis of the 1 percent bandwidth filter using standard tabulated values for the conductivity of brass and silver, and the loss tangent of Teflon, and a roughness factor of 1.8 indicated that bandwidth remained essentially unchanged. However the ripples near the band-edges started to deteriorate, as was confirmed experimentally.

2.8 Conclusions

A design procedure has been developed for band-pass coaxial filters, which is based on the readily available low-pass prototype circuit, and is applicable for bandwidths between approximately 1 percent and 20 percent. Numerical and experimental

results have shown that the filter characteristics are greatly improved when the impedance inverters are synthesized as short sections of transmission line rather than as lumped capacitances. The emphasis has been on band-pass filters with 50 ohm terminations, but the design theory may readily be applied to impedance transformers. These impedance transformers are used in the design of the lower sideband upconverter.

CHAPTER III

DESIGN THEORY FOR THE LOWER SIDEBAND UPCONVERTER

3.1 Introduction

The analyses of parametric devices found in most textbooks and journal articles are performed with very simple lumped circuits. However, most LSUC's operate at microwave frequencies and therefore are built using distributed circuits. The analysis in this chapter will consider various distributed element circuits, which could be used in designing a LSUC. Section 3.2 contains a review of the design and analysis relationships for LSUC's and includes a discussion of the cause for the nonresonant gain maximum seen in later calculations. A low reactance at the upper sideband frequency is shown in Section 3.3 to produce deleterious effects on the gain and noise figure. Section 3.4 includes a description of three LSUC circuit configurations. This is followed with numerical calculations of gain, gain bandwidth product, and noise figure for these three circuits when the diodes are tuned by constant impedances a specified distance from the diode, by single-stub tuners, and by double-stub tuners. The effects of diode parasitic elements and higher order sidebands are also explored. Finally in Section 3.5 the filter theory developed in Chapter II is used to design several LSUC circuits with coaxial impedance matching transformers.

3.2 Review of Existing LSUC Design Theory

As mentioned in Chapter I, the progress in parametric amplifier design has been hastened by the development in the late 1950's of high quality varactor diodes. A reverse biased varactor diode chip now can be accurately modeled as a voltage dependent depletion layer capacitance in series with a small resistance. The basic design theory described below uses this model. The addition of diode parasitic elements and external circuit impedances can be easily accommodated in the design theory and therefore does not detract from its usefulness.

The fundamental relationships between power and frequency for lossless nonlinear reactances were derived by Manley and Rowe (Ref. 6) in 1956 and have since been named after these two authors. They are given by

$$\sum_{m=0}^{\infty} \sum_{n=-\infty}^{\infty}{}' \frac{mP_{mn}}{m\omega_p + n\omega_s} = 0 \tag{3.1}$$

$$\sum_{m=-\infty}^{\infty} \sum_{n=0}^{\infty}{}' \frac{nP_{mn}}{m\omega_p + n\omega_s} = 0 \tag{3.2}$$

where P_{mn} is the power flow into the device at frequency $m\omega_p + n\omega_s$. In this formulation the frequencies ω_p and ω_s are either incommensurate or commensurate and incoherent (Ref. 29). These relations are useful in understanding the principles of such devices as frequency multipliers, reflection parametric amplifiers, frequency upconverters, and frequency down-converters. They also can be used to find the ultimate power gain and conversion efficiency of parametric devices. Although the Manley-Rowe relations illustrate the feasibility of frequency conversion in parametric (nonlinear reactive) devices, they do not contain detailed circuit design information.

3.2.1 Method of Harmonic Balance. Nonlinear circuits can be modeled by a series of nonlinear differential equations, which in general cannot be solved analytically. However, if a small signal assumption is made, they can be reduced to linear differential equations with time-varying coefficients. The circuit problem may then be solved either by direct solution of the differential equations or by use of the principle of harmonic balance. The latter approach has been the most successful in analysis of parametric circuits. In either case once the nonlinear differential equations are linearized, analysis of the ferroresonant effect as well as higher order instabilities occurring at certain harmonics and fractions of the pump frequency is no longer possible. However Oliver (Ref. 15) was able to explain these effects by exploring the original nonlinear equations.

For the small signal assumption, the pump voltage (or charge) is much larger than the incoming signal voltage (or charge) or any components at the generated sideband frequencies. Thus the varactor elastance variation is caused solely by the pump source,

and the small incoming signal sees a time-varying elastance oscillating at harmonics of the pump frequency.

The small signal (differential) elastance of a varactor diode can be written in terms of the total charge q_t stored in the diode junction and the total voltage v_t across the junction:

$$S(q_t) = \frac{dv_t}{dq_t} \quad . \tag{3.3}$$

The total applied voltage and charge is the sum of the pump $(v_p\ ,\ q_p)$ components, plus the signal and sideband components $(v_s'\ ,\ q_s')$

$$v_t = v_p + v_s'$$

$$q_t = q_p + q_s'$$

where $v_p >> v_s'$ and $q_p >> q_s'$. Expansion of v_t into a Taylor series yields an incremental voltage-charge relationship

$$v_s' = S(q_p)\, q_s' \tag{3.4}$$

where

$$S(q_p) = \sum_{m=-\infty}^{\infty} S_m\, e^{jm\omega_p t} \quad . \tag{3.5}$$

Applying the principle of harmonic balance (Ref. 30) to (3.4), two infinite, but equivalent, sets of equations are obtained. One of these sets is written in matrix form in (3.6).

$$\begin{bmatrix} V_1 \\ V_2^* \\ V_3 \\ V_4^* \\ \vdots \end{bmatrix} = \begin{bmatrix} Z_{11} & \frac{jS_1}{\omega_2} & \frac{-jS_{-1}}{\omega_3} & \frac{jS_2}{\omega_4} & \cdots \\ \frac{-jS_{-1}}{\omega_1} & Z_{22}^* & \frac{-jS_{-2}}{\omega_3} & \frac{jS_1}{\omega_4} & \cdots \\ \frac{-jS_1}{\omega_1} & \frac{jS_2}{\omega_2} & Z_{33} & \frac{jS_3}{\omega_4} & \cdots \\ \frac{-jS_{-2}}{\omega_1} & \frac{jS_{-1}}{\omega_2} & \frac{-jS_{-3}}{\omega_3} & Z_{44}^* & \cdots \\ & \vdots & \vdots & \vdots & \end{bmatrix} \begin{bmatrix} i_1 \\ i_2^* \\ i_3 \\ i_4^* \\ \vdots \end{bmatrix} \tag{3.6}$$

The notation used in (3.6) is defined as follows:

$$\omega_k = \left[\frac{k}{2}\right]\omega_p + (-1)^{k+1}\omega_s \tag{3.7}$$

where $k = 1, 2, 3, \ldots, [x]$ is the symbol for the greatest integer less than x, ω_p is the radian pump frequency, ω_s is the radian signal frequency. V_k, I_k and Z_{kk} are the voltages, currents, and impedances at ω_k respectively, and $Z_{kk} = \frac{-jS_0}{\omega_k}$ + diode parasitic elements + circuit impedance. The time origin is ordinarily chosen so that $S_1 = S_{-1}$. This matrix can be written more concisely as

$$\begin{bmatrix} V_1 \\ V_2^* \\ V_3 \\ V_4^* \\ \vdots \end{bmatrix} = \begin{bmatrix} Z_{11} & -jX_{12} & jX_{13} & -jX_{14} & \cdots \\ jX_{21} & Z_{22}^* & jX_{23} & -jX_{24} & \cdots \\ jX_{31} & -jX_{32} & Z_{33} & -jX_{34} & \cdots \\ jX_{41} & -jX_{42} & jX_{43} & Z_{44}^* & \cdots \\ \vdots & \vdots & \vdots & \vdots & \end{bmatrix} \begin{bmatrix} i_1 \\ i_2^* \\ i_3 \\ i_4^* \\ \vdots \end{bmatrix} \tag{3.8}$$

where

$$X_{mn} = \frac{-S_j}{\omega_n}$$

and

$$j = (-1)^n \frac{2n-1}{4} - (-1)^m \frac{2m-1}{4} \quad .$$

Two additional assumptions are often invoked to simplify (3.6): (1) S_1 is assumed to be the only significant pumped elastance component, and (2) the open circuit assumptions are employed at the higher sideband frequencies. Most of the non-diagonal terms in (3.6) can be set to zero by means of the first assumption. Removal of this assumption is discussed in the following section. The open circuit assumption is equivalent to saying that all currents above a given frequency are open-circuited by the external circuit. The simplest analysis of a LSUC would assume all currents at

frequencies $> \omega_2$ are zero. This leaves two currents but an infinite number of voltages. However since no power is propagated at these higher frequencies, these voltages may be safely ignored and (3.6) is reduced to a 2×2 matrix. In the numerical analysis presented in Sections 3.4 and 3.5 the first assumption is removed and the second relaxed.

The same analysis can be performed to obtain an admittance matrix rather than the impedance matrix of (3.6). The number of equations is reduced by using a short circuit assumption, i.e., voltages above a specified frequency are short-circuited by the external circuit. In general the open-circuit assumption is considered superior since the package lead inductance presents a high reactance to the diode chip at high frequencies, although if the lead inductance is resonated this argument fails.

3.2.2 Elastance Coefficients. The theory developed thus far for the LSUC can be applied only if the nonlinear characteristic of the varactor diode is precisely known. For a diode heavily doped on one side, and having a doping distribution of

$$N(x) = ax^b \tag{3.9}$$

on the other side, the nonlinear depletion layer elastance is

$$S = S_b(1-V/\phi_v)^\gamma \tag{3.10}$$

where $\gamma = 1/(b+2)$, ϕ_v is the built-in potential, V is the applied voltage ($V>0$ for forward bias), and S_b is the zero bias elastance.

One method of finding the harmonic elastance components is to expand (3.10) in a Fourier series by assuming a sinusoidal voltage source and allowing harmonic currents to flow (short-circuit assumption). Alternately the expansion can be made by assuming a sinusoidal charge source and allowing harmonic voltages to exist (open-circuit assumption). These two cases have been studied by Oliver (Ref. 15, Appendix B). Leeson (Ref. 31) noticed this expansion could be expressed as a solution of the Laplace integral where the answer was found in terms of gamma functions and the associated Legendre function of nonintegral degree. However, a more accurate method has been found which is not subject to either of these assumptions. Oliver (Ref. 15) has solved

the nonlinear differential equation describing a varactor diode in a particular circuit to obtain a set of elastance components for (3. 5). In the numerical work which follows, Oliver's method is used to obtain the elastance components for a graded junction diode embedded in the particular circuit configuration under study.

3. 2. 3 Gain Relationship for the LSUC. The power gain of an amplifier can be expressed in at least five different ways, of which the transducer power gain has been found to be the most meaningful for negative resistance devices like the LSUC. In the following discussion the amplifier accepts a signal from a voltage source with internal impedance Z_g and the amplified output power is dissipated in a load Z_ℓ.

1. The power gain is defined as the ratio of power dissipated in the load to the power delivered to the input of the amplifier. This gain definition depends only on Z_ℓ, and since the properties of a LSUC depend strongly on Z_g and Z_ℓ, this definition is of limited use.

2. The available gain is the ratio of the amplifier output power to source available power. Since this gain depends only on Z_g and not on Z_ℓ, this definition suffers a similar drawback to that of the first.

3. The exchangeable gain of an amplifier is the ratio of output exchangeable power to input exchangeable power. The exchangeable power of a source with internal impedance Z and voltage V is

$$P = \frac{|V|^2}{4\mathrm{Re}(Z)} \qquad \mathrm{Re}(Z) \neq 0$$

which can be < 0 for negative resistance devices (Ref. 32). The exchangeable gain is an extension of available gain and suffers from the same limitation: it does not depend on Z_ℓ.

4. The insertion gain is the ratio of output power to the power dissipated in the load if the amplifier were not present. Exactly what replaces the amplifier in this definition is unspecified, and this becomes a major problem in frequency conversion devices such as the LSUC. Therefore this definition of gain is too vague to be useful here.

5. The transducer power gain is the ratio of the power delivered to the load to the source available power. This definition depends on both Z_g and Z_ℓ, an advantage the other definitions lack. Also in contrast to the exchangeable gain, the present definition gives positive gain.

When the transducer power gain is applied to frequency conversion devices it is given by

$$G_{mn} = \frac{\text{average power delivered to the load at } \omega_m}{\text{average available power from the source at } \omega_n}$$

If the source voltage V_n is conducted through a source resistance R_{gn} and the resulting output current i_m is absorbed by a load resistance $R_{\ell m}$, the transducer power gain is

$$G_{mn} = \frac{|i_m|^2 R_{\ell m}}{|V_n|^2/4R_{gn}}$$

$$G_{mn} = |Y_{mn}|^2 4R_{\ell m}R_{gn} \tag{3.11}$$

where Y_{mn} is the (m, n) element of the inverse of the impedance matrix (3.6).

Synthesis of LSUC's to obtain a specified gain presently is limited to using only the signal and lower sideband frequencies. The open-circuit assumption is used for all frequencies $> \omega_2$, so the infinite impedance matrix (3.6) is reduced to a 2×2 matrix. Since there is only one voltage source V_1, the matrix may be reduced to a lower triangular form even when more than two frequencies are considered. Thus a complete matrix inversion is unnecessary to find Y_{mn}. After some striaght forward algebra the gain for the LSUC is

$$G_{21} = \frac{4Q_{11}^2 R_{g1} R_{\ell 2} R_s^2}{|Z_{11}Z_{22}^* - Q_{11}Q_{21}R_s^2|^2} \tag{3.12}$$

where $Q_{ij} = \frac{S_j}{\omega_i R_s}$. R_s is the diode series bulk resistance, and Z_{mn} is a matrix element in (3.6). At midband this expression can be written as

$$G_{21} = \frac{4x_g y_\ell r K_q}{[(1+x_g)(1+y_\ell) - K_q]^2} \tag{3.13}$$

where

$$x_g = \frac{R_{g1}}{R_s} \tag{3.14}$$

$$y_\ell = \frac{R_{\ell 2}}{R_s} \tag{3.15}$$

$$K_q = Q_{11}Q_{21} \tag{3.16}$$

$$r = \frac{\omega_{20}}{\omega_{10}} \tag{3.17}$$

and ω_{10}. ω_{20} are the midband signal and lower sideband radian frequencies. When x_g is set to a nonzero constant $> (K_q-1)$, (3.13) shows that the gain is always finite. For a specified value of $x_g > (K_q-1)$, y_ℓ can be varied to maximize the midband gain (Ref. 11) yielding

$$G_{21} = \frac{Q_{11}^2 x_g}{(1+x_g)(1+x_g-K_q)} \tag{3.18}$$

$$y_\ell = 1 - \frac{K_q}{1+x_g} \tag{3.19}$$

Since the gain expression (3.13) is symmetrical in x_g and y_ℓ, a similar expression for maximum gain is obtained for a specified value $y_\ell > (K_q-1)$.

In reflection parametric amplifiers (RPA) and upconverters, the maximum gain often occurs slightly below the resonant frequency (Ref. 33). The reason for the nonresonant gain maximum can be seen more clearly by rearranging (3.12):

$$G_{21} = \frac{4R_{g1}R_{\ell 2}(S_1/\omega_1)^2}{\left|Z_{11}Z_{22}^* - S_1^2/(\omega_1\ \omega_2)\right|^2} \quad .$$

As the frequency falls slightly below resonance, the denominator decreases because the parametrically induced negative resistance term has increased. The other frequency dependent terms in the gain expression are of less significance in many microwave structures. An analytical expression for the true maximum gain and the frequency shift can be found for the ideal LSUC in a fashion similar to that used for the ideal RPA (Refs. 34, 35). If the amplifier uses single-tuned signal and lower sideband circuits, then the transducer power gain near resonance is

$$G_{21} = \frac{4R_{g1}R_{\ell 2}S_1^2\,(1-2\delta\omega/\omega_{10})}{|Z_{22}|^2\,\omega_{10}^2\,[(R_{g1}-R_{v0}-a_r\delta\omega)^2+(a_x\delta\omega)^2]}$$

where

$$\delta\omega = \omega_1 - \omega_{10}$$

$$Z_v = \frac{S_1^2}{\omega_1\omega_2 Z_{22}^*} - R_s - jX_{11}$$

$$= R_v + jX_v$$

$$Z_{v0} = Z_v\big|_{\omega_1=\omega_{10}}$$

$$a_r = \left.\frac{dR_v}{d\omega_1}\right|_{\omega_1=\omega_{10}}$$

$$= -\frac{S_1^2\,(\omega_{20}-\omega_{10})}{R_{22}\omega_{10}^2\omega_{20}^2}$$

$$a_x = \left.\frac{dX_v}{d\omega_1}\right|_{\omega_1=\omega_{10}}$$

$$= \frac{S_1^2}{\omega_{10}\omega_{20}R_{22}^2}\left.\frac{dX_{22}}{d\omega_1}\right|_{\omega_1=\omega_{10}} - \left.\frac{dX_{11}}{d\omega_1}\right|_{\omega_1=\omega_{10}}.$$

Maximizing the gain with respect to $\delta\omega$ gives an expression for the frequency deviation from resonance $\delta\omega_m$ where the gain is maximum. After some algebra this gives

$$\frac{\delta\omega_m}{\omega_{10}} = -\left(\frac{1}{a_r^2 + a_x^2}\right)\left(\frac{R_{g1} - R_{v0}}{\omega_{10}}\right)\left(\frac{R_{g1} - R_{v0}}{\omega_{10}} - a_r\right)$$

where the approximation $X_{22} = 0$ is used. The maximum gain can be found simply by using $\delta\omega_m$ in the gain expression. This expression demonstrates the existence of the nonresonant gain maximum. However since the microwave circuits used in LSUC's are so complicated, accurate, tractable analytical expressions for the maximum gain cannot be found.

3.2.4 Bandwidth and Gain-Bandwidth Product. If the varactor diode contains no parasitic elements, and if the external circuit is assumed to consist of ideal filter elements, then approximate analytical expressions may be derived for bandwidth and gain-bandwidth product. Under high-gain conditions, the primary frequency dependence of gain is the reactive term in the denominator of the gain expression (Ref. 36). Thus when the frequency-dependent reactance increases to where the denominator is doubled, the gain is approximately halved, and the bandwidth as a fraction of the input frequency can be found:

$$w = \frac{1-\alpha_w}{\frac{Q_{10}}{1+x_g} + \frac{\alpha_w}{r}\frac{Q_{20}}{1+y_\ell}} \qquad (3.20)$$

where

$$\alpha_w \triangleq \frac{K_q}{(1+x_g)(1+y_\ell)} .$$

The definition of gain-bandwidth product used here is the square root of the transducer power gain multiplied by the fractional bandwidth (3.20). The square root of the gain is used since the frequency dependence of the gain-bandwidth product is minimized. The gain-bandwidth expression is

$$GBW \triangleq w(G_{21})^{\frac{1}{2}}$$

$$GBW = \left[\frac{4x_g y_\ell \alpha_w r}{(1+x_g)(1+y_\ell)}\right]^{\frac{1}{2}} \left[\frac{Q_{10}}{1+x_g} + \frac{\alpha_w}{r}\frac{Q_{20}}{1+y_\ell}\right]^{-1} \tag{3.21}$$

Because of the assumptions used, these two expressions are useful only in finding the approximate upper limits for a particular LSUC or for comparing different designs.

3.2.5 Noise Figure Relationship for the LSUC. Noise sources in an upconverter circuit can be broadly divided into two classes: thermal noise caused by random motion of electrons in a resistor and shot noise caused by random fluctuations of charge carriers in an electric current. The thermal noise in the LSUC is assumed to be caused entirely from $R_{rr} = R_s + R_r$, where R_s is the series bulk resistance of the diode and R_r is the circuit resistance at ω_r. The shot noise is assumed to be caused by the charge carriers traversing the depletion layer of the varactor diode. Shot noise in varactor diodes is generally considered negligible in comparison with thermal noise in uncooled parametric amplifiers. This is based on the simple calculation made by Uhlir (Ref. 37) who showed that the noise current when both shot and thermal noise are present is

$$\langle i^2 \rangle = \frac{4kTB_w}{R} + 2qB_w i_0 \tag{3.22}$$

where i_0 is the dc current. k is Boltzmann's constant, and T is the absolute temperature. Substituting numbers for a typical parametric amplifier into this expression shows that the first term is much larger than the second. Indeed, Uhlir has shown elsewhere (Ref. 38) that the ideal nonlinear capacitor (zero storage time) has no shot noise output. However the shot noise effect is more complicated than that implied by (3.22) and cannot be automatically neglected. Even if the diode is open circuited as is the case of the LSUC discussed here, shot noise can still arise from forward-and-back current (Ref. 38).

Josenhans (Ref. 39) calculated the shot and thermal noise in a reflection parametric amplifier subject to several simplifying assumptions. The assumptions that will be retained for the calculation given here are the following.

1. The diode has a large dynamic Q at the signal and sideband frequencies.

2. The charge carrier makes one pass across the space charge layer and recombines on reaching the far side.
3. The transit time of the carrier is short compared to the period of the pump.
4. The effect of any fast surface states is negligible.

In addition to these assumptions, Josenhans assumed high gain and no higher order sideband frequencies. The first is unnecessary, as tractable results can be obtained for arbitrary gain while the second will be employed after the general expression is obtained. The noise equivalent circuit of the varactor chip shown in Fig. 3.1 can be reduced to that in Fig. 3.2 when the dynamic $Q >> 1$. In these figures T_d is the diode temperature and T_a is the ambient temperature. The forward diode current

$$i_0 = i_s(e^{qV/kT} - 1)$$

is used to find the equivalent diode noise resistance:

$$R_x = \frac{kT}{qi_0} .$$

The shot noise source may be regarded as an equivalent resistance at ω_r given by

$$R_{er} = \frac{\left(\frac{S_0}{\omega_r}\right)^2 R_x}{R_x^2 + \left(\frac{S_0}{\omega_r}\right)^2}$$

so that mathematically this noise source can be treated as a thermal noise source of mean square voltage $< v^2 > = 4kTB_w R_{er}$.

There are several definitions of noise figure in the literature, but the "actual noise figure" proposed by Kurokawa (Ref. 40) is the most meaningful and the most convenient for negative resistance amplifiers. This definition includes the noise contribution from the load, so that two amplifiers which are not necessarily optimally loaded may be compared. The actual noise figure is defined as

$$F_m = \frac{\text{noise power delivered to the load at } \omega_m}{\text{available noise input power at } \omega_n} \cdot \frac{1}{G_{mn}}$$

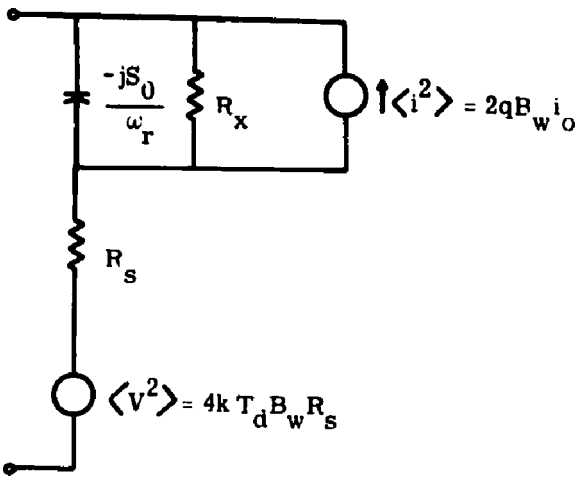


Fig. 3.1. Noise equivalent circuit

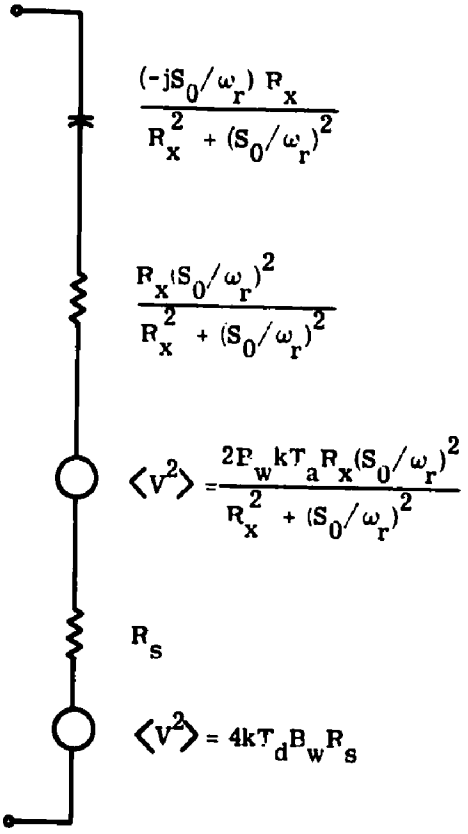


Fig. 3.2. Transformed noise equivalent circuit

The noise power delivered to the load can be analyzed as three components:

1. noise from sources at $f_r (r \neq m)$,
2. noise from internal sources of the amplifier at f_m,
3. and noise from the load itself which is amplified and returned to the load.

The first noise component is

$$N_{mr} = |Y_{mr}|^2 R_{\ell m} \{4kB_w[R_s T_d + T_a(R_r + R_{er})]\} \quad r \neq m \quad .$$

The second component is generated at f_m from the resistance $R_{mm} - R_{\ell m}$:

$$N_{mma} = |Y_{mm}|^2 R_{\ell m}\, 4kB_w[R_s T_d + R_m T_a + R_{em} T_a - R_{\ell m} T_a] \quad .$$

The third component is the thermal noise arising from the load $R_{\ell m}$ and is obtained by multiplying the output reflection gain of the amplifier by the available noise of the load.

$$N_{mmb} = kT_a B_w \left| \frac{R_{\ell m} - [(Y_{mm})^{-1} - R_{\ell m}]}{R_{\ell m} + [(Y_{mm})^{-1} - R_{\ell m}]} \right|^2$$

$$= kT_a B_w \left| 1 - 2R_{\ell m} Y_{mm} \right|^2$$

Summing these three noise contributions up gives the total output noise power

$$N_m = kB_w \left\{ 4R_{\ell m} \left[\sum_{r=1}^{n} |Y_{mr}|^2 (R_s T_d + R_r T_a + R_{er} T_a) - |Y_{mm}|^2 R_{\ell m} T_a \right] + T_a \left| 1 - 2R_{\ell m} Y_{mm} \right|^2 \right\}$$

where $n - 1$ is the number of sidebands considered. The noise figure is then

$$F_m = \frac{N_m}{kT_a B_w G_{mn}} \qquad (3.23)$$

The impedance matrix has been modified by the inclusion of the shot noise impedance in Fig. 3. 2 so that the diagonal of the matrix is augmented by

$$2R_{er} + (-1)^r \frac{jR_x^2 (S_0/\omega_r)}{R_x^2 + (S_0/\omega_r)^2}$$

This effects the values of Y_{mr} and G_{mn}. A tractable expression for the noise figure is obtained by evaluating (3. 23) at resonance for the 2×2 matrix approximation. After some algebra this reduces to

$$F_2 = 1 + \frac{1}{r}(1 + \frac{1}{x_g}) + \frac{T_d}{T_a x_g} + \frac{x_s}{x_g}(1 + \frac{2}{r}) + \frac{(1 + 2x_s + x_g)^2}{x_g r K_q} (\frac{T_d}{T_a} - 1) \qquad (3.24)$$

where

$$x_s = \frac{R_{e1}}{R_s}$$

$$y_s = \frac{R_{e2}}{R_s}$$

and

$$G_{21} = \frac{4x_g y_\ell r K_q}{[(1 + x_g + 2x_s)(1 + y_\ell + 2y_s) - K_q]^2}$$

When there is no shot noise $(x_s = y_s = 0)$, (3. 24) gives the noise figure for the diode heated above ambient by the pump source. If in addition $T_d = T_a$, (3. 24) reduces to

$$F_2 = (\frac{1}{x_g} + 1)(\frac{1}{r} + 1) + \frac{1}{G_{21}} \quad . \qquad (3.25)$$

This expression is valid for any value of gain while the expression derived by Kurokawa and Uenohara (Ref. 10) is valid only for infinite gain.

It was shown in Section 3. 2. 3 that the midband gain expression is symmetrical in x_g and y_ℓ. For some fixed $x_g > (K_q - 1) \geq 0$ the gain is maximized for some

$y_\ell \leq 1$, and for some fixed $y_\ell > (K_q - 1) \geq 0$, the gain is maximized for some $x_g \leq 1$. The first maximum gain condition implies $x_g > y_\ell$, and the second implies $y_\ell > x_g$. Equation (3. 25) clearly shows that the first maximum gain condition (with large x_g) gives superior noise figure and that noise decreases with increasing upconverter gain.

When the noise figure is optimized with respect to the set of maximum gains of (3. 18). the minimum noise figure as determined by Khan (Ref. 11) is

$$F_2 = 1 + \frac{2}{Q_{11}^2}\left(1 + \sqrt{1 + Q_{11}^2}\right) \tag{3. 26}$$

and the resulting gain is

$$G_{21} = r\left(1 + \frac{1}{\sqrt{1 + Q_{11}^2}}\right)^{-1}\left(\frac{\sqrt{1 + Q_{11}^2}}{K_q} + \frac{1}{K_q} - 1\right)^{-1} \tag{3. 27}$$

where

$$x_g = \sqrt{1 + Q_{11}^2} \tag{3. 28}$$

$$y_\ell = 1 - \frac{K_q}{1+x_g} \tag{3. 29}$$

$$r > r_c \triangleq \sqrt{1 + Q_{11}^2} - 1 \tag{3. 30}$$

If the diode Q_{11} is known and a specified gain is desired consistent with the minimum noise figure (3. 26). then the optimum frequency ratio is determined from (3. 27):

$$r_{opt} = r_c\left[1 - \frac{r_c(r_c + 1)}{(r_c + 2)G_{21}}\right]^{-1} . \tag{3. 31}$$

The desired gain obviously must be sufficiently large to give a finite optimum frequency ratio.

3. 2. 6 Origin of Shot Noise. The measurements of shot noise made by Josenhans on gallium arsenide and germanium diodes were all in error by less than 46 percent when compared to his theory. but for silicon diodes the measurements differed from the

theory by a factor of 10 to 15. A similar descrepency was observed earlier by Uenohara (Ref. 41). He had ruled out circuit loss, pump noise, shot noise on the basis of (3. 22), microplasma noise. and higher order sideband noise. However he noted his theory is inadequate for diodes with a static $Q_c = S_0/(\omega R_s) > 5$. No quantitative reason is given for the discrepency. but he suggested that the diode Q deteriorates with increase in applied pump power. His assumptions of neglecting circuit loss. pump noise. and higher order sideband noise are verified later in Chapter IV as being reasonable. so the shot and microplasma noise were probably larger than he expected.

Both Uenohara and Josenhans neglected carrier lifetime. Uhlir (Ref. 38) in discussing the noise contribution of the forward-and-back current still assumes $\omega\tau << 1$: an invalid assumption for silicon at microwave frequencies. Although an analytical treatment of this large shot noise is not available. a qualitative explanation is.

Siegel (Ref. 42) observed that when a diode was pumped by an RF source, the dc current-voltage characteristic exhibited a negative resistance region. He postulated that this was caused by some anomalous charge multiplication mechanism. Lindmayer and Wrigley (Ref. 43) verified that this is the case and described this effect in the following way.

When a forward current step is applied to a p^+n diode, holes begin to flow across the junction into the n region. At the same time an equal quantity of electrons flow from the n side ohmic contact. and since electron mobility is large in the n region. charge neutrality is established. When the junction is suddenly reverse biased, the faster moving electrons leave excess holes behind in the n region near the junction, thus initially giving the appearance of being heavily doped. The advance of the space charge is retarded. a high electric field is formed. and carrier multiplication occurs as the holes return to the p region. When all of the holes are returned. the electric field decays to that determined by the impurity concentration. The net result of this is that more charge is moved during the reverse transient than during the forward pulse. The same phenomena occur if a periodic signal is used rather than a voltage step.

3. 2. 7 Summary of Existing Design Theory. The fundamental design relationship is the midband gain expression (3. 13), which assumes a small input signal level and ideal circuit filters (i. e. no higher order sidebands propagate beyond f_{p-s}) . The same as-

sumptions are used in finding the midband noise figure (3. 25). These two expressions can be manipulated to find the conditions for maximum gain or minimum noise figure.

The design procedure for a LSUC exhibiting minimum noise figure can be outlined as follows.

1. The input signal frequency is first specified.
2. The diode dynamic Q_{11} is then specified. This parameter increases with the pump power and should normally be as large as possible.
3. The optimum lower sideband to signal frequency ratio is determined from (3. 31) for a specified gain.
4. The generator and load resistances are found from (3. 28) and (3. 29).

The optimum frequency ratio is not used in the designs of the following sections, because the ratio is so large that the required pump frequency is beyond the capabilities of the available equipment. Nevertheless low noise amplifiers with a specified gain are designed by choosing a large generator resistance and deriving the resulting low load resistance from (3. 13). Although the synthesis technique described here is based on only the 2×2 matrix approximation, analysis of the resulting design can be performed for a much larger number of frequencies.

3. 3 Effects of Upper Sideband Reactance on the LSUC

The theory outlined in Section 3. 2 provides a method for designing the impedances at signal and lower sideband frequencies. However, impedances at the higher order sidebands may significantly change the upconverter performance. To show explicitly how the reactance at the upper sideband frequency X_{33} affects the upconverter, (3. 8) is truncated to a 3×3 matrix rather than a 2×2 matrix. With this more accurate approximation, various impedances, the gain, gain stability with variations in pump power, gain-bandwidth product, and noise figure can all be modified by X_{33} and the second harmonic of the pumped varactor elastance S_2.

3. 3. 1 Effects of X_{33} on Gain.

The effects of X_{33} on gain is more clearly seen if the 3×3 matrix derived from (3. 8) is reduced to a 2×2 matrix, because this shows what additional impedances are induced into the signal and lower sideband circuits. Since there is no applied voltage source at the upper sideband frequency, the term i_3

can be eliminated from the first two equations resulting in

$$\begin{bmatrix} V_1 \\ V_2^* \end{bmatrix} = \begin{bmatrix} Z_{11} + \dfrac{X_{31}X_{13}}{Z_{33}} & -jX_{12} - \dfrac{X_{13}X_{32}}{Z_{33}} \\ jX_{21} + \dfrac{X_{23}X_{31}}{Z_{33}} & Z_{22}^* - \dfrac{X_{32}X_{23}}{Z_{33}} \end{bmatrix} \cdot \begin{bmatrix} i_1 \\ i_2^* \end{bmatrix} \tag{3.32}$$

$$\triangleq \begin{bmatrix} Z'_{11} & Z'_{12} \\ Z'_{21} & Z'_{22} \end{bmatrix} \begin{bmatrix} i_1 \\ i_2^* \end{bmatrix} . \tag{3.33}$$

If $Z_{33} = R_s + jX_{33}$, then

$$Z'_{11} = R_g + R_s + \frac{R_s X_{31} X_{13}}{R_s^2 + X_{33}^2} - j \frac{X_{33} X_{31} X_{13}}{R_s^2 + X_{33}^2}$$

$$\triangleq R_g + R_s + \Delta R_{11} - j\Delta X_{11}$$

$$Z'_{12} = - \frac{R_s X_{32} X_{13}}{R_s^2 + X_{33}^2} + j\left(-X_{12} + \frac{X_{33} X_{13} X_{32}}{R_s^2 + X_{33}^2}\right)$$

$$Z'_{21} = \frac{R_s X_{31} X_{23}}{R_s^2 + X_{33}^2} + j\left(X_{21} - \frac{X_{33} X_{31} X_{23}}{R_s^2 + X_{33}^2}\right)$$

$$Z'_{22} = R_\ell + R_s - \frac{R_s X_{32} X_{23}}{R_s^2 + X_{33}^2} + j \frac{X_{33} X_{32} X_{23}}{R_s^2 + X_{33}^2}$$

$$\triangleq R_\ell + R_s - \Delta R_{22} + j\Delta X_{22}$$

$$Z_{in1} \triangleq - \frac{Z'_{12} Z'_{21}}{Z'_{22}}$$

$$Z_{in2} \triangleq - \frac{Z'_{12} Z'_{21}}{Z'_{11}} .$$

Thus the equivalent circuit for the LSUC when X_{33} is finite is shown in Fig. 3.3.

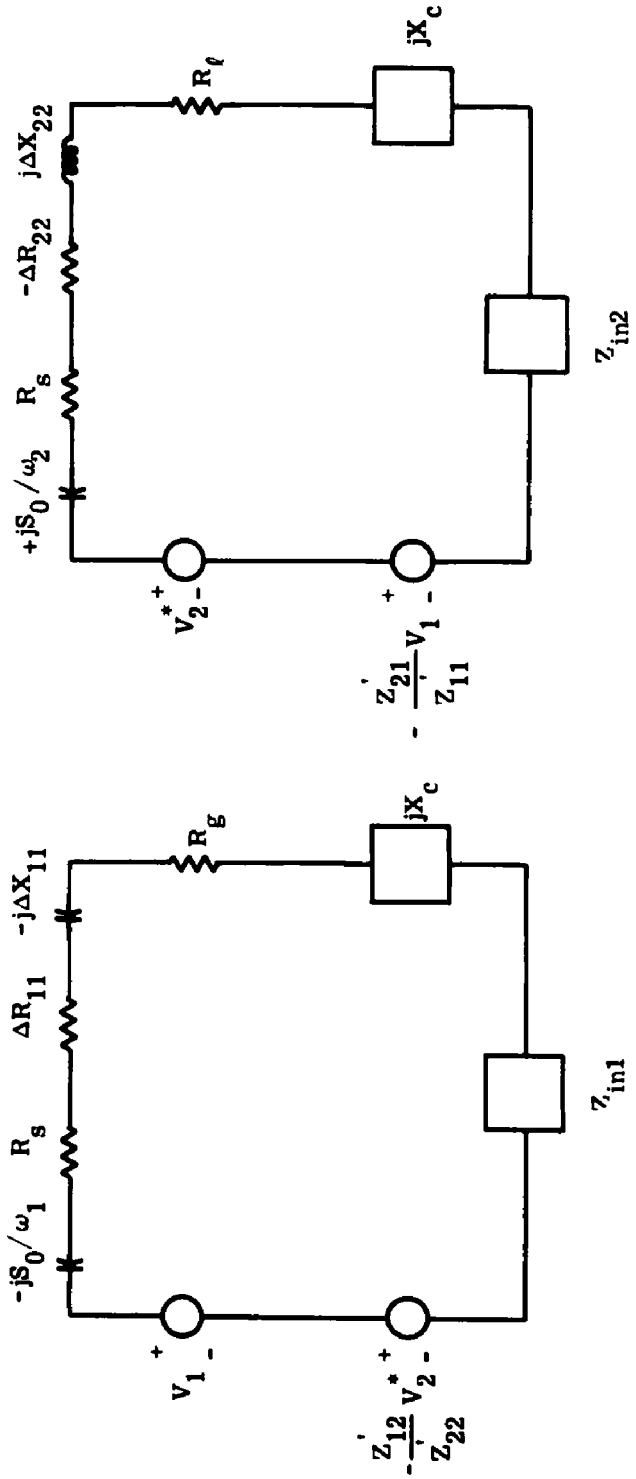


Fig. 3.3 Equivalent circuit of LSUC where X_c is the circuit reactance and X_{33} is finite

In the usual 2×2 matrix approximation at midband the only impedance induced into the signal circuit is $Z_{in1} = -S_1^2/[\omega_1\omega_2(R_\ell + R_s)]$: the negative resistance arising from the double reactive mixing. However, for finite X_{33} the induced impedance Z_{in1} is complex, and consists of terms which show the interaction between the circuits at ω_1 and ω_3, between ω_3 and ω_2, and between ω_2 and ω_1. In addition there is the added impedance ΔZ_{11}, which is dependent on the coupling between the circuits at ω_1 and ω_3. Similar remarks apply to the lower sideband circuit. Both ΔZ_{11} and ΔZ_{22} attain their maximum values when $X_{33} = R_s$.

The curves shown in Fig. 3.4 provide further insight into the magnitude of the impedances that might be expected in a typical LSUC. The parameters used here to make the calculations are listed below:

$$S_0 = 6.283\ 10^{11}\ F^{-1}$$

$$S_1/S_0 = 0.35$$

$$S_2/S_0 = 0.044$$

$$R_g = 100 \text{ ohms}$$

$$R_\ell = 1.3 \text{ ohms}$$

$$R_s = 1.0 \text{ ohms}$$

$$f_p = 9.000 \text{ GHz}$$

$$f_s = 1.000 \text{ GHz} \quad .$$

The large variation in these impedance values fortunately occur over a small range of X_{33} near zero. Except for R_{in2} the corresponding impedances in the lower sideband circuit are negligibly small, all being less than 1 ohm. If $S_2 = 0$ (or $X_{23} = X_{32} = 0$), Z_{in1} is equal to the negative resistance obtained from the usual 2×2 matrix analysis, while ΔZ_{11} varies with X_{33} in the same manner since it is independent of S_2. With these impedance variations, it is expected that the gain would also be seriously affected.

The transducer power gain is given by (3.11) where Y_{21} is the row 2, column 1 element of the inverse of either (3.32) or the truncated 3×3 matrix derived from (3.8). At midband where S_0 is resonated out, the gain is found to be

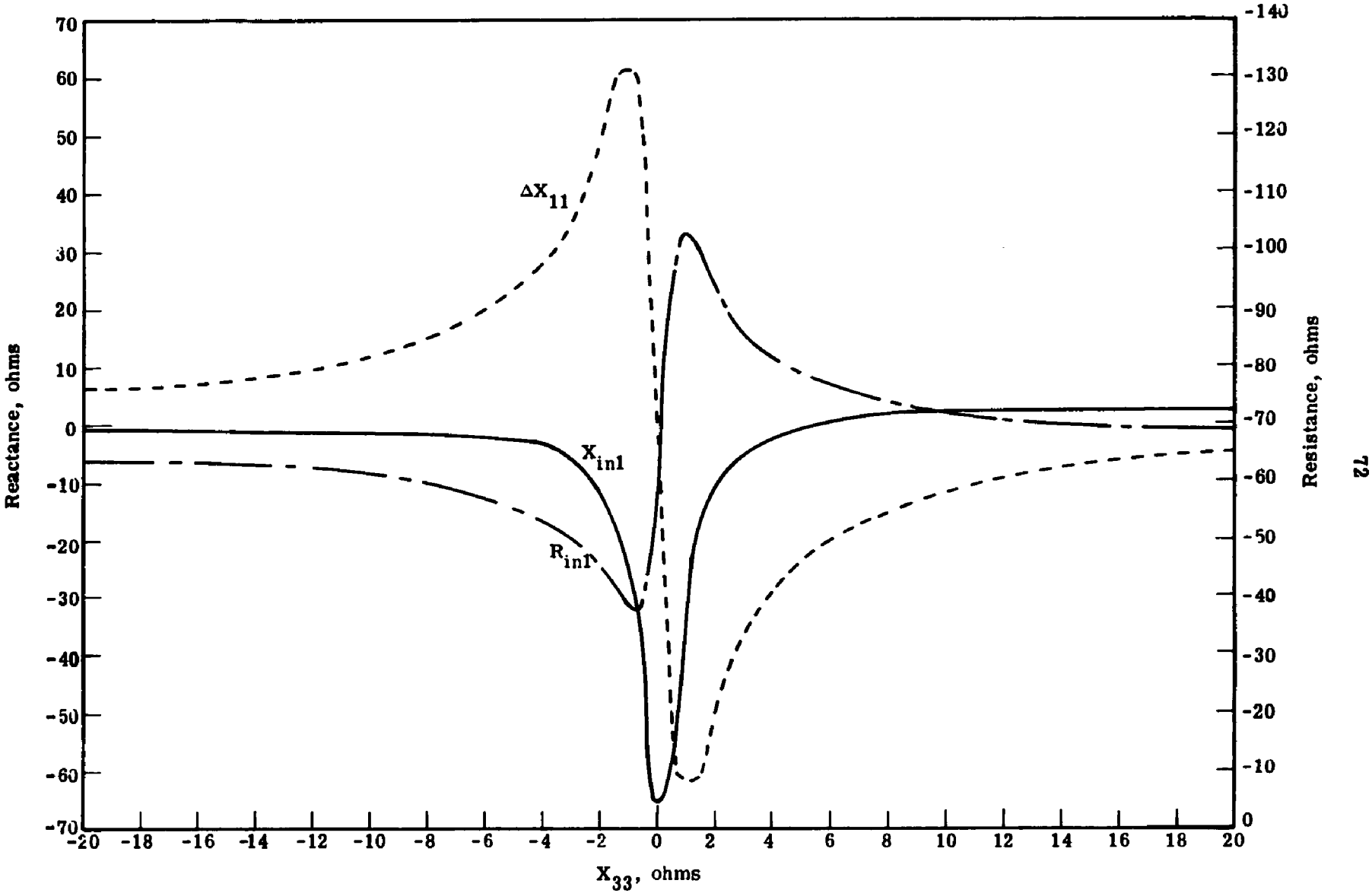


Fig. 3.4 The impedances induced into the signal circuit by the finite value of X_{33}

$$G_{21} = 4R_g R_f \frac{(X_{23}X_{31} - X_{21}X_{33})^2 + (R_s X_{21})^2}{M_a + (X_{33}M_b + M_c)^2} \tag{3.34}$$

where

$$M_a = [(R_g + R_s)(R_f + R_s)R_s - (R_g + R_s)X_{23}X_{32} + (R_f + R_s)X_{13}X_{31} - R_s X_{12}X_{21}]^2$$

$$M_b = (R_g + R_s)(R_f + R_s) - X_{12}X_{21}$$

$$M_c = X_{21}X_{13}X_{32} + X_{23}X_{31}X_{12}$$

$$M_d = M_a + M_c^2 \quad .$$

Although there is an additional negative resistance term in M_a proportional to S_2^2, there are other terms which would tend to degrade the gain. If the additional assumption is made that $S_2 = 0$, the gain simplifies to

$$G_{21} = \frac{4R_g R_f |X_{21}|^2}{[(R_f + R_s)(R_g + R_s + \Delta R_{11}) - X_{12}X_{21}]^2 + [(R_f + R_s)\Delta X_{11}]^2} \quad . \tag{3.35}$$

If ΔX_{11} as well as S_0 is tuned out by the external circuit, the gain is given by (3.35) with $\Delta X_{11} = 0$. Clearly midband gain can be enhanced only when X_{33} is finite and $S_2 \neq 0$.

The maximum and minimum gain can be found by differentiating (3.34) with respect to X_{33}. This yields the following quadratic equation:

$$X_{33}^2(-M_b M_c X_{21}^2 - M_b^2 X_{23}X_{31}X_{21}) + X_{33}[-M_d X_{21}^2 + (M_b X_{23}X_{31})^2 + (M_b R_s X_{21})^2]$$
$$+ M_d X_{23}X_{31}X_{21} + M_c M_b (X_{23}X_{31})^2$$
$$+ M_b M_c (R_s X_{21})^2 = 0 \quad . \tag{3.36}$$

This can be easily solved by use of the quadratic formula. Using the previously defined parameters for the LSUC, the maximum and minimum values of gain can be found.

$X_{33} = 9\ 77\ \Omega$ $G_{21} = 21.9$ dB (Maximum gain)

$X_{33} = -0.538\ \Omega$ $G_{21} = 6.48$ dB (Minimum gain)

$|X_{33}| = \infty\ \Omega$ $G_{21} = 20.06$ dB

When $S_2 = 0$, the minimum gain occurs at $X_{33} = 0$. The midband gain plotted in Fig. 3.5 for the typical LSUC described above clearly shows the minimum and maximum gain. In addition when the reactances X_{in1}, X_{in2}, ΔX_{11}, and ΔX_{22} are tuned out by the external circuit, even larger variations in the gain occur (Fig. 3.5). When $S_2 = 0$, the midband gain curve shown in Fig. 3.6 is symmetrical about $X_{33} = 0$. However the nonresonant maximum gain, also plotted for this case, does exhibit a peak for $X_{33} \lesssim 0$.

3.3.2 Effects of X_{33} on Gain Sensitivity. One possible source of gain instability in a LSUC is variation in the pump power source. The pump provides all the harmonic elastance coefficients S_1, S_2, S_3, ..., but to a first order approximation the gain sensitivity can be found by assuming that only the fundamental elastance coefficient is nonzero. Applying the formula

$$S_{pp} = \frac{S_1^2}{G_{21}} \frac{\partial G_{21}}{\partial S_1^2}$$

to (3.35), the gain sensitivity is

$$S_{pp} = 1 + \frac{S_1 G_{21}^{\frac{1}{2}}}{\omega_{20}(R_g R_\ell)^{\frac{1}{2}}} M_s \tag{3.37}$$

where

$$M_s = \{X_{33}^2[(R_g + R_s)(R_\ell + R_s) - S_1^2/(\omega_{10}\omega_{20})]$$

$$+ [(R_g + R_s)(R_\ell + R_s)R_s + (R_\ell + R_s)S_1^2/(\omega_{10}\omega_{30}) - R_s S_1^2/(\omega_{10}\omega_{20})]$$

$$\cdot [R_s - (R_\ell + R_s)\omega_{20}/\omega_{30}]\} \Big/ \Big((R_s^2 + X_{33}^2)^{\frac{1}{2}}\{X_{33}^2[(R_g + R_s)(R_\ell + R_s)$$

$$- S_1^2/(\omega_{10}\omega_{20})]^2 + [(R_g + R_s)(R_\ell + R_s)R_s + (R_\ell + R_s)S_1^2/(\omega_{10}\omega_{30})$$

$$- R_s S_1^2/(\omega_{10}\omega_{20})]^2\}^{\frac{1}{2}}) \quad . \tag{3.38}$$

The multiplying factor $M_s = 1$ if $|X_{33}| = \infty$. For a specified value of gain it will now be shown under what conditions the sensitivity can be improved by the finite value of X_{33}, i.e., when $M_s < 1$. The factor M_s can be written in the form

$$M_s = \frac{X_{33}^2 M_a + M_b M_c}{[(R_s^2 + X_{33}^2)(X_{33}^2 M_a^2 + M_b^2)]^{\frac{1}{2}}} < 1 \tag{3.39}$$

where the importance of the factor

$$M_c = R_s - (R_\ell + R_s)\omega_{20}/\omega_{30}$$

will be seen shortly, and where the other factors are defined from (3.38). After squaring (3.39) and cancelling the X_{33}^4 terms, the condition for improved gain sensitivity reduces to

$$0 < X_{33}^2(M_b^2 - 2M_a M_b M_c + M_a^2 R_s^2) + M_b^2(R_s^2 - M_c^2) \quad . \tag{3.40}$$

The inequality (3.39) is therefore satisfied if the coefficient of $X_{33}^2 > 0$ and $(R_s^2 - M_c^2) > 0$. However both of these conditions are equivalent. The coefficient of X_{33}^2 is a quadratic function in M_b and is always positive if the constant term $(M_a R_s)^2 > 0$, (obviously true), and the discriminant is less than zero. The discriminant is

$$4(M_a M_c)^2 - 4(R_s M_a)^2 < 0$$

or

$$R_s^2 > M_c^2 \quad .$$

On substituting for M_c, the requirement that gain sensitivity decrease reduces to the following restriction on the load resistance:

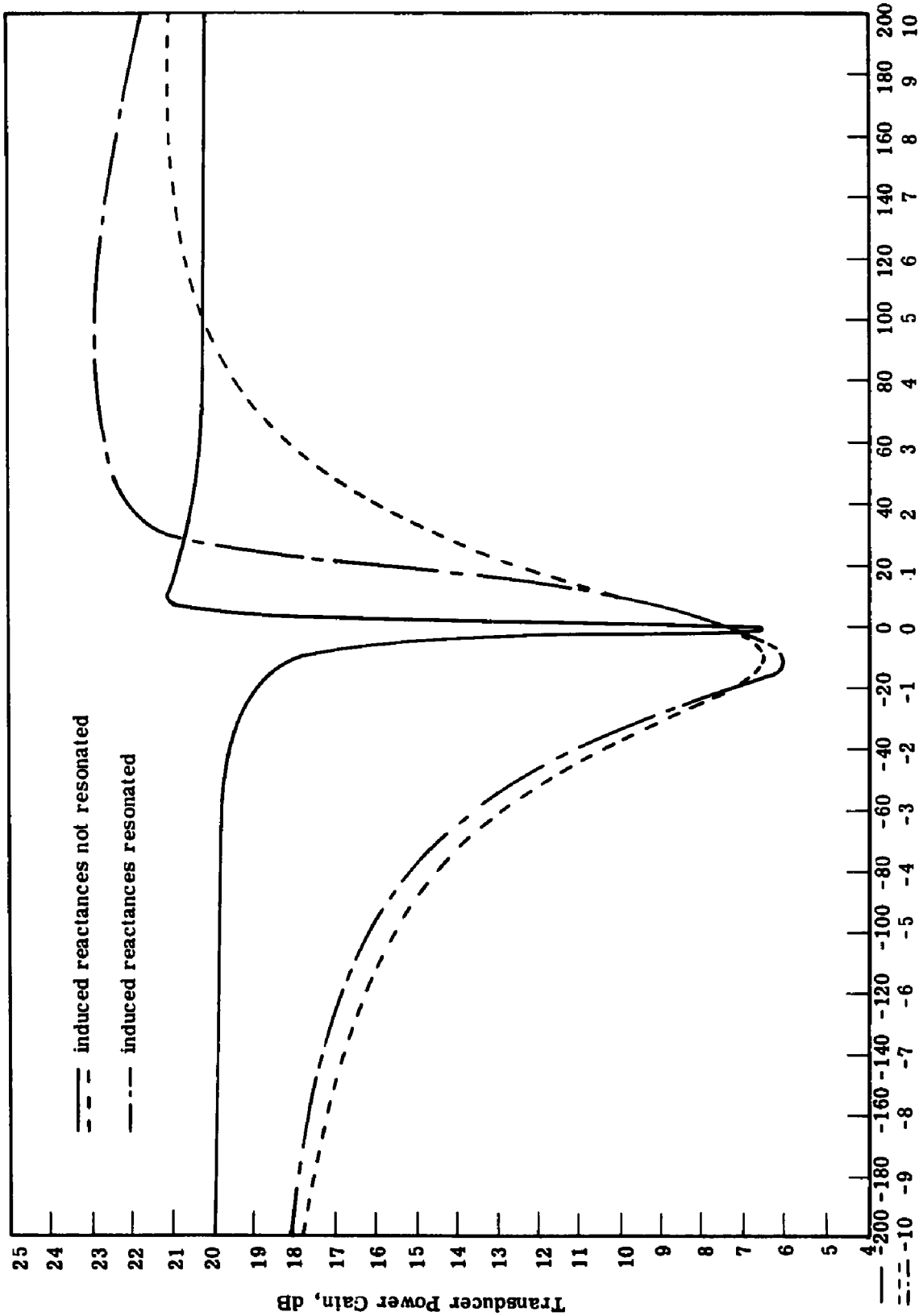


Fig. 3.5. Midband transducer power gain when $S_2/S_0 = 0.044$

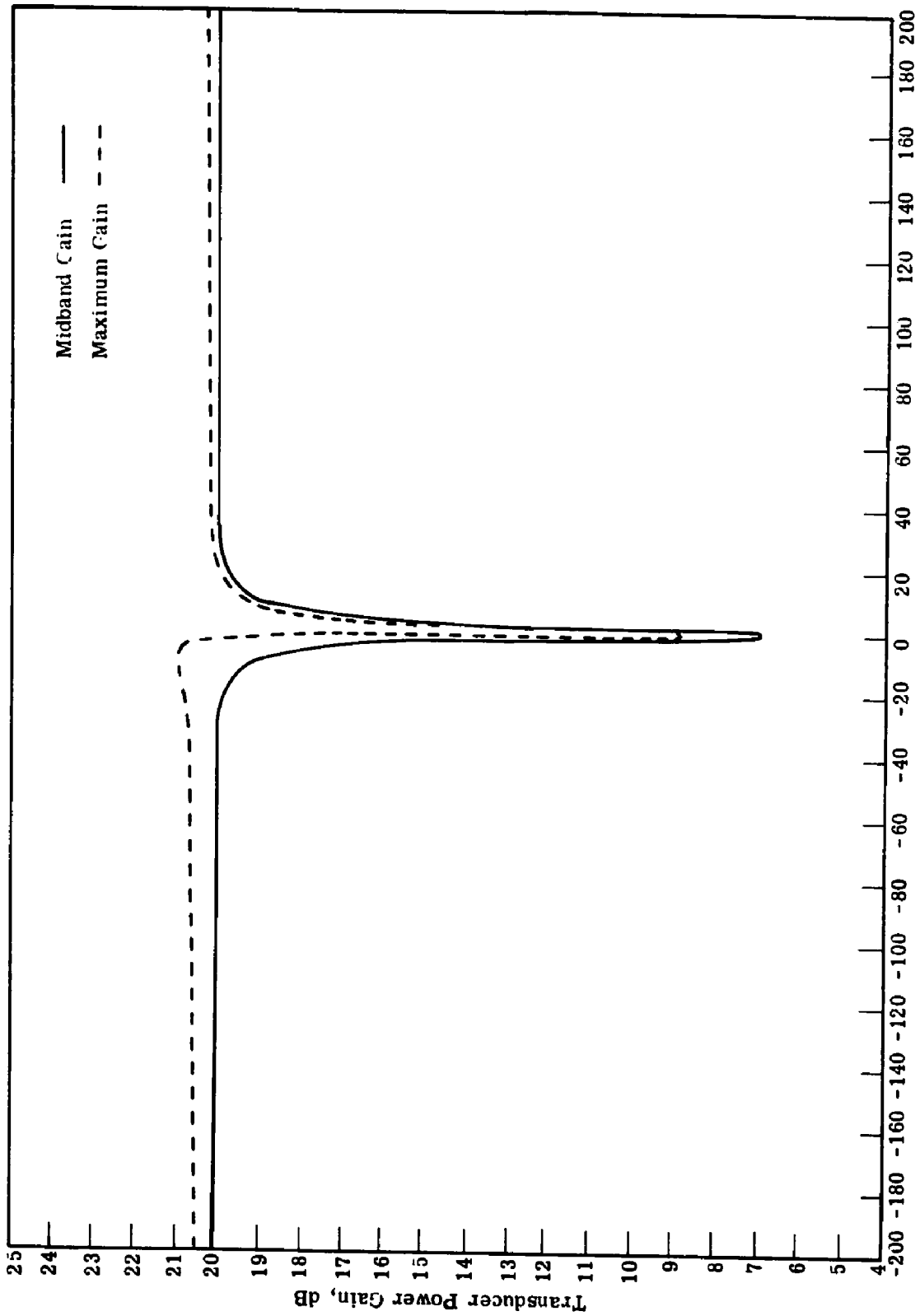


Fig. 3.6 The transducer power gain when $S_2 = 0$

$$R_\ell < R_s(2\omega_{30}/\omega_{20} - 1) \quad . \tag{3.41}$$

This expression, being independent of X_{33}, merely determines the boundary where gain sensitivity can always be improved. The amount of improvement is found from (3.39).

3.3.3 Effects of X_{33} on Gain-Bandwidth Product. The gain-bandwidth product expression obtained in Section 3.2.4 was derived subject to a high gain assumption. A similar expression can be found when X_{33} is finite and $S_2 = 0$, i.e., by using (3.35). If ΔR_{11} and ΔX_{11} are assumed frequency independent, the gain-bandwidth product will be very similar to the previous value:

$$GBW = \left[\frac{4x_g y_\ell r \alpha'_w}{(1 + x_g + x'_g)(1 + y_\ell)}\right]^{\frac{1}{2}} \left[\frac{Q_{10}}{1 + x_g + x'_g} + \frac{\alpha'_w Q_{20}}{r(1 + y_\ell)}\right] - 1 \tag{3.42}$$

where $x'_g \triangleq \frac{\Delta R_{11}}{R_s}$ and $\alpha'_w = \frac{K_q}{(1 + x_g + x'_g)(1 + y_\ell)}$. Since both numerator and denominator decrease by the factor

$$\frac{1 + x_g}{1 + x_g + x'_g}$$

the gain-bandwidth product remains unchanged when X_{33} is finite, at least for this first order approximation.

A more accurate picture of this parameter as X_{33} is varied can be obtained by removing the frequency independent assumption on the induced reactances, allowing $S_2 \neq 0$, assuming X_{33} is a single tuned lumped reactance, and calculating the gain as a function of frequency when X_{33} is the desired reactance at midband. Using the same LSUC parameters defined in Section 3.3.1, the gain-bandwidth product was calculated and plotted in Fig. 3.7. If the reactances induced into the signal and lower sideband ports by X_{33} are resonated by a single tuned reactance, the gain-bandwidth product is not changed enough to be seen on the scale of this graph. If $S_2 = 0$, the gain-bandwidth product increases for $X_{33} < 0$ and decreases for $X_{33} > 0$, but never by more than 0.002. If S_2 is increased rather than decreased, the gain-bandwidth product changes in the opposite direction.

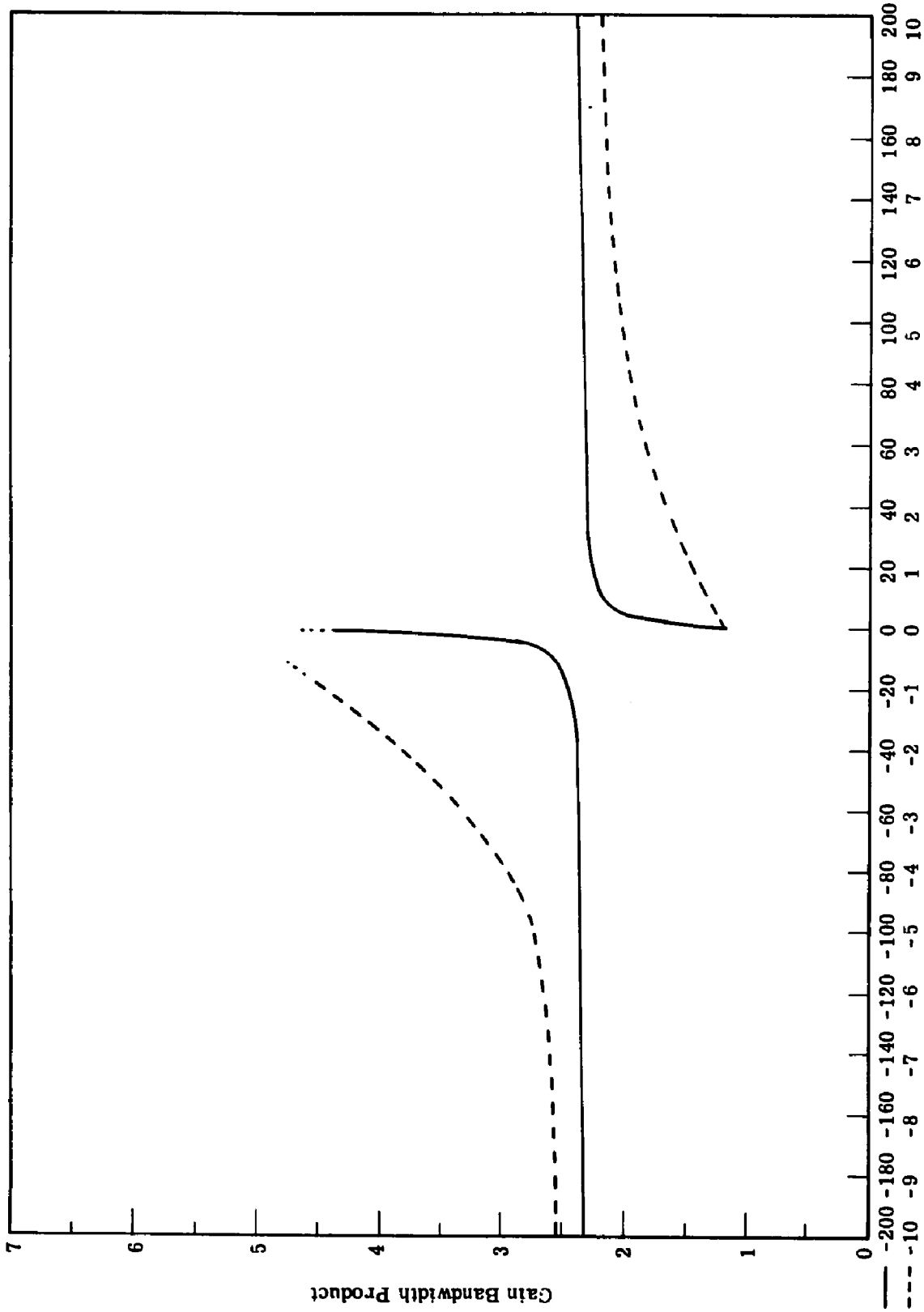


Fig. 3.7. The gain-bandwidth product ($G^{\frac{1}{2}}w$) when $S_2/S_0 = 0.044$ where the dashed curve corresponds to the expanded X_{33} scale

The behavior of the gain-bandwidth product near $X_{33} = 0$ needs some explanation. When $X_{33} \lesssim 0$, the gain is low and bandwidth wide, so values for the product are difficult to obtain. When $X_{33} \gtrsim 0$, the gain versus frequency curve has a large dip near the resonant point. For values of X_{33} in this range the maximum gain occurs at a frequency above resonance (rather than below as expected from the theory presented in Section 3. 2. 3), and the bandwidth is greatly reduced. Consequently the gain-bandwidth product is low for $X_{33} \gtrsim 0$.

3. 3. 4 Effects of X_{33} on Noise Figure. The noise figure for the LSUC is obtained from (3. 23) where for these calculations X_{33} is finite, the shot noise is assumed to be zero, and the diode temperature is assumed to be equal to the ambient temperature. The noise figure is

$$F_2 = 1 + \frac{R_s}{R_g} + \frac{4R_\ell R_s(|Y_{22}|^2 + |Y_{23}|^2)}{G_{21}} + \frac{|1 - 2R_\ell Y_{22}|^2}{G_{21}} \tag{3.43}$$

where G_{21} is given by (3. 34). After some algebraic manipulation this can be reduced to a form similar to (3. 25):

$$F_2 = 1 + \frac{R_s}{R_g} + \frac{1}{G_{21}} + \left(1 + \frac{R_s}{R_g}\right)\left(\frac{X_{12}}{X_{21}}\right) \frac{X_{21}^2(R_s^2 + X_{33}^2)}{[(X_{31}X_{23} - X_{21}X_{33})^2 + (X_{21}R_s)^2]}$$

$$+ \Bigg\{ \frac{R_s}{R_g} [X_{23}^2(R_g + R_s)^2 + (X_{21}X_{13})^2 + X_{13}X_{31}X_{12}X_{21}]$$

$$+ \left(1 + \frac{R_s}{R_g}\right) [X_{23}X_{32}R_s(R_g + R_s) + X_{23}X_{32}X_{13}X_{31}$$

$$- X_{33}(X_{12}X_{23}X_{31} + X_{21}X_{13}X_{32})] \Bigg\} \Big/ [(X_{31}X_{23} - X_{21}X_{33})^2 + (X_{21}R_s)^2] . \tag{3.44}$$

This equation by comparison provides explicit demonstration of the effect of X_{33} on the upconverter noise. When $|X_{33}| = \infty$, (3. 44) reduces to the simple expression (3. 25); when $S_2 = 0$, (3. 44) reduces to

$$F_2 = (1 + \frac{1}{x_g})(1 + \frac{1}{r}) + \frac{1}{G_{21}} + \frac{X_{13}(X_{13} + X_{31}/r)}{x_g(R_s^2 + X_{33}^2)} \tag{3.45}$$

where x_g is the normalized generator resistance and $r = \omega_2/\omega_1 = X_{21}/X_{12}$.

Just as the gain exhibited a minimum and maximum as a function of X_{33}, so also does the noise figure. To find these extrema, (3.44) may be written in the following form:

$$F_2 = 1 + \frac{R_s}{R_g} + \frac{M_a + M_b X_{33} + M_c X_{33}^2}{[(X_{31}X_{23} - X_{21}X_{33})^2 + (R_s X_{21})^2]} \tag{3.46}$$

where

$$M_a = \left(1 + \frac{R_s}{R_g}\right) X_{12}X_{21}R_s^2 + \frac{R_s}{R_g}[X_{23}^2(R_g + R_s)^2 + (X_{21}X_{13})^2 + X_{13}X_{31}X_{12}X_{21}]$$

$$+ \left(1 + \frac{R_s}{R_g}\right)[X_{23}X_{32}R_s(R_g + R_s) + X_{23}X_{32}X_{13}X_{31}]$$

$$+ \left\{[(R_g + R_s)(R_\ell + R_s)R_s - (R_g + R_s)X_{23}X_{32} + (R_\ell + R_s)X_{13}X_{31}\right.$$

$$\left. + R_s X_{12}X_{21}]^2 + [X_{21}X_{13}X_{32} + X_{23}X_{31}X_{12}]^2\right\} \Big/ (4R_\ell R_g)$$

$$M_b = \left(1 + \frac{R_s}{R_g}\right)(-X_{12}X_{23}X_{31} - X_{21}X_{13}X_{32}) + 2(X_{21}X_{13}X_{32} + X_{23}X_{31}X_{12})$$

$$\cdot [(R_g + R_s)(R_\ell + R_s) - X_{12}X_{21}] / (4R_g R_\ell)$$

$$M_c = \left(1 + \frac{R_s}{R_g}\right) X_{12}X_{21} + [(R_g + R_s)(R_\ell + R_s) - X_{12}X_{21}]^2 / (4R_g R_\ell)$$

Differentiating (3.46) with respect to X_{33} results in the following quadratic equation in X_{33}:

$$0 = X_{33}^2 [-M_b X_{21}^2 - 2M_c X_{31} X_{23} X_{21}] + X_{33}[2M_c (X_{31} X_{23})^2 + 2M_c (X_{21} R_s)^2$$

$$- 2M_a X_{21}^2] + [M_b (X_{31} X_{23})^2 + M_b (X_{21} R_s)^2 + 2M_a X_{21} X_{31} X_{23}]$$

which may be easily solved by the quadratic formula. When $S_2 = 0$ (i.e., $X_{23} = X_{32} = 0$) the noise figure has only the one extremum at $X_{33} = 0$. Clearly from (3.45) this extremum is a maximum since, when $S_2 = 0$, the noise figure can only be increased by the finite X_{33}. However, when $S_2 \neq 0$, some improvement in the noise figure is possible. Using the LSUC parameters defined in Section 3.3.1, the noise figure extrema are found:

$X_{33} = -0.480\ \Omega$	$F = 1.8124$	(Maximum noise)
$X_{33} = 24.50\ \Omega$	$F = 1.1453$	(Minimum noise)
$X_{33} = \infty\ \Omega$	$F = 1.1463$	.

These extrema are also observed in Fig. 3.8 which is a plot of (3.44). It appears that the enhanced noise performance at $X_{33} = 24.50$ is very small, although it could be improved by increasing S_2.

The "actual" noise measure, defined by Kurokawa (Ref. 40) as

$$M = \frac{F-1}{1 - \frac{1}{G_{21}}}$$

is plotted in Fig. 3.9. This parameter is particularly useful in assessing the noise characteristics of a low gain amplifier, a condition that occurs for X_{33} near zero. The noise measure parameter permits choosing between a low gain, low noise amplifier or a high gain, higher noise amplifier for the front end of a system. The noise measure in Fig. 3.9 reached a maximum of 0.791 at approximately the same place the maximum noise figure occurs.

3.3.5 Conclusions on the Effects of X_{33}. All of the major effects on the LSUC that are caused by a finite value of X_{33} for the example chosen here occur for $X_{33} \lesssim 20$. However for any LSUC, the large variations between the 2 x 2 and 3 x 3 matrix approximations will diminish as X_{33} gets large. In a given upconverter design

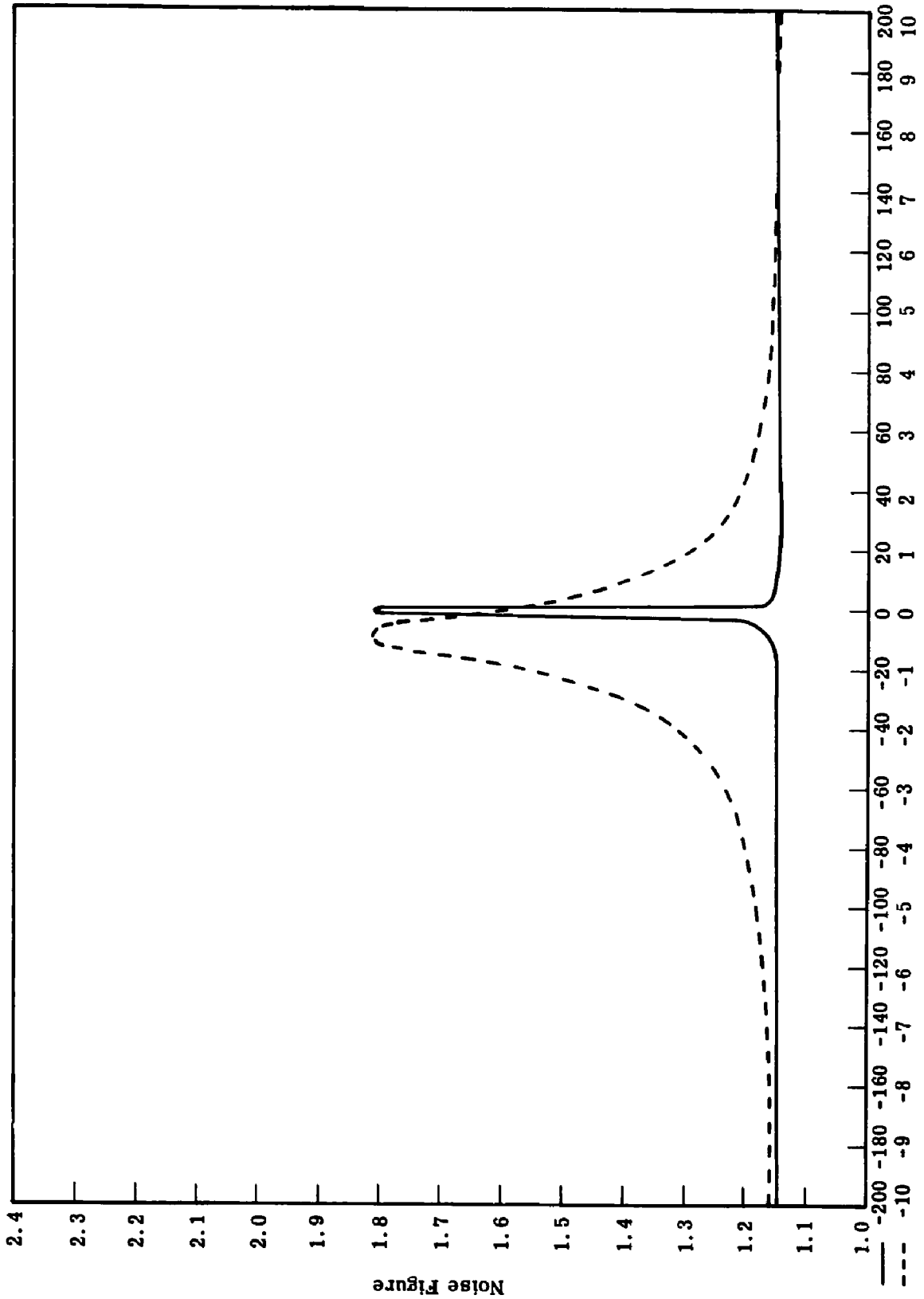


Fig. 3.8. The noise figure when $S_2/S_0 = 0.044$ where the dashed curve corresponds to the expanded X_{33} scale

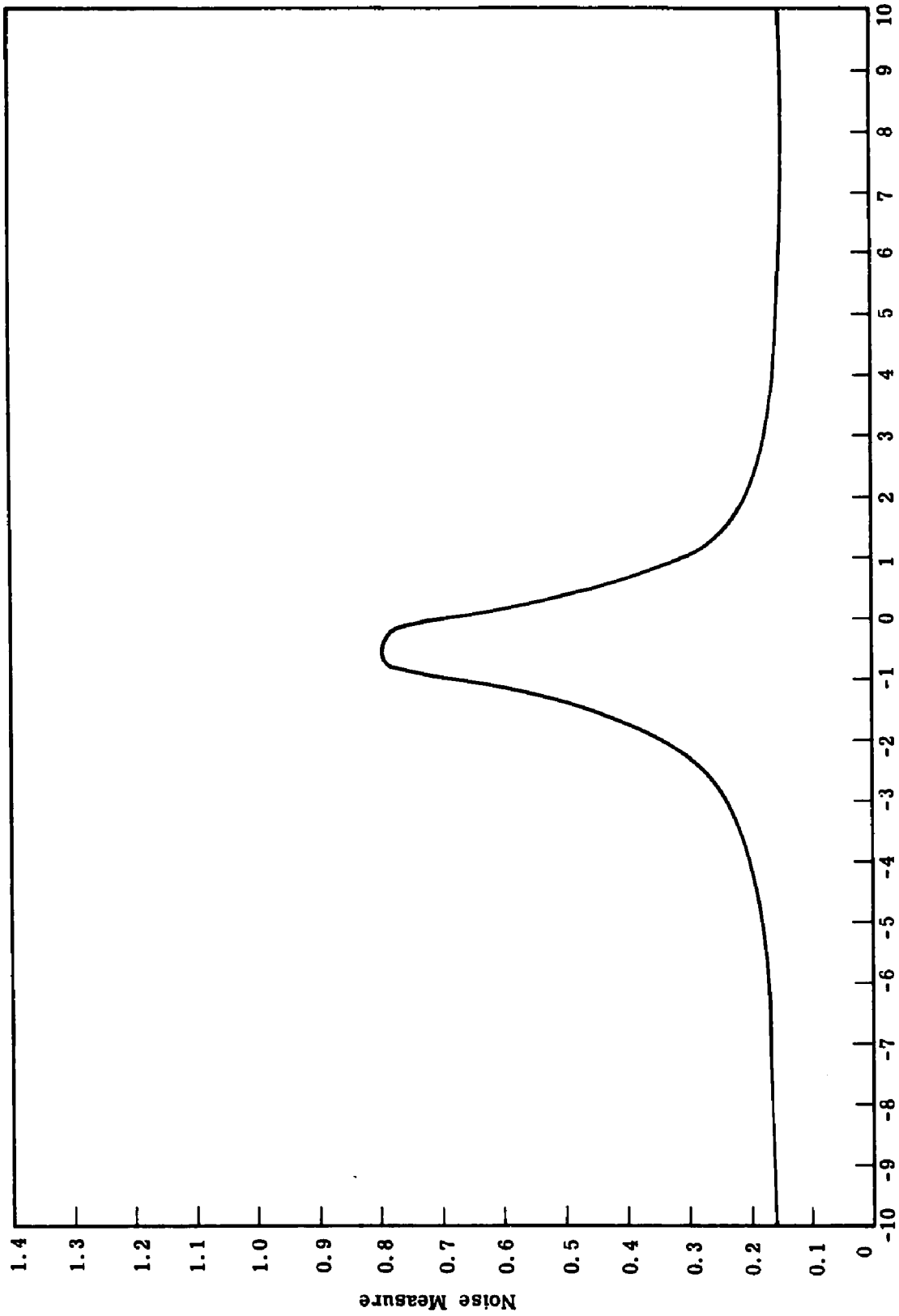


Fig. 3.9. The actual noise measure of the LSUC when $S_2/S_0 = 0.044$

the values of X_{33} where the minimum and maximum gain and noise figure occur are a function of the magnitude of S_2 (Table 3. 1).

	$S_2 = 0$	$S_2/S_0 = 0.044$	$S_2/S_0 = 0.1$
Maximum Gain	$\infty\ \Omega$	9. 77 Ω	5. 62 Ω
Minimum Gain	0 Ω	-0. 538 Ω	-1. 151 Ω
Min. Noise Fig.	$\infty\ \Omega$	24. 50 Ω	15. 19 Ω
Max. Noise Fig.	0 Ω	-0. 480 Ω	-1. 062 Ω

Table 3. 1. Values of X_{33} where the gain and noise figure extrema occur

Therefore measurement of X_{33} where the midband maximum and minimum gain occur offers at least the theoretical possibility of measuring S_2 under operating conditions. The method would proceed by resonating the signal and lower sideband circuits for some large value of $|X_{33}|$. Then the values of X_{33}, namely X_{33a} and X_{33b}, are found for which the gain is minimum and maximum respectively. Since these two values satisfy (3. 36), then $-(X_{33a} + X_{33b})$ equals the ratio of the coefficient of X_{33} to the coefficient of X_{33}^2 in (3. 36). Thus a linear expression in S_2^2 is obtained in terms of the known circuit values and S_1. Enhancement of S_2 not only moves the extrema to lower X_{33} values, but also provides larger maximum gain and lower minimum noise figure.

3. 4. Numerical Comparison of Three Possible LSUC Circuits

There are at least three possible circuits which could be used in fabricating a LSUC using a coaxial tee junction. If the diode is mounted at the tee junction between the center and outer conductors, then all three ports of the tee are in parallel with the diode (Fig. 3. 10a). This first circuit is designated LSUC1. If the diode is mounted completely within the center conductor with one end in the signal port, then the diode sees the signal port in series with the parallel combination of the pump and lower sideband ports (Fig. 3. 10b). This second circuit is designated as LSUC2. If the diode is mounted a short distance away from the tee junction and in the lower sideband port, then

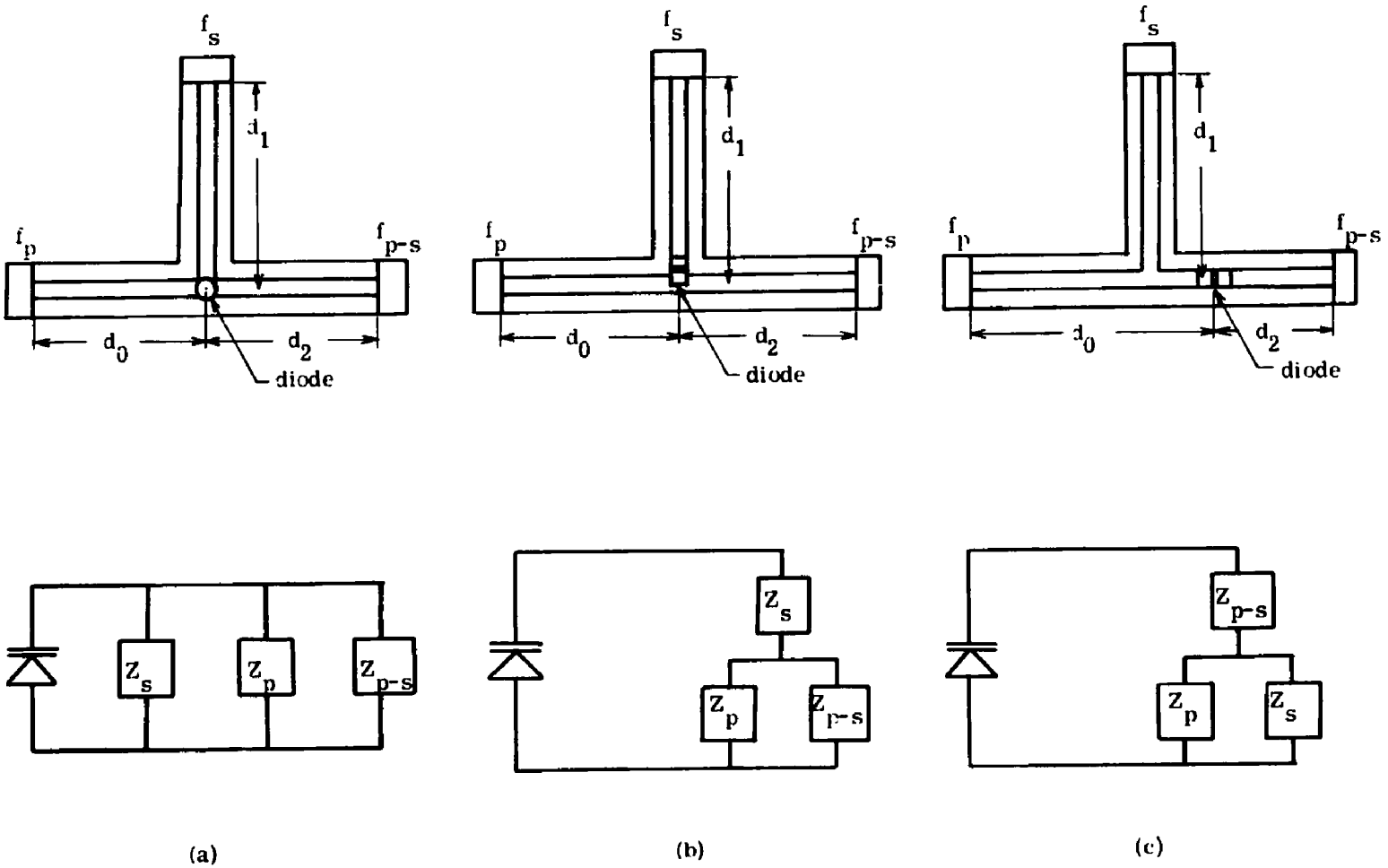


Fig. 3. 10. Drawings of LSUC1, LSUC2, and LSUC3 together with the corresponding schematics of the circuits are shown in (a), (b), and (c) respectively. d_0, d_1, and d_2 are the distances between the diode and the corresponding impedance transformers respectively. Z_s, Z_p, and Z_{p-s} are the impedances of the signal, pump, and lower sideband ports as seen by the diode

the diode sees the lower sideband port in series with the parallel combination of the pump and signal ports (Fig. 3. 10c). This third circuit is designated as LSUC3.

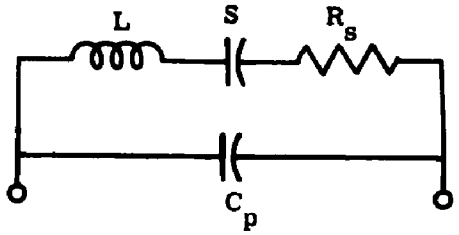
In the analysis that follows, the tee junction for LSUC1 and LSUC2 is assumed to be an ideal junction. However at X-band frequencies and higher, this assumption is not valid. Hence in LSUC3, a more accurate assumption is used; the leg of the tee junction appears as an open circuit to power flowing between the two arms of the tee circuit for frequencies in X-band or higher.

To make these circuit configurations into LSUC's, two additional factors must be considered: (1) the diode with its package parasitic elements, and (2) the external circuit which performs the impedance matching and filtering functions. A typical diode model, which is used throughout a large portion of this chapter, is shown in Section 3. 4. 1. In Section 3. 4. 2 the gain and gain-bandwidth product are found for a LSUC with frequency independent filters and impedance matching transformers using both an unpackaged and packaged diode. Under these circumstances all three circuit configurations give identical results. In the following sections each of the three LSUC circuits are examined under a variety of conditions: (1) ideal band-pass impedance transformers for the three ports are located a given distance away from the diode, (2) the diode package parasitic inductance is changed so that the diode is self resonant at f_{20}, and (3) the ideal transformers are replaced by single- and double-stub tuners. Finally in Section 3. 4. 7 some conclusions are drawn, and the relative merits of these three circuit configurations are discussed.

3. 4. 1 Diode Model and Desired Circuit Parameters. The basic diode model is shown in Fig. 3. 11, with the typical parasitic values:

$$R_s = 1 \text{ ohm}$$
$$L = 2 \text{ nH}$$
$$C_p = 0.7 \text{ pF}$$
$$S_0 = 2\pi 10^{11} \text{ F}^{-1}$$

The design of a LSUC must include these package parasitic elements since they have a major effect on the amplifier operation. To avoid needless repetition in later sections,



$$S = \sum_{n=-\infty}^{\infty} S_n \exp(jn\omega_p t)$$

Fig. 3.11. Package varactor diode model

this model with these particular parasitic element values is termed the "standard diode model."

In the designs which follow, the signal center frequency $f_{10} = 1.000$ GHz, the pump frequency $f_p = 9.500$ GHz, and the lower sideband center frequency $f_{20} = 8.500$ GHz. The desired midband transducer power gain is 19 dB. From (3.13) this value of gain can be obtained with small noise figure if $R_g = 100$ ohms and $R_f = 1.3$ ohms.

3.4.2 Gain for the Ideal Circuit with Unpackaged and Packaged Diode. The broadest bandwidth possible for a LSUC would occur with no diode package parasitic elements present. If the circuit presents to the unpackaged diode terminals a constant $R_g = 100$ ohms at all signal frequencies and a constant $R_f = 1.3$ ohms at all lower sideband frequencies, the transducer power gain as a function of frequency would appear as shown in Fig. 3.12. This curve also provides a clear demonstration of the frequency dependence of the parametrically induced negative resistance. The maximum gain has increased by a factor of 1.14 over the resonant gain while the frequency of maximum gain is 0.96 of the resonant frequency. Subsequent analysis shows that when circuit Q increases, the frequency of maximum gain is closer to the resonant frequency.

The gain-bandwidth product is shown in Fig. 3.13 and is compared to the value given by Robinson in (3.21). Clearly the gain-bandwidth product increases with pump level. Also, the high gain assumption made by Robinson is shown to be quite good for the normal pump level chosen here, i.e., $S_1/S_0 = 0.35$. However Robinson's expression is normally not of much help in determining the gain-bandwidth product since the diode

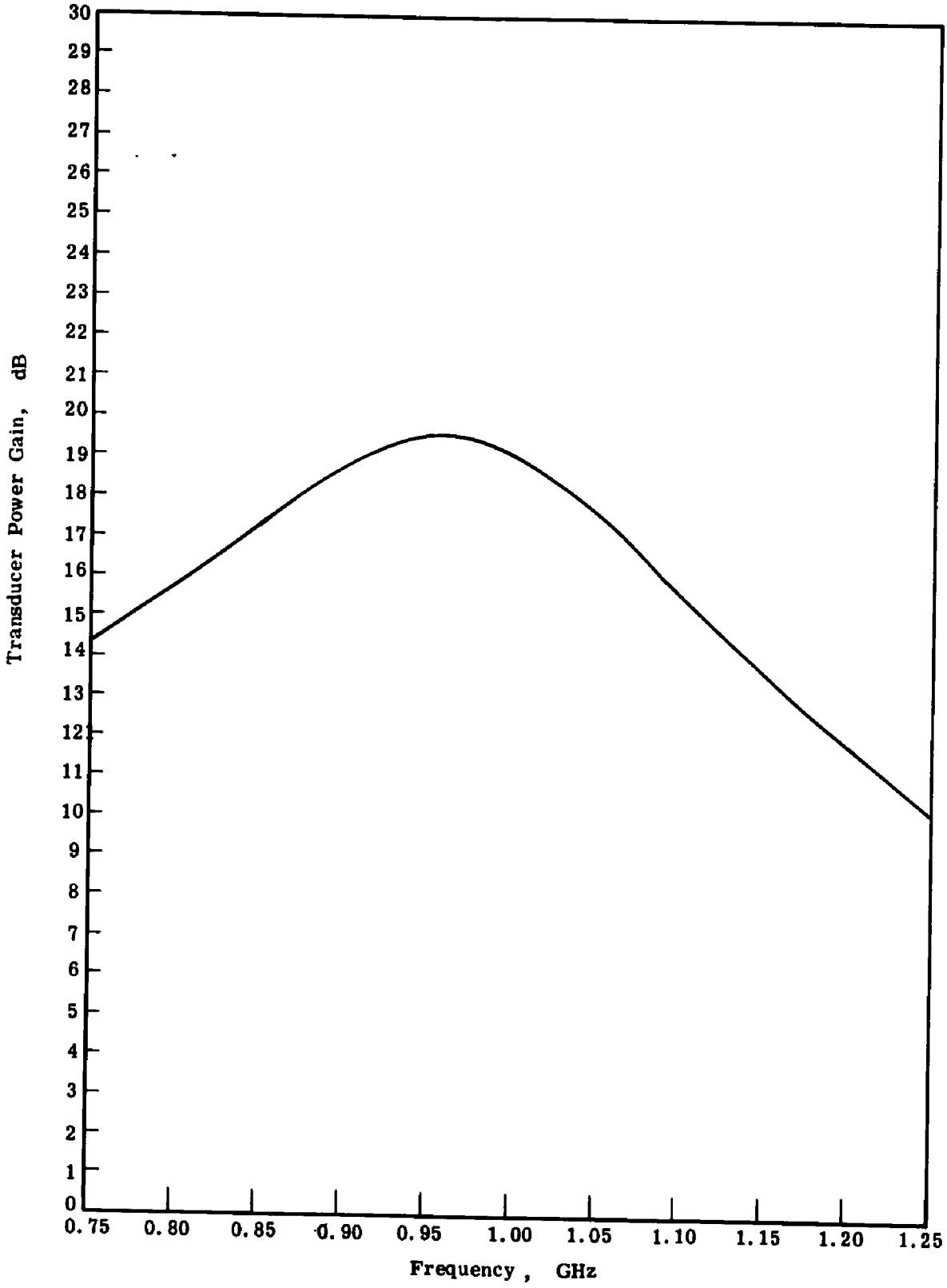


Fig. 3.12. LSUC transducer power gain with out-of-band circuits completely isolated and the diode has no parasitic elements

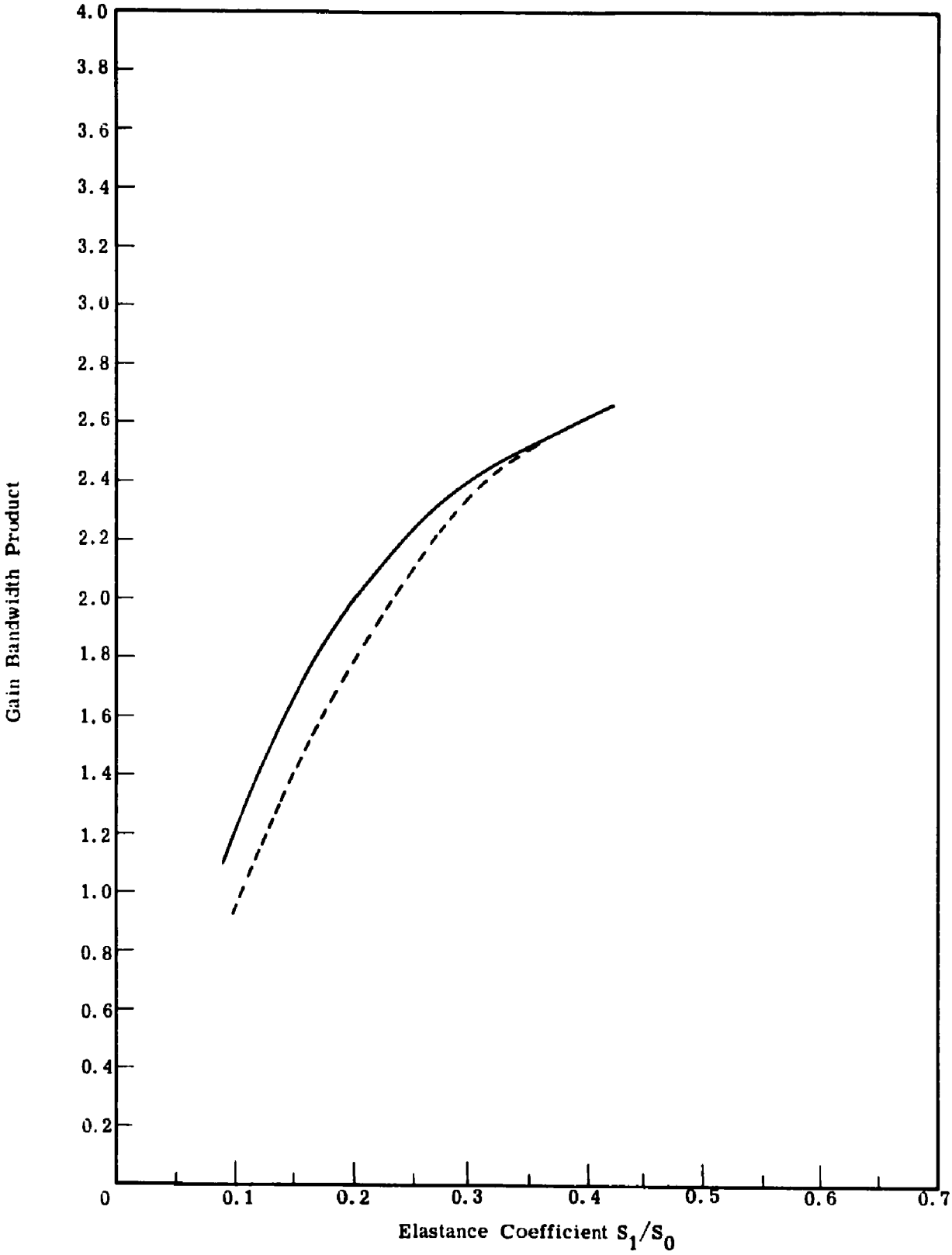


Fig. 3.13. Variation of gain-bandwidth product ($G^{\frac{1}{2}}w$) with pumping level when out-of-band circuits are completely isolated and there are no diode parasitics ———, and Robinson's gain-bandwidth formula – – – –

parasitic elements and complicated circuit arrangements seriously degrade upconverter bandwidth. Rather than trying to predict the gain-bandwidth product analytically, it is obtained by finding the half power points in the numerical gain curve.

In actual upconverter circuits using packaged diodes and frequency sensitive circuits the bandwidth and gain-bandwidth product is reduced considerably from that indicated in Figs. 3.12 and 3.13. Here only the effect of package parasitic elements is considered while in the following sections various external circuit arrangements are analyzed.

When the diode package shown in Section 3.4.1 is resonated by a single tuned circuit, the gain versus frequency and gain-bandwidth product are shown as the solid lines in Figs. 3.14 and 3.15 respectively. In particular the gain-bandwidth product has been reduced from 2.5 for the unpackaged diode to 0.19 for the "standard" packaged diode when it is pumped to give $S_1/S_0 = 0.35$. These curves also show that the bandwidth progressively increases when C_p is halved but L is the same, when L is halved but C_p is the same, and when both L and C_p are halved.

3.4.3 Comparison of Three circuit Designs Using Ideal Impedance Transformers. In each of the three LSUC circuits to be described here, the impedance presented by the signal port at all signal frequencies is a constant but is located a specified distance away from the diode. At the other frequencies, the signal port is assumed to be a short circuit at this same distance from the diode. Similarly the impedances presented by the lower sideband and pump ports are constant but are located specified distances away from the diode. Thus the frequency sensitivity of the upconverter model is caused by the line lengths and package parasitic elements.

The actual impedance presented by the signal and lower sideband ports (Z_t and Z_i respectively) are different from the desired R_g and R_ℓ. The impedances Z_t and Z_i must be chosen so that when they are combined with the reactances of the other two ports and the diode parasitic elements, the diode chip itself is presented with R_g at f_{10} and R_ℓ at f_{20}. The expressions for Z_t and Z_i as well as Z_{kk} for all three LSUC configurations are found in Appendix B.

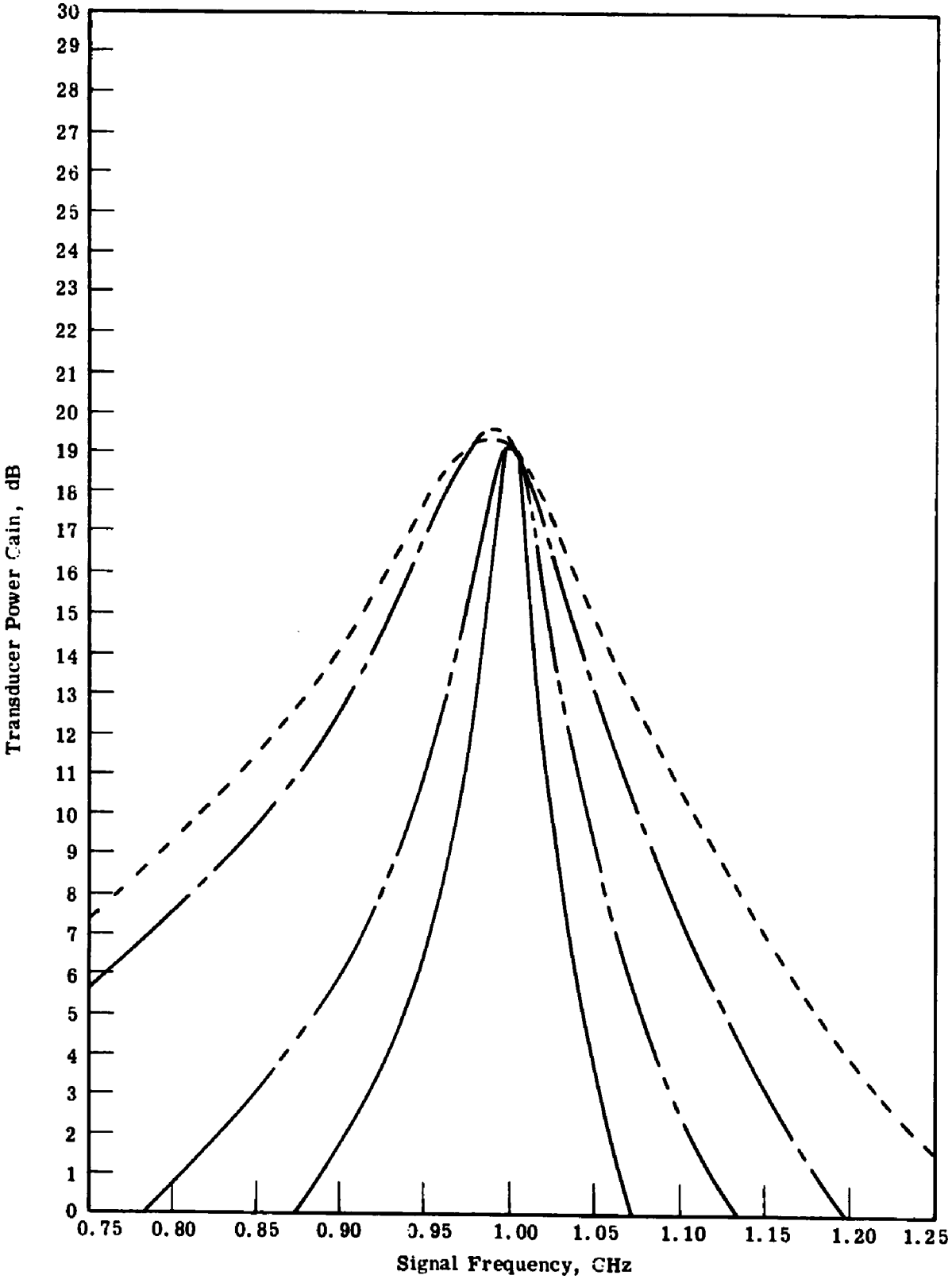


Fig. 3.14. LSUC transducer power gain with out-of-band circuits completely isolated where the diode parasitic elements are as follows: L = 2 nH and $S_p = 2.856\ 10^{12}\ F^{-1}$ ——— — — ———, L = 1 nH and $S_p = 1.428\ 10^{12}\ F^{-1}$ ——— — ———, L = 1 nH and $S_p = 2.856\ 10^{12}\ F^{-1}$ -----

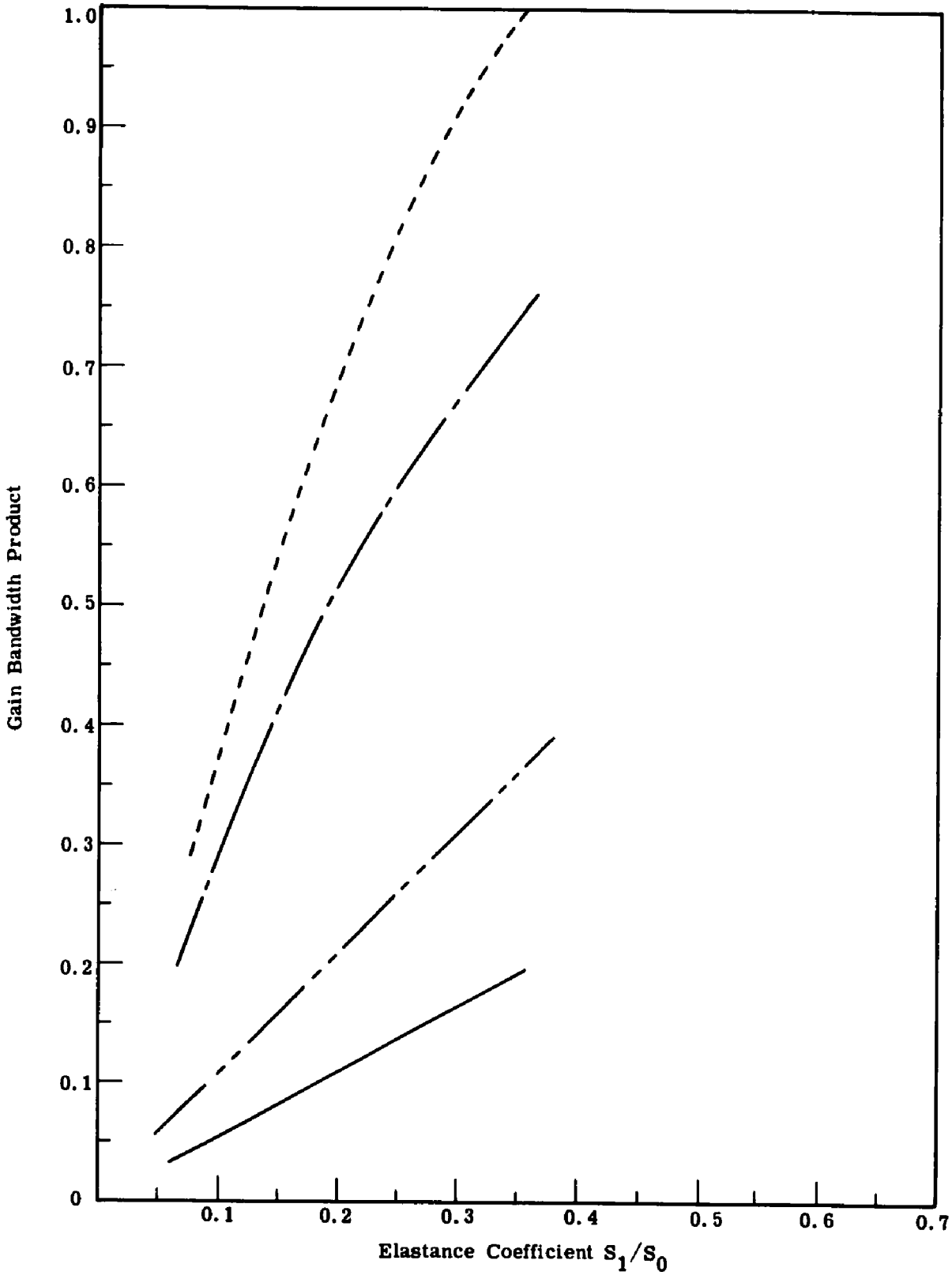


Fig. 3.15. LSUC gain-bandwidth product ($G^{\frac{1}{2}}w$) with out-of-band circuits completely isolated from one another where the diode parasitic elements are as follows: L = 2nH and $S_p = 1.428\ 10^{12}\ F^{-1}$ ——, L = 2nH and $S_p = 2.856\ 10^{12}\ F^{-1}$ — — —, L = 1nH and $S_p = 2.856\ 10^{12}\ F^{-1}$ ------

The various circuit distances from the diode can be specified so that the up-converter bandwidth is optimized. However since the gain expression for these circuits is complicated, the optimization must be done numerically. The approximate technique used here is based on the assumption that the overall bandwidth is limited by the impedance at the signal frequency. For a given LSUC circuit configuration, diode model, and signal filter to diode distance, a search is made for the pump and lower sideband port distances which minimize the "slope function"

$$\sqrt{\left(\frac{dR_{11}}{d\omega}\right)^2 + \left(\frac{dX_{11}}{d\omega}\right)^2} \quad . \tag{3.47}$$

The procedure begins by choosing trial pump and lower sideband distances. Then Z_t is found which is located at the plane of the signal filter. The impedance Z_{11} is calculated at two closely spaced frequencies and the above slope function is obtained. The process is repeated for various pump and lower sideband distances until the minimum value for (3.47) is found. The approximate optimum distances are shown in Table 3.2 for the four cases when the signal port distances are $\lambda_s/4$ and $\lambda_p/4$, and when two values for diode inductance are used. These distances are used in the subsequent analysis.

	LSUC1		LSUC2		LSUC3	
	LSB Dist.	Pump Dist.	LSB Dist.	Pump Dist.	LSB Dist.	Pump Dist.
Signal Dist. $=\lambda_s/4$ L = 2 nH	6.3 or 6.0	6.0 or 6.3	4.8	4.8	3.9	4.2
Signal Dist. $=\lambda_p/4$ L = 2 nH	5.7	5.7	1.5*	1.5*	4.5	1.8
Signal Dist. $=\lambda_s/4$ L = 0.2203 nH	6.3 or 6.0	6.0 or 6.3	4.8	4.8	4.5	3.0
Signal Dist. $=\lambda_p/4$ L = 0.2203 nH	5.7	5.7	1.5*	1.5*	4.8	1.5

Table 3.2 Distances in cm between the diode and lower sideband (LSB) or pump filters. The * values are not true minima as the slope in these cases is monotonically increasing

When the standard diode model of Section 3.4.1 is used (i.e. L = 2 nH) and the signal port is $\lambda_s/4$ away from the diode, the transducer power gain for the three circuits is shown in Fig. 3.16. In these calculations a 5 x 5 matrix approximation is used (signal frequency plus four sideband frequencies), and the pump modulation coefficient is $S_1/S_0 = 0.35$. In each of these circuits the maximum gain occurs at resonance rather than at a frequency lower than resonance as was found in circuits containing less reactance (Figs. 3.6 and 3.8). Evidently the frequency sensitivity of the circuit masks the asymmetry of the negative resistance. The bandwidth of LSUC3 is larger than that for LSUC2 since the assumption of a nonideal junction in LSUC3 eliminates the frequency sensitivity of the signal port at the lower sideband frequency.

When the gain is calculated there is only one applied voltage. This means a complete inversion of the impedance matrix is unnecessary. However, for noise calculations there are noise voltages at all the relevant frequencies, and thus in this case a complete matrix inversion is necessary. Although this impedance matrix is complex, it can be separated into its real and imaginary parts and manipulated as two real matrices (Ref.44). If the matrix is $C = A + jB$, then

$$C^{-1} = D - jDBA^{-1}$$

where

$$D = (A + BA^{-1}B)^{-1} \quad .$$

Thus a computer program which inverts real matrices can be used to invert complex matrices. A program using this technique called CMINV, is listed in Appendix A. This technique was applied in calculating the noise figure from (3.23) to obtain the plot of noise figure in Fig. 3.17 for the 5 x 5 matrix approximation. These curves again show the inverse relationship between noise figure and gain.

The gain-bandwidth product is defined as the square root of the maximum transducer power gain multiplied by the fractional bandwidth

$$w = \frac{f_b - f_a}{f_{max}}$$

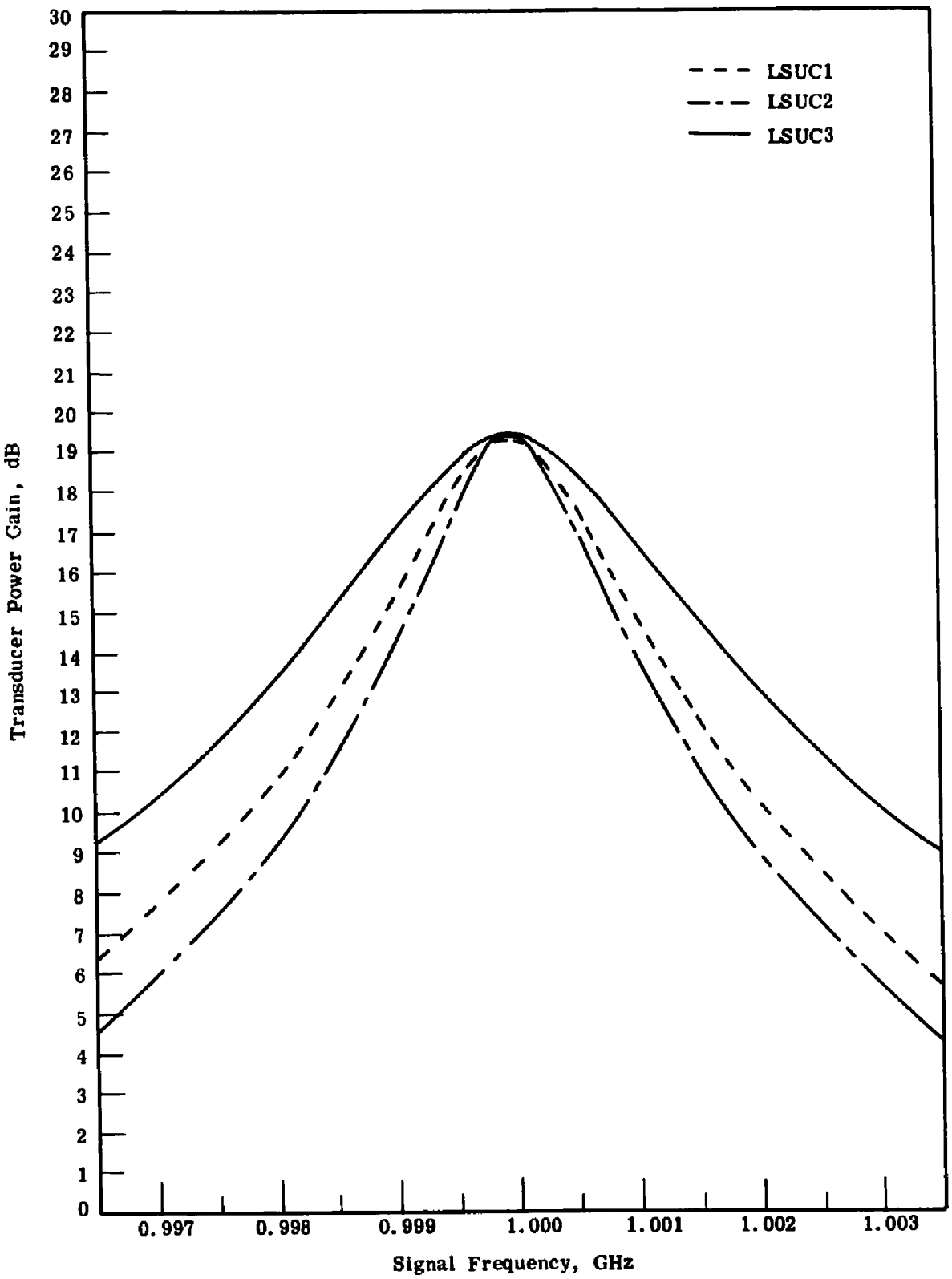


Fig. 3.16. Transducer power gain for the three LSUC circuits when ideal impedance matching circuits and the 5 x 5 matrix approximation are used

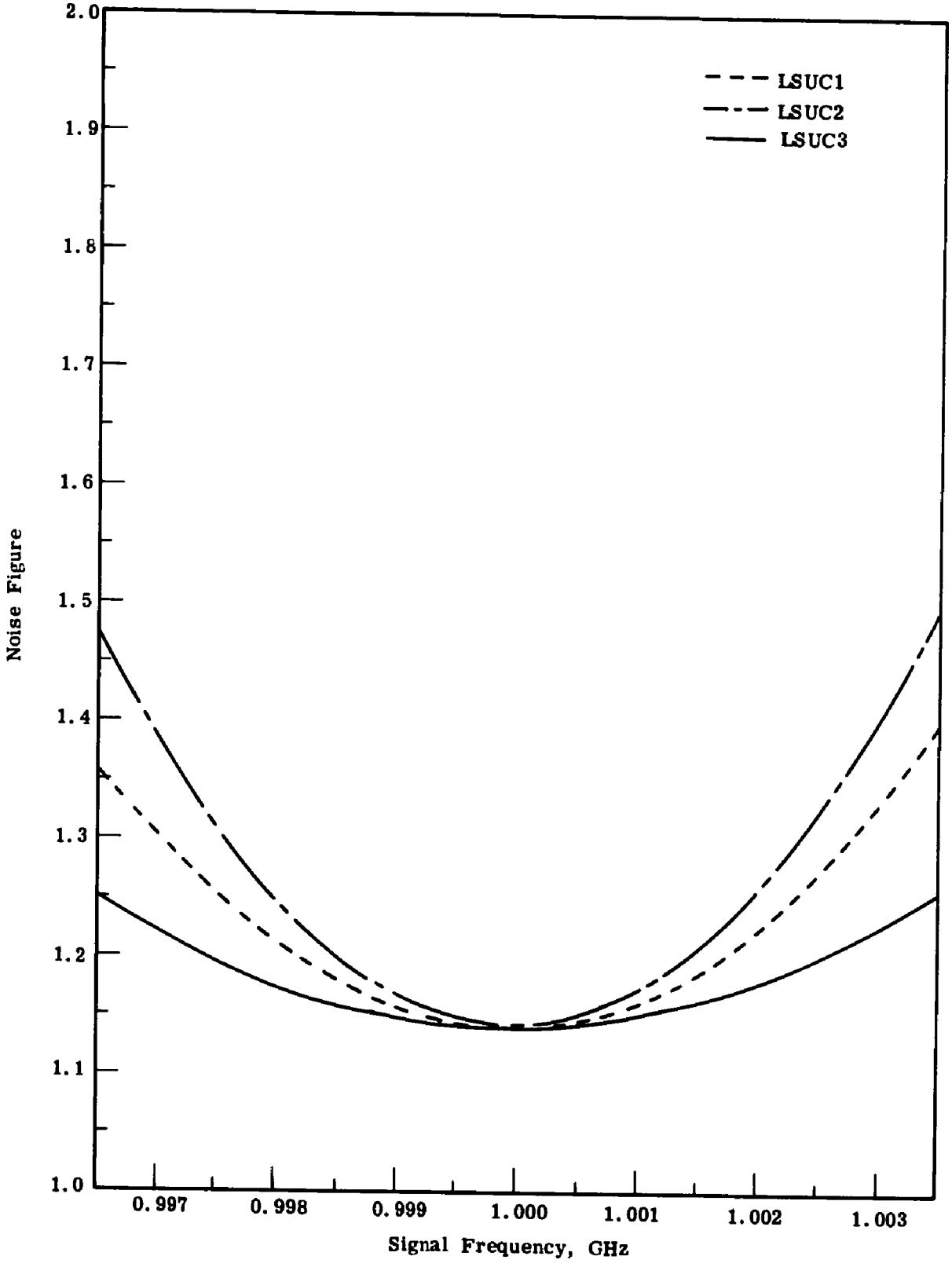


Fig. 3.17. Noise figure for the three LSUC circuits when ideal impedance matching circuits and the 5 x 5 matrix approximation are used

where f_{max} is the frequency of maximum gain and f_a, f_b are the half power frequencies. The gain-bandwidth product is shown in Fig. 3.18 for the standard diode model of Section 3.4.1 and in Fig. 3.19 when the diode series inductance is reduced to 0.2203 nH where the diode is series resonant at the lower sideband frequency. The gain-bandwidth product is plotted as a function of the elastance modulation coefficient. Since the maximum gains for all three circuits are almost the same (Fig. 3.10) the gain-bandwidth product for LSUC3 is larger than that for the other two circuits when the standard diode model is used.

3.4.4 Effect of Signal Circuit Length. Shortening the signal circuit length and finding the corresponding approximate optimum lower sideband and pump port distances in the LSUC, increases the gain-bandwidth product. The curves of Figs. 3.18 and 3.19 show that when $S_1/S_0 = 0.35$ the gain-bandwidth product increases by a factor between 1.22 and 1.64 depending on the diode inductance, when the signal port distance is decreased from $\lambda_s/4$ to $\lambda_p/4$. Contrary to what is expected the gain-bandwidth product for LSUC2 decreases rather than increases. The reason for this behavior is unclear, but it may be related to the lack of a minimum in the "slope function" (3.47) for LSUC2 when the signal port distance is $\lambda_p/4$. The impedance slope for this case monotonically increases with pump and lower sideband distances, so that the values used in Table 3.2 are actually the minimum practical distances.

3.4.5 Effect of Diode Parasitic Inductance. The diode parasitic element values were seen to have a major effect on the LSUC where the three circuit ports were completely isolated from one another (Figs. 3.14 and 3.15). For the three circuits discussed here, if the diode series inductance is reduced from 2 nH to 0.2203 nH so that the diode is series resonant at f_{20}, the gain-bandwidth curves are significantly changed. Comparison of Figs. 3.18 and 3.19 shows that each LSUC circuit has a larger gain-bandwidth product when the diode parasitic inductance is decreased. The largest increase occurs with the LSUC1 where the gain-bandwidth product increases by a factor between 15.3 and 18 depending on the choice of signal circuit. The curve in Fig. 3.20 shows explicitly the effect of diode inductance on LSUC1 when the signal port distance is $\lambda_s/4$. Similar curves for LSUC2 and LSUC3 are difficult to obtain because the optimum pump and lower sideband port distances change when the diode model changes.

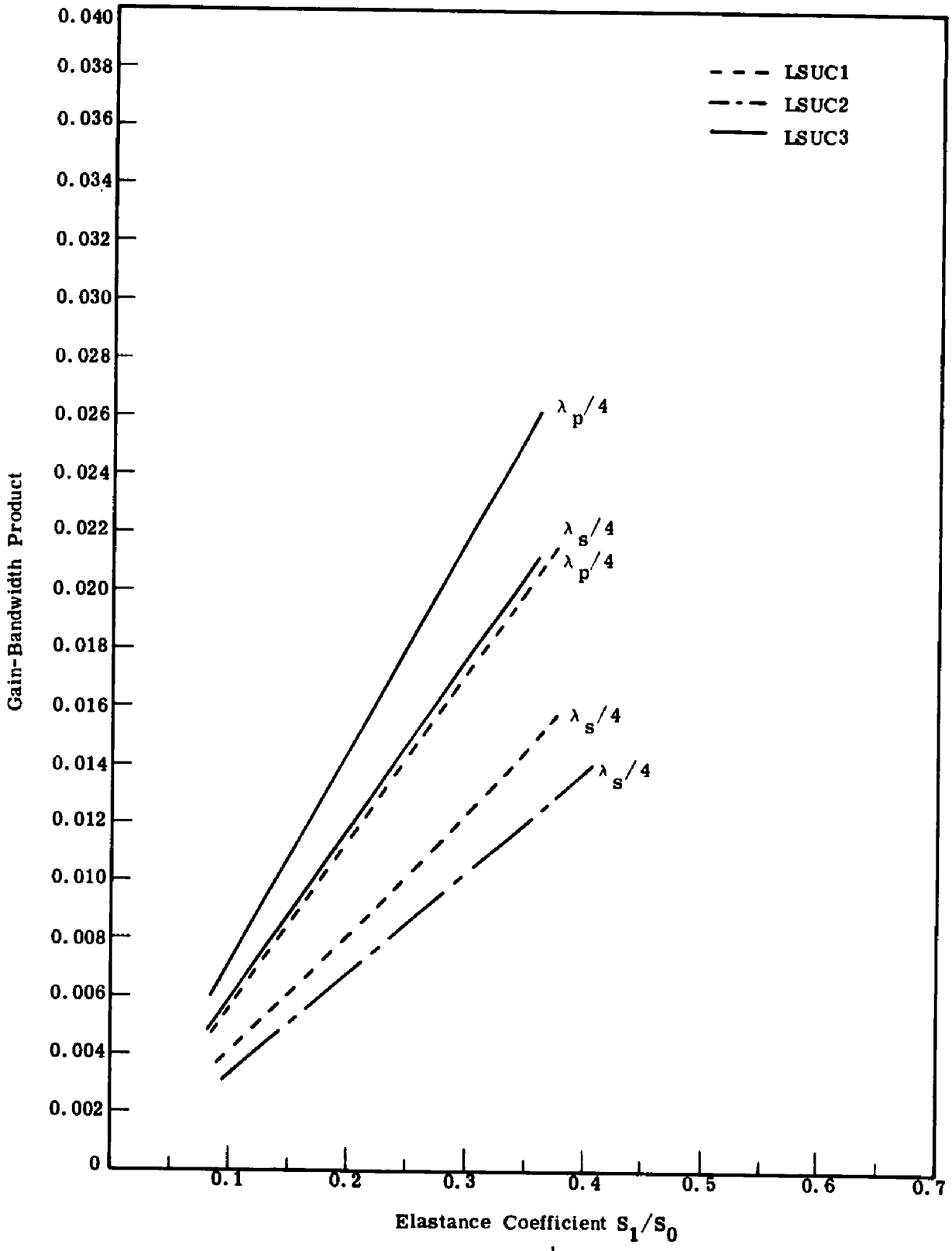


Fig. 3.18. Variation of gain-bandwidth product ($G^{\frac{1}{2}}w$) versus pumping level with signal circuit distance as a parameter, using ideal impedance matching circuits, the 5 x 5 matrix approximation, and standard diode inductance of 2 nH

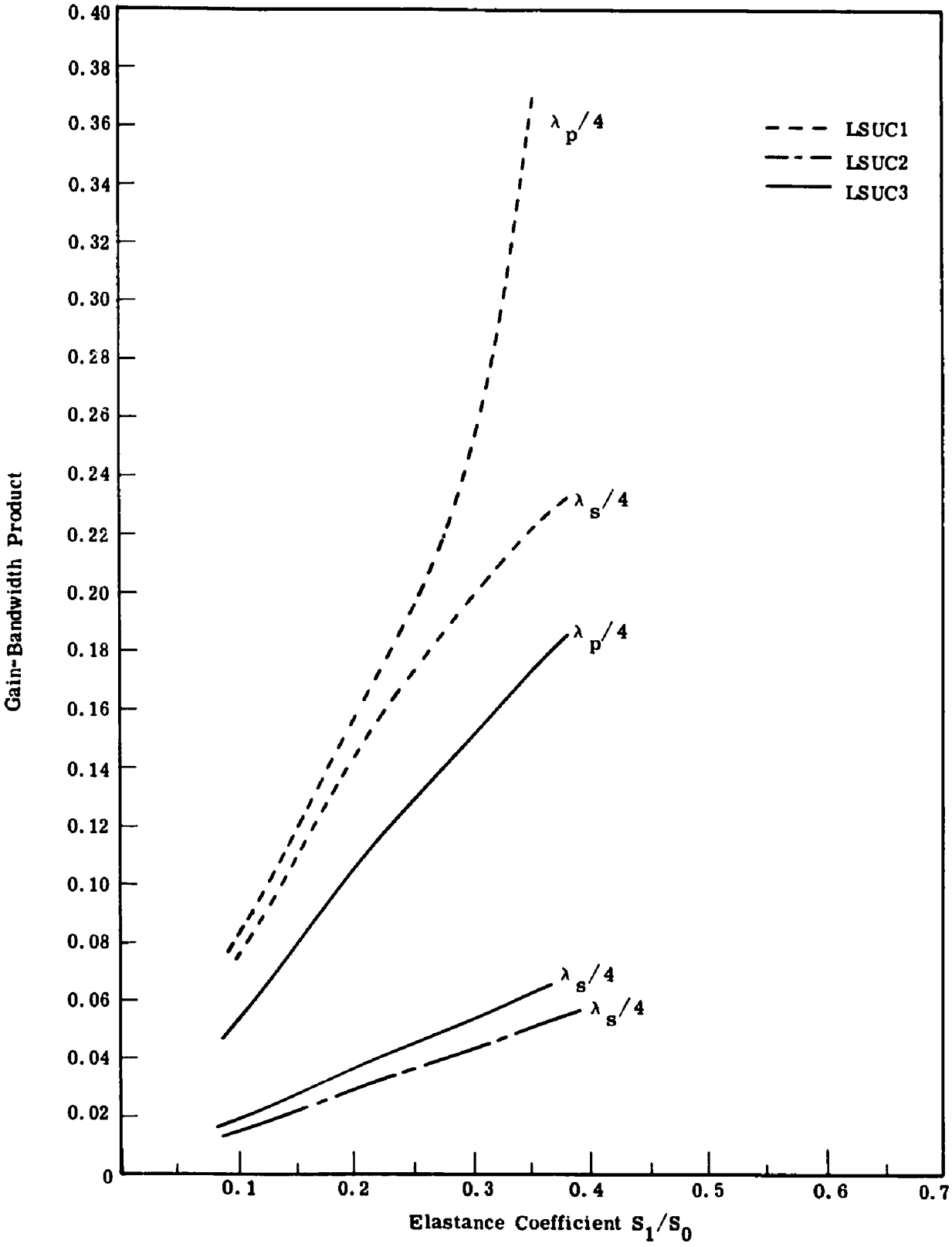


Fig. 3.19. Variation of gain bandwidth product ($G^{\frac{1}{2}}w$) versus pumping level with signal circuit distance as a parameter, using ideal impedance matching circuits, the 5 x 5 matrix approximation, and a diode package inductance of 0.2203 nH

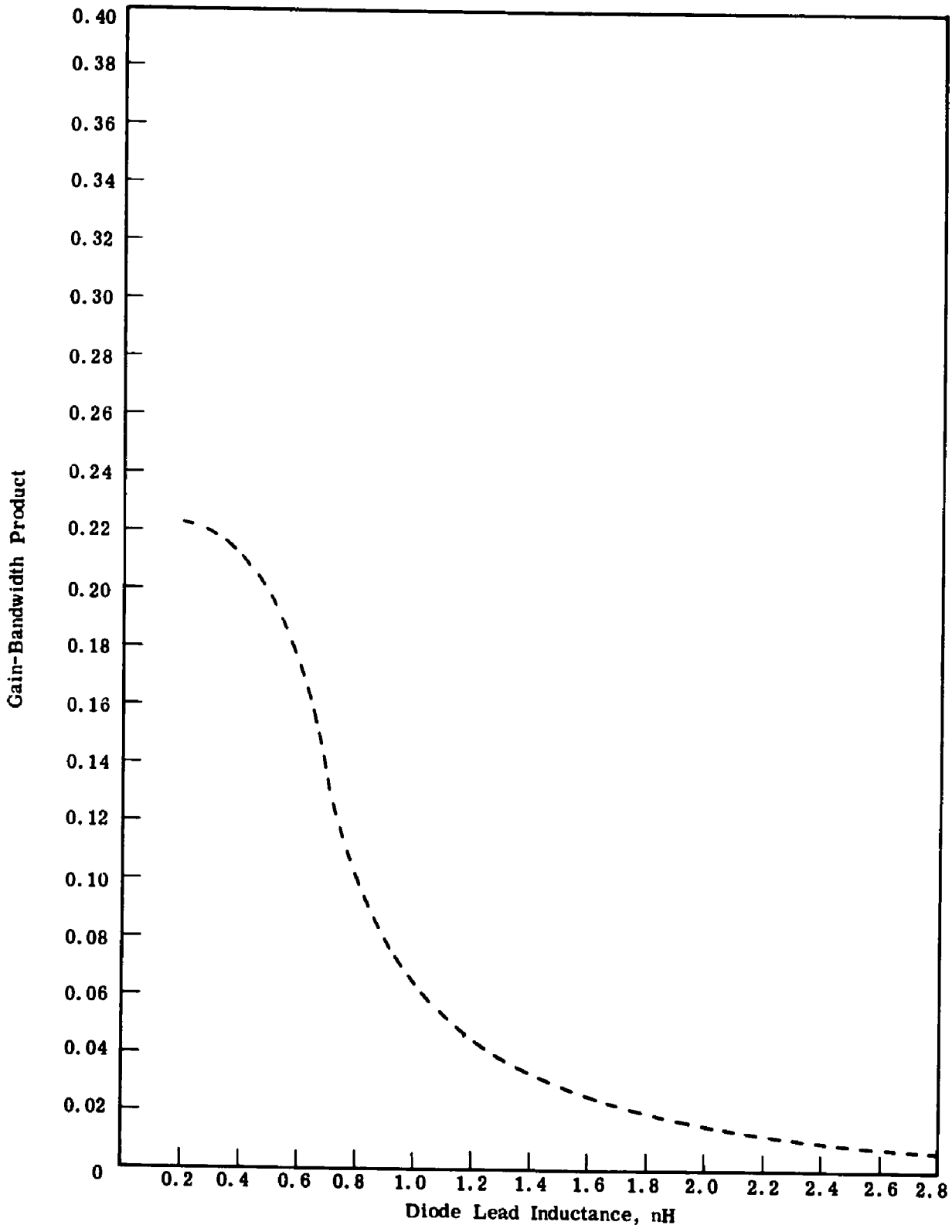


Fig. 3.20. Variation of gain-bandwidth product ($G^{\frac{1}{2}}w$) with diode package inductance for LSUC1, using the 5 x 5 matrix approximation and a signal port distance of $\lambda_g/4$

3.4.6 Effect of Shunt-Stub Tuners. Two common impedance matching mechanisms are the single-stub and double-stub tuners. In this section a comparison is made between the ideal impedance matching elements used previously and these two types of tuners.

The single-stub tuner can match any impedance by choosing the proper stub position and stub length. The double-stub tuner can match a given range of impedances which is dependent on the distance between the two stubs. In the numerical work, a stub distance of $\lambda/8$ at the center of the respective passband frequencies is used as this usually provides an adequate matching range. These tuners are placed at least the distance given in Table 3.2 away from the diode. At out-of-band frequencies the ideal filters which act as short-circuits are located the distance specified in Table 3.2 away from the diode.

The change in the gain-bandwidth product is negligible when the ideal matching circuits are replaced by either single-stub or double-stub tuners. The largest deviation occurs with the LSUC3 circuit where the single-stub tuner degrades the gain-bandwidth product by only 8.9 percent. The double-stub tuners failed to provide the required matching in LSUC1, but by changing the pump and lower sideband port distances a circuit was found in which the double-stub tuners work. In this revised LSUC1 circuit, the gain-bandwidth product is degraded much less than 8.9 percent when the double-stub tuners are used in place of ideal matching circuits.

3.4.7 Conclusions on the Use of the Three LSUC Configurations. The results of the previous sections are briefly summarized in Table 3.3 where each value uses the approximate optimum lower sideband and pump port distances shown in Table 3.2. For the diode and frequencies used here, LSUC3 provided the best performance for all cases except one.

The best value in Table 3.3 however still falls short of the maximum obtainable gain-bandwidth product for the unpackaged diode (Fig. 3.13) by a factor of 7. Therefore, even though the simple theory presented in Section 3.2 is useful for designing LSUC's an analysis similar to that presented here in Section 3.4 is still needed to evaluate final upconverter performance.

Circuit	Ideal Circuits				L = 2 nH Signal Dist. = $\lambda_s/4$	
	Signal Dist. = $\lambda_s/4$		Signal Dist. = $\lambda_p/4$		Single-stub Tuner	Double-Stub Tuner
	L = 2nH	L = 0.2203 nH	L = 2nH	L = 0.2203 nH		
LSUC1	0.01446	0.2205	0.02037	0.3616	0.01357	———
LSUC2	0.01201	0.0511	small	small	0.01190	0.01184
LSUC3	0.02090	0.06203	0.02558	0.1733	0.01905	0.02102

Table 3.3. Gain-bandwidth product when $S_1/S_0 = 0.35$

In practical situations, the choice of a circuit configuration is often dictated by criteria such as the frequencies involved or the type of transmission line that is to be used. The LSUC1 structure would probably not be useful in a coaxial tee or wye junction, because the diode would have to be mounted between the center and outer conductors. The fields surrounding the diode would be distorted in some unknown manner, making an analytical design difficult. However, analysis of this structure is performed because of the light it sheds on the circuit in which the diode is mounted between the two conductors in a microstrip tee or wye junction. Here a reasonable approximation could be made of the field configuration around the shunt mounted diode.

The LSUC2 design is the obvious solution to the field distortion problem associated with a shunt mounted diode in a coaxial tee junction. Although an experimental LSUC was designed and built using this approach, several empirical modifications were required to obtain satisfactory operation. This deficiency is a result of the nonideal tee junction characteristics.

The LSUC3 design attempts to use the nonideal tee junction characteristics advantageously. Table 3.3 shows that the gain-bandwidth product for this design is superior to the LSUC2 design, as well as being the most practical in a coaxial system.

3.5 LSUC Design with Coaxial Band-pass Impedance Matching Circuits

In the previous sections the three LSUC circuits studied used ideal filters and either ideal impedance matching circuits or shunt-stub tuners. In the following sections these three LSUC configurations are investigated using the physically realizable coaxial

impedance matching transformers developed in Chapter II. These filter networks provide both the filtering and impedance matching functions and thereby replace the tuner and ideal filter used in the earlier models. The "standard" diode model described in Section 3. 4. 1, is used throughout the following discussion although the element values are sometimes changed. General design rules applicable to all three LSUC circuits are outlined in Section 3. 5. 1. The subsequent sections describe the individual design methods needed for each circuit configuration.

3. 5. 1 General Design Procedure for the Three LSUC Circuits. In designing each of the three LSUC's the pump circuit is designed first, then the lower sideband circuit, and finally the signal circuit. The design method described here does not use an iterative process so each circuit is designed independent of the other two. In the first two LSUC circuits described, this assumption means that ideal band-stop filters are needed. However, the third circuit, LSUC3, does not use any ideal band-stop filters but uses realizable distributed elements only.

3. 5. 1. 1 Pump Circuit. The pump circuit is designed first because, of the three, it is the least critical to the LSUC operation. The basic problem is to transfer power at the pump frequency to power at the signal and lower sideband frequencies. If the varactor were lossless, the power at ω_p, which is converted to power at ω_1, can be modeled by the resistance induced into the pump circuit by the signal voltage. Even in a lossy varactor, pump power must be "absorbed" in this induced resistance in order to produce parametric gain.

Perlman and Bossard (Ref. 45) obtained an approximate expression for this induced resistance when all voltages at frequencies $> f_2$ were shorted. Since the open circuit assumption has been used here, an approximate expression for the induced resistance when all currents at frequencies $> f_2$ are open circuited is given here. The varactor elastance as a function of stored chrage is

$$S(Q) = S(0)\left[1 - \frac{(1-\gamma)S(0)Q}{\phi_v}\right]^{\frac{\gamma}{1-\gamma}} \tag{3.48}$$

$$= S(0) + \sigma_1 Q + \sigma_2 Q^2 + \ldots \tag{3.49}$$

where

$$\sigma_1 = \left.\frac{dS}{dQ}\right|_{Q_0} = -\frac{S(0)^2\gamma}{\phi_v}\left[1 - \frac{(1-\gamma)S(0)Q_0}{\phi_v}\right]^{\frac{2\gamma}{1-\gamma}} .$$

The approximate voltage across the varactor is

$$V = [S(0) + \sigma_1 Q]Q .$$

If the charge is given by

$$Q = 2Q_p \cos(\omega_p t) + 2Q_1 \cos(\omega_1 t) + 2Q_2 \cos(\omega_2 t + \psi_2)$$

and assuming $S(0)Q$ can be resonated, the voltages at ω_p, ω_{10}, and ω_{20} are

$$V_p = 2\sigma_1 Q_1 Q_2 \tag{3.50}$$

$$V_1 = 2\sigma_1 Q_2^* Q_p \tag{3.51}$$

$$V_2 = 2\sigma_1 Q_1^* Q_p \tag{3.52}$$

where these voltages and charges are coefficients of $e^{j\omega t}$. Manipulation of these expressions give

$$R_{ind} = \frac{V_p}{i_p} = \frac{4\sigma_1^2 |Q_1|^2}{\omega_{20}\omega_p R_\ell} . \tag{3.53}$$

In a typical LSUC where f_p = 9.500 GHz, f_{20} = 8.500 GHz, R_ℓ = 3.1 ohms, $\gamma = 1/3$, ϕ_v = 0.7 volts, and $S(0) = 10^{12}\ F^{-1}$, the induced resistance is 4×10^{-8} ohms when $V_1 = 20\ \mu V$ and 1 ohm when $V_1 = 98$ mV.

If the pump circuit were as shown in Fig. 3.21a, it would be unnecessary to match to R_{ind}. In fact the smaller the pump source resistance, the more power there is available to the induced resistance. If however there is an ideal impedance transformer between R_{ind} and the pump source (Fig. 3.21b), then the power delivered to R_{ind} is

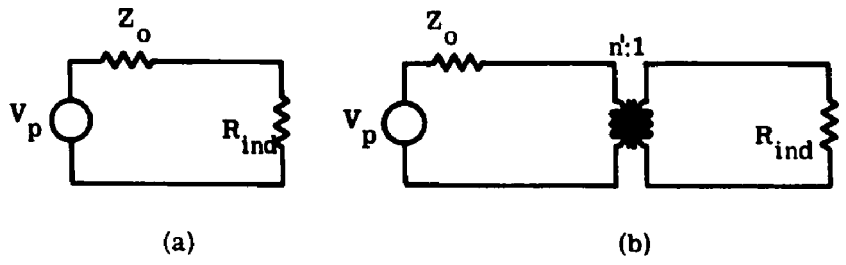


Fig. 3.21. Pump circuit without (a) and with (b) ideal transformer

$$P = \frac{n'^2 R_{ind} V_p^2}{(n'^2 R_{ind} + Z_o)^2} \quad .$$

This is maximized with respect to the transformer ratio n' when $R_{ind} = Z_o / n'^2$. As noted above, R_{ind} is usually too small to be matched with available microwave impedance transformers, so a value of one ohm is used as the transformed pump source resistance.

The design of the pump impedance transformer is based on the load being the varactor diode model including the parasitic elements (Fig. 3.11) in which R_s is replaced by the one ohm resistor and the average elastance S_0 is used. The resonated load Q_c at f_p needed for the filter design procedure is obtained, and with the desired fractional bandwidth, which in this case can be fairly narrow, the decrement $\delta = 1/(wQ_c)$ can be found. From δ the low-pass prototype g values and the K values for the impedance inverters are found (Fig. 2.8). The impedance transforming network is then designed using the distributed design procedure.

3.5.1.2 Lower Sideband Circuit. The lower sideband circuit is designed so that the impedance presented to the diode variable elastance at the center of the lower sideband frequency band, f_{20}, is $R_\ell + R_s$. The external circuit impedance is found by substituting the load resistance R_ℓ for R_s in the diode equivalent circuit (Fig. 3.11) and resonating this circuit at f_{20}. In the LSUC1 and LSUC2 circuits this modified diode is resonated with two external circuit elements, while in the LSUC3 circuit the diode is resonated with only one external circuit element.

In the first two configurations the package capacitance is resonated by a shunt inductive reactance. This reactance is provided by adjusting the distance between the end of the pump circuit and the diode. Since f_{20} is an out-of-band frequency, the impedance of the pump circuit is almost entirely reactive. Using this approximation the angular distance between the pump circuit and the diode is readily obtained from the transmission line equation:

$$\theta_p = \text{Arctan}\left\{\frac{Z_o[X - X_p(\omega_{20})]}{[Z_o^2 + X \cdot X_p(\omega_{20})]}\right\} \tag{3.54}$$

where

$$X = +\frac{1}{\omega_{20}C_p} \quad .$$

Although this procedure will change the impedance presented to the diode at f_p, pump power can be increased to overcome the additional mismatch. The actual resulting pump port impedance is obtained later for the LSUC3.

The remaining diode reactance, which at these frequencies is inductive, is resonated by a semilumped series capacitance placed $\lambda_{p-s}/2$ away from the diode in the lower sideband port. The signal port impedance is eliminated from consideration by using ideal band-stop filters at f_{20} making $Z_s(f_{20}) = \infty$ for LSUC1 and $Z_s(f_{20}) = 0$ for LSUC2. The diode now being resonated, the lower sideband band-pass impedance transformer can be designed using methods discussed in Chapter II.

A slightly different method is used in the LSUC3 design. Here the total reactance of the diode (not just $-\frac{1}{\omega_{20}C_p}$) is resonated by adjusting the pump circuit to diode distance. This procedure is practical when the diode parasitic reactances transform the R_f to a value that can be easily matched. It will be shown later that the condition $Z_s(f_{20}) = \infty$ can be obtained without using ideal band-stop filters, so the signal port need not be considered in the lower sideband port design. Having resonated the diode, the lower sideband circuit is designed as before.

3.5.1.3 Signal Circuit. The signal circuit is designed so that the impedance presented to the diode variable elastance is $R_g + R_s$ at the center of the signal frequency

band f_{10}. The design of this circuit differs from the procedures used on the other two ports for two reasons: (1) f_{10} is the comparatively low frequency of 1 GHz, and (2) R_g is a relatively large value between 100 and 150 ohms. The low signal frequency implies that a filter consisting of a series of impedance inverters separated by half wavelengths of line would be impractically long. A better method is to use either alternate K and J inverters separated by $\lambda/4$ lengths of line or to use a low-pass Chebyshev matching network (Ref. 46) based on semilumped inductors and capacitors.

The relatively large value of R_g means that when R_s is replaced by R_g in the diode model (Fig. 3.11), the resulting impedance can be easily resonated by simply inserting a length of transmission line between the diode and the signal circuit. This approach differs from that used for the lower sideband circuit where an external reactance was used to resonate the diode.

The procedure for designing the signal circuit begins with obtaining the diode impedance $Z_d = R_d + jX_d$ as shown in Fig. 3.22.

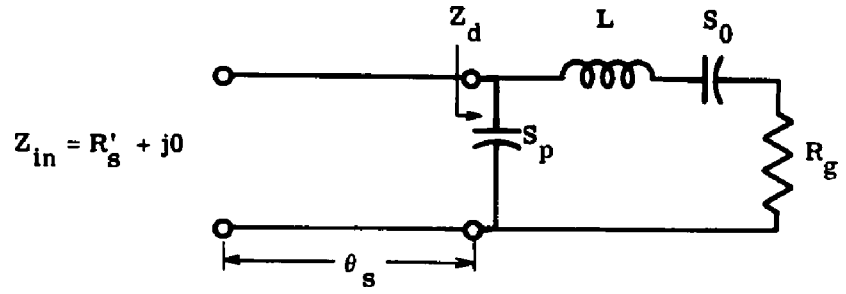


Fig. 3.22. Circuit model used to design the signal circuit

The diode impedance Z_d seen a distance θ away from the diode terminals is

$$Z_{in} = \frac{R_d Z_o^2(1 + \tan^2\theta) + jZ_o[(Z_o^2 - R_d^2 - X_d^2)\tan\theta + Z_o X_d(1 - \tan^2\theta)]}{(Z_o - X_d \tan\theta)^2 + (R_d \tan\theta)^2}$$

The distance $\theta = \theta_s$ where Z_{in} is resonate is

$$\tan\theta_s = \frac{Z_o^2 - R_d^2 - X_d^2}{2Z_o X_d} \pm \sqrt{\frac{Z_o^2 - R_d^2 - X_d^2}{2Z_o X_d} + 1} \qquad (3.55)$$

and the corresponding input resistance at the signal frequency is

$$R'_s = \frac{R_d Z_o^2 (1 + \tan^2 \theta_s)}{(Z_o - X_d \tan \theta_s)^2 + (R_d \tan \theta_s)^2} \quad . \tag{3.56}$$

Once θ_s is known, R'_s can be found. The two values of θ_s in (3.55) are a quarter wavelength apart. The value of θ_s which gives $R'_s \leq Z_o$ is the value chosen in the designs used here. When the values for the diode model of Section 3.4.1 and $R_g = 100$ ohms are used, the resulting $R'_s = 11.48$ ohms and $\theta_s = 1.108$ radians or 5.38 cm at 1.000 GHz. This value of R'_s can be easily matched with either the band-pass or low-pass impedance matching circuits.

In designing the signal circuit, it was assumed that the lower sideband and pump circuits could be ignored. This means that at f_{10} $Z_p = Z_{p-s} = \infty$ for LSUC1, $Z_p \,||\, Z_{p-s} = 0$ for LSUC2, and $Z_p = \infty$, $Z_{p-s} = 0$ for LSUC3. Appropriately placed band-stop filters in these two out-of-band ports is an impractical method for obtaining these impedances because of the large size of the filters. However in Chapter II it was shown that the coaxial band-pass filters will pass low frequencies. This means that the positions of high-pass filters at the input of the pump port and at the output of the lower sideband port could be adjusted to provide the desired impedances at f_{10}. Since both the pump and lower sideband frequencies are in X-band, these high-pass filters can be realized simply as X-band coax-to-waveguide adapters.

3.5.2 Special Design Considerations for LSUC1. The LSUC1 circuit was designed and analyzed using the band-pass circuit in the signal port. Fortuitously the signal circuit reactance at f_{20} is large, so the ideal band-stop filter in the signal circuit is not used. The resulting gain curve (Fig. 3.23) shows this circuit has a bandwidth of approximately 4 MHz.

3.5.3 Special Design Considerations for LSUC2. For LSUC2 the circuit represented in Fig. 3.10b must be designed so that (1) pump power can get into the diode $Z_{p-s}(\omega_p) = \infty$ and $Z_s(\omega_p) = 0$, (2) signal power can get into the diode $Z_p(\omega_{10}) \,||\, Z_{p-s}(\omega_{10}) = 0$, (3) lower sideband power can leave through the lower sideband circuit

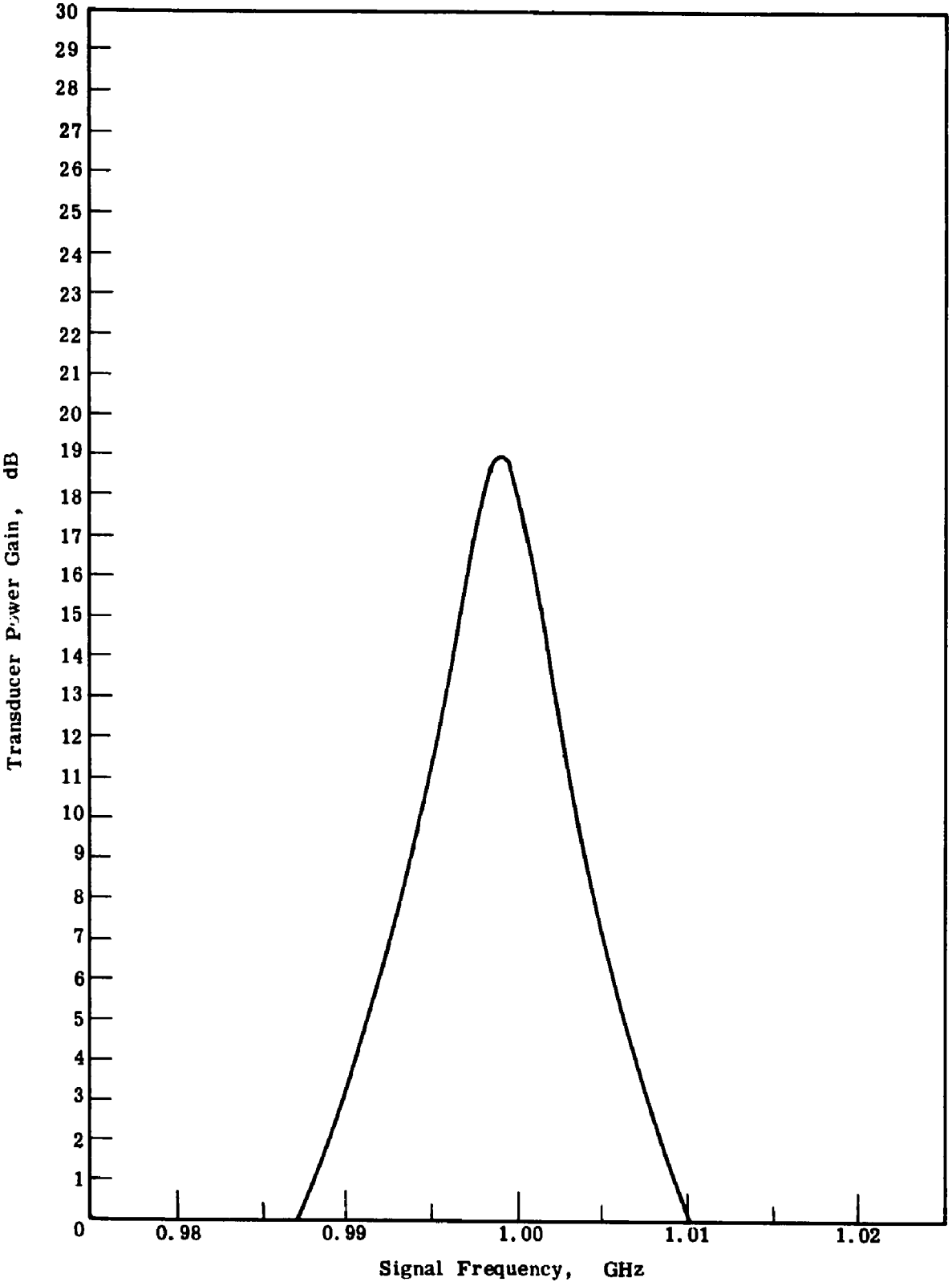


Fig. 3.23. Gain of LSUC when all filters in parallel with one another

$Z_s(\omega_{20}) = 0$, $Z_p(\omega_{20}) = \infty$, and (4) the impedance seen by the voltage dependent capacitance at f_{10} is $R_g + R_s$ and at f_{20} is $R_\ell + R_s$.

No special consideration is given to requirement (1) since the amount of pump power can be changed to compensate for mismatch. If this assumption is unwarranted, additional band-stop filters may be needed to fulfill condition (1) more closely. Condition (2) is fulfilled by using the high-pass filters external to the pump and lower sideband ports. As for condition (3), $Z_s(\omega_{20}) = 0$ is accomplished by placing a band-stop filter $\lambda_{p-s}/4$ away from the diode in the signal port, and $Z_p(\omega_{20}) = \infty$ is accomplished by resonating the diode package capacitance with the pump circuit.

3.5.3.1 LSUC2 with the Low-pass Signal Matching Circuit. The signal circuit used in this model is a pseudo low-pass matching network described by Matthaei (Ref. 46). The circuit chosen for this LSUC is a 10 pole Chebyshev network which requires 5 shunt capacitors and 5 series inductors. They can be realized as coaxial disks and No. 20 wire (0.03196 in. dia.) respectively, and the resulting network is less than 2 inches long. The complete LSUC2 circuit is shown in Fig. 3.24. From the numerical analysis shown in Fig. 3.25 the bandwidth for the diode of Section 3.4.1 is only 9.0 MHz. It is evident from Fig. 3.25 that the diode parasitic elements have a strong effect on the amplifier bandwidth. Physically this low-pass circuit is difficult to realize because some of the series inductors are very short allowing the neighboring disks to introduce a sizeable series capacitance.

3.5.3.2 LSUC2 with the Band-pass Signal Matching Circuit. The signal circuit used here in Fig. 3.26 is a three pole band-pass impedance transformer discussed in Chapter II. The graphs in Figs. 3.27 to 3.29 and Table 3.4 show the resulting gain, bandwidth, and gain-bandwidth product for this circuit. The different graphs indicate the variation in the characteristics when the LSUC is designed for diodes with different parasitic element values. The different gain characteristics for the 2×2 and 5×5 matrix approximations are clearly evident in these plots. The noise figure shown in Fig. 3.30, which corresponds to Fig. 3.27, resembles the reciprocal of the gain curve, and the minimum noise figure corresponds closely to the design objective expressed by (3.25). The sharp dips in the gain curve illustrate the importance of including in the gain calculation the higher order sidebands. These calculations confirm the theory presented

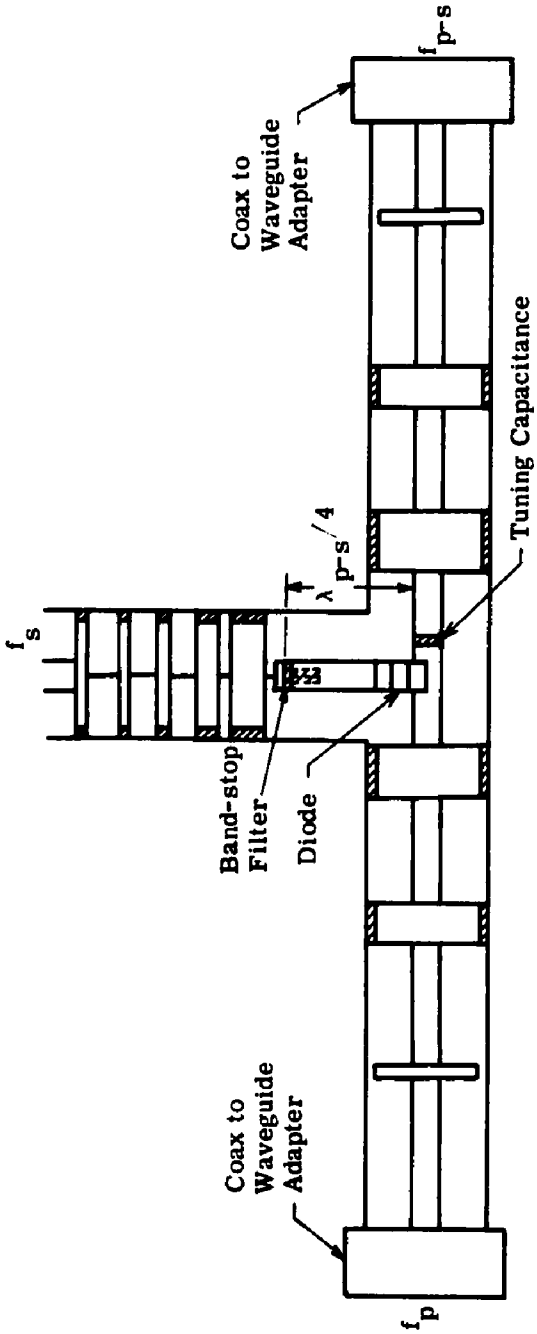


Fig. 3.24. LSUC1 circuit using a semilumped low-pass signal circuit

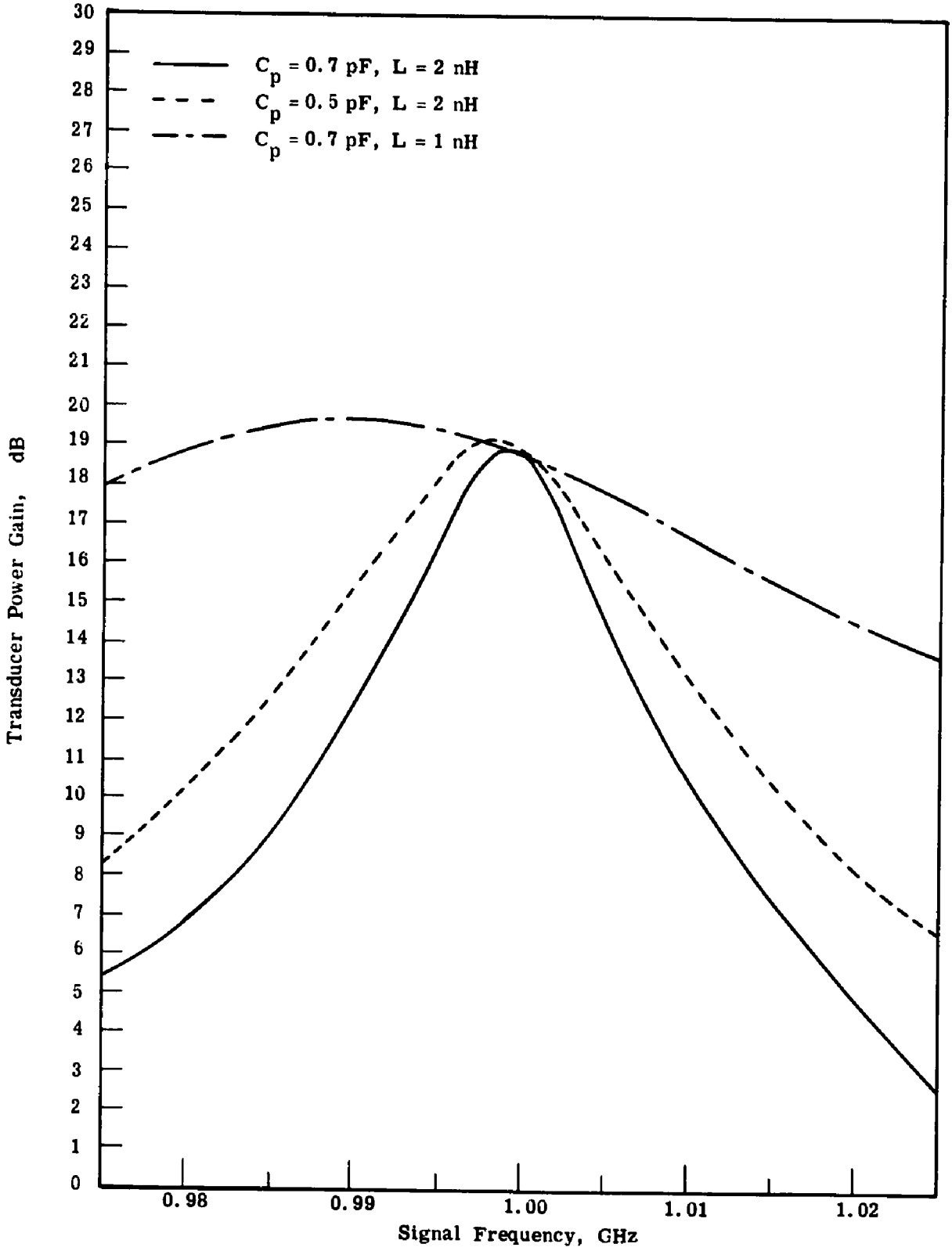


Fig. 3.25. Gain of LSUC using coaxial filters with diode in center conductor

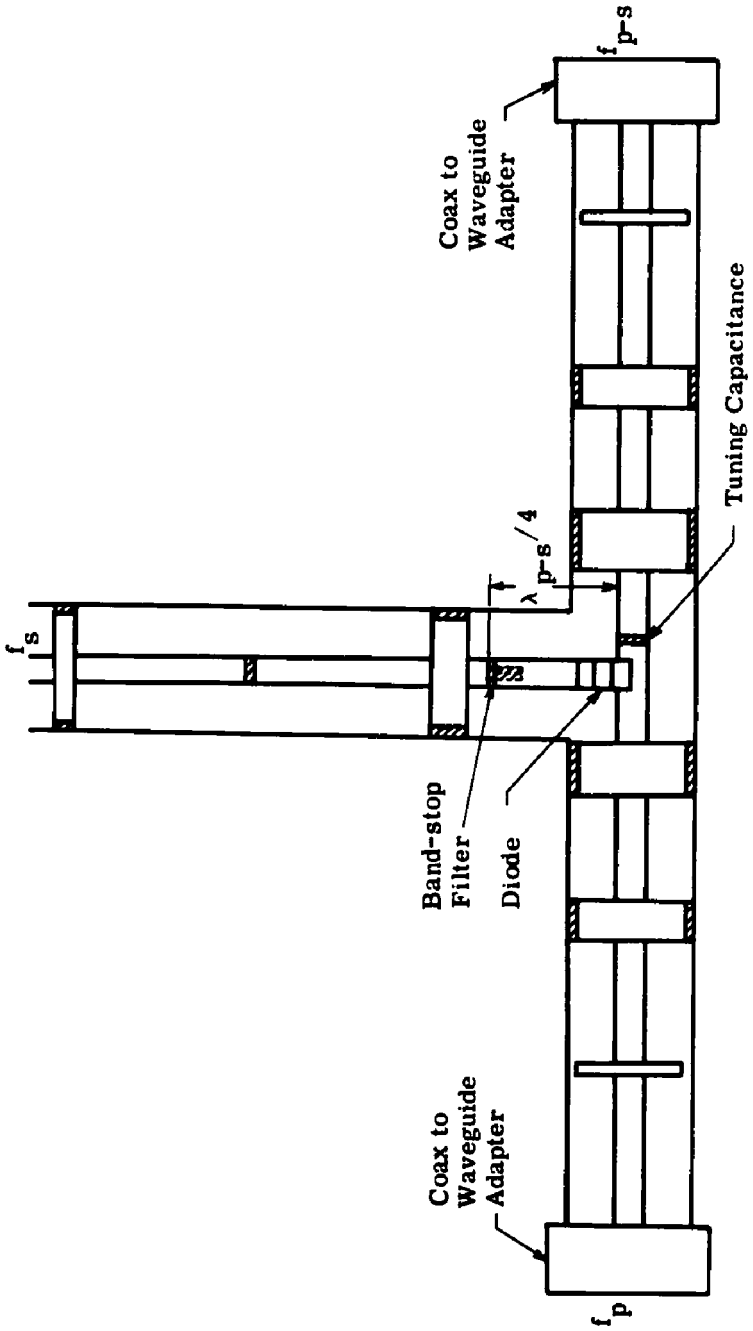


Fig. 3.26. LSUC1 circuit using a distributed band-pass signal circuit

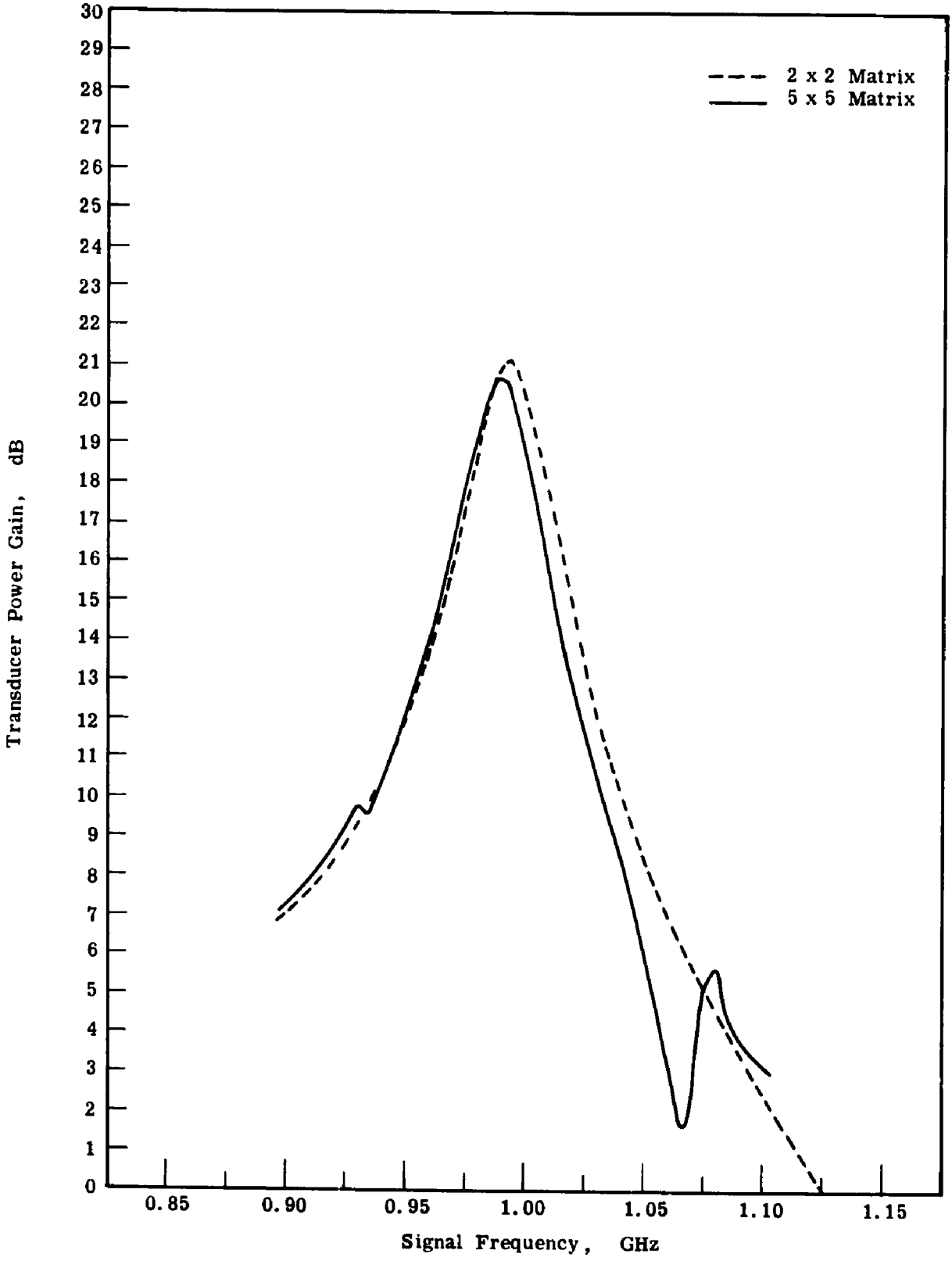


Fig. 3.27. LSUC transducer power gain using the coaxial microwave filters when the diode model has the following elements: R_S = 1 ohm, L = 2 nH, C_p = 0.7 pF, $S_0 = 6.28\ 10^{11}\ F^{-1}$, and $S_1/S_0 = 0.35$

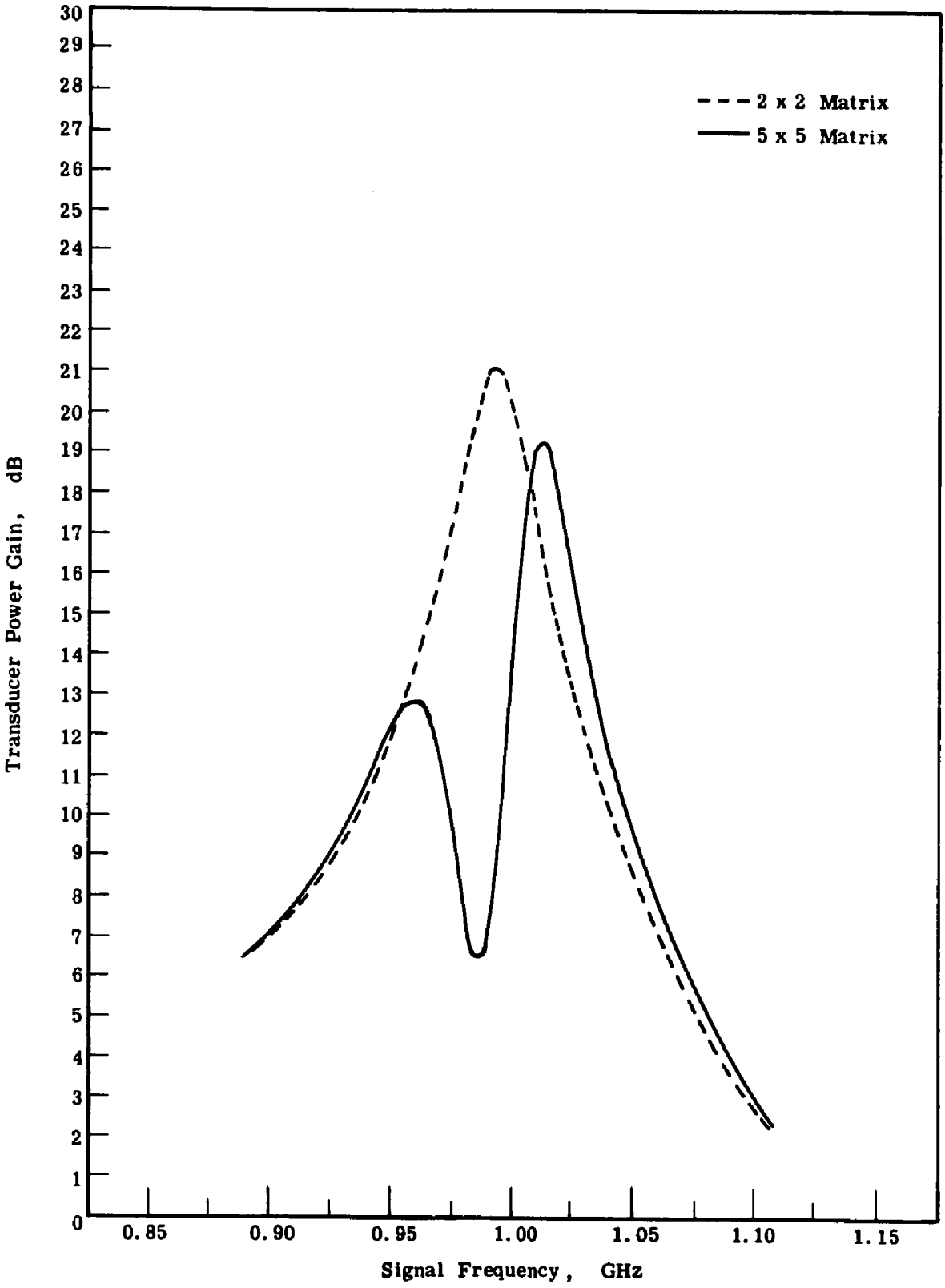


Fig. 3.28. LSUC transducer power gain using the coaxial microwave filters when the diode model has the following elements: R_s = 1 ohm, L = 2 nH, C_p = 0.5 pF, $S_0 = 6.28\ 10^{11}\ F^{-1}$, and $S_1/S_0 = 0.35$

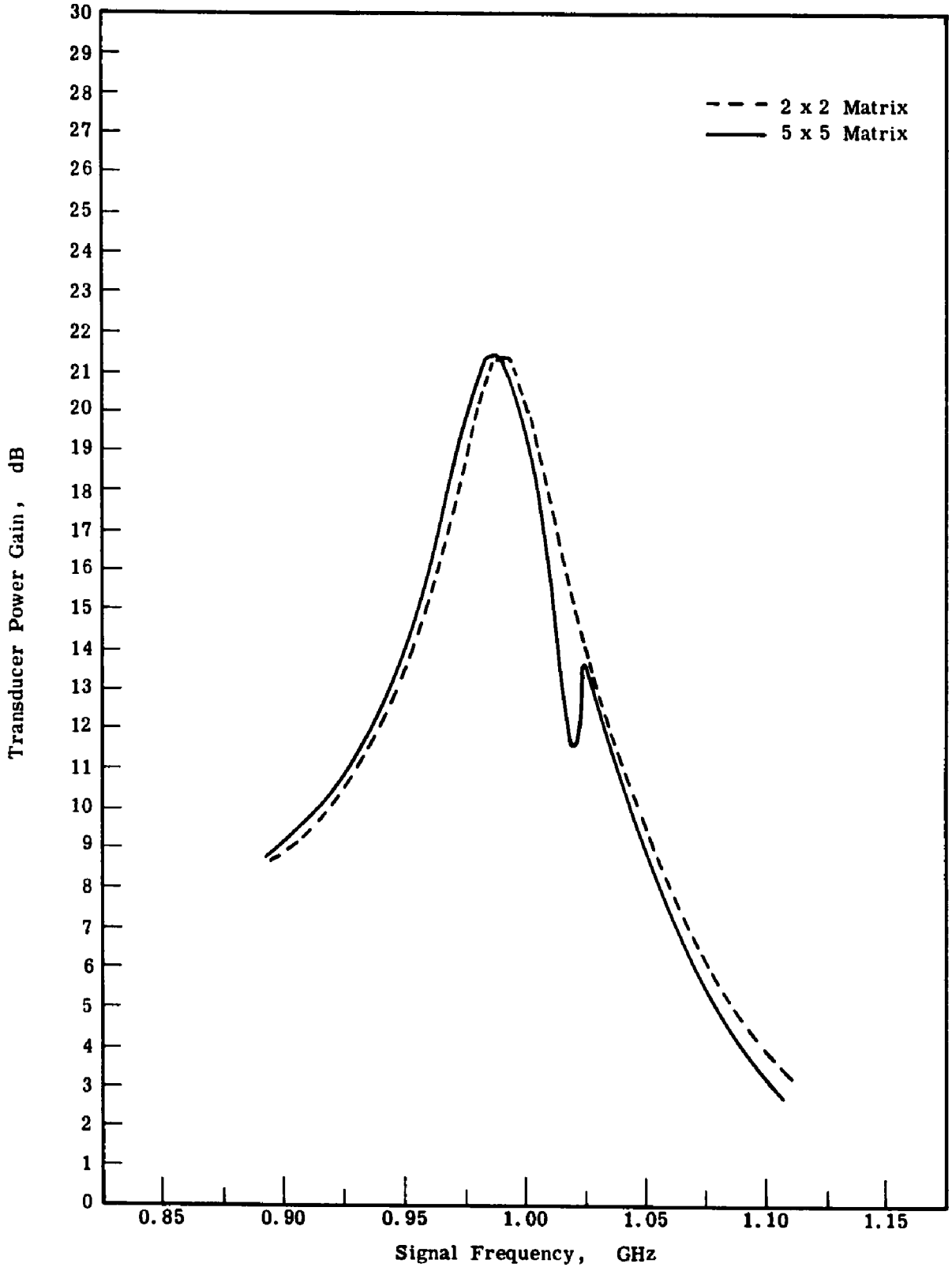


Fig. 3.29. LSUC transducer power gain using the coaxial microwave filters when the diode model has the following elements: R_s = 1 ohm, L = 1.428 nH, C_p = 0.7 pF, $S_0 = 6.28\ 10^{11}\ F^{-1}$, and $S_1/S_0 = 0.35$

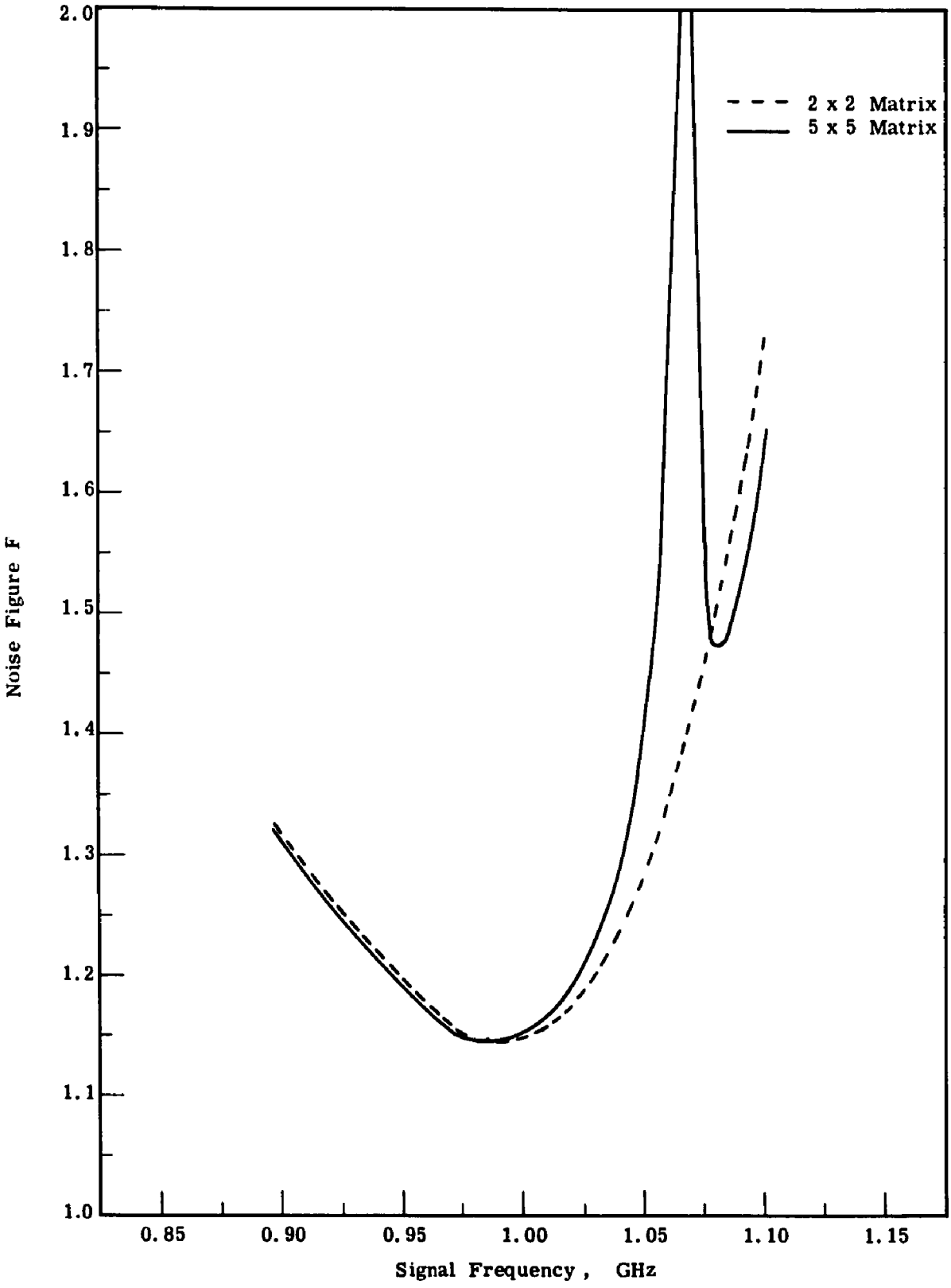


Fig. 3.30. LSUC noise figure using the coaxial microwave filters when the diode model has the following elements: R_S = 1 ohm, L = 2 nH, C_p = 0.7 pF, $S_0 = 6.28\ 10^{11}\ F^{-1}$, and $S_1/S_0 = 0.35$

in Section 3. 3 on the effects of the reactance at the upper sideband frequency on the midband gain.

Matrix Size	L nH	C_p pF	Max. Gain dB	BW GHz	$\sqrt{G}$ w	Freq. of Max. Gain GHz
2 x 2	2	0. 7	21. 04	0. 031	0. 349	0. 995
5 x 5	2	0. 7	20. 64	0. 032	0. 345	0. 990
2 x 2	2	0. 5	20. 98	0. 031	0. 348	0. 995
5 x 5	2	0. 5	19. 23	0. 022	0. 201	1. 015
2 x 2	1. 428	0. 7	21. 36	0. 086	1. 009	0. 990
5 x 5	1. 428	0. 7	21. 44	0. 038	0. 449	0. 985

Table 3. 4. Gain and bandwidth of the LSUC2 using coaxial band-pass filters in all three ports

3. 5. 4 Special Design Considerations for LSUC3. The primary reason for considering this configuration is that experimentally it was found (see Section 4. 3. 2) that at X-band frequencies most power entering one arm of the coaxial tee junction will go to the opposite port while most power entering the leg will be reflected back. Therefore, the diode is placed in the lower sideband circuit to avoid complications from the nonideal tee junction.

The only unresolved design problem is the isolation of the signal port from the diode at the lower sideband frequencies. To insure this isolation the entire signal circuit may be moved toward or away from the tee junction without changing the electrical properties of the structure at f_{10} as long as the total distance between the diode and the signal filter remains constant. If, for example, the signal circuit is moved away from the junction, the diode and lower sideband circuit must be moved the same distance toward the junction. This degree of freedom allows one to choose the distance between the junction and signal circuit so that $Z_s(f_{20}) = \infty$. There are thus two mechanisms that isolate the signal circuit from the power at the lower sideband frequency -- the nonideal tee and the optimum placement of the signal circuit.

The LSUC3 has been designed using only realizable distributed elements without recourse to an iterative process. Thus this circuit may be readily tested experimentally. Following the design procedure given in Section 3. 2. 6, the input signal frequency is

given as $f_{10} = 1.000$ GHz. The diode used in this design was measured according to the method outlined in Chapter 4 with the following results:

$$S_0 = 1.049 \times 10^{12}\ F^{-1}$$

$$L = 1.840\ nH$$

$$C_p = 0.1675\ pF$$

$$R_s = 1.41\ ohms \quad .$$

The assumed pumping modulation coefficient is chosen as $S_1/S_0 = 0.35$ which from (3.31) gives the optimum frequency ratio $r_{opt} = 66.72$. This ratio is much too high for the chosen signal frequency, available circuit components, and available pump sources. Since the specifications for the 14-mm 50-ohm coaxial line are exceeded above 8.50 GHz, the center lower sideband frequency is chosen at $f_{20} = 8.500$ GHz. Although the minimum noise figure is therefore not achievable, a glance at (3.25)

$$F_2 = (\frac{1}{x_g} + 1)(\frac{1}{r} + 1) + \frac{1}{G_{21}} \qquad (3.25)$$

shows that the noise figure is insensitive to the choice of x_g as long as x_g is sufficiently large. If x_g is chosen to be 100, then from (3.13), $y_\ell = 2.201$, or $R_g = 141$ ohms and $R_\ell = 3.104$ ohms. When these parameters are used in the algorithm described here, the circuit specified in Table 3.5 and Fig. 3.31 results. The analysis of this design is shown in Fig. 3.32.

When the diode is resonated at f_{20} by adjusting the distance between the pump circuit and the diode, a significant mismatch at f_p can occur, although the effects of this mismatch can be overcome by increasing the pump power. Analysis of this design shows that the impedance external to the diode at f_p is $0.456 + j\,49.64$ ohms and the transformed impedance seen by the variable elastance of the diode is $1.791 + j\,191$ ohms.

The main computer program, used to generate this design and the accompanying analysis, is found in Appendix A as program B. The necessary subroutines required with this program are also listed there.

	i	Distance d_i inches	Length ℓ_i inches	Diameter $_i$ inches	Relative Dielectric Constant ϵ_{r_i}	d_w inches
Pump Circuit						
	1	0.6956	0.1600	0.542	2.03	
	2	0.6333	0.08292	0.532	2.03	
	3	0.6797	0.03897	0.502	1.00	1.833
Lower Sideband Circuit						
	1	0.7394	0.03791	0.502	2.03	
	2	0.7500	0.1446	0.502	2.03	
	3	0.7778	0.02022	0.502	1.00	5.893
Signal Circuit						
	1	2.8337	0.6332	0.502	2.03	
	2	2.6940	1.1066 pF	-----	----	
	3	3.4221	0.09781	0.502	2.03	

d_{tv} = 1.7817 in., d_{st} = 1.0520 in.

d_1 in the pump circuit is the distance between disk 1 and the tee junction.

d_1 in the other two circuits is the distance between disk 1 and the diode.

Table 3.5. Design parameters for the LSUC when the diode is in the lower sideband port

3.6 Conclusions

This chapter contains a theoretical discussion on the design and properties of a LSUC. The simple design relationships reviewed in Section 3.2 were applied to LSUC circuits that used a coaxial tee junction in three different ways: (1) the diode is mounted between the center and outer conductors, (2) the diode is mounted in the center conductor at the tee junction, and (3) the diode is mounted in the center conductor in the lower sideband arm of the tee. These three configurations were investigated using ideal filters for frequency isolation of the separate ports, and ideal or shunt-stub tuners for impedance matching. Later these elements were replaced by the coaxial band-pass impedance matching transformers discussed in Chapter II. The methods employed here are valuable in designing and analyzing LSUC circuits with different diodes or tuning elements, but because of the large number of variables no general conclusions can be

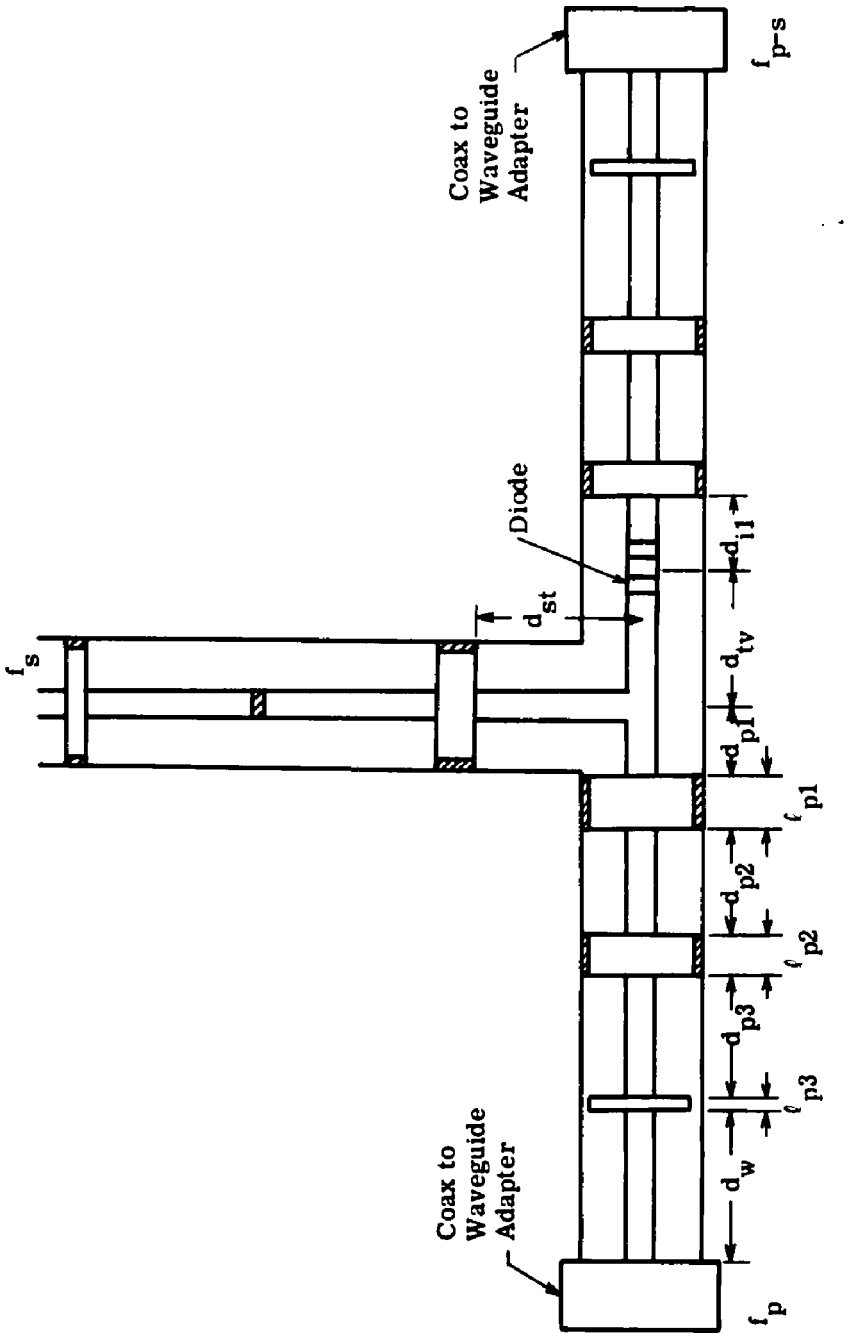


Fig. 3.31. LSUC3 using coaxial disk band-pass impedance transformers

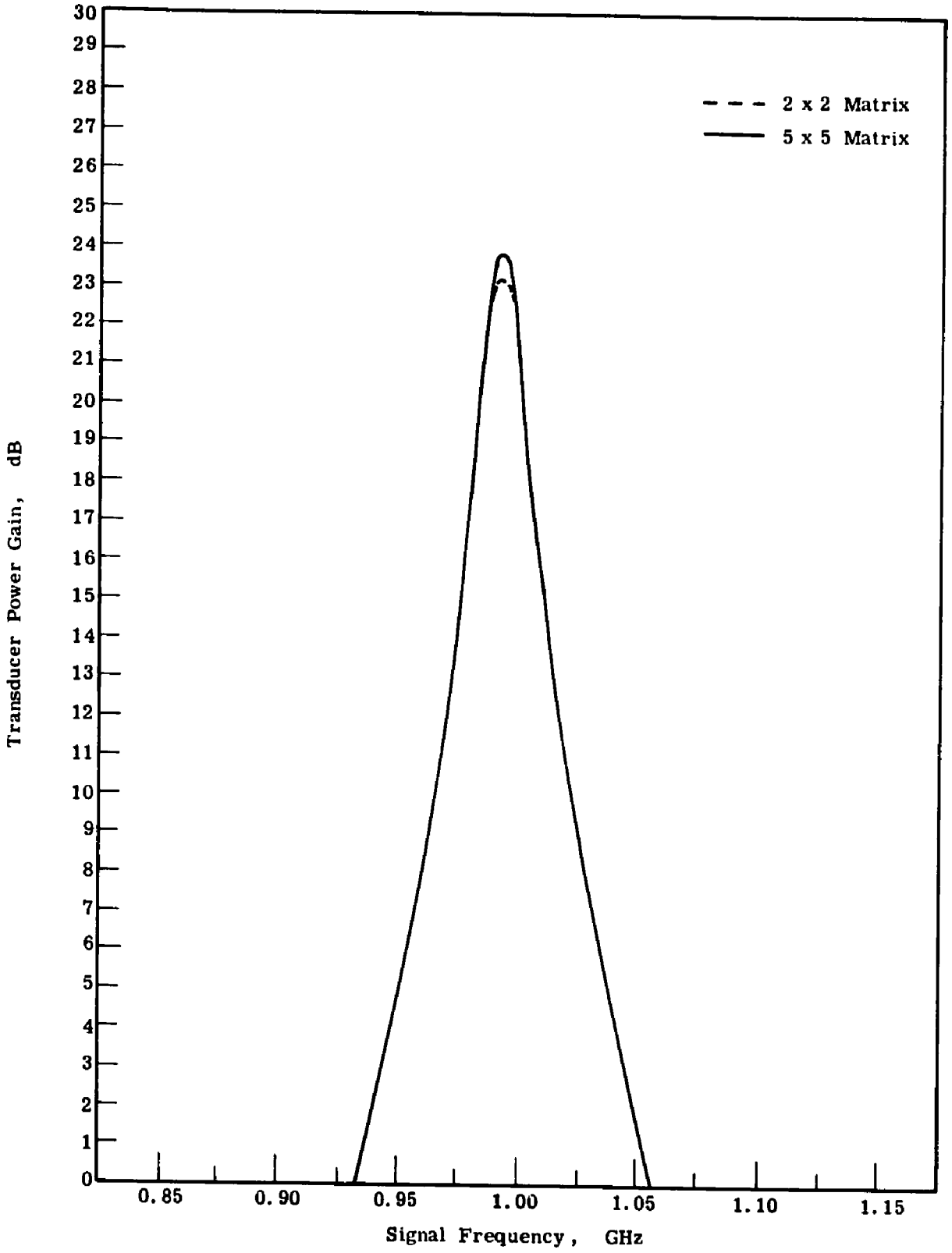


Fig. 3.32. LSUC transducer power gain using coaxial microwave filters when the diode is mounted in the lower sideband port. The diode model elements are $R_s = 1.41$ ohm, $L = 1.834$ nH, $C_p = 0.1633$ pF, $S_0 = 1.0456\ 10^{12}\ F^{-1}$, and $S_1/S_0 = 0.35$

drawn as to which circuit is best. However the LSUC3 circuit is superior in coaxial systems for practical experimental reasons.

The analyses of these circuits point out the importance the diode parasitic elements play in restricting the bandwidth of the amplifier, the importance the reactance at the upper sideband frequency has on the performance of the upconverter, and the effect of the nonresonant gain maximum.

The work in this chapter culminated with a detailed design of a LSUC using coaxial filters, which, with a minor modification, accurately models the experimental LSUC3 discussed in Chapter IV.

CHAPTER IV

EXPERIMENTAL EVALUATION OF THE LOWER SIDEBAND UPCONVERTER

4. 1 Introduction

The previous chapters have dealt with design considerations for the LSUC and the practical problem of constructing band-pass impedance matching circuits in coaxial line. Since the circuit design is heavily dependent on the values of the diode equivalent circuit elements, these diode elements were measured first. The method and results of this measurement are outlined in Section 4. 2. Since three frequencies must enter or leave the amplifier through a coaxial tee circuit, the properties of the impedance transformers and the tee junction were also measured, and are reported in Section 4. 3. Using this information two upconverters were designed and built; detailed measurements on the second one showed a close correspondence to the design theory. The measurements of gain, bandwidth, and noise figure are presented in Section 4. 4. Since the measured noise figure is larger than that predicted from thermal noise sources alone, other sources of noise are considered in this section to explain the discrepancy.

4. 2 Diode Measurement

The packaged diode is a complex circuit element that presents several measurement problems to the experimenter. The resolution of these difficulties has been the subject of numerous papers of which the most pertinent are reviewed below. From the three basic methods presented in these papers, the third is chosen to measure the diode used in the experimental LSUC design.

4. 2. 1 Diode Measurement Review. The equivalent circuit for the varactor diode shown in Fig. 3. 5 of the previous chapter is actually a simplified version of a more complex structure. The diode is considered to be physically much smaller than the wavelength at its highest operating frequency, so it can be represented by a lumped circuit. An equivalent circuit for a packaged varactor diode together with its more

common simplified circuit is shown in Fig. 4. 1. To be a valid equivalent circuit, the circuit elements must be independent of frequency. The depletion layer capacitance, lead inductance, and package capacitance are frequency independent for microwave frequencies through X-band. The bulk series resistance R_s is usually assumed frequency and voltage independent. However, careful measurements show this is not the case. At frequencies higher than 10 GHz, R_s increases with frequency because of the skin effect resistance (Ref. 47). The applied voltage across the diode can vary R_s by two mechanisms. First, when the applied voltage varies the depletion layer capacitance, it also changes the width of the epitaxial base material (Ref. 48, p. 69). This is sufficient to cause a large variation in the series resistance. For an abrupt junction diode this variation is given by

$$R_s = \rho(W_{max} - W)/A$$

where ρ is the resistivity, A is the diode area, and W is the depletion layer width. Second, in a packaged diode the fringing capacitance will cause the effective series resistance R_s to increase with applied voltage (Ref. 49). This can be seen by equating the impedances of Fig. 4. 1(a) to that of Fig. 4. 1(b). The effective resistance is

$$R_s = \frac{RX_f^2}{R^2 + (X_j + X_f)^2}$$

$$\cong \frac{R}{[1 + C_f/C_j(V)]^2} \qquad 1 >> \omega C_f R$$

where X_f and X_j are the capacitive reactances of C_f and C_j respectively. For zero and reverse bias the junction conductance G_j is very large and therefore can be safely neglected. The fringing capacitance commonly associated with the capacitance between the pillar and the top cap is also considered small enough to be neglected in most cases. However, as was just seen, this assumption may not always be warranted.

One of the difficulties in accurately characterising a varactor diode is now already evident: the semiconductor region is accessible only through the equivalent components of the package. There are in addition other difficulties. Special care must be

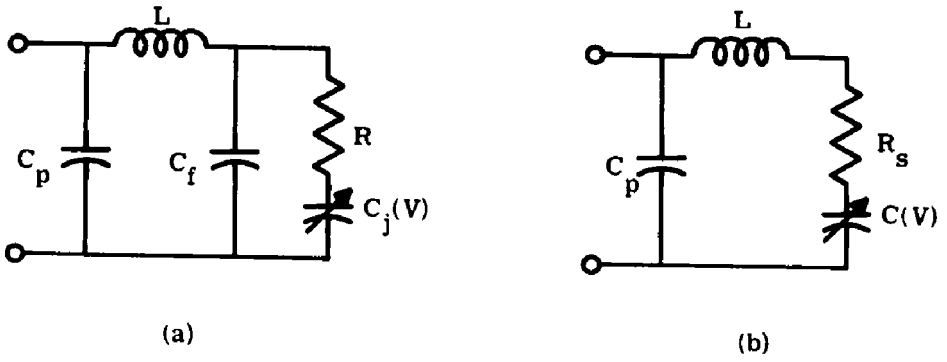


Fig. 4.1. (a) The varactor diode equivalent circuit and (b) the modified simple equivalent circuit

exercised in measuring R_s as this is usually between 1 and 5 ohms; the high quality factor Q_c of the diode implies that small losses in the measuring system can produce significant errors in the measurement of this important parameter. Also the diode is nonlinear, so low RF power must be used to avoid pumping the diode. In one method to be described, it is desirable to obtain the parallel resonant frequency of the diode. In some cases, this frequency is so high that TEM mode coaxial line is not available while impedance measurements in waveguide suffer from having a nonunique characteristic impedance.

These difficulties have resulted in basically three measurement techniques: (1) low-frequency bridge measurement of the capacitance, (2) single-frequency measurement of the diode Q_c at varying bias voltages, and (3) measurement of diode impedance including package parasitic elements, performed at a single bias voltage but over a range of frequencies. In the first case the package parasitic elements can be neglected; in the second case they are tuned out and the diode Q_c is measured directly, while in the third case, the diode is measured with the package parasitic elements.

4.2.1.1 Method 1. In the frequency range between 100 kHz and 10 MHz R_s and L can be safely neglected so that the total measured capacitance as found on a transformer ratio-arm bridge is

$$C_T = C_p + C_f + C_j(V)$$

$$\cong C_p + C(V) \quad .$$

Crook (Ref. 50) assumes C_f is negligible and separates C_p from $C(V)$ by an independent measurement of C_p on an empty diode cartridge. Roberts and Wilson (Ref. 49) describe an alternative way of separating these two capacitances. The capacitance law, i.e., γ and the built-in potential can be found by measuring a large number of diodes at two bias values, e.g., 0 and -6 V. From the slope of the straight line plot of $C_T(-6)$ versus $C_T(0) - C_T(-6)$, the capacitance law can be determined. Knowing this law, two bias levels enable finding C_p and $C(V)$. Data given by Roberts and Wilson (Ref. 49), however, show these low-frequency measurements are in error by over 0.1 pF in 0.28 pF at -6V when compared to microwave measurements. Since the diode is to be used at microwave frequencies, the high-frequency measurement values are to be preferred. Therefore, method 1 is not recommended for diode characterization.

4.2.1.2 Method 2. This method provides a direct method of finding the diode $Q_c = 1/[\omega R_s C(V)]$. It is based on normalization of the measured impedance to R_s rather than Z_o, and impedance matching the diode at a particular frequency and bias with a lossless transformer. Impedance matching is not strictly necessary, but is readily accomplished and simplifies the mathematics. Houlding (Ref. 51) used this technique to find the diode Q_c by determining the change in reactance with a change in bias. However, his method requires knowledge of the capacitance-voltage law for the particular diode. Harrison (Ref. 52) soon afterward described a method of finding the Q_c without having to know the capacitance-voltage law of the diode. In this method the bias on the matched diode is varied, the impedance is plotted on a Smith chart, and this plot is rotated until it coincides with the unit circle. The location on the unit circle where the diode is a short circuit is numerically equal to the diode Q_c. Harrison showed that this short circuit can be provided either by replacing the diode with a shorted package or by forward biasing the diode until it is an effective short. This latter technique works well for silicon diodes, but in gallium arsenide diodes the effective short is obtained near maximum permissible power dissipation. Mavaddat (Ref. 53) extended Harrison's method by eliminating the need of a short-circuited diode. He shows that a plot of $1/\Delta C$ versus $1/\Delta X$ for various bias values gives $1/Q_c$ as well as $1/C(V)$

at the intersection of the curve with the $1/\Delta X$ and $1/\Delta C$ axes respectively. The value of $C(V)$ so obtained does not include the fringing capacitance C_f.

Criticism of this general approach was made by Hyde and Smith (Ref. 54) who showed, after analyzing several loss mechanisms, that the diode Q_c found by this method may lead to erroneous results. Their conclusions may be summarized as follows. Additional series resistance whether within the diode cartridge or between the diode and the plane of measurement always reduces ΔQ_c (or ΔX). Distributed loss either inside or outside the cartridge causes the relative impedance locus to lie inside the unit resistance circle when reverse biased and outside it when forward biased. In addition ΔQ_c is reduced and the short-circuit point does not lie on the periphery of the chart. Shunt conductance loss, which occurs near the reverse breakdown voltage and the forward conduction region, results in an impedance locus that lies inside the unit circle in both regions but does not disturb the short-circuit point. When using method 2 it is necessary to plot experimental data on a Smith chart at an arbitrary reference plane. These data points are rotated to fit the unit circle as closely as possible. But it is clear that qualitative adjustment for the asymmetries that arise may be necessary, and the possible failure of the short position to lie on the periphery of the Smith chart could be caused by either an unknown loss mechanism or the lack of a good short. Since the mathematical representation of these alternate loss mechanisms is complicated, Hyde and Smith conclude it is not possible to extract lossless results from lossy data. Nevertheless, Sard (Ref. 55) does attempt to separate circuit losses from varactor losses by assuming the lossy matching network is a standard form. However, correcting for the circuit loss in series with diode bulk resistance requires extreme measurement care.

4.2.1.3 Method 3. The first method is a low-frequency technique to find $C(V)$, while the second is a high-frequency technique to find Q_c. The third method gives the diode equivalent circuit elements from impedance data as a function of frequency. This method can be divided into two techniques: transmission loss measurements of a diode shunt mounted in a waveguide and direct impedance measurement of the varactor diode when series mounted in a coaxial short-circuited line.

The transmission technique was first proposed by DeLoach (Ref. 56) for the measurement of unencapsulated varactors. It requires measuring the ratio of the power

received by the load in the absence of the diode to that received when the diode is tuned to resonance, together with the two frequencies for which the transmitted power is doubled. With this information, the depletion layer capacitance, the series resistance, and the lead inductance can be found. This method has been extended to packaged diodes since at series resonance, the shunt package reactance is quite large.

Roberts and Wilson (Ref. 49) use a variation of the transmission method to find R_s, L, and C(V). Since

$$C(V) = \frac{1}{4\pi^2 f_a^2 L}$$

a plot of $1/f_a^2$ versus bias gives a plot of $M_a C(V)$ versus bias, where f_a is the series resonant frequency and M_a is an unknown constant. With the frequency set to f_a at zero bias, the forward bias and reverse bias required to double the transmitted power are measured. The corresponding values of $M_a C(V)$ at these two bias values are read on the graph from which the Q_c is readily calculated. This gives the cut-off frequency, $f_c = Q_c f_a$, C(V), L, and the capacitance variation coefficient.

The most obvious disadvantage of this method is that it provides no way of determining the package capacitance since the diode is assumed to be a series RLC circuit. Houlding (Ref. 57) has pointed out that the equivalent circuit of the more common diode packages (rather than the Sharpless package used by DeLoach) would be considerably more complex than a simple RLC circuit. Uncertainty in the exact transformation of the diode junction diode, compounded by the need to vary the frequency, would introduce further error in this method. In addition there is some doubt of the appropriateness of the choice of waveguide characteristic impedance used by DeLoach. The value he used was derived by Schelkunoff and is the impedance seen by a thin wire placed between two broad walls of a reduced height waveguide (small compared to $\lambda_g/4$). Packaged diodes usually cannot be considered as thin wires. Furthermore, a diode measured in a reduced height waveguide would be expected to operate in a similar diode mount, and this unduly restricts the circuit design.

In none of the methods reviewed thus far is there a satisfactory method for obtaining the package capacitance C_p. Roberts (Ref. 58) has shown that all four elements

of Fig. 4. 1(b) can be obtained by series mounting the packaged diode in a short-circuited coaxial line and measuring the impedance over a broad range of frequencies. To obtain the three energy storage elements, the series resistance R_s is assumed negligible and three pairs of frequency-reactance variables are chosen. Roberts chooses the series resonant frequency f_a, $f_a/2$, and the parallel resonant frequency f_b. The corresponding reactances are $X(f_a) = 0$, $X(f_a/2)$, and $X(f_b) = \infty$. The corresponding parameters are then given by

$$C_p = -\frac{3}{\pi f_a X(f_a/2)} \left[4\left(\frac{f_b}{f_a}\right)^2 - 1\right]^{-1} \tag{4.1}$$

$$C(V) = C_p \left[\left(\frac{f_b}{f_a}\right)^2 - 1\right] \tag{4.2}$$

$$L = \frac{1}{(2\pi f_a)^2 C(V)} \quad . \tag{4.3}$$

This method works well as long as $f_b < 18$ GHz. Above this frequency, the unavailability of coaxial line and connectors makes this method cumbersome. Roberts and Wilson (Ref. 49) overcome this problem by recognizing that a minimum of transmission occurs at f_b. They, therefore, measure this frequency with the diode mounted in the inner conductor of the coaxial line between two coax-to-waveguide adapters.

The series resistance may now be evaluated by one of the Q-measurement techniques described in method 2. This has the advantage of finding R_s at the operating frequency and the disadvantage of incurring additional circuit loss. Alternatively a straightforward SWR measurement at series resonance can be used. Account must be taken of losses in the measuring system, since these losses can easily mask the true diode resistance. Crook (Ref. 50) minimizes these losses by using a 10-ohm quarter-wave impedance transformer between the slotted line and the diode. Bandler (Ref. 59) has shown for high standing waves

$$\frac{1}{S_m} = \frac{1}{S_L} + \frac{1}{S_{max}} \tag{4.4}$$

where S_m = measured SWR, S_L = desired SWR of the load, and S_{max} = maximum SWR when the load is replaced by a short. The diode series bulk resistance is determined from S_L rather than S_m.

4.2.1.4 Conclusions on the Three Methods. Table 4.1 summarizes the references which should be consulted for measuring the various diode parameters. Of the three basic methods described above the first seems the least useful at microwave frequencies. In the design of a LSUC, the basic problem is knowing the values of the package parasitic elements, R_s, and the average depletion layer capacitance, while knowing Q_c is of secondary interest. Hence, method 3 is the most appropriate.

Author	C(V)	R_s	L	C_p	C_f	Q_c
Crook (Ref. 50)	x	x		x		
Houlding (Ref. 51)						x
Harrison (Ref. 52)						x
Mavaddat (Ref. 53)	x	x				x
Roberts and Wilson (Ref. 49)	x	x	x	x	x	
DeLoach (Ref. 56)	x	x	x			
Roberts (Ref. 58)	x	x	x	x		
Bandler (Ref. 59)		x				

Table 4.1. References for measuring diode parameters

Addition of a fifth element to the circuit in Fig. 4.1(b) provides a more accurate representation of the physical diode. The fringing capacitance shunting the diode wafer and an extra inductance external to the diode package capacitance are two possibilities that have been suggested for a fifth element.

Roberts and Wilson (Ref. 49) found that the fringing capacitance is larger than expected, and as has been shown, its presence can account for voltage dependence of the

effective series resistance. They found that the major part of the series inductance comes from the pillar on which the wafer rests (not the wires connecting the chip to the top cap) and that the magnitude of C_f cannot be explained only by the existence of capacitance between the top cap and the wafer. The pillar is actually a distributed line and the additional fringing capacitance can be explained by the capacitance from the sides of the pillar to the top cap through the ceramic ring (Fig. 4. 2). This distributed line can be approximated by an equivalent circuit that includes the fringing capacitance.

An additional external inductance has been proposed by Houlding (Ref. 57) who criticized the four-element equivalent circuit for the error it produces, particularly at the higher frequencies. He proposed neglecting the fringing capacitance and including an extra inductance L_T, which approximates additional transforming action of the package (Fig. 4. 3).

Both of these five-element models give improved correlation with experimental measurements. However, the four-element equivalent circuit seems to be sufficiently accurate for the LSUC design.

4. 2. 2 Experimental Diode Measurement Results. The basic technique credited to Roberts (Ref. 38) has been employed to find the reactive elements of the circuit in Fig. 4. 1(b). The transmission technique was not used because, in the LSUC, the diode in not shunt-mounted in a reduced height waveguide. Furthermore, the objection to Roberts' method which is based on a high parallel resonant frequency, does not materialize since the diode package used here had a parallel resonant frequency somewhere in the lower half of the X-band frequency range. The diode is therefore mounted in a shorted piece of 14-mm coaxial line as shown in Fig. 4. 4. Since the diode diameter is less than the coaxial center conductor, the latter is tapered to make a smooth transition from the 50-ohm line to the diode. Any error introduced by this taper is at least partially offset by a corresponding taper in the diode mount in the LSUC. The reference plane used in the measurement is taken at the edge of the diode ceramic nearest the generator. The diode was measured under self-bias conditions on the Hewlett Packard No. 8410A network analyzer using the No. 8413A phase-gain indicator from 1 to 11. 5 GHz. The results are plotted in Fig. 4. 5. Equations (4. 1) to (4. 3), when used in conjunction with this plot, give the following values for the reactive elements:

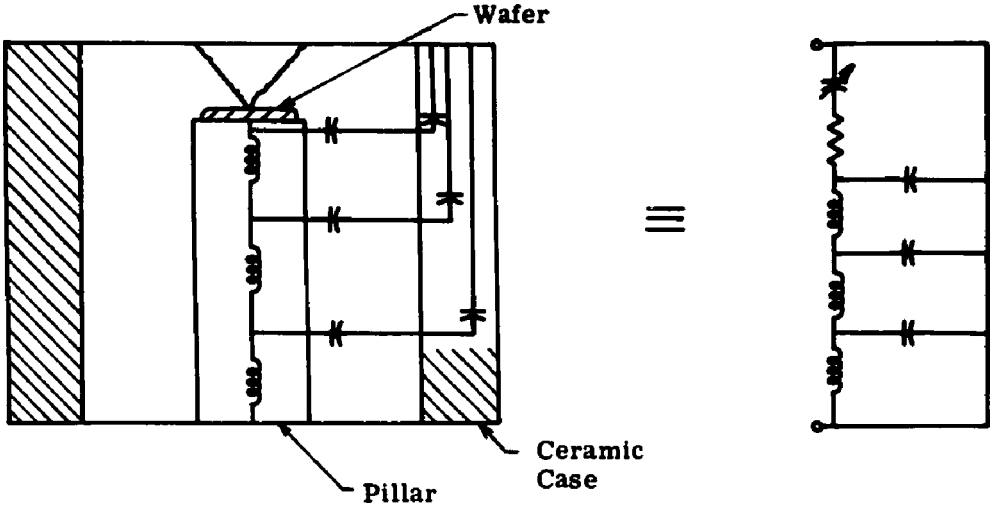


Fig. 4.2. Distributed diode model

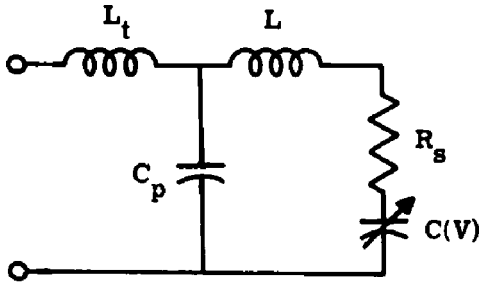


Fig. 4.3. Houlding's varactor diode model

$$S_p = 6.12 \times 10^{12}\ F^{-1}$$

$$S_0 = 1.05 \times 10^{12}\ F^{-1}$$

$$L = 1.83\ nH\ .$$

The series resistance was found using both Harrison's Q measurement technique and a standard slotted line measurement with Bandler's modification. The measuring system used for the first method is shown in Fig. 4.6, and the resulting bulk resistance is found to be $R_s = 1.55$ ohms. Using Bandler's method, the resistance is found to be $R_s = 1.41$ ohms. Although both methods give approximately the same result, the first method is

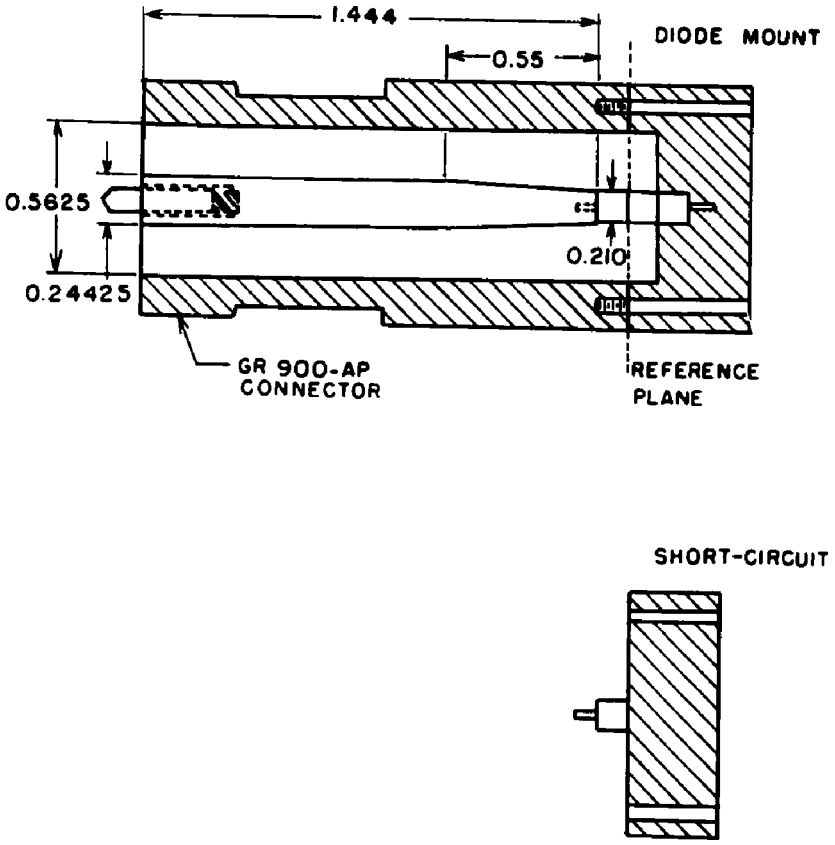


Fig. 4.4. Diode measurement mount with (a) the varactor diode and (b) the short-circuit reference plane where all dimensions are in inches

less accurate because of the additional losses in the double-stub tuner, the bias tee, and the additional connectors. The series resistance of the diode is therefore taken as 1.41 ohms.

The analysis of the resulting equivalent circuit is shown in Fig. 4.5. The reactance of the measured diode and the equivalent circuit are shown in Fig. 4.7. A comparison shows that the worst discrepancies occur at frequencies beyond parallel resonance, but these frequencies are also higher than the operating frequency of the LSUC, and so the discrepancies do not disturb the design.

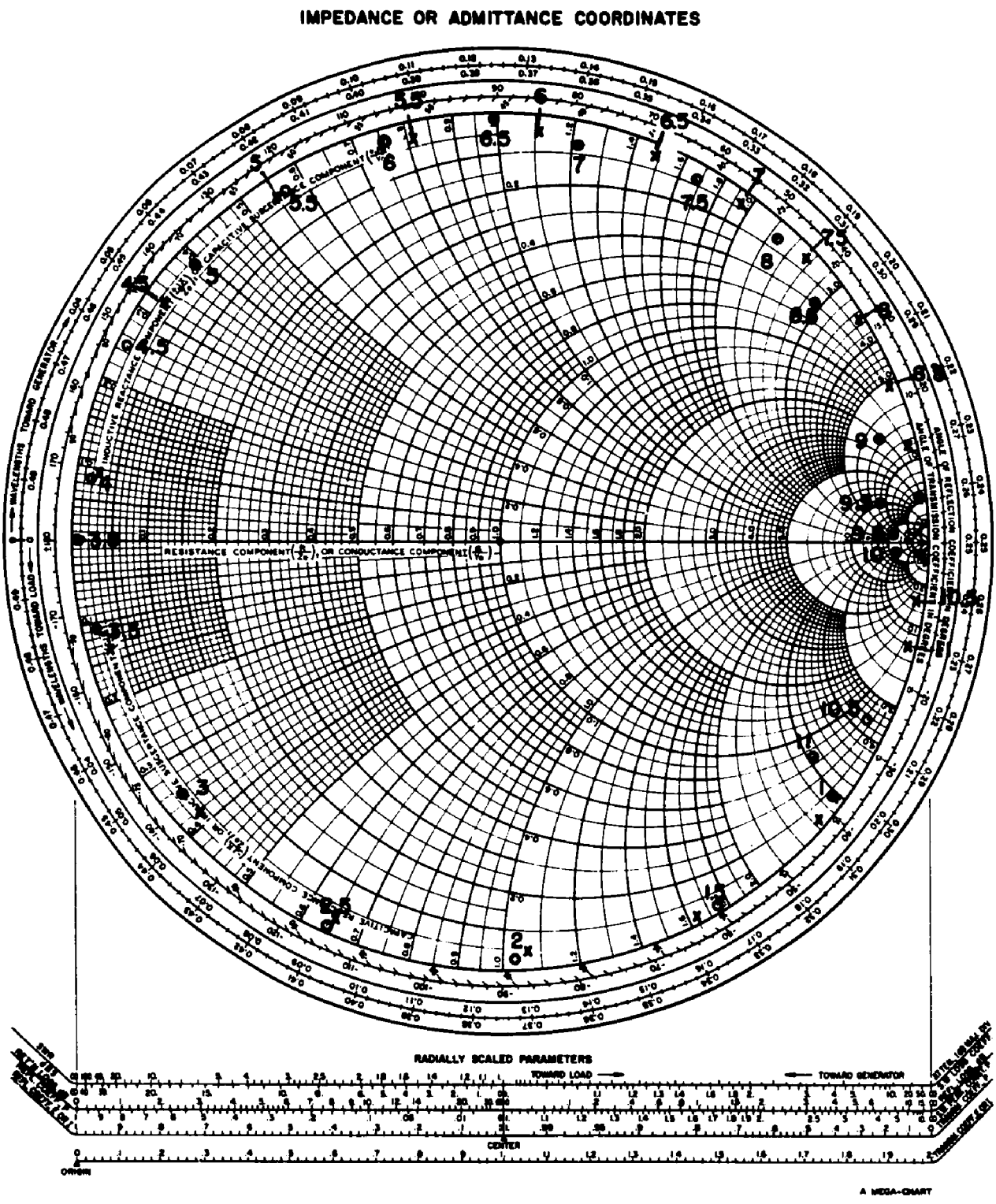


Fig. 4.5. The measured diode impedance data points are designated by o and the selected points obtained from analysis of the resulting diode model are designated by ×

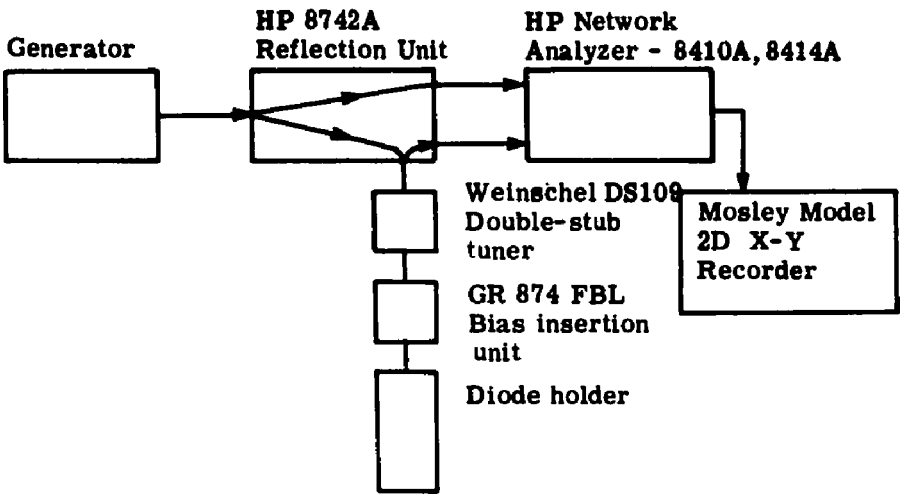


Fig. 4.6. Diode measurement circuit

4.3 External Microwave Circuit Measurements

The two problems considered in this section are the measurement of the band-pass impedance transformers used in the signal and lower sideband ports, and the measurement of the equivalent tee junction.

4.3.1 Band-pass Transformers. In the design for LSUC3 discussed in Chapter III the signal transformer is designed to have a bandwidth of 40 percent of the center frequency and to transform the 50-ohm generator impedance to 7.630 ohms (which normalized to 50 ohms is 0.153) at the reference plane where the impedance is real. The lower sideband port is designed to have a bandwidth of 7 percent of the center frequency and to transform the 50-ohm load impedance to 30.04 ohms (which normalized to 50 ohms is 0.6). These two transformers were measured on the Hewlett-Packard No. 8410A network analyzer using the No. 8414A polar display and an X-Y recorder. The results shown in Figs. 4.8 and 4.9 indicate the bandwidths of these filters are somewhat narrower than the design bandwidth. However, this is in qualitative agreement with the analysis presented in Chapter II. Although the bandwidth is narrower than the design goal, the impedance transformers are sufficiently broad so as not to restrict the amplifier bandwidth.

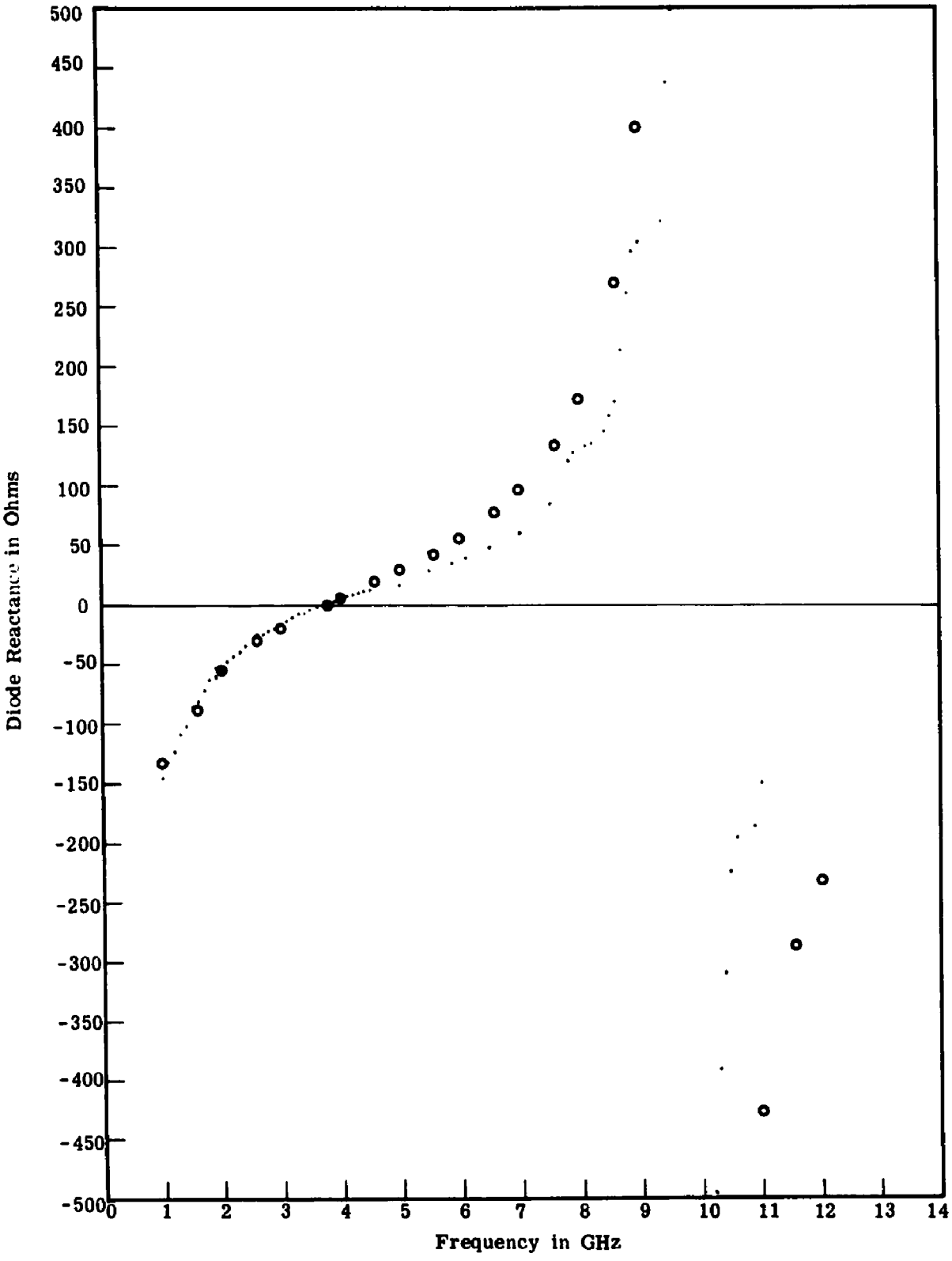


Fig. 4.7. Comparison of the reactance for the measured diode · · · and the diode model o o o

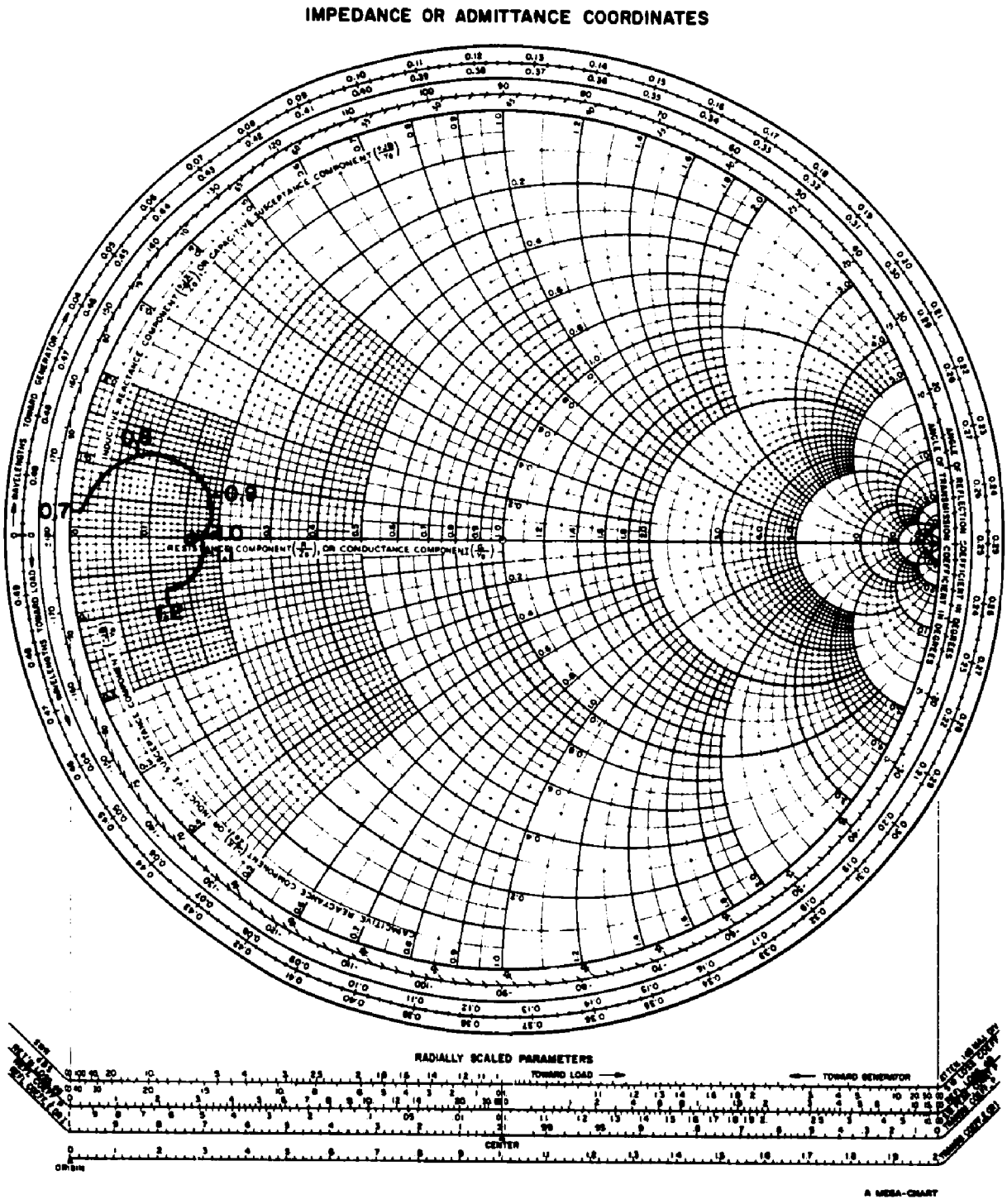


Fig. 4.8. Impedance of the signal frequency transformer

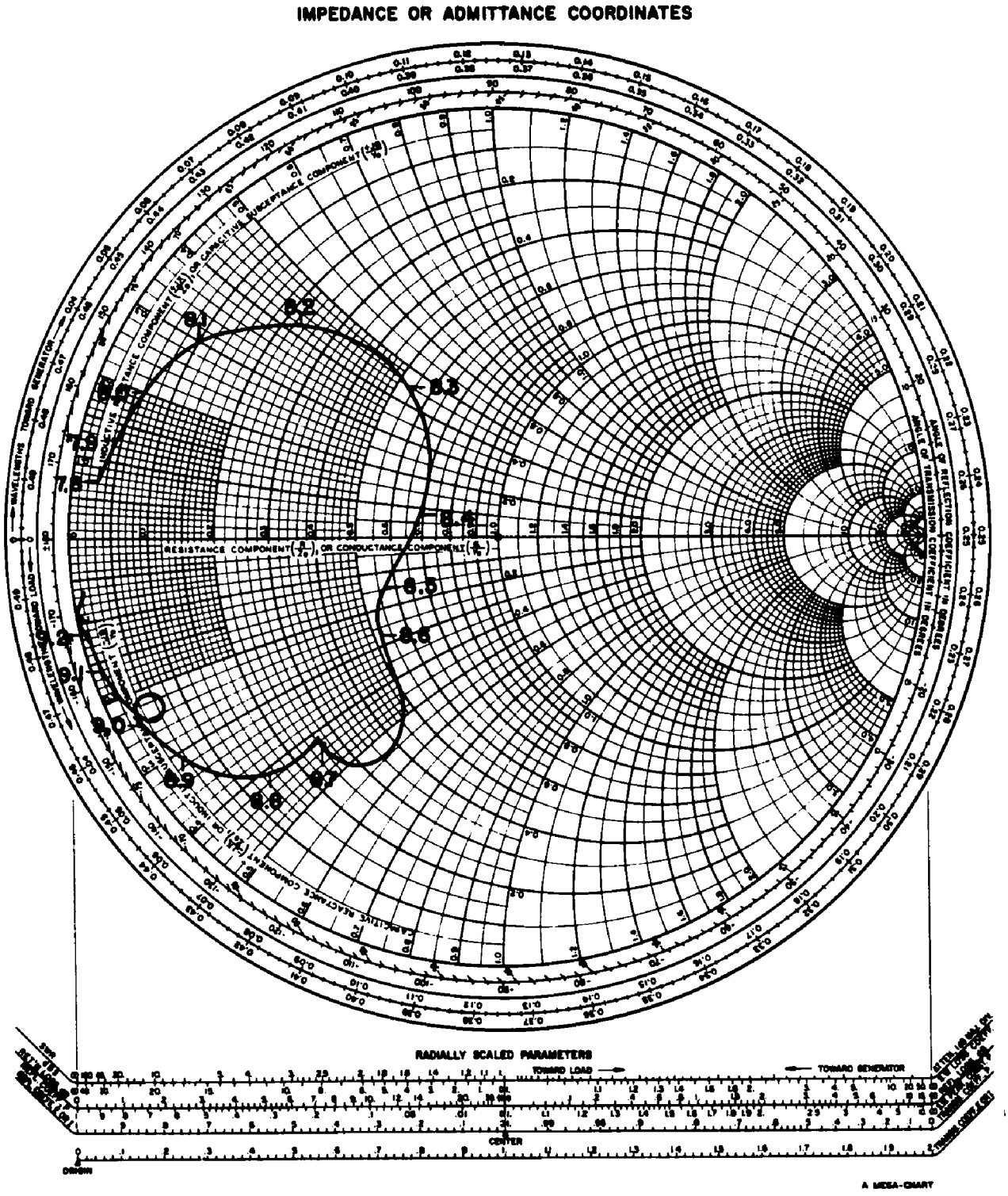


Fig. 4. 9. Impedance of the lower sideband frequency transformer

4. 3. 2 The Tee Junction. In much of the theoretical work described in Chapter III, it has been assumed that all three ports of the coaxial tee junction are symmetrical, so that power entering one port divides equally between the other two. However, empirically this assumption is found to be invalid at high frequencies. In connection with realizing multiplexing networks, Wenzel (Ref. 60) found that coaxial shunt stubs caused some difficulties at X-band and were very unpredictable at K_u-band. To gain further insight into the tee junction characteristics, two ports of the tee were terminated by 50-ohm loads, and the input impedance was measured at the third port with the reference plane at the center of the junction (Fig. 4. 10). These measurements indicate that the tee junction is not an ideal power splitter above 2 GHz for the 14 mm coaxial tee and above 4 GHz for the 7mm coaxial tee. The measurements of the 7 mm tee in Fig. 4. 11 show that beyond this border line frequency the input impedance Z_a looks increasingly reactive while Z_b tends to look more like 50 ohms. Thus power entering the input port of Fig. 4. 10(a) is almost totally reflected at sufficiently high frequencies, while at these same frequencies most of the power entering the input port of Fig. 4. 10(b) is absorbed in the opposite arm. These characteristics are used to advantage in the LSUC3 design.

To obtain a more quantitative model of the 14 mm tee junction used in the LSUC, parameters are obtained for a three port equivalent circuit shown in Fig. 4. 12. The matrix equation for the tee junction is

$$\begin{bmatrix} i_1 \\ i_2 \\ i_3 \end{bmatrix} = \begin{bmatrix} Y_{11} & Y_{12} & Y_{13} \\ Y_{21} & Y_{22} & Y_{23} \\ Y_{31} & Y_{32} & Y_{33} \end{bmatrix} \cdot \begin{bmatrix} V_1 \\ V_2 \\ V_3 \end{bmatrix} . \qquad (4.5)$$

From symmetry, $Y_{11} = Y_{22}$ and $Y_{13} = Y_{23}$, and from reciprocity, the nine terms in (4. 5) can be reduced to only four terms:

$$\begin{bmatrix} i_1 \\ i_2 \\ i_3 \end{bmatrix} = \begin{bmatrix} Y_{11} & Y_{12} & Y_{13} \\ Y_{12} & Y_{11} & Y_{13} \\ Y_{13} & Y_{13} & Y_{33} \end{bmatrix} \cdot \begin{bmatrix} V_1 \\ V_2 \\ V_3 \end{bmatrix} .$$

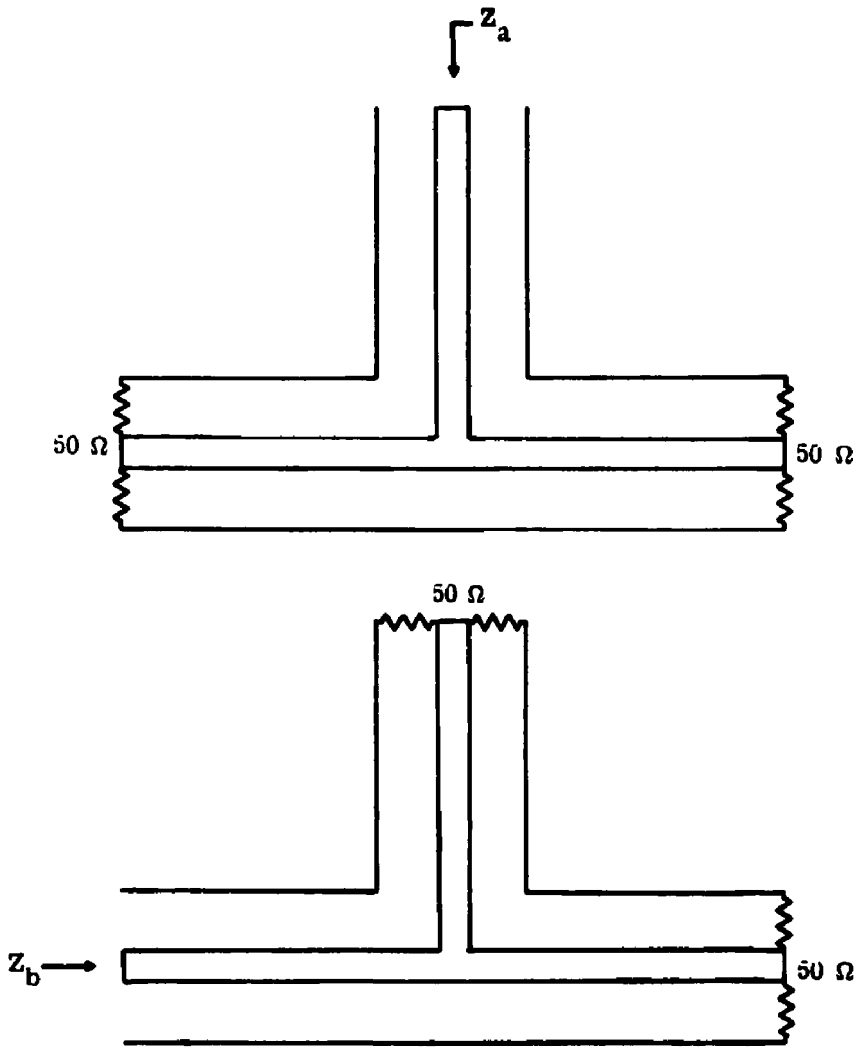


Fig. 4.10. The impedance of the coaxial tee circuit as seen from (a) the leg port, and (b) the arm port

The measurement of $Y_{11} = Y_{22}$ and Y_{33} is easily accomplished by putting shorts at the reference planes of two ports and measuring the input admittance of the third. Measuring the off diagonal terms is slightly more involved. To measure Y_{12}, for example, port 3 is shorted at the reference plane, reducing the 3 x 3 matrix above to

$$\begin{bmatrix} i_1 \\ i_2 \end{bmatrix} = \begin{bmatrix} Y_{11} & Y_{12} \\ Y_{21} & Y_{22} \end{bmatrix} \cdot \begin{bmatrix} V_1 \\ V_2 \end{bmatrix} \quad . \tag{4.6}$$

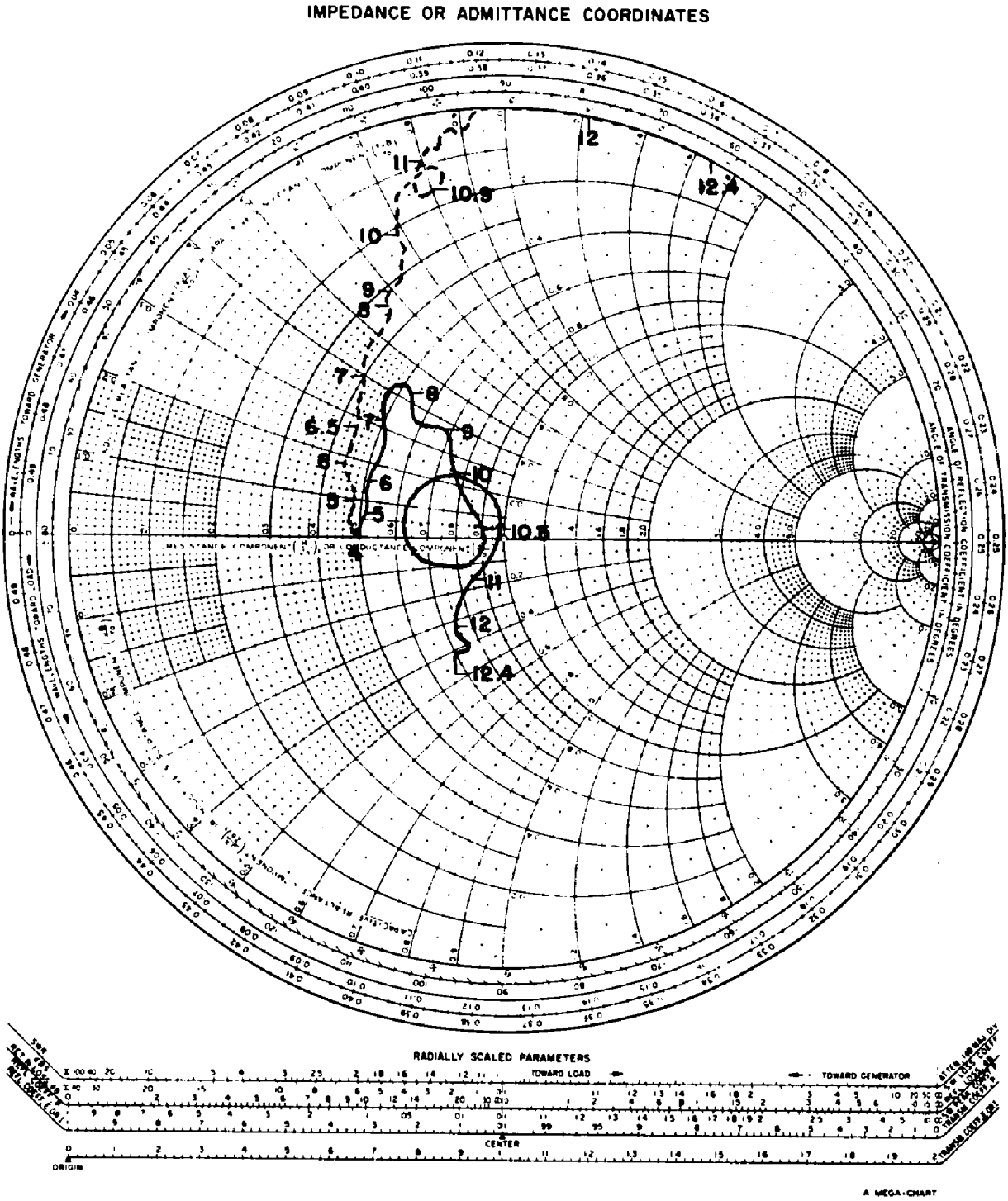


Fig. 4. 11. The impedance as a function of frequency in GHz of a 7 mm coaxial tee junction as seen from the leg Z_a, ----, and the impedance as seen from the arm Z_b, ——, when the other two ports are terminated with 50 ohms

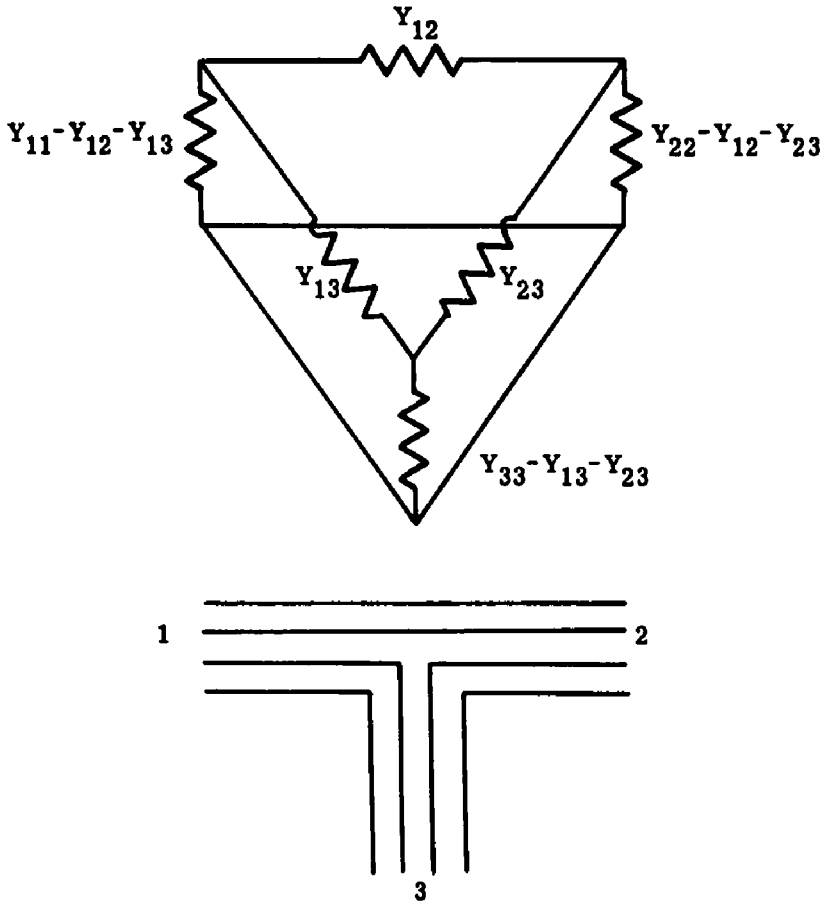


Fig. 4. 12. (a) The coaxial tee junction and (b) the equivalent circuit of the tee junction at the reference planes

Equation (4. 6) can be solved for the unknown $Y_{12} = Y_{21}$ in terms of the easily measured values Y_{11}, Y_{22}, $Y_{1in} = i_1/V_1$, and $Y_2 = i_2/V_2$:

$$Y_{12}^2 = (Y_{1in} - Y_{11})(Y_2 - Y_{22}), \qquad V_3 = 0 \quad . \tag{4.7}$$

Similarly Y_{13} is

$$Y_{13}^2 = (Y_{1in} - Y_{11})(Y_3 - Y_{33}), \qquad V_2 = 0 \tag{4.8}$$

where $Y_3 = i_3/V_3$. The value Y_{1in} in both (4. 7) and (4. 8) is the input admittance looking into the junction from port 1 for some finite Y_2 or Y_3, while Y_2 and Y_3 are the

admittances looking away from the tee junction at the reference planes of ports 2 and 3 respectively. In the measurements reported here, a short was placed a quarter wavelength from the reference plane in either one of ports 2 or 3 so that Y_2 or Y_3 was $-jY_o \cot(\frac{\pi\lambda_o}{2\lambda})$ where λ_o is the midband wavelength. The measured equivalent circuit for the 14 mm coaxial tee junction for frequencies between 8.40 and 8.60 GHz is given by

$$B_{11} = \omega C_{11} - 0.148 \text{ mhos}, \qquad C_{11} = 2.96 \text{ pF}$$

$$B_{33} = -(\omega L_{33} - 0.275)^{-1} \text{ mhos}, \qquad L_{33} = 55.7 \text{ nH}$$

$$B_{12} = \omega C_{12} - 0.138 \text{ mhos}, \qquad C_{12} = 2.92 \text{ pF}$$

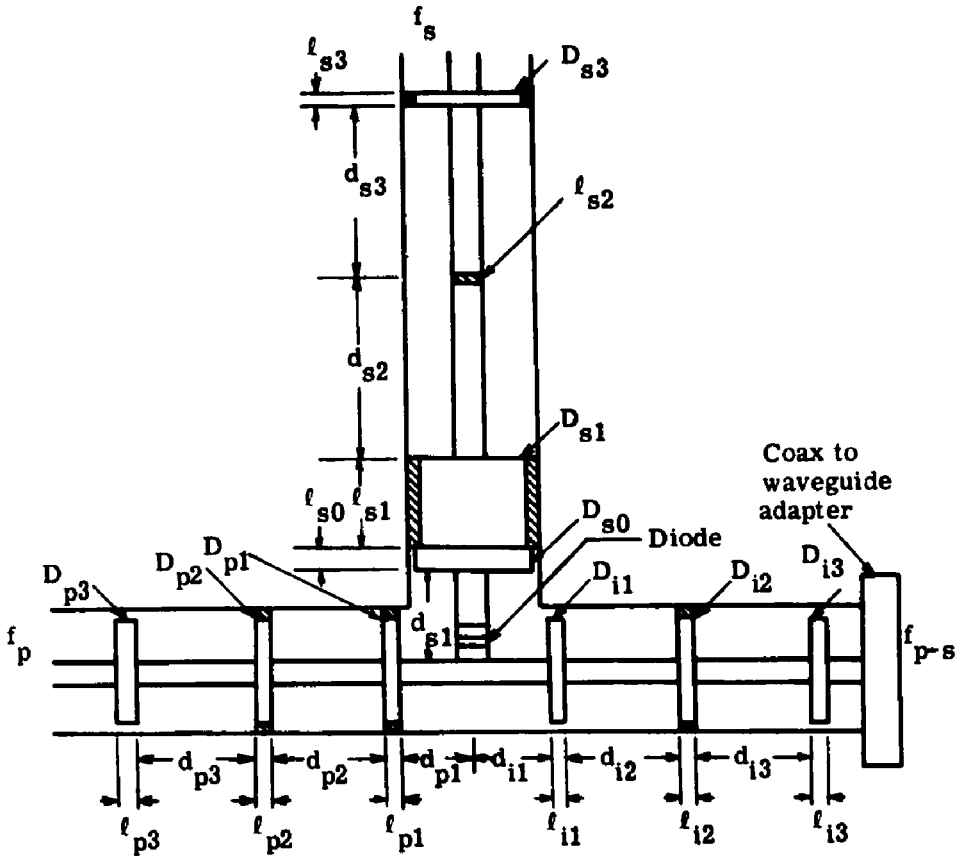
$$B_{13} = \omega C_{13} - 0.0915 \text{ mhos}, \qquad C_{13} = 2.00 \text{ pF} \quad .$$

Although the coaxial tee junction is a common microwave component, no accurate analysis has been given for it. King (Ref. 61, pp. 389-397, 426-430) has analyzed the two wire transmission line tee junction and indicated how this method might be extended to give an approximate equivalent circuit for the coaxial tee junction. However, his approach is complex and would not cover the problem of higher order modes which are excited at sufficiently high frequencies. In the absence of an accurate theoretical description of the tee junction, the above empirical model is used in the analysis of the LSUC.

4.4 The Experimental LSUC Circuits

Two LSUC circuits were designed and tested: one based on the LSUC2 design and the other on the LSUC3 design. Although 20 dB of stable gain was obtained in both upconverters, the LSUC2 required several empirical modifications before this gain was achieved while the LSUC3 did not require these modifications.

The theoretical LSUC2 used an ideal band-stop filter to help isolate the signal port from the lower sideband frequency. However, experimentally it was found expedient to not use a band-stop filter. This together with the effects of the nonideal tee junction made it necessary to modify both the signal and lower sideband circuits to obtain the desired gain. The final experimental amplifier is shown in Fig. 4.13. In contrast to the preceding design, the LSUC3 required neither a band-stop filter nor an ideal tee



Distances in.	Disk Lengths in.	Disk Diameters in.
$d_{p1} = 0.386$	$\ell_{p1} = 0.1544$	$D_{p1} = 0.542$
$d_{p2} = 0.6338$	$\ell_{p2} = 0.0817$	$D_{p2} = 0.532$
$d_{p3} = 0.6804$	$\ell_{p3} = 0.0375$	$D_{p3} = 0.502$
$d_{i1} = 0.427$	$\ell_{i1} = 0.0103$	$D_{i1} = 0.499$
$d_{i2} = 0.8143$	$\ell_{i2} = 0.0860$	$D_{i2} = 0.502$
$d_{i3} = 0.7966$	$\ell_{i3} = 0.0111$	$D_{i3} = 0.502$
	$\ell_{s0} = 0.1222$	$D_{s0} = 0.554$
$d_{s1} = 2.301$	$\ell_{s1} = 0.952$	$D_{s1} = 0.502$
$d_{s2} = 2.599$	$\ell_{s2} = 0.020$	
$d_{s3} = 3.424$	$\ell_{s3} = 0.1094$	$D_{s3} = 0.502$

Fig. 4.13. Schematic diagram of the experimental LSUC2 including the final experimental dimensions. The transmission line is standard 14 mm 50 ohm coaxial line and the cross-hatched sections are Teflon

junction, so this upconverter provided the desired gain without recourse to empirical design modifications. A cut away view of the LSUC3 is shown in Fig. 4. 14, and the upconverter together with the associated equipment is shown in Fig. 4. 15.

4. 4. 1 Gain. Both amplifiers were designed to have a transducer power gain of 20 dB based on an elastance pumping coefficient $S_1/S_0 = 0.35$. When the input power was set to -80 dBm , the output power was 20 dB higher as measured on a calibrated spectrum analyzer. The gain can be increased or decreased by simply changing the applied pump power. The LSUC2 had a maximum gain of 37 dB, and the LSUC3 had a maximum gain of 33 dB before oscillations occurred.

4. 4. 2 Bandwidth. If the amplifier bandwidth were limited by the pass-band of the signal or lower sideband impedance transformers, then its value would exceed 400 MHz. However both the measurements and the theoretical gain versus frequency calculations show the amplifier bandwidth to be much less than this. Evidently the complicated circuit impedance and the diode package parasitic elements, rather than the filters themselves, are primarily responsible for limiting the bandwidth.

The 3 dB bandwidth of the LSUC2 was measured and found to be 3. 5 MHz. Because of the various above mentioned modifications in this circuit, a comparison with theory is not possible.

The experimental gain curve for the LSUC3 is shown in Fig. 4. 16 for various values of pump power (or various values of maximum gain). The 3 dB bandwidth for the 20 dB curve is 2. 6 MHz. These curves cannot be compared directly with the corresponding theoretical calculation of the LSUC3 (Fig. 3. 22) in Chapter III because of some minor differences in the two amplifiers. These differences are listed below.

1. The experimental amplifier has a maximum gain of 20 dB while the theoretical amplifier has a midband gain of 20 dB.
2. The distance between the diode and the lower sideband filter is increased by $\lambda_{p-s}/2$ so as to make a gradual transition from the diode cartridge diameter to the coaxial center conductor diameter.
3. The distance between the tee junction and the pump filter is increased by $\lambda_{p-s}/2$ so that the pump filter does not extend into the tee junction area itself.

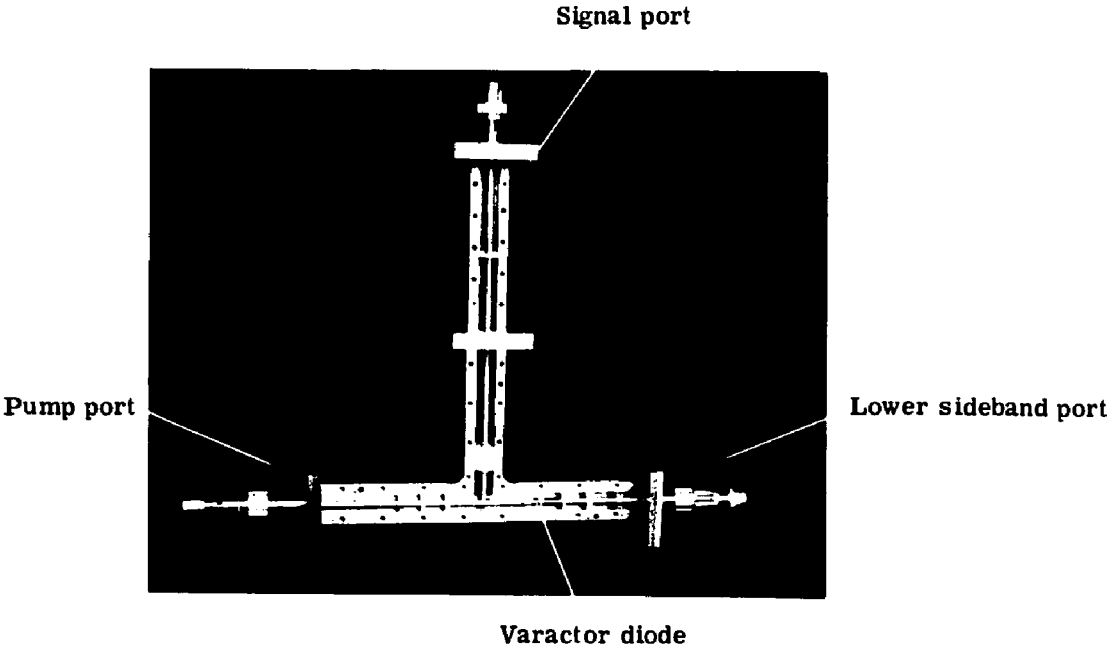


Fig. 4.14. Photograph of the LSUC

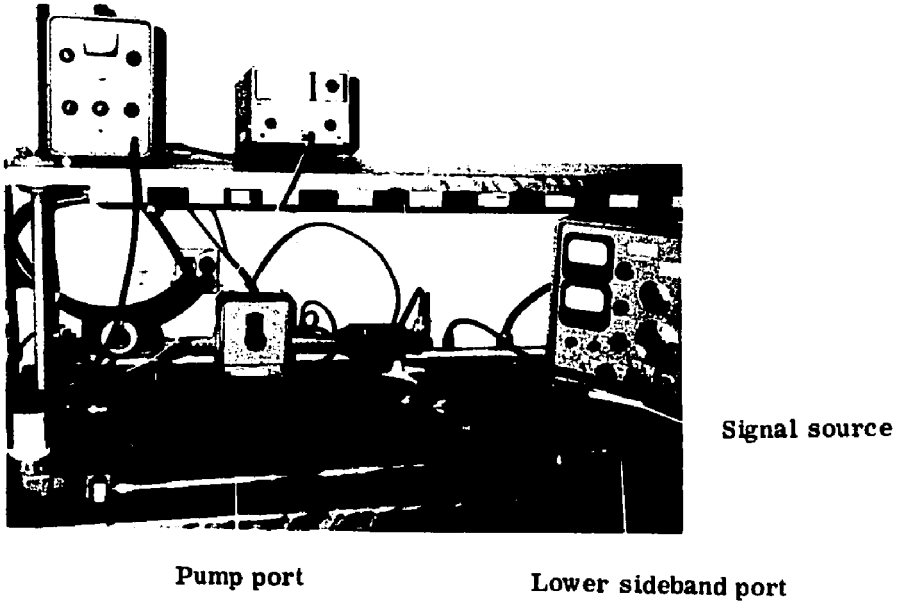


Fig. 4.15. Photograph of the LSUC when in operation

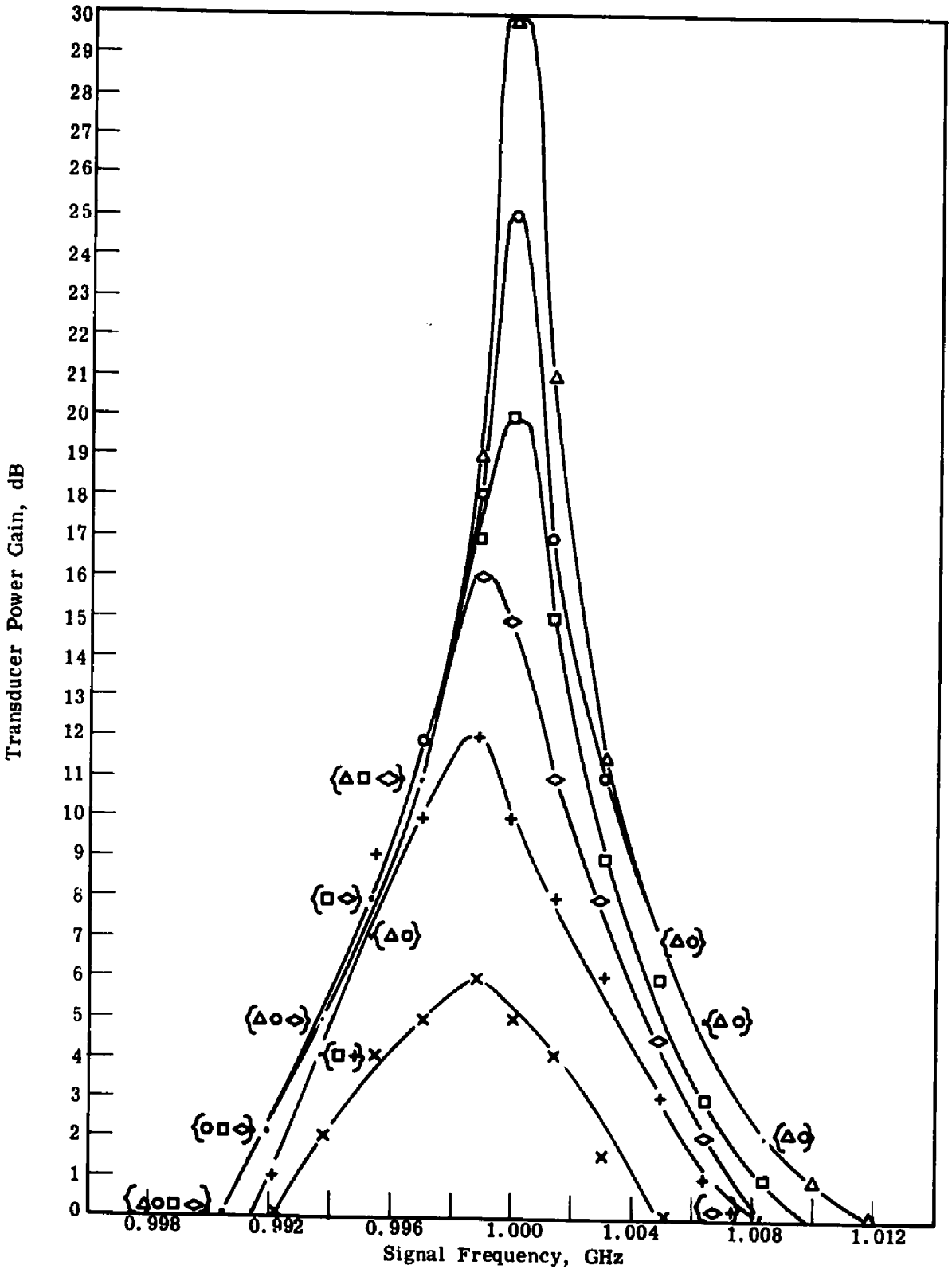


Fig. 4.16. Experimental power gain of LSUC3 when the midband gain is 30 dB (△), 25 dB (o), 20 dB (□), 15 dB (◇), 10 dB (+), and 5 dB (×)

4. The distance between the lower sideband filter and the high-pass filter is approximately 3. 5 λ_s because of the long line stretcher used.
5. The distance between the pump filter and the corresponding high-pass filter is approximately 1. 5 λ_s because of the long line stretcher used in the circuit.
6. The actual tee junction frequency sensitivity is neglected in the theoretical LSUC3 in Chapter III.

All these differences do not change the basic design philosophy of the LSUC3, but they must be incorporated in the analysis of the amplifier to obtain correspondence between theory and experiment. When these changes are made the theoretical gain curves are shown in Fig. 4. 17 which at 20 dB gives a bandwidth of 4. 63 MHz. Shown in Fig. 4. 18 is a comparison of the gain-bandwidth product for various pump levels. The complex behavior of the element values for the equivalent circuit of the tee junction (the equations given in Section 4. 3. 2 are the best linear approximations to the actual susceptances), the connector reactances, the line stretcher reactances, and the SWR of the high-pass filters in the pass-band, all contribute to bandwidth reduction beyond that calculated for Fig. 4. 17. The major limitation to the bandwidth, however, seems to be the long line stretchers, for if they could be removed and the high-pass filters brought next to the pump and lower sideband filters respectively, a bandwidth of 21. 6 MHz would be expected.

4. 4. 3 Noise Figure. When the output impedance of an amplifier is negative, care must be taken in correctly measuring the amplifier noise figure. In systems using a LSUC an isolator is normally attached to the output of the amplifier, so the noise figure of the LSUC and output isolator was measured as a single unit. There are several definitions of noise figure, but the one most convenient when dealing with negative resistance amplifiers is the "actual" noise figure (Ref. 40). The actual noise figure is consistent with the definition of the transducer power gain and accounts for the noise generated in the load and generator impedances. A block diagram of the noise measuring circuit is shown in Fig. 4. 19 while a photograph of the system is shown in Fig. 4. 20. The noise figure for a cascade of stages is

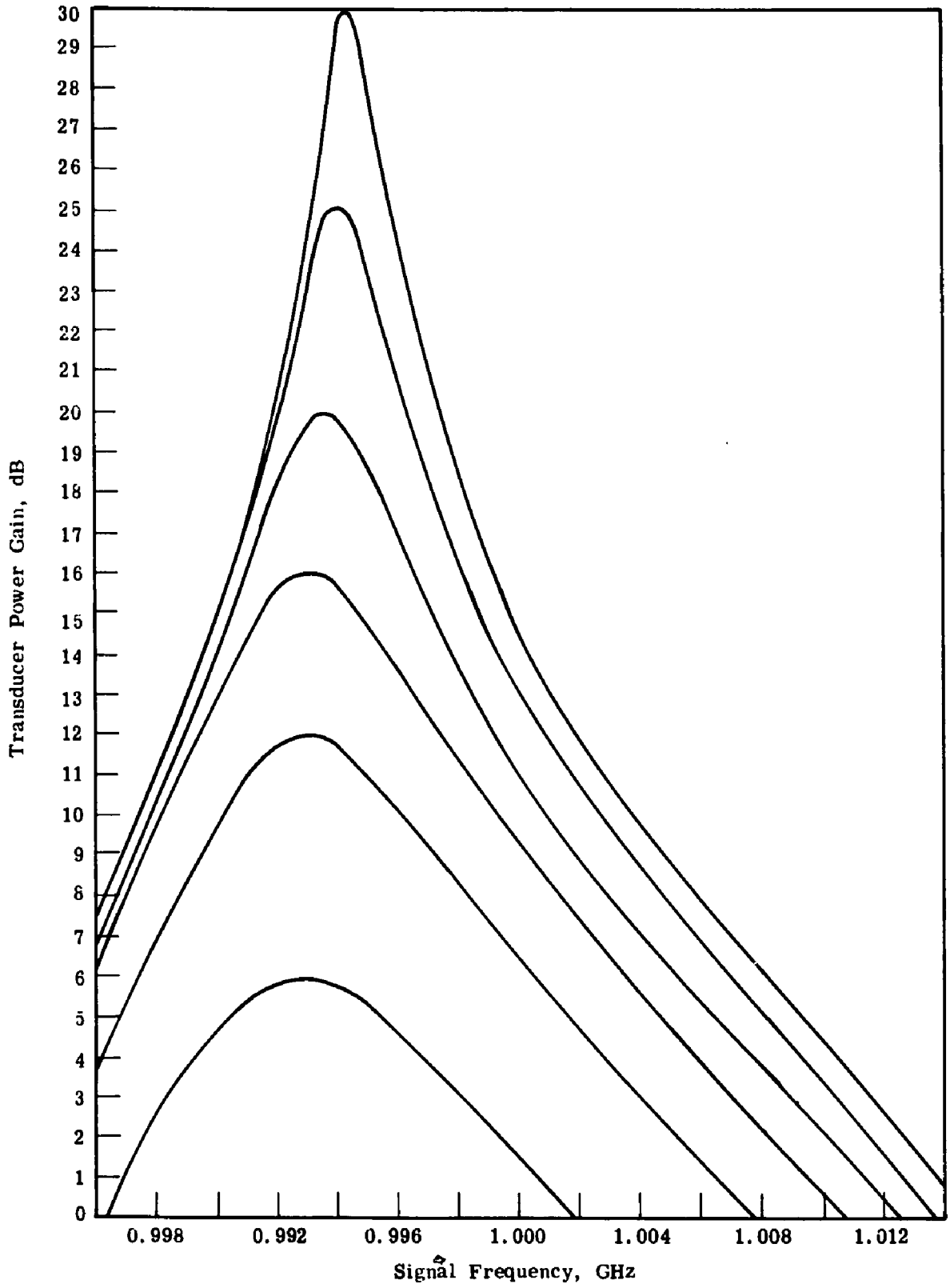


Fig. 4.17. Theoretical gain curves for LSUC3 when the circuit is modified because of physical requirements

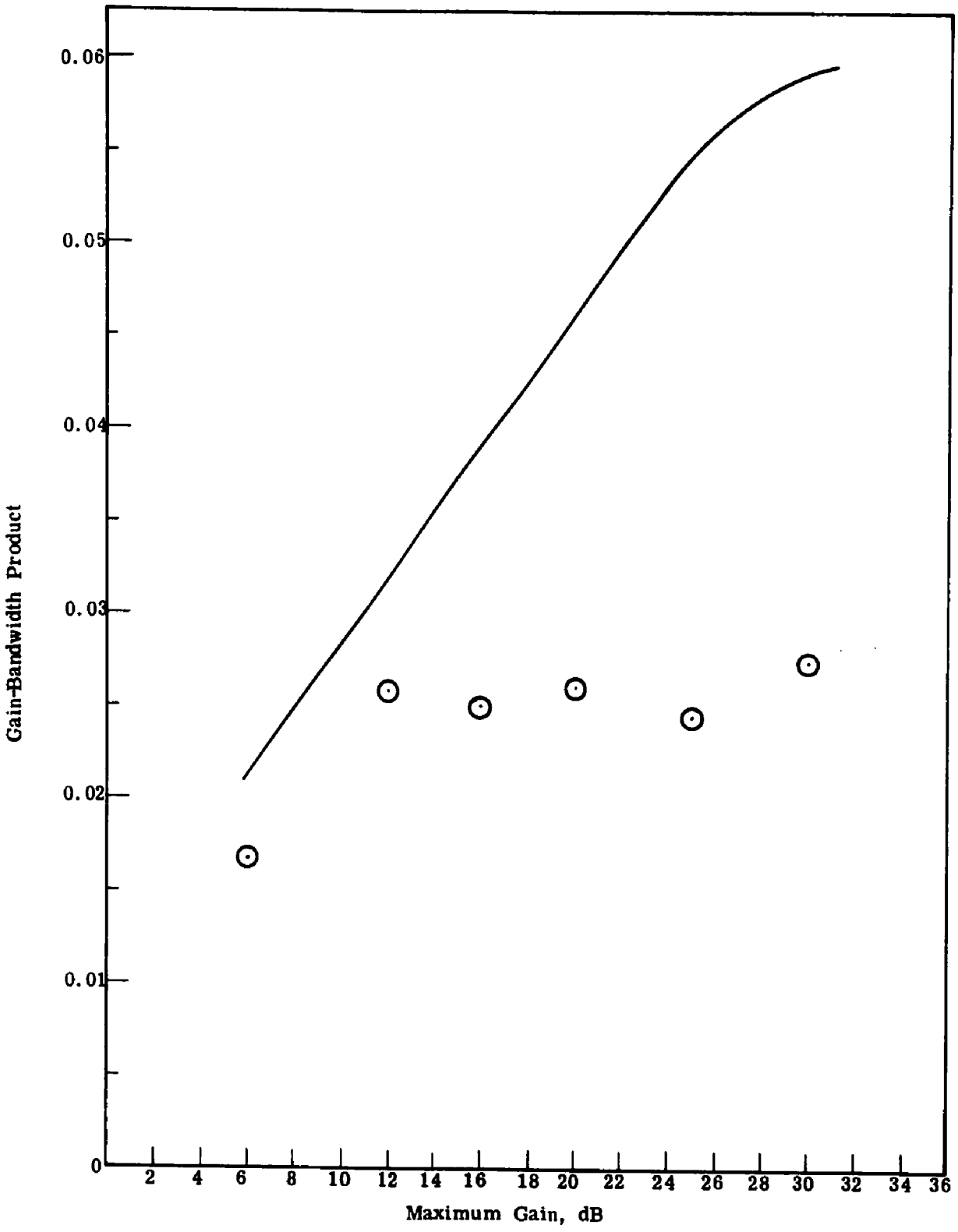


Fig. 4.18. Comparison of theoretical and experimental gain-bandwidth product

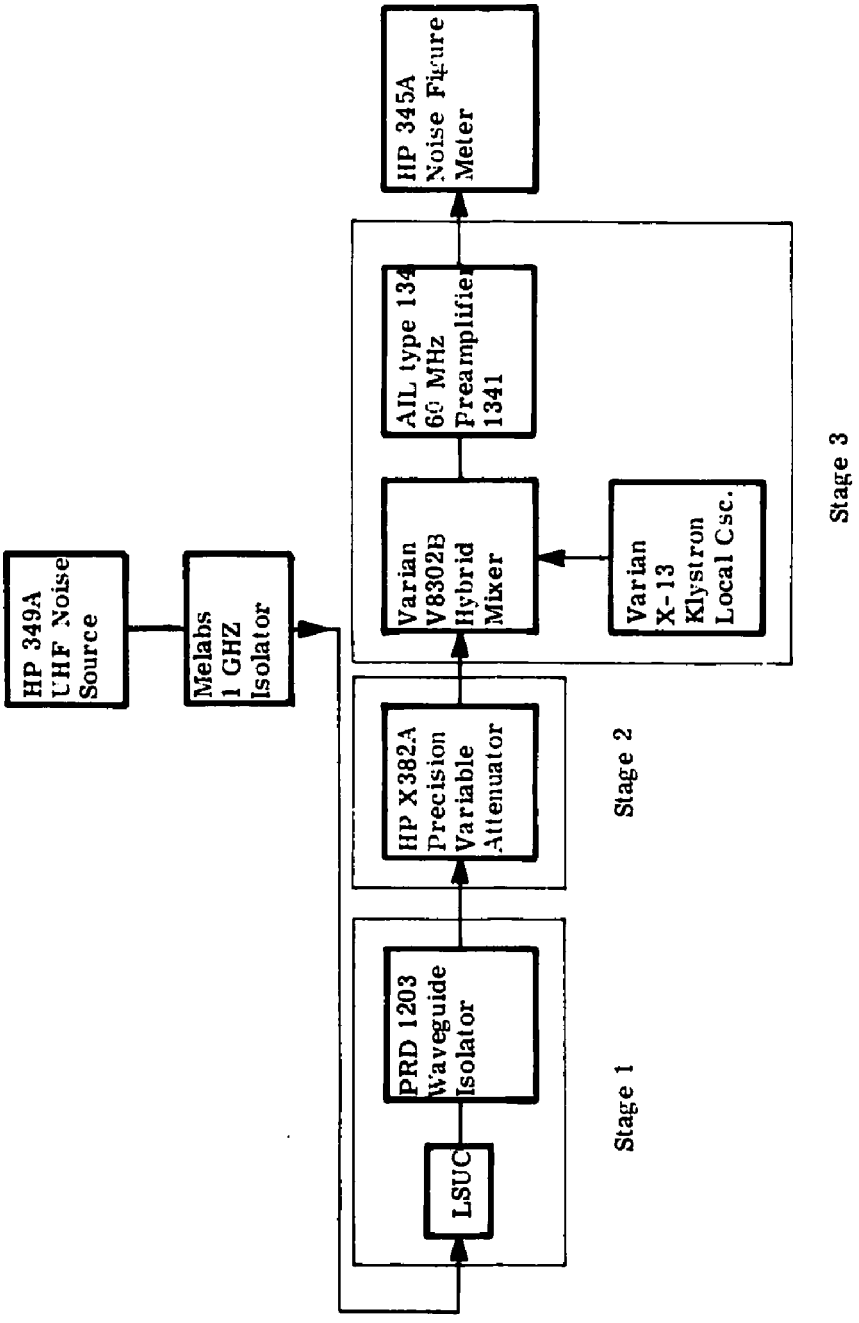


Fig. 4.19. Noise figure measuring circuit

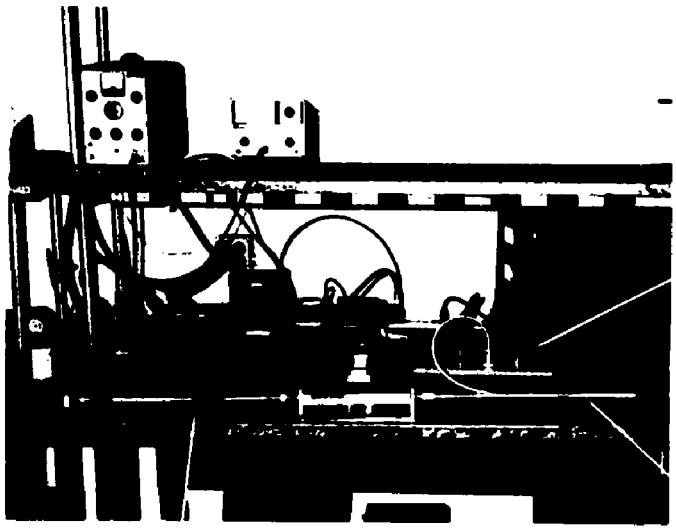


Fig. 4. 20. Photographs of the noise figure measuring circuit

$$F = F_1 + \frac{F_2 - 1}{G_{21}} + \frac{(F_3 - 1)L_2}{G_{21}}$$

where G_{21} is the gain of the LSUC (stage 1) and L_2 is the loss in the variable attenuator (stage 2). If the ambient temperature is $290^{\circ}K$, then $F_2 = L_2$ and the total noise figure reduces to

$$F = F_1 - \frac{1}{G_{21}} + \frac{L_2 F_3}{G_{21}} \quad .$$

When the total noise figure is measured as a function of L_2, the result is a straight line with slope = F_3/G_{21} and intercept at $F = F_1 - 1/G_{21}$. Since F_3 can be found by an independent measurement, G_{21} and finally F_1 can be obtained, where F_1 is the noise figure of the amplifier and isolator combination. This method gives accurate results since individual measurement errors can be averaged.

The noise figure of both amplifiers was measured by setting the gain at 5 dB, 10 dB, and 20 dB by an appropriate choice of pump power when a sine wave was applied at the signal port. The noise figure of stage 3 was 10.0 when the noise figure for LSUC2 was to be found, and 9.5 for the LSUC3 measurement. The difference in F_3 between the two cases is ascribed to the difference in frequency and output power of the local oscillator. The straight line graphs generated for these measurements are shown in Figs. 4.21 and 4.22 and the final results in Table 4.2. These two figures experimentally confirm the result cited in (3.25) : $F - 1/G_{21}$ is a constant.

The results shown in Table 4.2 indicate the upconverter amplifies noise power as much as 5 dB less than CW power. The reason for this discrepancy is unknown, but when the CW and noise gain of an Aertech TY538, X-band, tunnel diode amplifier were measured, they both came out to be 10 dB. The discrepancy therefore seems to be inherent in the upconverter itself.

The theoretical spot noise figure obtained from (3.24) when the 5×5 matrix approximation is used is shown in Fig. 4.23. To relate this with the measured value, a relationship between the spot noise figure $F(f)$ at frequency f and the average noise figure $\overline{F}$ is needed. This expression is

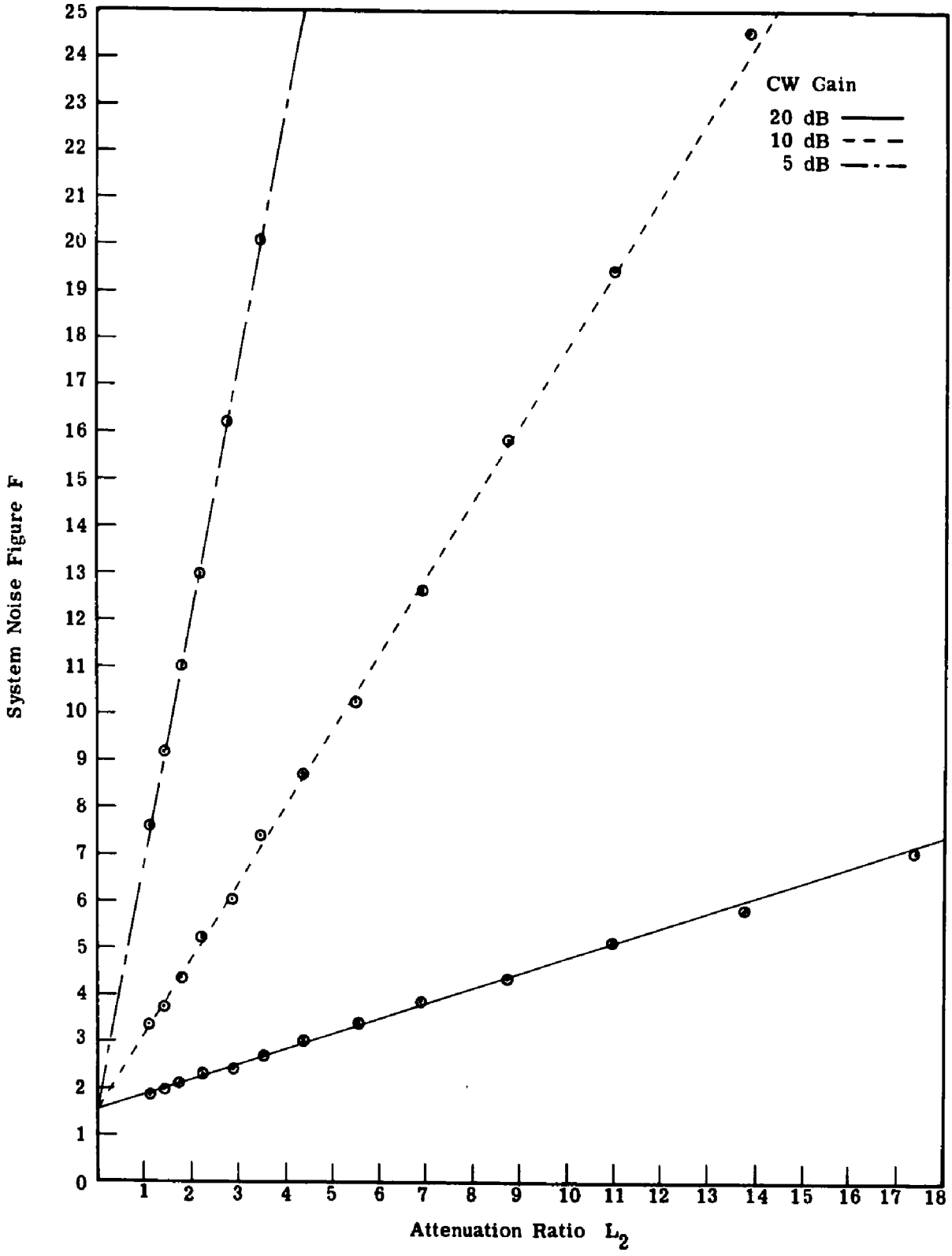


Fig. 4.21. Noise figure of LSUC2

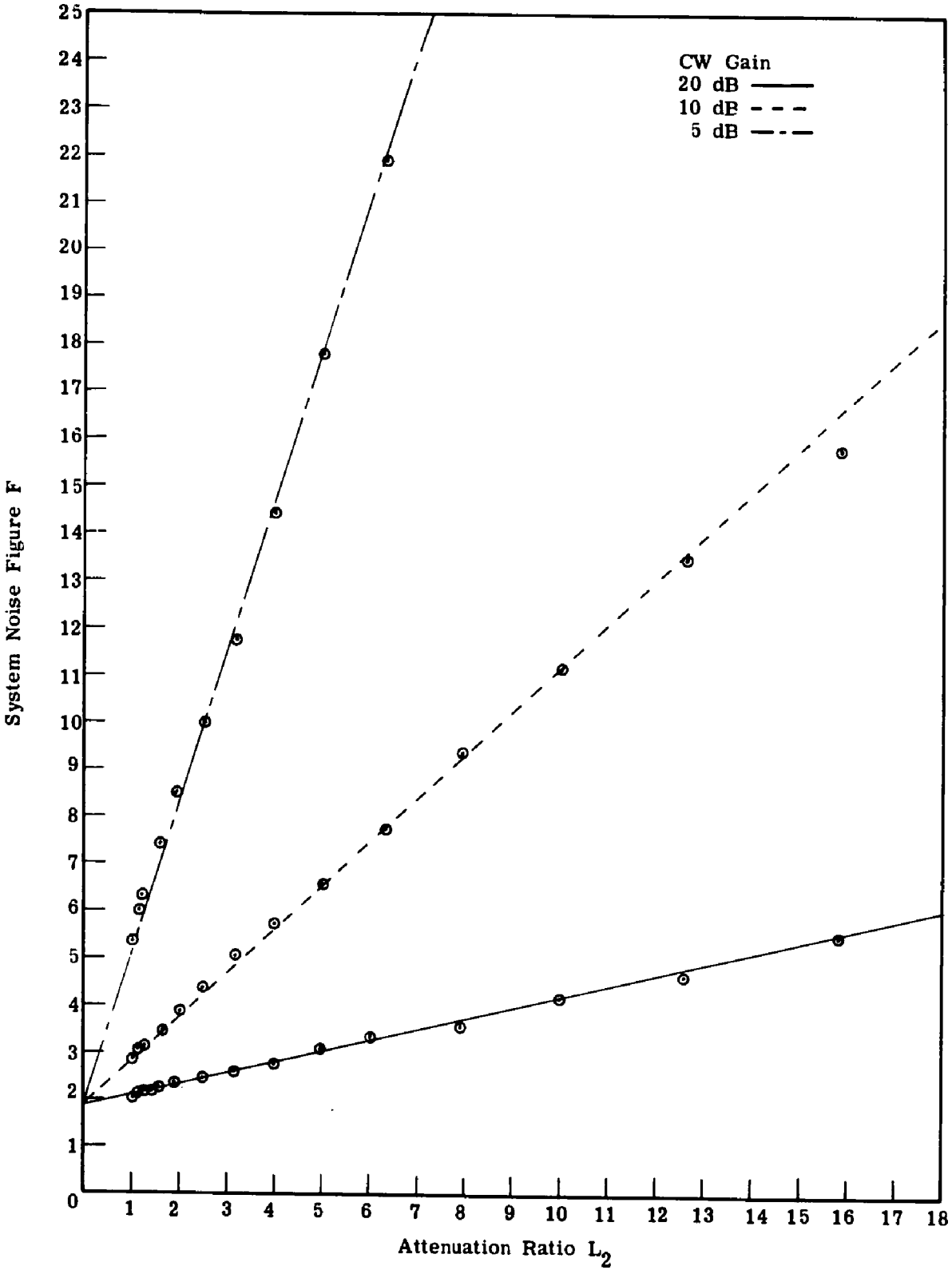


Fig. 4. 22. Noise figure of LSUC3

	CW Gain dB	Slope	Noise Gain dB	Noise Figure F_1	Excess Noise Temperature
LSUC2	20	0. 326	14. 87	1. 58	$168^{o}K$
	10	1. 632	7. 87	1. 71	$206^{o}K$
	5	5. 362	2. 71	2. 09	$316^{o}K$
LSUC3	20	0. 236	15. 77	1. 88	$255^{o}K$
	10	0. 931	9. 81	1. 95	$276^{o}K$
	5	3. 210	4. 44	2. 21	$351^{o}K$

Table 4. 2. Noise figure of the LSUC

$$\overline{F} = \frac{\int F(f)\, G_{21}(f)\, df}{\int G_{21}(f)\, df} \tag{4. 9}$$

where G_{21} is the upconverter gain (Ref. 62). When the data used in plotting Figs. 4. 23 and 4. 17 are numerically integrated, the theoretical average noise figure is found to be 1. 187: a value significantly lower than the measured noise figure. In the following paragraphs, various other sources of noise are investigated to explain this discrepency.

4. 4. 3. 1 Circuit Losses. Resistive circuit losses adds some thermal noise to the amplifier. However when the LSUC was numerically analyzed in a circuit taking account of this loss, the change in the noise figure was negligible. In the calculation the standard values for the resistivity for brass ($6. 4\ 10^{-8}$ ohm-meter), the standard loss tangent for Teflon ($3. 7\ 10^{-4}$), and a roughness factor of 1. 8 (Ref. 63) were used. The result is a change in the thermal noise figure of only 0. 0023: a value too small to be measured with a standard noise figure meter.

4. 4. 3. 2 Incorrect Value of Diode Bulk Resistance. One important source of noise is the series bulk resistance of the diode. If this resistance increases, the noise figure also increases. However when the noise figure was calculated for the LSUC with R_s = 1. 41 ohms replaced by R_s = 7. 71 ohms, the noise figure with the gain adjusted to give 20 dB increased to only 1. 19 . Observation of the midband noise figure expression for the uncooled LSUC,

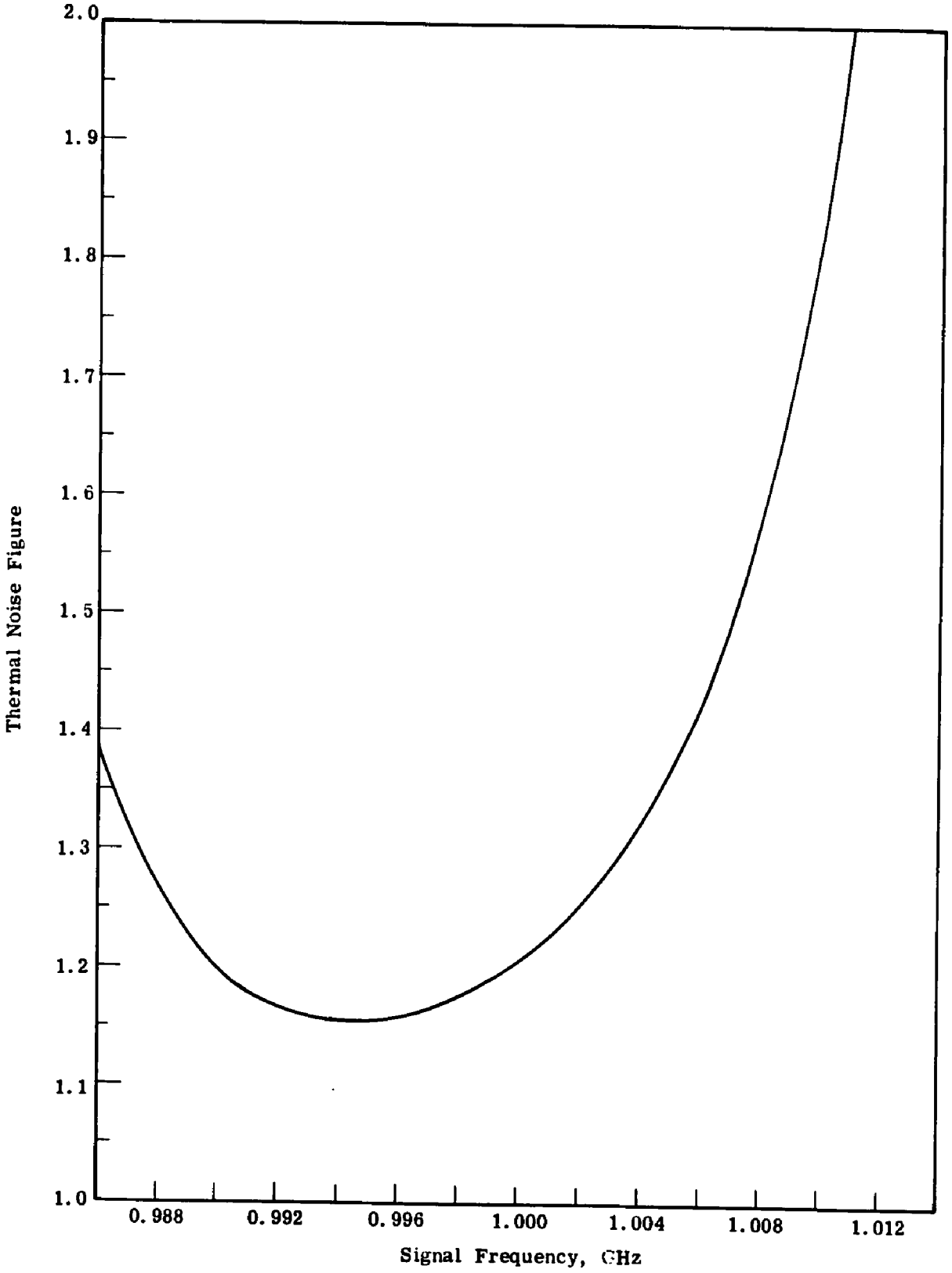


Fig. 4.23. Theoretical noise figure for LSUC3

$$F = \left(1 + \frac{1}{x_g}\right)\left(1 + \frac{1}{r}\right) + \frac{1}{G_{21}} \qquad (4.10)$$

shows that when x_g is large (= 100 in this case), decreasing it by a factor of 5.5 as done here does not greatly degrade the noise figure.

4.4.3.3 Noisy Pump Source. The noise fluctuations of the pump oscillator are generally considered to have an insignificant effect on the noise figure of parametric amplifiers. Uenohara (Ref. 41) assumed this on the basis that for a properly adjusted amplifier, the gain is almost constant for small variations in pump power. More recently IMPATT diodes have been used for parametric amplifier pump sources. Although FM and AM noise of IMPATT diodes are considered to be from 20 to 25 dB higher than that found in klystrons (Ref. 64), Gray, Kikushima, Morenc, and Wagner (Ref. 65) found that the noise figure, bandwidth, and gain were the same for the klystron and IMPATT diode pump sources.

A first order approximation to the FM noise introduced by the pump source can be obtained from (4.10) which is valid for the 2×2 matrix approximation when the generator and load resistances are independent of frequency. The FM noise of the pump effects both the frequency ratio r and the gain G_{21}, while the AM noise effects only the gain. The pump FM, which causes fluctuations only in ω_2, increases the frequency ratio term by the factor

$$1 + \frac{\delta\omega}{\omega_{20}}$$

where $\delta\omega = \omega_2 - \omega_{20}$. Assuming single tuned circuit elements, the reactance at the lower sideband frequency is

$$-X_{22} = -2\frac{S_0}{\omega_{20}}\frac{\delta\omega}{\omega_{20}} \quad .$$

Using these expressions in (3.12) and substituting into (4.10), the modified noise figure is

$$F = \left(1 + \frac{1}{x_g}\right) + \left(1 + \frac{1}{x_g}\right)\frac{1}{r}\left(1 + \frac{\delta\omega}{\omega_{20}}\right) + \frac{1}{G_0}\left\{1 + \frac{\delta\omega}{\omega_{20}}\,\frac{2K_q}{(1 + x_g)(1 + y_\ell) - K_q}\right.$$

$$\left.\left(\frac{\delta\omega}{\omega_{20}}\right)^2 \frac{K_q^4 + 4(1 + x_g)^2 Q_{20}^2}{[(1 + x_g)(1 + y_\ell) - K_q]^2} + \mathcal{O}\left(\frac{\delta\omega}{\omega_{20}}\right)^3\right\} \qquad (4.11)$$

where G_0 is the midband gain. The additional noise figure due to the FM noise alone F_{FM} is readily obtained from this expression. The pump klystron used for the LSUC had an FM bandwidth of approximately 25 KHz at $f_p = 9.50$ GHz. Using this value plus the LSUC parameters used in the design,

$$F_{FM} = 1.75 \times 10^{-7} + \frac{1}{G_0}(4.86 \times 10^{-6})$$

$$\cong 2.24 \times 10^{-7} \quad .$$

Thus the increase in the noise figure from frequency fluctuations in the pump source is negligible.

An amplitude fluctuation in the pump source leads to AM noise in the upconverter through variations in S_1^2 . The reciprocal of the gain under this condition is given by

$$\frac{1}{G_{21}} = \frac{1}{G_0}\left\{1 + \frac{\delta S_1^2}{S_1^2}\left[1 + \frac{2K_q}{(1 + x_g)(1 + y_\ell) - K_q}\right]\right.$$

$$+\left(\frac{\delta S_1^2}{S_1^2}\right)^2\left[\frac{2K_q}{(1 + x_g)(1 + y_\ell) - K_q} + \frac{K_q^2}{[(1 + x_g)(1 + y_\ell) - K_q]^2}\right]$$

$$\left.+\mathcal{O}\left[\left(\frac{\delta S_1^2}{S_1^2}\right)^3\right]\right\}$$

which reduces to $1/G_0$ when there is no AM noise. If the parameters used in the design of the LSUC are used, the additional AM noise in the upconverter is

$$F_{AM} = \frac{1}{G_0}\left[\frac{\delta S_1^2}{S_1^2}(4.31) + \left(\frac{\delta S_1^2}{S_1^2}\right)^2 (6.03)\right] \quad .$$

Assuming a gain of 20 dB and a pessimistic elastance variation of $\delta S_1^2/S_1^2 = 0.01$, this AM noise reduces to

$$F_{AM} = 4.31 \times 10^{-4} \quad .$$

Clearly both the AM and FM noise from the pump source add negligible noise figure to the upconverter. Thus from both experimental substitution of a noisy pump source for a quiet one and observation of (4.10), the noise in the pump source can be neglected as a major contributor to the upconverter noise figure.

4.4.3.4 Pump Heating of Diode. Garbrecht (Ref. 66) proposed that the heating effect of the pump power on the diode spreading resistance determines the lower limit of noise temperature for cooled parametric amplifiers. An expression which describes the effect of diode heating can be obtained from (3.24) by setting the shot noise components to zero. Under large pumping conditions the diode temperature can be expected to rise approximately $40^{\circ}K$ above ambient, which increases the noise figure by less than 0.009. Although the pump heating effect is important for cooled parametric upconverters it is not important for room temperature upconverters.

4.4.3.5 Shot Noise. In Chapter III an expression was derived for the shot noise in a LSUC caused by the dc bias current i_0. This relationship, which is plotted in Fig. 4.24 with diode temperatures $T_d = 290^{\circ}K$ and $330^{\circ}K$, shows that the diode would have to draw an excessive current for the noise figure to be close to the measured value of 1.9. However Josenhans (Ref. 39) noticed that the slope of the corresponding curve for his reflection parametric amplifier using silicon diodes was a factor of 10 to 15 higher than what his theory predicted. At the same time, when he measured germanium and gallium arsenide diodes, his theoretical and experimental values matched within the experimental error. If this same factor is applied here, only $10\mu A$ of dc current (or an equivalent forward-and-back current) is needed to give a noise figure of 1.9. Apparently the zero minority carrier lifetime assumption used in deriving the noise figure

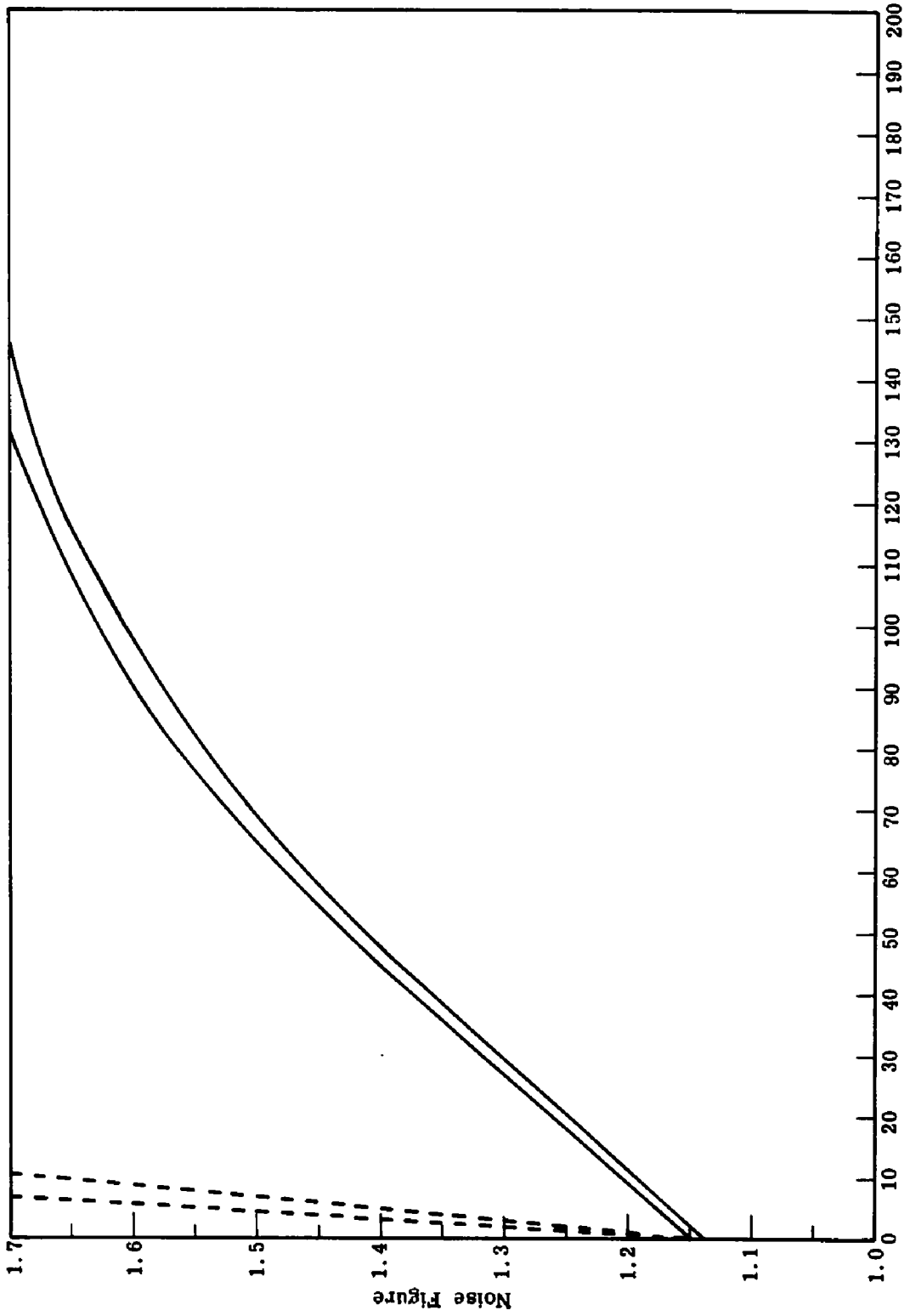


Fig. 4.24. Thermal plus shot noise figure of a LSUC at 290°K when the diode is at 290°K and 330°K. The dashed curves have slopes 10 and 15 times larger than the noise figure curve

expression (3. 24) is in error for silicon diodes. The remainder of this section describes an experimental investigation of the effects of nonzero minority carrier lifetime.

In the experimental LSUC3 described in this chapter, the diode circuit at dc is open. Thus any shot noise arising in the upconverter must be caused by forward-and-back current. Unfortunately this current cannot be directly measured, but there are two indications that it is responsible for the high noise figure. The first is that the noise figure increases significantly as the diode bias increases, and the second is that the diode exhibits changes in the dc characteristic when pumped by an RF source, suggesting the existence of significant forward-and-back current.

To verify the first of these indications, the noise figure of a LSUC as a function of bias voltage was measured. Since a change in bias changes the diode capacitance, variable tuning elements were needed to compensate for this change so that the gain and pump power could be kept constant. This is accomplished by replacing the impedance transformers in LSUC3 with numerous filters and variable tuning elements. The pump frequency in this case was 10. 59 GHz and the signal frequency 1. 843 GHz . The bias voltage was applied through a General Radio 874-FBL bias insertion unit placed in the signal port. The dc current was thus conducted through the center conductor to the diode and returned to the outer conductor by the shorted double-stub tuner in the lower sideband circuit. The noise figure was measured using the same techniques described in Section 4. 4. 3, and the results are shown in Fig. 4. 25. Although the magnitude of the noise figure for this empirically designed LSUC was poor (partly because of the low gain of this device) the noise figure clearly increased with increase in bias voltage. By allowing $7\mu A$ current to flow, the noise figure of the LSUC increased by 10 dB over the reverse bias configuration. (The break in the curve at $V_b = 0$ results solely from the change in scale of the abscissa.) The existence of nonzero forward dc current, which is indicated near the appropriate data points, even when the dc voltage is zero shows that the pump source is producing some dc current.

The second indication of significant forward-and-back current can be seen in the dc volt-ampere characteristics of the varactor when pumped by a large RF signal (Fig. 4. 26). These measurements were made by series mounting the same varactor

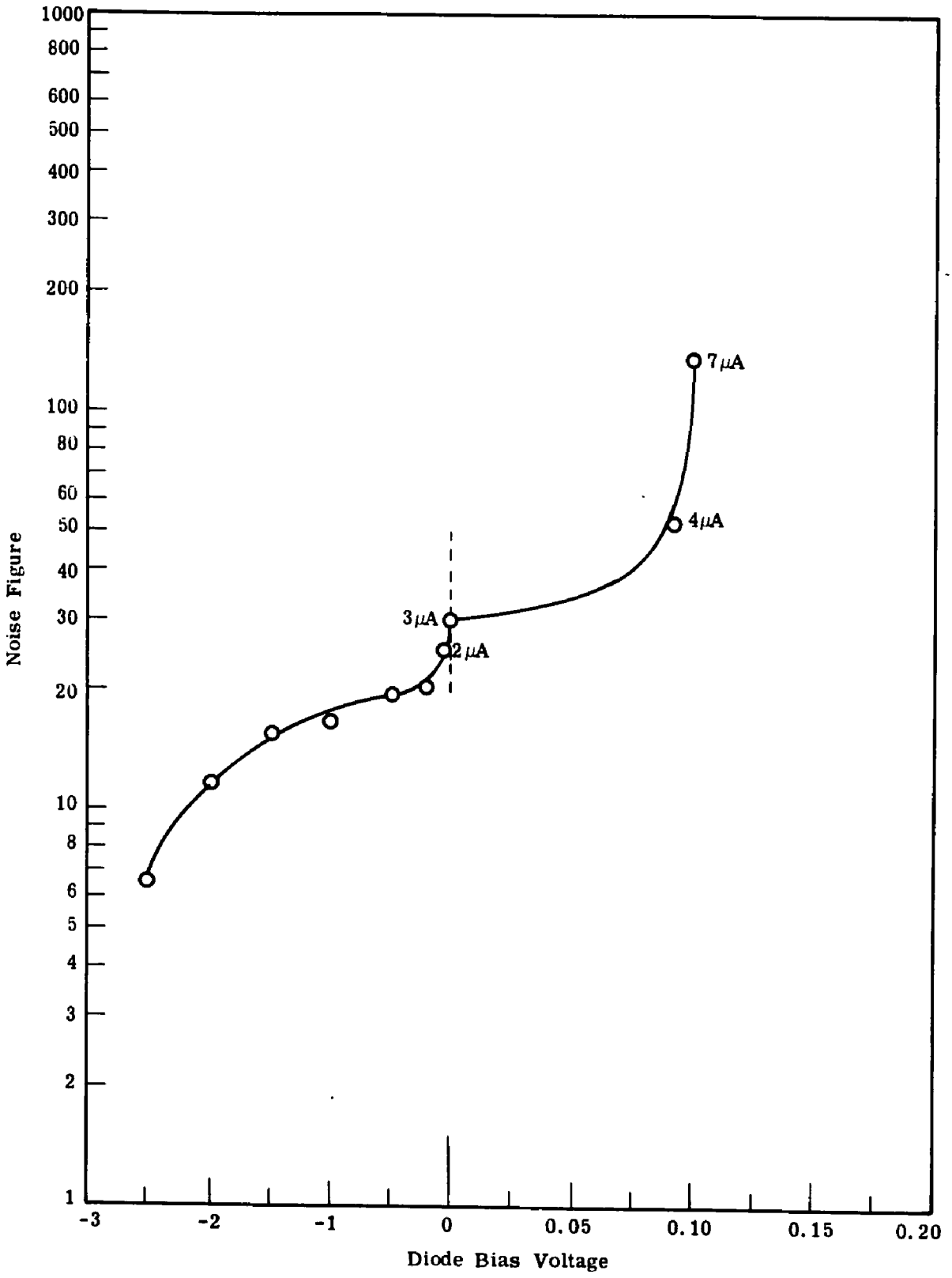


Fig. 4. 25. Noise figure of a LSUC as a function of bias voltage when the gain and pump power is constant

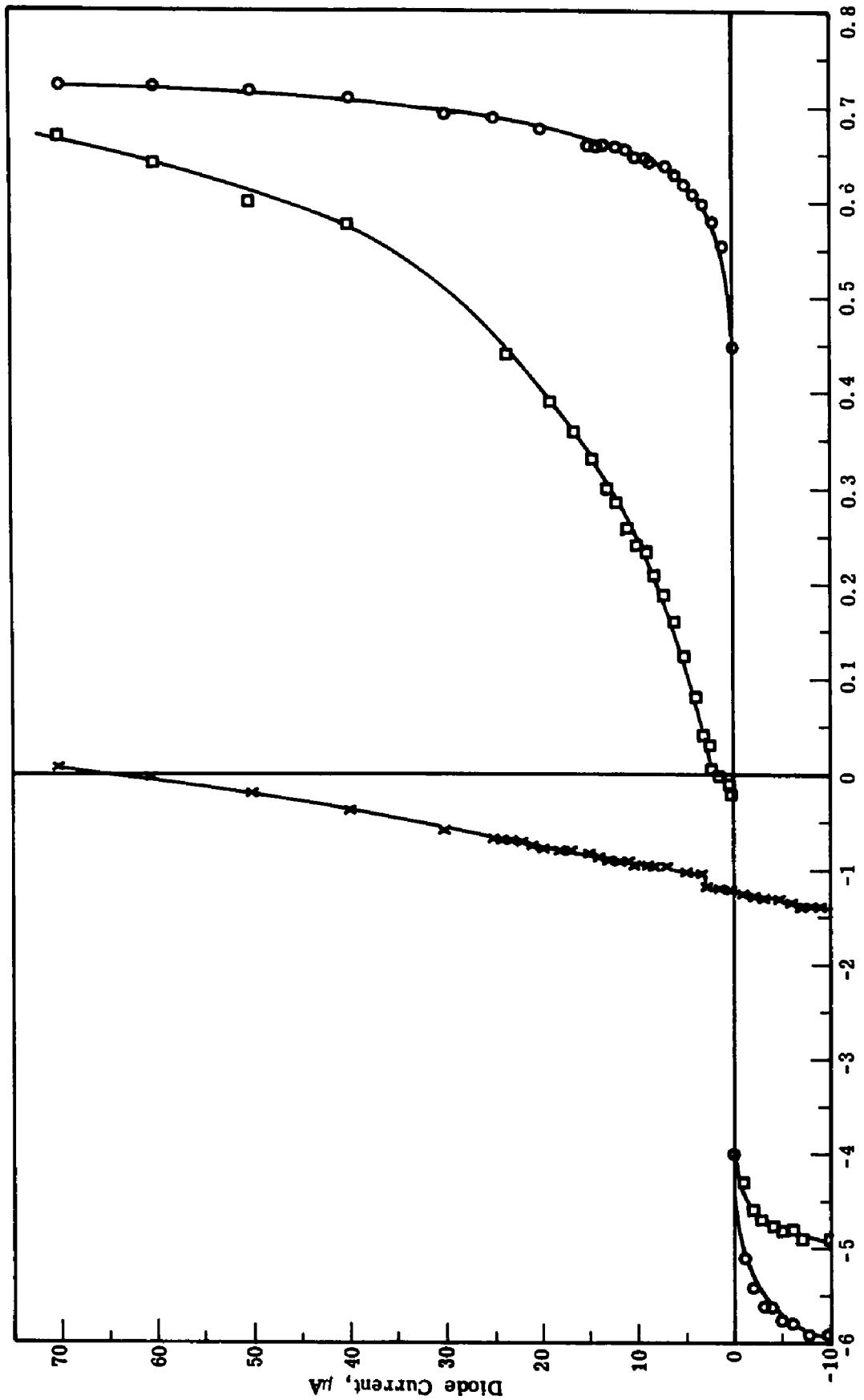


Fig. 4.26. Varactor diode dc current-voltage characteristics with no RF power (○), with 71 mW RF (□), and with 0.71 W (×). The applied RF is 9.5 GHz, and the diode is series mounted in a terminated 14 mm coaxial line

diode used previously in a 14 mm terminated coaxial line (Fig. 4. 27). This circuit, like Siegel's (Ref. 42), was used to avoid tuning the diode at a particular frequency. Although the measurement results found in Fig. 4. 26 failed to show any negative resistance region, the application of pump power clearly had a significant effect on the diode. Siegel found after careful investigation that the negative resistance he observed was not caused by the ac signal swinging from reverse breakdown to forward conduction. The same conclusion is valid here, since even under heavy pumping (0. 71 W), the voltage swing across the diode chip would be approximately $\pm$ 0. 40 volts: a value much smaller than the reverse bias to forward conduction voltage range for the unpumped varactor. Thus the pump in the LSUC may well cause charge multiplication in the varactor which in turn contributes to the shot noise figure of the amplifier.

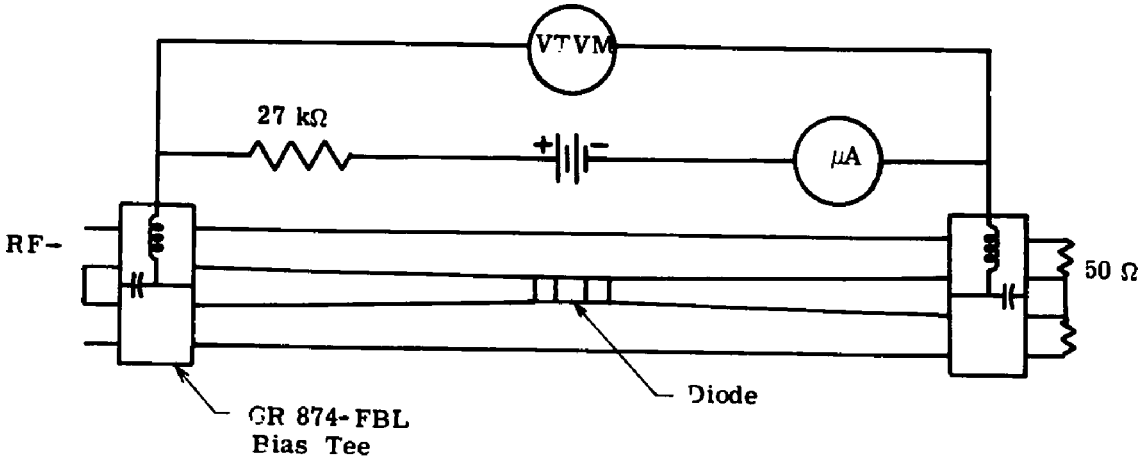


Fig. 4. 27. Mount for measuring diode current-voltage characteristic under pumped conditions

4. 5 Conclusions

The results presented here verify the synthesis techniques developed in Chapter III for the LSUC. The additional adjustments in the analysis needed to account for the extra half wavelength line sections used in the experimental LSUC and the nonideal tee junction do not affect the basic design theory. The measured noise figure was however significantly larger than that calculated on the basis of thermal noise alone. Shot noise with an additional charge multiplication mechanism appear to be the primary cause of this extra noise.

CHAPTER V

DIFFUSION ADMITTANCE

5. 1 Introduction

The work described in Chapters II, III, and IV has dealt primarily with circuit aspects of the LSUC. Even the diode is considered as an equivalent circuit with a time varying elastance. Here the varactor diode chip itself is analyzed with special attention given to the evaluation and effects of diffusion admittance. Diffusion capacitance arises when a pn junction is biased in the forward conduction region for at least part of an RF cycle. Charge carriers driven across the junction become minority carriers and would recombine if they stayed there long enough. However if the lifetime of the carriers is much longer than the period of the applied ac voltage, most of the minority carriers will return across the junction before they recombine. This charge storage effect produces a circuit element known as diffusion capacitance.

The diode elastance harmonics used in Chapter III were derived using the depletion layer capacitance alone. Since varactors used in parametric circuits are often forward biased during part of the pump cycle, diffusion admittance plays an important role in amplifier performance. The analysis presented here indicates how the diode characteristic can be optimized to enhance LSUC performance.

A review of the literature in Section 5. 2 shows that overdriving the diode improves frequency converter and multiplier performance. This section also describes some work on diffusion admittance. In Section 5. 3 an expression for the diffusion admittance is obtained, unrestricted by small signal approximations, as a function of the doping profile of the diode. Previously this theory had been applied only in improving the design of a multiplier. Here a large signal analysis of a LSUC in conjunction with short circuit assumptions using only the diffusion admittance (no depletion capacitance) is presented in Section 5. 4. Following in Section 5. 5 is a small signal analysis of a LSUC when (1) the diode has only diffusion admittance, and (2) the diode has both diffusion

and depletion admittance. These calculations show the particular characteristics needed to improve LSUC performance when the diffusion admittance is significant.

5.2 Literature Review

Varactor diodes are used not only in small signal frequency converters, but in large signal frequency converters, frequency multipliers, reflection parametric amplifiers, and voltage controlled frequency tuners. Although varactor diodes manufactured specifically for parametric amplifiers, frequency multipliers, or voltage controlled tuners differ in such details as capacitance variation, cut off frequency, etc., the theory developed for a diode used in one application can often be transferred to a diode used in another application.

Most analyses of either a LSUC or one of these other devices assume that the diode can be represented by a depletion layer capacitance under reverse bias, and by a short-circuit under forward bias. Mathematically this can be stated as follows:

$$\overline{V} = \begin{cases} -(-\overline{Q})^{1/(1-\gamma)} & \overline{Q} < 0 , \\ 0 & \overline{Q} > 0 , \end{cases} \tag{5.1}$$

where

$$\overline{V} = -\frac{\phi_v - V}{\phi_v - V_B}$$

$$\overline{Q} = -\frac{Q_\phi - Q}{Q_\phi - Q_B}$$

V_B = breakdown voltage

Q_B = charge on varactor at V_B

Q_ϕ = charge on varactor at $V = \phi_v$

$V > 0$ for forward bias .

This means that for $Q \geq Q_\phi$, the diode is assumed to act like an infinite capacitance, presumably a result of large diffusion effects.

Although this model assumes the minority carrier lifetime in the diode to be infinite and therefore does not specifically consider the effects of diffusion admittance, it has been used extensively in the analysis of large signal frequency converters and multipliers. Analysis of both multipliers (Refs. 67 to 70) and large-signal upper sideband upconverters (USUC) (Refs. 71 to 73) with this simple model show that increased power output and efficiency are obtained when the varactor "drive" > 1, where

$$\text{drive} = \frac{Q_{max} - Q_B}{Q_\phi - Q_B} \quad . \tag{5.2}$$

More specifically Davis (Ref. 68) calculated the output power and efficiency of varactor doublers based on the work of Penfield and Rafuse (Ref. 48). He found that overdriving a graded junction diode improves the doubler performance by a larger factor than overdriving an abrupt junction diode, although overdrive improves doublers using diodes of either profile. Burckhardt (Ref. 69) showed by a more complete numerical analysis of several multipliers, with and without idlers, that overdriven diodes with small γ gives the greatest output power and efficiency.

Similar conclusions have been reached with regard to γ and drive for the USUC. Penfield and Rafuse (Ref. 48) assumed that if the total charge is

$$Q = q_b + q_p \cos(\omega_p t + \psi_p) + q_s \cos(\omega_s t + \psi_s) + q_u \cos(\omega_u t + \psi_u) \tag{5.3}$$

where q_b is the bias charge and subscripts u, p, and s refer to the upper sideband, pump, and signal respectively, then the maximum charge for the fully driven diode is restricted by

$$q_p + q_s + q_u = \text{constant} \quad . \tag{5.4}$$

Conning (Ref. 72) using this restriction compared the output power and efficiency for $\gamma = 0$ and $\gamma = 1/2$, and shows that output power is larger for drive > 1.8 and efficiency is larger for drive > 1.5 when $\gamma = 0$. Nelson (Refs. 74, 75) showed that the estimate (5.4) of Penfield and Rafuse was unduly restrictive and developed a more accurate and larger charge restriction. Grayzel (Ref. 72) generalized Nelson's results to include an

overdriven diode. He proceeded to show that the greatest efficiency and power handling capability occurs for a drive = 2 . Also the maximum efficiency and maximum power handling capability increase with decreasing γ .

Gewartowski and Minetti (Ref. 73) pointed out that Grayzel had used the phase condition $\psi_p = \psi_s = \psi_u$. Rather than making this assumption, Gewartowski and Minetti choose ψ_u to correspond to the maximum output power for a prescribed drive level, and thus they achieve as much as 16 percent more power output thereby making a further improvement in the maximum charge restriction. They found that the maximum output power is larger for the abrupt-junction than the graded-junction diodes for all drive levels between 1 and 2, but that for high drive levels, the power-impedance product is higher for the graded junction. The up conversion gain and efficiency for high drive levels were both larger for the smaller γ varactors. For $\gamma = 1/2$ the maximum efficiency and gain occured at a drive = 1.4 to 1.6 while for $\gamma = 1/3$ the maximums occurred at drive = 1.8 . However they found the bandwidth is larger for the abrupt junction diode although the difference becomes negligible at drive = 2 .

These analyses show that the efficiency of these devices and the gain of the USUC increase when the varactor is overdriven and γ is small. However, all of these results are based on the simple diode model described by (5.1). If some forward conduction is so important to optimal use of the varactor, it appears that a better model of the varactor in the forward bias region is needed.

If the depletion layer capacitance is neglected under forward bias conditions, an approximation for the diffusion capacitance can be found. The usual small signal approach for calculating the diffusion admittance (Refs. 76, 77, 78) assumes the voltage and current on the diode are

$$V(t) = V_b + V_{ss} e^{j\omega t}$$

$$J(t) = J_b + J_{ss} e^{j\omega t}$$

where $V_{ss} << V_b$ and $J_{ss} << J_b$. Then the minority carrier densities are approximated as

$$p = p_n e^{\alpha V(t)}$$

$$\cong p_n (1 + \alpha V_{ss} e^{j\omega t}) e^{\alpha V_b}$$

$$n \cong n_p (1 + \alpha V_{ss} e^{j\omega t}) e^{\alpha V_b}$$

where p_n and n_p are the equilibrium minority carrier densities, q is the electron charge, and $\alpha \triangleq q/kT$. The small signal admittance found on the basis of these assumptions is

$$Y = \frac{J}{V} = \alpha q \left(\frac{D_p p_n}{L_p} \sqrt{1 + j\omega\tau_p} + \frac{D_n n_p}{L_n} \sqrt{1 + j\omega\tau_n} \right) e^{\alpha V_b} \qquad (5.5)$$

where τ is the minority carrier lifetime, D is the diffusion constant, and $L = \sqrt{D\tau}$ is the diffusion length.

The most prominent feature of this expression is that the diffusion capacitance is proportional to $e^{\alpha V_b}$, which explains why it is dominant in the forward conduction region. For high frequencies $(\omega\tau >> 1)$ the diffusion susceptance due to the holes only is

$$B_p = \frac{q\alpha D_p p_n}{L_p} \sqrt{\frac{\omega\tau_p}{2}} e^{\alpha V_b}$$

$$= q\alpha p_n \sqrt{\frac{D_p \omega}{2}} e^{\alpha V_b} .$$

Hence at high frequencies the susceptance is proportional to $\sqrt{\omega}$ rather than ω as in the ordinary parallel plate capacitor. Also B_p is independent of τ_p. At low frequencies

$$B_p = \frac{\alpha q D_p p_n}{L_p} \omega\tau_p e^{\alpha V_b}$$

$$= \alpha q p_n \omega \sqrt{D_p \tau_p} e^{\alpha V_b}$$

which indicates that the susceptance is directly proportional to ω and increases with $\sqrt{\tau_p}$. This analysis shows that at high frequencies, changing the minority carrier lifetime will not affect the susceptance since all of the minority charge is recovered. Increasing τ_p will not increase the charge storage because all of the charge is already stored.

Although this analysis displays several important characteristics of diffusion admittance, it is restricted to small signals. It therefore cannot be used with confidence to analyze large-signal frequency converters or multipliers; also there is no way other than by experiment to determine its degree of accuracy for small-signal converters. Although Shpirt (Ref. 79) calculated the diffusion currents of a forward biased diode without using small signal assumptions, his analysis was restricted to abrupt junction diodes. Parygin and Maneshin (Ref. 80) found the diffusion currents under large signal conditions for a wider range of doping profiles and applied the results to an analysis of a frequency multiplier. Later Romanova (Ref. 81) showed from low frequency experiments (1 to 60 MHz) that the varactor diode can be modeled by a depletion layer capacitance in parallel with the diffusion admittance.

Soviet authors apparently have been more concerned than U. S. researchers in developing a more accurate model of the diffusion capacitance found in the forward biased diode. Of particular importance is the paper by Parygin and Maneshin, whose results are used extensively in this chapter. Since this study is largely unknown in the United States, the analysis is restated in Section 5. 3. 2.

5. 3 Varactor Diode Model

The diode model described here allows for the depletion capacitance and diffusion admittance to occur in the same model. The varactor diode is characterized primarily by the depletion layer capacitance when the diode is reversed biased and by diffusion admittance when it is forward biased.

5. 3. 1 Depletion Layer Capacitance. The depletion layer capacitance is found by solving Poisson's equation and is given by

$$C = \frac{C_b}{(1 - V/\rho_v)^\gamma} \tag{5.6}$$

where C_b is the zero bias capacitance and ϕ_v is the built-in potential. If the profile is $N(x) = ax^b$, then the exponent γ in (5.6) is $\gamma = 1/(b+2)$. Thus for a graded junction diode $\gamma = 1/3$ and for an abrupt junction diode $\gamma = 1/2$.

5.3.2 Diffusion Admittance. The diffusion admittance calculated by Parygin and Maneshin (Ref. 80) is rederived below. Since the diffusion admittance is proportional to the highly nonlinear exponential function, harmonically related currents are generated in the diode. Harmonically related admittances $\frac{\partial J_m}{\partial V}$ also result from the analysis.

In general, a pn junction diode can be described by the following six basic equations.

$$\vec{J}_p = q(\mu_p p\vec{E} - D_p \vec{\nabla}p) \tag{5.7}$$

$$\vec{J}_n = q(\mu_n n\vec{E} + D_n \vec{\nabla}n) \tag{5.8}$$

$$-\vec{\nabla} \cdot \vec{J}_p = q(\frac{\partial p}{\partial t} + \frac{p-p_n}{\tau_n} - g_p) \tag{5.9}$$

$$\vec{\nabla} \cdot \vec{J}_n = q(\frac{\partial n}{\partial t} + \frac{n-n_p}{\tau_n} - g_n) \tag{5.10}$$

$$\rho = q(p-n + N_d - N_a) \tag{5.11}$$

$$\vec{\nabla} \cdot (\epsilon\vec{E}) = \rho \tag{5.12}$$

The hole and electron minority carrier densities are p and n respectively, the equilibrium hole and electron minority carrier densities are p_n and n_p respectively, J is the current density, N_d and N_a are the donor and acceptor atom densities, ρ is the net charge density, and g is the generation term which will normally be neglected. The calculations that follow are based on a $p^+ n$ diode so that the depletion layer extends into the n region from $x = 0$ to $x = W$. At equilibrium the sum of the drift and diffusion electron currents at the edge of the depletion region is approximately zero, so J_n in (5.8) is set to zero. If the impurity concentration is $N_d(x) = ax^b$, then from (5.8) and the Einstein relationship, $D_n = \frac{kT}{q}\mu_n$, the electric retarding field in the n region is

$$E = -\frac{kT}{q}\,\frac{1}{N_d}\,\frac{dN_d}{dx} = -\frac{kT}{q}\,\frac{b}{x} \quad . \tag{5.13}$$

The hole current is then given by (5.7):

$$J_p = -qD_p\left(\frac{bp}{x} + \frac{\partial p}{\partial x}\right) \quad . \tag{5.14}$$

This can be combined with the continuity equation (5.9) to yield

$$D_p\left(\frac{\partial^2 p}{\partial x^2} + \frac{b}{x}\,\frac{\partial p}{\partial x} - \frac{bp}{x^2}\right) - \frac{p - p_n}{\tau_p} = \frac{\partial p}{\partial t} \quad .$$

When a periodic voltage is applied to the diode, the hole concentration can be represented by a Fourier series:

$$p(x, t) = p_o + \sum_{m=1}^{\infty} (p_{mc} \cos m\omega t + p_{ms} \sin m\omega t) \, .$$

If this is substituted into the above equation, and the harmonic balance technique is applied (coefficients of corresponding frequency terms are equated), the following two sets of equations are formed:

$$D_p\left(\frac{d^2 p_{mc}}{dx^2} + \frac{b}{x}\,\frac{dp_{mc}}{dx} - p_{mc}\,\frac{b}{x^2}\right) - \frac{p_{mc}}{\tau_p} = m\omega p_{ms}$$

$$D_p\left(\frac{d^2 p_{ms}}{dx^2} + \frac{b}{x}\,\frac{dp_{ms}}{dx} - p_{ms}\,\frac{b}{x^2}\right) - \frac{p_{ms}}{\tau_p} = m\omega p_{mc} \quad .$$

Since

$$\mathrm{Re}\left[(p_{mc} - jp_{ms})\, e^{jm\omega t}\right] = p_{mc} \cos m\omega t + p_{ms} \sin m\omega t$$

the above two equations can be combined into one by defining

$$p_m \triangleq p_{mc} - jp_{ms}$$

where this is not to be confused with $p_n(W)$.

$$x^2 \frac{d^2 p_m}{dx^2} + bx \frac{dp_m}{dx} - \left(b + \frac{1 + jm\omega\tau_p}{L_p^2} x^2 \right) p_m = 0 \qquad (5.15)$$

To transform this into the usual form for a modified Bessel equation the following substitutions are made:

$$\bar{x} = \xi x$$

$$p_m = u\bar{x}^{(1-b)/2}$$

where

$$\xi^2 = \frac{1 + jm\omega\tau_p}{L_p^2} \quad . \qquad (5.16)$$

Using the first substitution, (5.15) can be written as

$$\bar{x}^2 \frac{d^2 p_m}{d\bar{x}^2} + b\bar{x} \frac{dp_m}{d\bar{x}} - (b + \bar{x}^2) p_m = 0 \quad .$$

The second substitution transforms this expression into

$$\bar{x}^2 \frac{d^2 u}{d\bar{x}^2} + \bar{x} \frac{du}{d\bar{x}} - [(1 + b)^2/4 + \bar{x}^2]u = 0 \quad .$$

This is the well-known modified Bessel equation, with the solution

$$p_m(x) = x^{(1-b)/2}[M_1 I_{b'}(\bar{x}) + M_2 K_{b'}(\bar{x})]$$

where $b' \triangleq (b+1)/2$. Two boundary conditions are now applied to evaluate the constants M_1 and M_2. Since $p_m(x) = 0$ as $x \to \infty$, $M_1 = 0$. The constant M_2 is found by using the hole concentration at the edge of the depletion region, $x = W$. If the resistance of the semiconductor is much less than the resistance of the depletion layer, the entire applied voltage, $V(t)$, is across the junction. Therefore the hole density at the edge of the depletion region is

$$p(W) = p_n(W)\, e^{\alpha V} = p_n(W)\left[g'_0 + \sum_{m=1}^{\infty} (g'_{mc} \cos m\omega t + g'_{ms} \sin m\omega t)\right]$$

where the g'_0, g'_{mc} and g'_{ms} are the Fourier coefficients of $e^{\alpha V}$. If W is considered to be independent of the voltage, and $p_m(W) \triangleq p_n(W)\,(g'_{mc} - jg'_{ms})$, then

$$M_2 = \frac{p_n(W)\,(g'_{mc} - jg'_{ms})}{W^{(1-b)/2} K_{b'}(\xi W)} \quad .$$

The final solution for $p_m(x)$ is then

$$p_m(x) = p_n(W)\left(\frac{x}{W}\right)^{(1-b)/2} \frac{K_{b'}(\xi x)}{K_{b'}(\xi W)} \cdot \frac{1}{\pi} \int_0^{2\pi} e^{\alpha V} (\cos m\omega t - j \sin m\omega t)\, d\omega t . \qquad (5.17)$$

The current can be expanded into a Fourier series just as was the hole density.

$$J = J_0 + \sum_{m=1}^{\infty} J_{mc} \cos m\omega t + J_{ms} \sin m\omega t$$

If $J_m \triangleq J_{mc} - jJ_{ms}$, the expression for $p_m(x)$ of (5.17) can be substituted into (5.14) to obtain an expression for the current. If $b'' \triangleq (b-1)/2$, then

$$J_m(x) = \left(\frac{x}{W}\right)^{-b''} \xi \frac{K_{b''}(\xi x)}{K_{b'}(\xi W)} \frac{qD_p p_n(W)}{\pi} \int_0^{2\pi} e^{\alpha V} (\cos m\omega t - j \sin m\omega t)\, d\omega t \qquad (5.18)$$

where the identity $\frac{d}{dz}\left[z^n K_n(z)\right] = -z^n K_{n-1}(z)$ has been used. This expression gives the harmonic current components due to the applied voltage V(t). If

$$\alpha_m + j\beta_m \triangleq \xi W \frac{K_{b''}(\xi W)}{K_{b'}(\xi W)} \quad , \qquad (5.19)$$

then the coefficients for the cosine and sine terms for the currents are

$$J_{mc} = \frac{qD_p p_n(W)}{\pi W} \int_0^{2\pi} e^{\alpha V} (\alpha_m \cos m\omega t + \beta_m \sin m\omega t)\, d\omega t \qquad (5.20)$$

$$J_{ms} = \frac{qD_p p_n(W)}{\pi W} \int_0^{2\pi} e^{\alpha V} (\alpha_m \sin m\omega t - \beta_m \cos m\omega t)\, d\omega t \quad . \tag{5.21}$$

The α_m should not be confused with $\alpha = q/kT$.

If the admittance is defined as

$$Y_m = A \frac{dJ_m}{dV}$$

$$= A\alpha J_m \tag{5.22}$$

where A is the diode area, then there is clearly a resistive part (conductance) and a reactive part (diffusion capacitance). The conductance term is lossy and introduces thermal noise. Although the large nonlinearity of the exponential function is desirable, this loss term limits the usefulness of diffusion capacitance in low-noise amplifiers.

5.3.3 Alternate Formulation. The method used by Parygin and Maneshin consists of first finding the diffusion currents, and then by differentiation with respect to the applied voltage the diffusion admittance is found. In contrast to this, Sah (Ref. 82) first finds the total charge stored by the minority carriers and then differentiates this charge with respect to the applied voltage to obtain the diffusion capacitance. Thus using the second method, if the n region extends from $x = W$ to the ohmic contact at $x = d$, the expression for the diffusion capacitance is

$$C = \frac{dQ}{dV}$$

$$= qA \frac{d}{dV} \int_W^d p_n(x)\, dx \quad .$$

Using the expression for $p_m(x)$ of (5.17) the harmonic charge components stored in the n region are

$$Q_m = \frac{p_n(W) q A}{\pi W^{(1-b)/2} K_{b'}(\xi W)} \int_0^{2\pi} e^{\alpha V} (\cos m\omega t - j \sin m\omega t)\, d\omega t$$

$$\cdot \int_W^d x^{(1-b)/2} K_{b'}(\xi x)\, dx$$

This is the total charge for the p^+n diode since the charge stored in the p^+ region is negligible.

If the second integral is designated by M_i, then

$$M_i = \xi^{(b-3)/2} \int_{\xi W}^{\xi d} (x\xi)^{(1-b)/2} K_{b'}(\xi x)\, d(\xi x) \quad .$$

Using the identity $K_\nu(z) = K_{-\nu}(z)$ and the above cited derivative formula for a Bessel function, the expression for M_i becomes

$$M_i = -\frac{1}{\xi} K_{b''}(\xi x)\, x^{(1-b)/2} \Big|_W^d \quad ,$$

and when $\xi d >> 1$

$$M_i = \frac{W^{(1-b)/2}}{\xi} K_{b''}(\xi W) \quad .$$

A comparison of this value of Q_m with the value of J_m in (5. 18) shows that

$$Q_m = \frac{J_m \tau_p A}{1 + jm\omega\tau_p}$$

Thus the diffusion capacitance defined by Sah, expressed in terms of the previously calculated diffusion admittance Y_m is given by

$$C = \frac{dQ_m}{dV}$$

$$= \frac{\alpha J_m \tau_p A}{1 + jm\omega\tau_p}$$

$$= \frac{Y_m \tau_p}{1 + jm\omega\tau_p} \quad .$$

Sah's method yields a complex, frequency-dependent capacitance, and therefore it distorts the concept of capacitance. In fact it was shown previously in Section 5.2 that the diffusion susceptance is not proportional to ω for all frequencies; consequently, an attempt to determine a real and frequency independent diffusion capacitance is expected to fail. Thus the superior method is that of finding the admittance rather than trying to find the "capacitance" directly. The results obtained from the admittance method are used in the following analysis.

5.3.4 Numerical Calculations of the Diffusion Admittance. The numerical calculation of the diffusion admittance (5.22) was performed for the doping profiles $N(x) = ax^b$ where $b = 0, 1, 3$. These correspond to the abrupt junction $\gamma = 1/2$, graded junction $\gamma = 1/3$, and $\gamma = 1/5$ respectively, when the diode is reverse biased. Since a p^+n diode is used, the current resulting from the diffusion admittance in the p side can be neglected. The calculations were performed using program C in Appendix A.

The short circuit assumption is employed for all pump harmonics beyond the fundamental so the pump voltage is of the form

$$V_b + V_0 \cos(\omega_0 t) \quad . \tag{5.23}$$

Although in practice the external circuitry can be expected to impress other voltage harmonics on the diode, the short circuit assumption (on the basis of the results found in Chapter III) can be expected to give reasonably accurate results in most cases. When the pumping voltage is of this simple form, the integral contained in (5.22) can be readily integrated by using Sonine's expansion

$$e^{z \cos \theta} = I_0(z) + 2 \sum_{n=1}^{\infty} I_n(z) \cos n\theta \tag{5.24}$$

where $I_n(z)$ are modified Bessel functions. Using this expansion and making use of the orthogonality of the trigonometric functions, the m-th harmonic of the current is

$$J_m = \xi \frac{K_{b'}(\xi W)}{K_{b''}(\xi W)} 2qD_p p_n(W) I_m(\alpha V_0) e^{\alpha V_b} \tag{5.25}$$

where it should be recalled from (5. 16) that ξ is a function of ω and τ_p, and the diffusion admittance is found from (5. 22). Thus the large signal analysis shows the same low and high frequency dependence of admittance with ω and τ_p for the abrupt junction diode as did the small signal analysis.

The numerical calculation of (5. 25) requires the evaluation of the modified Bessel function $K_\nu(z)$ where z is complex. Since no computer program to carry this out was available in the IBM "Scientific Subroutine Package," an algorithm was developed to perform this calculation. The details for this algorithm are found in Appendix C while the actual program listing is found in Appendix A under BESKC .

The diffusion admittance is found using (5. 25) and (5. 22) as a function of $\omega\tau_p$ and is plotted together with its harmonics in Figs. 5. 1 to 5. 7. Since the admittance is a function of the diffusion length $L_p = (D_p \tau_p)^{\frac{1}{2}}$, the minority carrier lifetime must be specified independent of the frequency. In Figs. 5. 1 to 5. 7 the following parameters were used:

$$V_b = 0 \text{ volt}$$

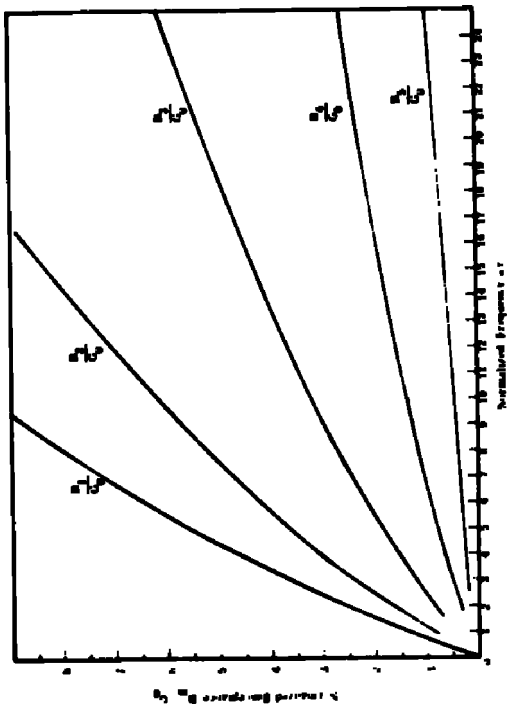
$$V_0 = 0.1 \text{ volt}$$

$$\mu_p = 401 \text{ cm}^2/\text{volt-sec}$$

$$\alpha = 40.1 \quad .$$

There is a tendency, in all but the high frequencies of the abrupt junction case (Fig. 5. 1), for the harmonic of the susceptance to be larger than the fundamental. Also the ratio B_1/G_1 is always less than 1 for the abrupt junction case but can be larger than 1 for sufficiently large frequencies for the other two profiles analyzed. This indicates that the lower b (higher γ) is, the more lossy is the diffusion admittance.

The plots in Fig. 5. 4 show that decreasing the depletion layer width by a factor of 10 increases the ratio B_1/G_1 for the graded junction. For the abrupt junction, there is no change in the diffusion admittance. Mathematically the reason for this is that the parameter W/L_p enters only in the argument of the modified Bessel functions, which for the abrupt case



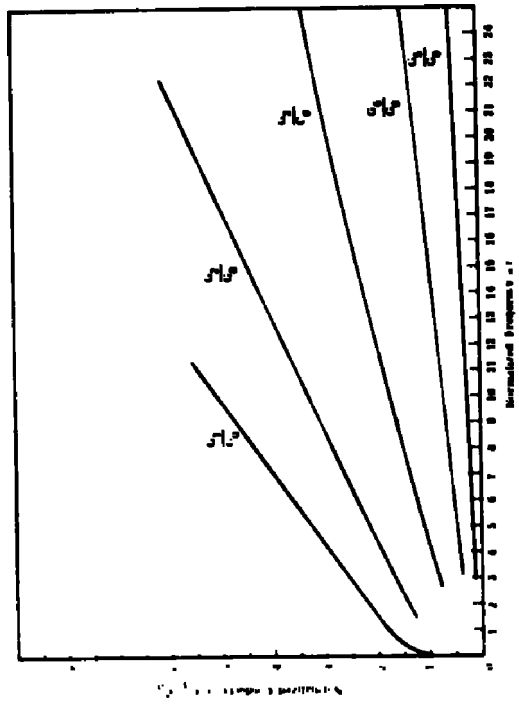
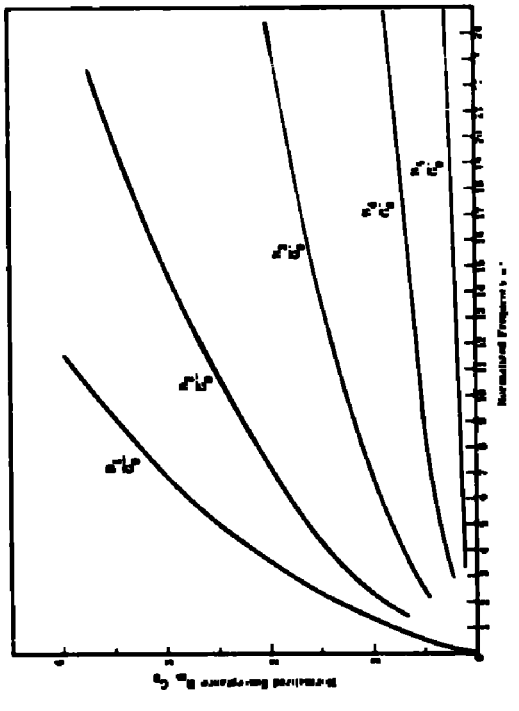


Fig. 5.2. Normalized diffusion admittance when $\gamma = 1/3$, $\tau_p = 10^{-7}$ sec, and $W/L_p = 0.1$



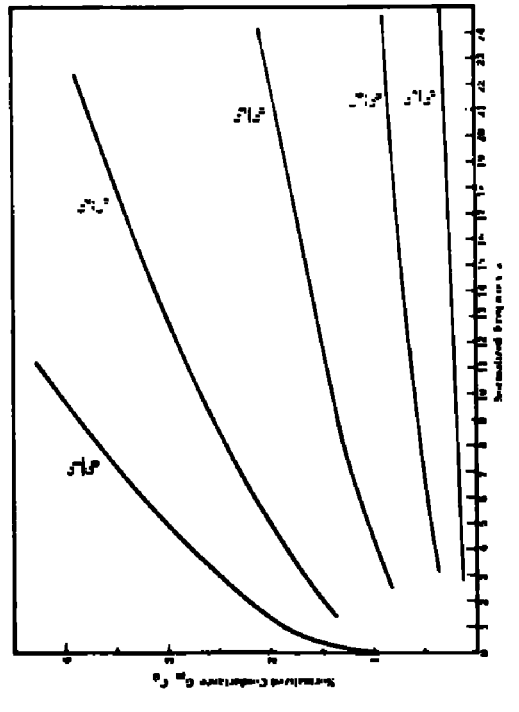


Fig. 5.1. Normalized diffusion admittance when $\gamma = 1/2$, $\tau_p = 10^{-7}$ sec, and $W/L_p = 0.1$

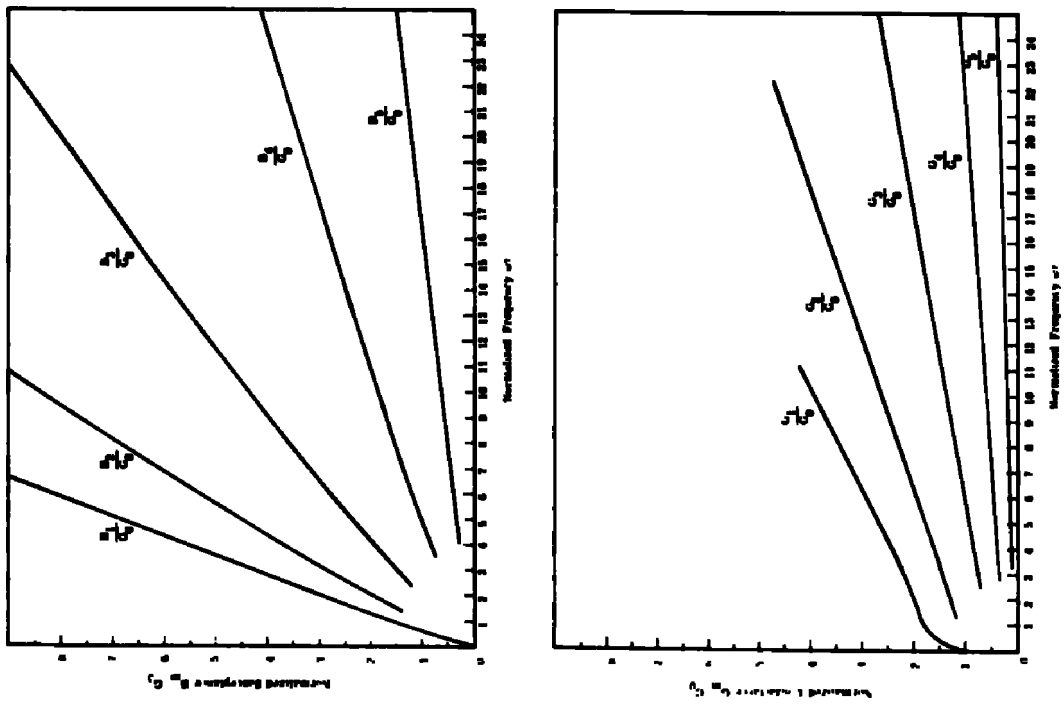


Fig. 5.4. Normalized diffusion admittance when $\gamma = 1/3$, $\tau_p = 10^{-7}$ sec, and $W/L_p = 0.01$

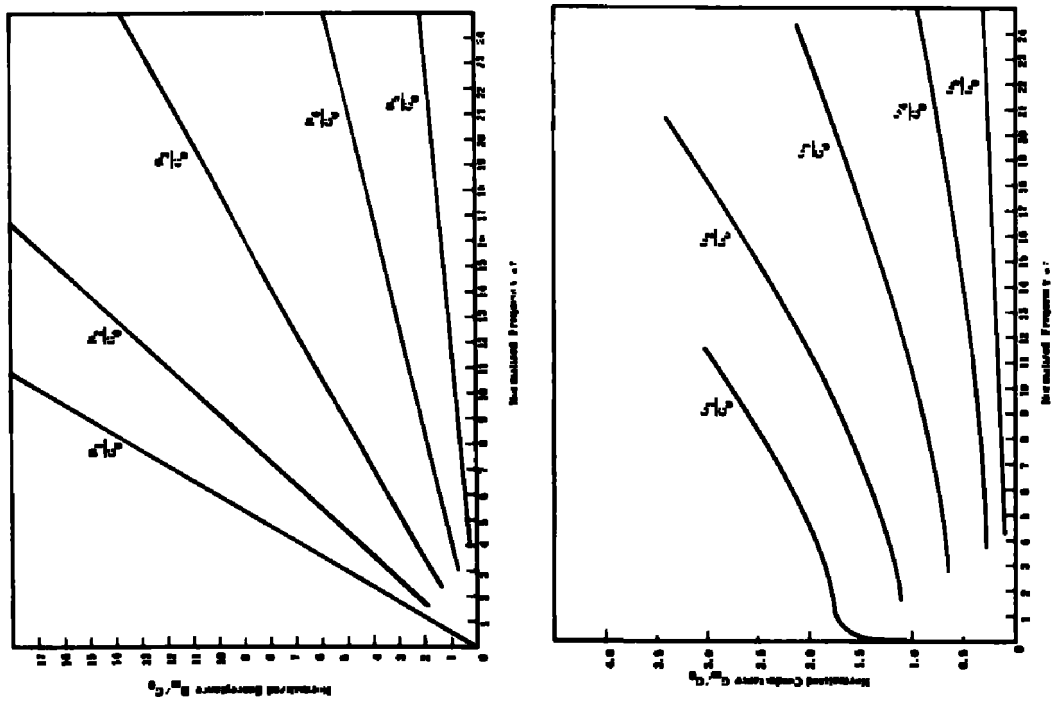


Fig. 5.3. Normalized diffusion admittance when $\gamma = 1/5$, $\tau_p = 10^{-7}$ sec, and $W/L_p = 0.1$

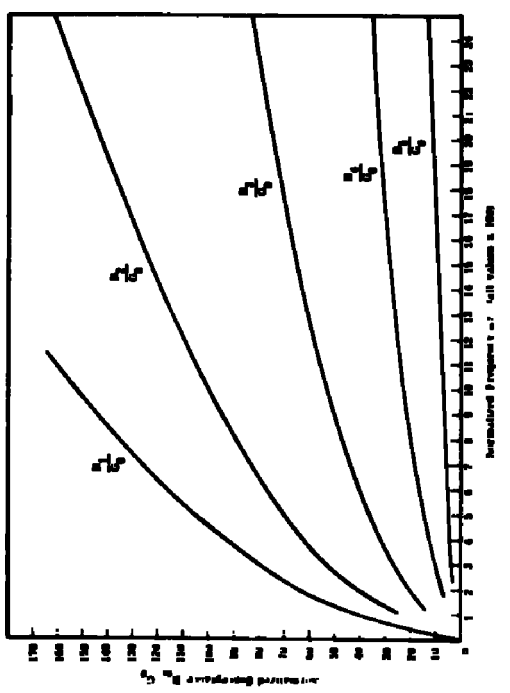


Fig. 5.6. Normalized diffusion admittance when $\gamma = 1/3$, $\tau_p = 10^{-5}$sec, and $W/L_p = 0.1$

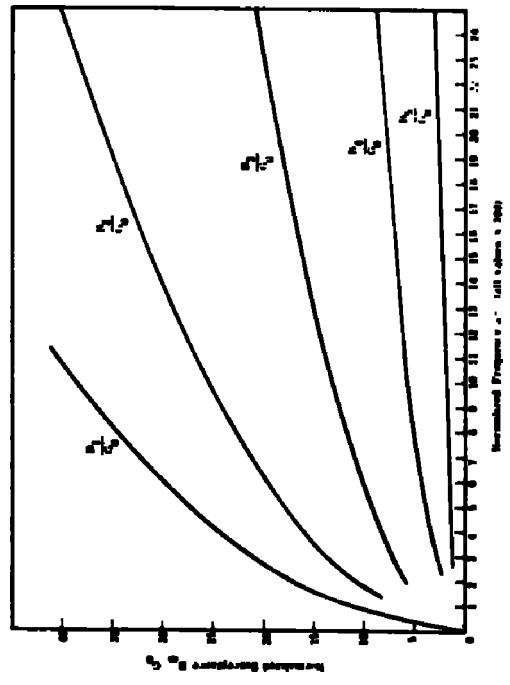


Fig. 5.5. Normalized diffusion admittance when $\gamma = 1/2$, $\tau_p = 10^{-5}$sec, and $W/L_p = 0.1$

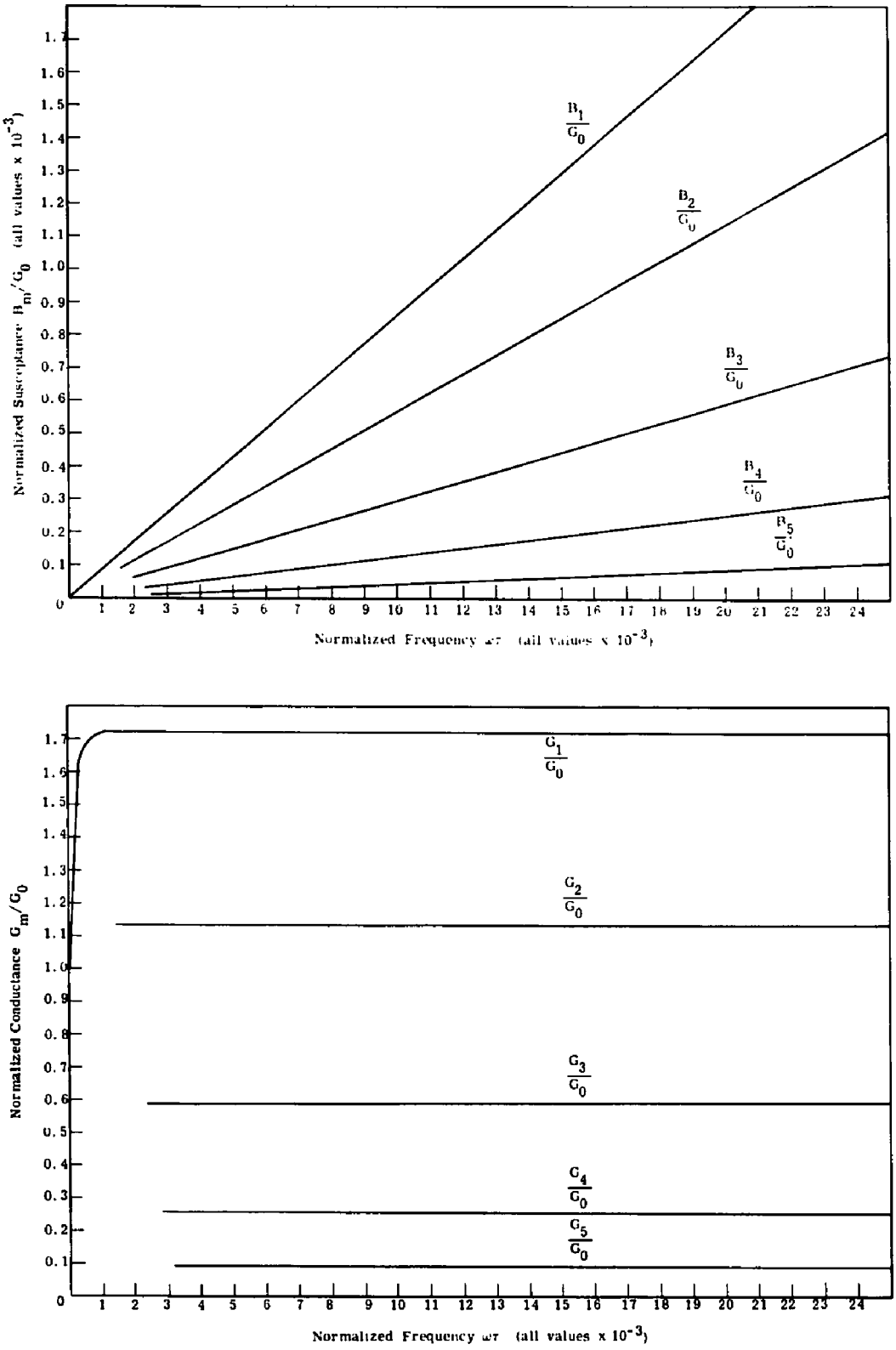


Fig. 5.7. Normalized diffusion admittance when $\gamma = 1/2$, $\tau_p = 10^{-10}$ sec, and $W/L_p = 0.1$

$$\frac{K_{b''}(\xi W)}{K_{b'}(\xi W)} = \frac{K_{-\frac{1}{2}}(\xi W)}{K_{\frac{1}{2}}(\xi W)} = 1 \quad .$$

The depletion layer width W entered the derivation for the admittance through the boundary condition $p(W) = p_n(W)\, e^{\alpha V}$. However, for the abrupt junction the donor concentration is constant throughout the n region, and hence the final solution for this case is independent of W .

Figures 5. 5 to 5. 7 show the variation of diffusion admittance with minority carrier lifetime for both the abrupt and graded junction cases. It is clear from these graphs that increasing the lifetime of the minority carriers increased the diffusion susceptance. For the abrupt junction, the B_1/G_1 ratio increased when τ_p increased although this ratio is still limited to a maximum of 1 . For short lifetimes Fig. 5. 7 shows the conductance is independent of frequency, and the susceptance almost directly proportional to frequency.

The plots of relative loss B_1/G_1 for various doping profiles in Figs. 5. 8 and 5. 9 indicate how the loss in the diffusion admittance can be controlled. The abrupt junction is seen to be inferior to the graded and cubic (b = 3) junctions at all frequencies. In general for a doping concentration profile given by $N(x) = ax^b$, as b increases, the loss in the diode decreases (B_1/G_1 increases). Also when the base width to diffusion length ratio $\frac{W}{L_p}$ decreases loss decreases. Furthermore as $\frac{W}{L_p}$ decreases, the angle $\omega\tau_p$ where the minimum loss occurs increases. These facts are summarized in Table 5. 1. An approximate calculation (Ref. 80) of the ratio B_1/G_1 for the graded junction where the arguments of the modified Bessel function are assumed small shows the minimum loss occurs at $\omega\tau_p = 6$ while the more exact analysis performed here shows the minimum loss occurs at $\omega\tau_p = 11$.

In the preceding analysis, the celebrated Shockley equation for the ideal diode has been used. This is

$$J(V) = J_s(e^{qV/\tilde{n}kT} - 1)$$

where J_s is the thermal saturation current and $\tilde{n} = 1$. Experimentally this is valid

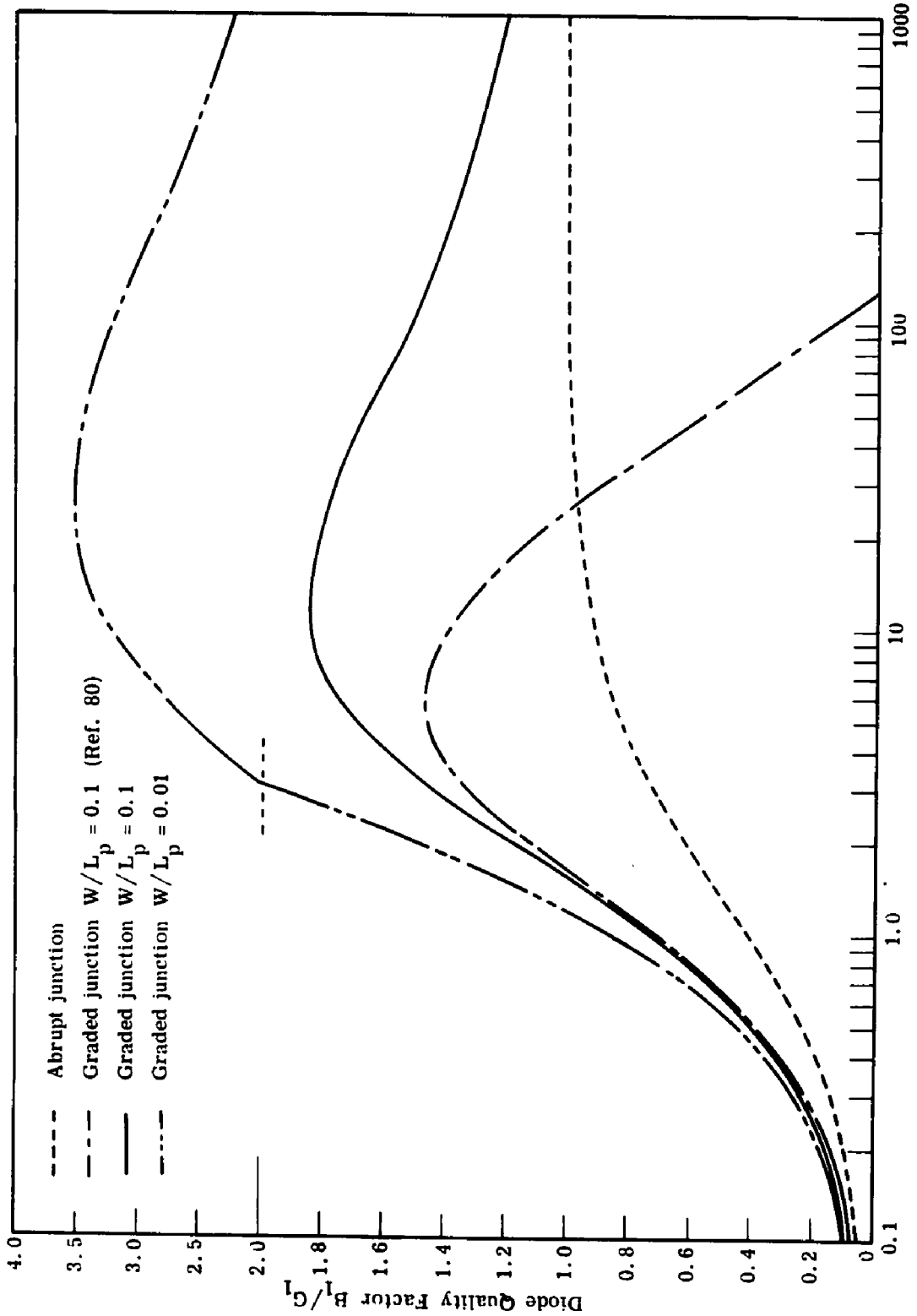


Fig. 5.8. Relative loss of an abrupt and graded junction diode under forward bias conditions

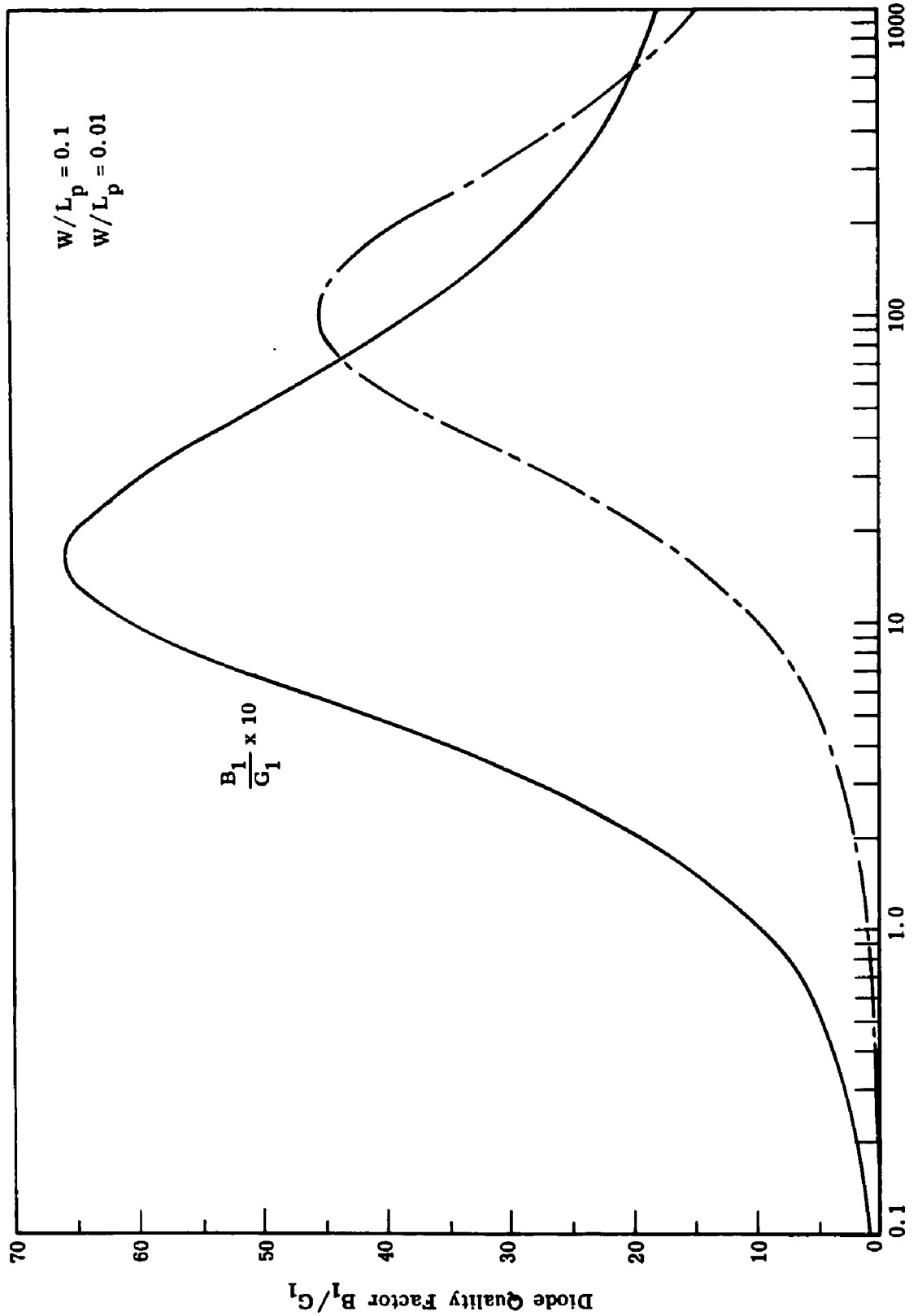


Fig. 5.9. Relative loss of diffusion admittance with doping profile $N(x) = ax^3$

b	γ	$\frac{W}{L_p}$	Max. B_1/G_1	$\omega\tau_p$ at Max. B_1/G_1
0	1/2	-----	1	∞
1	1/3	0.1	1.8490	11
1	1/3	0.01	3.5264	30
3	1/5	0.1	6.5421	17
3	1/5	0.01	45.198	100

Table 5.1. Variation of the minimum loss with doping profiles

for germanium, but for silicon $1 < \tilde{n} < 10$. Several explanations have been advanced for this nonideal behavior. Sah (Ref. 83) analyzes four mechanisms which could account for values of $\tilde{n} \neq 1$: (1) bulk diffusion current at high levels gives $\tilde{n} = 2$, (2) bulk recombination-generation current in the transition region gives $1 < \tilde{n} < 2$, (3) surface recombination-generation current gives $1 < \tilde{n} < 2$, and (4) surface channel current gives $2 < \tilde{n} < 4$. The actual value of $\tilde{n}$ thus depends on many factors, some of which are not fully understood. However, for silicon diodes $\tilde{n} = 2$ is often used. The effect of using $\alpha = q/2kT = 20\ (\text{Volt})^{-1}$ is a reduction in the magnitude of the diffusion admittance through the factor $e^{\alpha V_b} I_m(\alpha V_0)$ while the phase of the admittance remains unchanged.

5.3.5 Varactor Diode Model with both Diffusion and Depletion Admittance. The effects of both diffusion admittance and depletion admittance can be combined into a single diode model. At the edge of the depletion layer there are two current components. The first is the displacement current associated with the depletion capacitance and the second is the diffusion current which passes through the depletion layer. Since these two currents add, the depletion capacitance and the diffusion admittance are parallel elements as shown in Fig. 5.10. The resistor R_s is in series since it represents the bulk resistance of the base region (the n side of the p^+n diode). Since the diffusion admittance, being proportional to $e^{\alpha V}$, is larger than the depletion susceptance when the diode is forward biased, the latter does not short-circuit the former. In fact most diodes would burn out before the applied voltage reached the built-in potential.

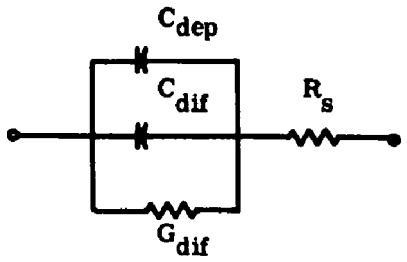


Fig. 5. 10. Total varactor model of diode wafer

The impedance of the total diode model of Fig. 5. 10 was calculated for the representative parameters listed below:

interrogation voltage $V(t) = 0.1 \cos(2\pi f_p t)$

frequency $f_p = 9.5$ GHz

depletion width to diffusion length ratio $\frac{W}{L_p} = 0.1$

minority concentration at depletion layer edge $p_n(W) = 10^{10}\ cm^{-3}$

diode area $A = 4.41\ 10^{-5}\ cm^2$

minority carrier lifetime $\tau_p = 1.84\ 10^{-10}$ sec

dielectric constant of silicon $\epsilon = 11.8\ \epsilon_o$

built-in potential $\phi_v = 0.9$ volt

series bulk resistance $R_s = 1$ ohm

exponential factor for silicon at room temperature $\alpha = 20\ V^{-1}$

mobility $\mu_p = 401\ cm^2/V\text{-sec}$

diffusion constant $D_p = 10$.

Except for the minority carrier lifetime, which was chosen to minimize the diffusion admittance losses, the above diode parameters are typical for silicon parametric varactor diodes.

The relative magnitude of the depletion and diffusion susceptances shown in Fig. 5. 11 can be compared for various bias voltages for both the abrupt and graded junction diodes. Clearly the diffusion admittance is important only in the forward bias region. The impedance at the diode terminals is plotted in Fig. 5. 12. This plot shows that the real part of the diode impedance increases when the bias voltage is between 0. 4

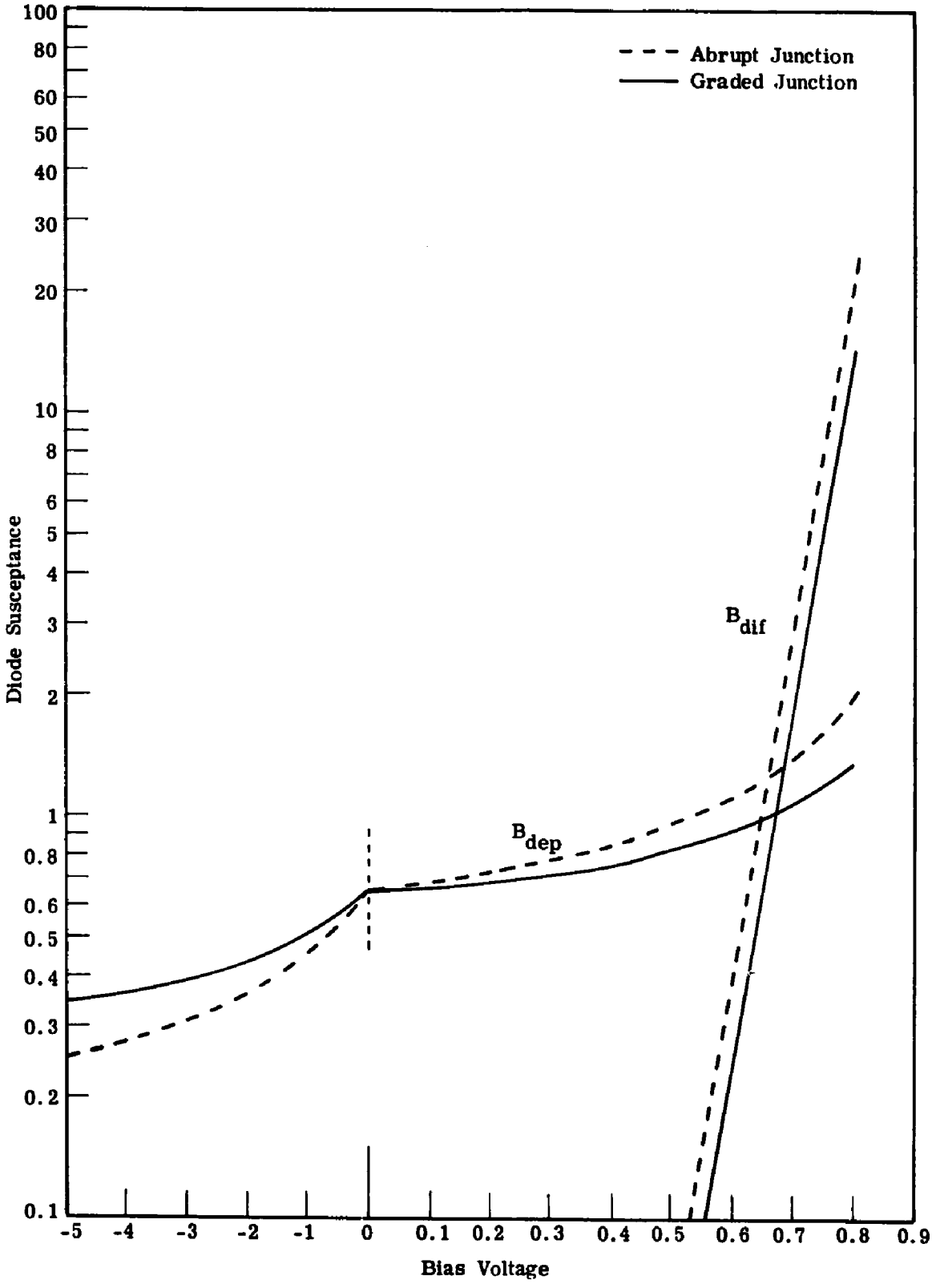


Fig. 5.11. The depletion and diffusion susceptance when the minority carrier lifetime is chosen to minimize loss in the graded junction diode, i.e., $\tau = 1.84 \times 10^{-10}$ sec

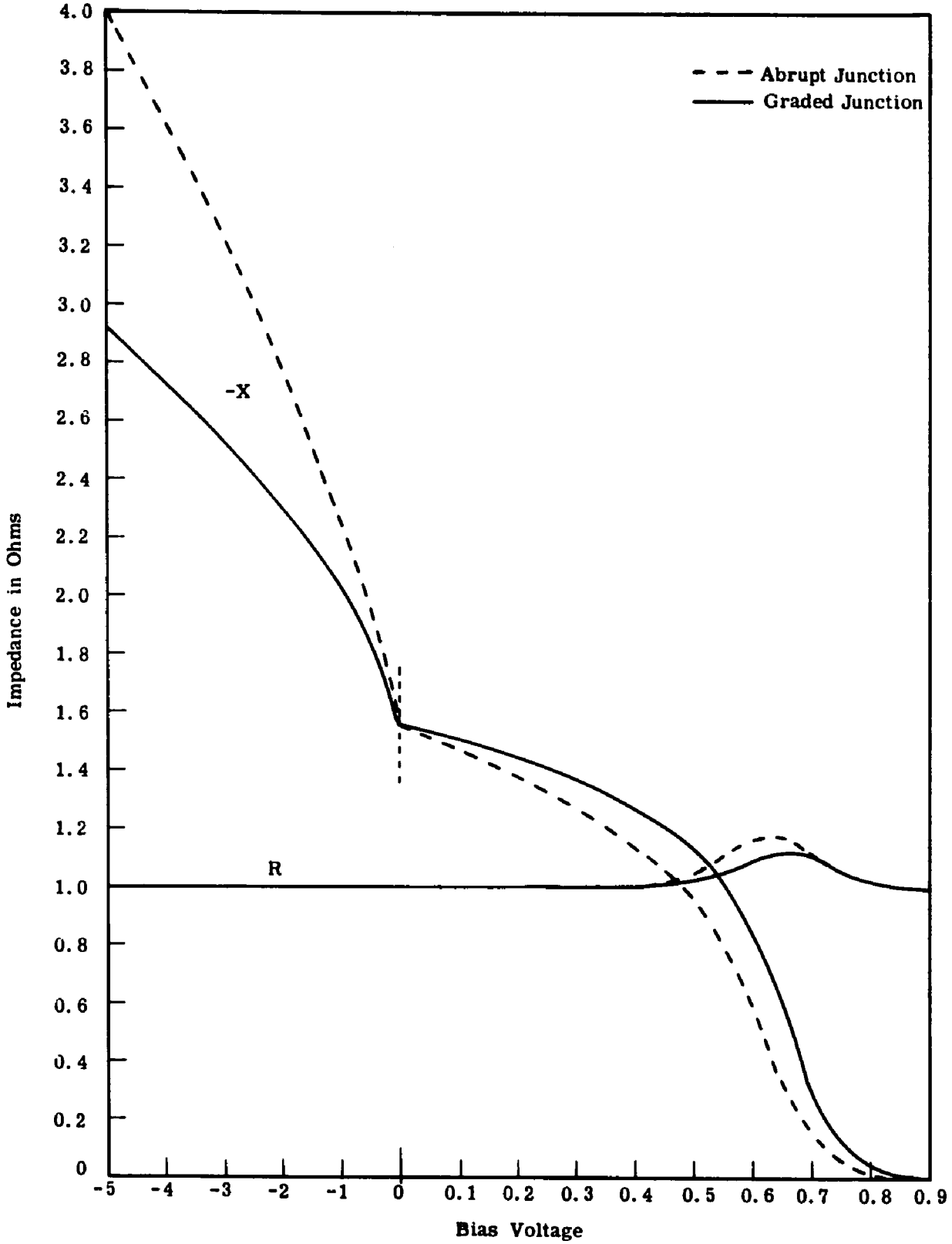


Fig. 5.12. The impedance of the total varactor model when the minority carrier lifetime is chosen to minimize loss in the graded junction diode

and 0.8 volts. Outside of this range the parallel combination of the diode capacitance and diffusion conductance is negligible because of the low conductance at small voltages and the high susceptance at large voltages. If a different value of τ_p is used, instead of the optimum value used above, the resistive part of the diode impedance can become quite large. For example when $\tau_p = 10^{-7}$ sec, this resistance has a maximum value of 6.5 ohms.

5.3.6 Comparison with Experimental Work. Several experimenters noticed some time ago that a forward-biased pn junction exhibits what is termed an "inductive effect." They noticed that the diode capacitance increases with applied voltage according to the standard depletion capacitance law until the voltage reaches a value between 0.60 and 0.75 V, at which point the capacitance decreases rapidly with further increase in voltage - hence the term "inductive effect."

Sah (Ref. 82) made a thorough analysis of the graded junction diode which included the forward bias region. His capacitance measurements clearly show the capacitance has a maximum value, after which it rapidly decreases. However, his theory based on finding the charge storage and taking the derivative with respect to the applied voltage, does not show the capacitance maximum. He considered this discrepancy to be possibly caused by conductivity modulation, i.e., a change in conductance with applied voltage. Wang (Ref. 84), following Sah's basic approach (i.e., obtain capacitance from $\frac{dQ}{dV}$), showed theoretically that the capacitance would have a maximum and decrease toward zero at large forward bias. His analysis of an abrupt junction diode differs primarily from earlier approaches in that, instead of assuming the quasi-Fermi levels are constant, he takes these levels to be actually proportional to $e^{\alpha V/2}$. O'Hearn and Chang (Ref. 85) also show experimental evidence for the maximum in the capacitance versus voltage curve. In their theory an approximate expression for the diffusion admittance of an abrupt junction diode is found from

$$\frac{i}{V} = \frac{Aq}{V} \int \frac{\partial p_n}{\partial t}\, dx \quad .$$

Analysis of this expression shows that, as the bias increases, the capacitance increases to a maximum, then falls to a local minimum; at voltages approaching the built-in potential, the capacitance starts to increase again. The maximum is here attributed to the conductance part of the admittance. This second increase in the capacitance predicted by O'Hearn and Chang is substantiated neither by their own experimental measurements nor by those of Sah. Furthermore, the existence of this local capacitance minimum is doubtful since it is unlikely that the diffusion capacitance would increase more rapidly than diode loss at high forward bias.

The experimental data in Refs. 83 and 85 show that as frequency increases the maximum diode susceptance remains practically unchanged, and the voltage where this maximum occurs, decreases. Also, when the bulk resistance increases, the maximum susceptance decreases and the voltage where this maximum occurs, decreases.

These characteristics are all consistent with the diffusion admittance theory presented in this chapter. The variation in the maximum diode susceptance with frequency and bulk resistance noted above can be predicted from (5. 22) and (5. 25). The curve shown in Fig. 5. 13 is the susceptance of the total diode model shown in Fig. 5. 10, calculated using the theory derived by Parygin and Maneshin (Ref. 80). It is seen here that there is one capacitance extremum as confirmed by the experimental points in Refs. 83 and 85. Figure 5. 13 also portrays the effect of changing the minority carrier lifetime, a parameter that was neglected in Ref. 84 and 85. The theory used here is valid for one sided abrupt and graded junction diodes as well as other doping profiles expressable as $N(x) = ax^b$ and is not restricted to low frequencies as are the theories of Sah and Wang. Furthermore this analysis is not restricted by small signal assumptions, and it gives the admittance, rather than the less valid "complex capacitance".

5. 4 Effects of Diffusion Admittance on a LSUC

The previous sections dealt with first finding the diffusion admittance of a varactor diode and then secondly with the total impedance of the diode when both diffusion admittance and depletion capacitance are combined in one diode model. A similar outline will be followed in evaluating the effects of diffusion admittance on the characteristics of a LSUC. First the diffusion admittance diode model will be used to analyze the LSUC

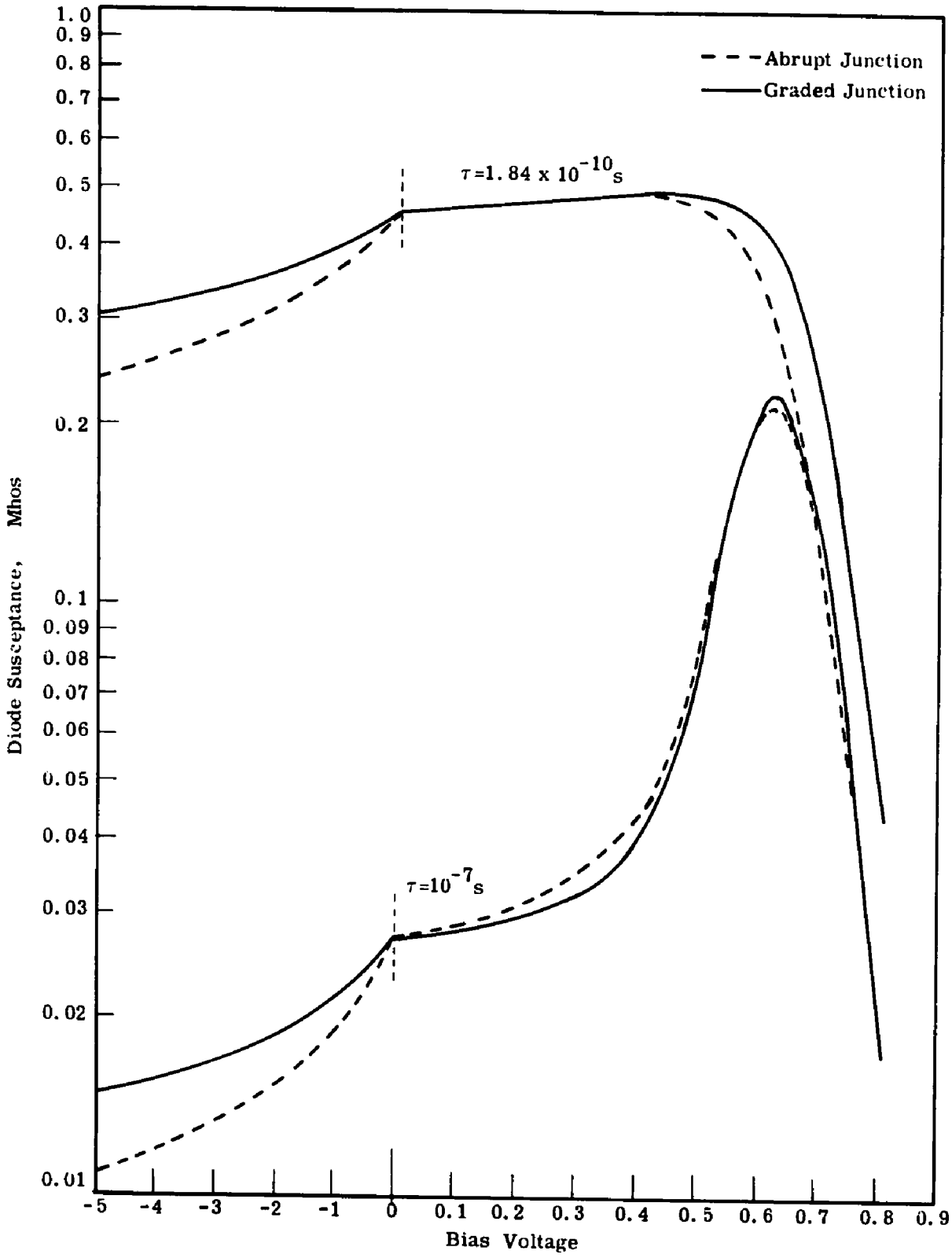


Fig. 5.13. The total diode susceptance for $\tau = 10^{-7}$ sec and $\tau = 1.84\ 10^{-10}$ sec (minimum loss) when the bulk series resistance $R_s = 1$ ohm

circuit on both large signal and small signal bases. Then a combined diode model will be used to determine LSUC gain and noise figure from a small signal analysis.

5.4.1 Large Signal Analysis of the Diffusion Admittance in a LSUC. Although most parametric amplifiers are designed to operate with a reverse biased varactor diode, high gain can be achieved in practice if some forward conduction is allowed. The previous formulation of diffusion admittance will be applied to the LSUC. The assumed circuit model is shown in Fig. 5.14 where the circuit elements are assumed to be ideal band-pass filters which act as short-circuits to out-of-band frequencies. This simple model can be contrasted with the more complex model used in Chapter III where the circuit impedances at out-of-band frequencies were neither necessarily open nor short circuits. However the results obtained from the model of Fig. 5.14 will clarify the basic properties of a LSUC using a diffusion-admittance model, and the results obtained will give a first order approximation to the gain and noise figure of an actual LSUC when the diode is forward-biased or pumped into the forward region. In addition a direct comparison between the depletion- and diffusion-admittance models can be obtained from this analysis. For convenience, the following notation will be used for the different LSUC frequencies.

$$\omega_k = \left[\frac{k}{2}\right] \omega_p + (-1)^{k+1}\omega_s$$

$$\omega_0 = \omega_p \qquad (5.26)$$

where $k = 1, 2, 3, \ldots$ and $[a]$ is the symbol for the greatest integer less than a. The subscript k will be hereafter reserved only for the above definition. It should be noted that only the upper and lower sidebands of the pump are considered here, but that the following analysis, in principle, is not restricted to this choice of frequencies. Although several current frequencies will be generated, the voltage across the diode will consist of only the pump, signal, lower sideband, and bias voltages. Even with these assumptions two additional computational problems arise: the calculation of the gain when there are incommensurable frequencies, and the relative phase of the diode voltages. Both problems are discussed below.

5.4.1.1 Incommensurate Frequencies in the LSUC. When the voltage applied to the diode chip is

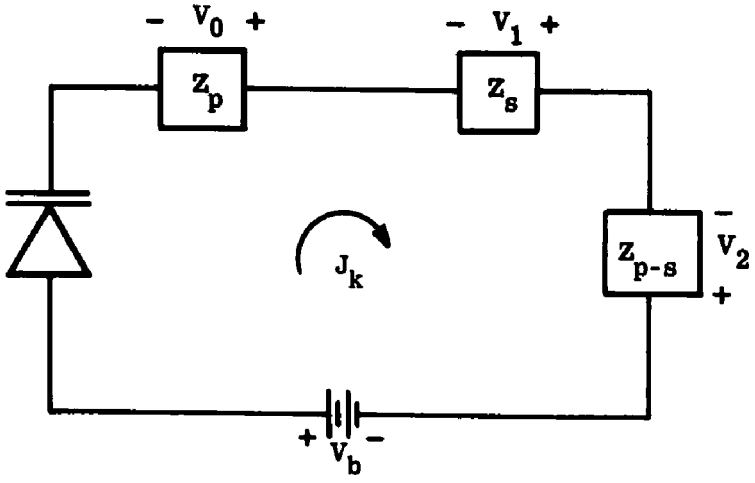


Fig. 5.14. LSUC circuit model for the diffusion admittance

$$V(t) = V_b + V_0 \cos(\omega_0 t) + V_1 \cos(\omega_1 t + \psi_1) + V_2 \cos(\omega_2 t + \psi_2) \qquad (5.27)$$

then equations (5.20) and (5.21) must be modified because the frequencies used there were all harmonically related. The problem can be resolved by choosing the frequency ω_f in (5.20) and (5.21) so that the signal, pump, and lower sideband frequencies in (5.27) are all harmonically related to ω_f. Such a choice can always be made if the frequencies are rational numbers, which is so in the physical world. This chosen frequency ω_f will hereafter be termed the fundamental frequency. The m in (5.20) and (5.21) therefore denotes the number of harmonics of the fundamental frequency and is related to the subscript k in (5.26) by the following expression:

$$\omega_k = m_k \omega_f \qquad (5.28)$$

For the frequencies chosen for the LSUC under investigation, $f_1 = 1$ GHz, $f_2 = 8.5$ GHz, and $f_0 = 9.5$ GHz. This means the fundamental frequency must be $f_f = 0.5$ GHz, and $m_0 = 19$, $m_1 = 2$, and $m_2 = 17$. In the work that follows the subscript k on m will usually be implied.

5.4.1.2 Phase of the Lower Sideband Voltage. The second problem which occurs in the LSUC is the calculation of the relative phases between pump, signal, and

lower sideband voltages. Since the pump and signal voltages are two independent input voltages, their relative phase will be arbitrary. However, the phase of the lower sideband voltage will be dependent on the signal and pump, and in order to find this relationship recourse must be made to a small signal assumption.

If the varactor is pumped with $V(t) = V_b + V_0 \cos(\omega_0 t + \psi_0)$, then (5.18) should be modified so that the Fourier series is expanded in terms of the angle $(m\omega_0 t + \psi_0)$. The admittance then from (5.18), (5.19) and (5.22) is

$$Y_p = (\alpha_{k=0} + j\beta_{k=0}) \frac{2qD_p p_n(W)}{W} I_1(\alpha V_0) e^{\alpha V_b}$$

$$\triangleq M_c(\alpha_0 + j\beta_0) \quad .$$

Thus the cosine admittance is $M_c \alpha_0 \cos(\omega_0 t + \psi_0)$ and the sine admittance is $-M_c \beta_0 \sin(\omega_0 t + \psi_0)$ so that

$$Y_p = M_c \alpha_0 \cos(\omega_0 t + \psi_0) - M_c \beta_0 \sin(\omega_0 t + \psi_0)$$

$$= M_c \sqrt{\alpha_0^2 + \beta_0^2} \cos[\omega_0 t + \text{Arctan}\,(\beta_0/\alpha_0) + \psi_0] \quad .$$

The current at the lower sideband frequency is obtained by multiplying the admittance by the signal voltage, $V_1 \cos(\omega_1 t + \psi_1)$.

$$J_{p-s} + J_{p+s} = M_c \sqrt{\alpha_0^2 + \beta_0^2} \cos\left(\omega_0 t + \psi_0 + \text{Arctan}\,\frac{\beta_0}{\alpha_0}\right) V_1 \cos(\omega_1 t + \psi_1)$$

$$J_{p-s} = \frac{M_c V_1 \sqrt{\alpha_0^2 + \beta_0^2}}{2} \cos\left(\omega_2 t + \psi_0 - \psi_1 + \text{Arctan}\,\frac{\beta_0}{\alpha_0}\right)$$

If the lower sideband current flows through a real impedance, then the voltage is

$$V_{p-s} = R_{p-s} J_{p-s} = \frac{R_{p-s} M_c V_1 \sqrt{\alpha_0^2 + \beta_0^2}}{2} \cos\left(\omega_2 t + \psi_0 - \psi_1 + \text{Arctan}\,\frac{\beta_0}{\alpha_0}\right) \quad .$$

Since the lower sideband voltage is

$$V_{p-s} = -V_2 \cos(\omega_2 t + \psi_2) = V_2 \cos(\omega_2 t + \psi_2 + \pi)$$

the relationship between the phases must be

$$\psi_2 = \psi_0 - \psi_1 + \text{Arctan}\frac{\beta_0}{\alpha_0} - \pi . \tag{5.29}$$

If the varactor were lossless, then $\alpha_0 = 0$ and

$$\psi_2 = \psi_0 - \psi_1 - \frac{\pi}{2}$$

which agrees with the usual phase relationship in an upconverter (Ref. 86).

5.4.1.3 Numerical Calculation of LSUC Currents. The numerical integration of (5.20) and (5.21) requires some care because the exponential term in the integrand varies over a wide range in the integration interval. The voltage applied to the diode chip,

$$V(t) = V_b + V_0 \cos(\omega_0 t) + V_1 \cos(\omega_1 t + \psi_1) + V_2 \cos(\omega_2 t + \psi_2)$$

$$= V_b + V_0 \cos(\omega_f t \frac{\omega_0}{\omega_f}) + V_1 \cos(\omega_f t \frac{\omega_1}{\omega_f} + \psi_1) + V_2 \cos(\omega_f t \frac{\omega_2}{\omega_f} + \psi_2)$$

has 19 maxima and 19 minima in the integration interval with the choice of frequencies made in Section 5.4.1.1. Since this voltage appears in the exponential, it dominates the magnitude of the variation of the integrand. In order to obtain accurate results the total interval was divided into 40 sections: the division being made at the 38 extreme values of $V(t)$ and the two end points. An IBM program which used a 12-point Gaussian quadrature formula was used on each of these subintervals, and the total was added together to give each J_{kc} or J_{ks} current component. The program listing is found in Appendix A under program D.

The numerical integration was carried out using the same parameters for a p^+n diode as were used in the calculation of the diffusion admittance in Section 5.3.4 except

now $\alpha = 20$, $W/L = 0.1$, $\psi_1 = 0$, $V_b = -0.7$, and $V_0 = 0.6$. Table 5.2 summarizes the results for the abrupt and graded junction when V_1 and V_2 are varied. The table indicates that the graded junction has a higher current gain, $|J_2|/|J_1|$, than the abrupt junction. Decreasing the signal and lower sideband voltage by a factor of 10 decreased the output current, but the current gain remained approximately constant.

In these calculations it was assumed that at $t = 0$, the relative phase between the pump and signal voltage is 0^o. When ψ_1 is changed to 30^o and 60^o the computer program shows that the phase of the output currents change, but the current magnitudes remain unchanged. The Gaussian quadrature method used here to perform the numerical integration took approximately 15 seconds of execution time for each set of 10 current densities. A much faster but less accurate method is described in Appendix D. The currents shown in Table 5.2 will be used later to gauge the accuracy of the small signal assumption employed in the next section.

The importance of the diffusion admittance is best seen when compared with the depletion capacitance. The currents generated by a nonlinear depletion capacitance when the same voltage is applied to the diode chip as in the diffusion case is shown in Table 5.3. These current densities were normalized so that the magnitude of the current at pump frequency $|J_0|$ is the same for both the diffusion and depletion admittances. In this way a direct comparison can be made between the two. In each case shown in Tables 5.2 and 5.3, the current sidebands arising from the diffusion admittance are much larger. This is further illustrated in Fig. 5.15 where current magnitudes for the high voltage condition are plotted as a function of the frequency f_k. This behavior is expected since $e^{\alpha V}$ is "more nonlinear" than $(1 - V/\phi_v)^{-\gamma}$. This enhanced capability of producing a sideband current is useful in LSUC operation in producing more negative resistance at a given pump level.

5.4.2 Small Signal Analysis of the LSUC. In low-noise parametric amplifier analysis, the usual approach is to make a small signal assumption for the signal and lower sideband voltages, and calculate an admittance or impedance matrix, from which an expression for gain can readily be found. The small signal assumption will now be applied to (5.20) and (5.21), leading to a diffusion admittance matrix and a gain expression.

		Abrupt Junction			Graded Junction		
V_1 = 0.01	k	J_{kc} A/cm^2	J_{ks} A/cm^2	$\|J_k\|$ A/cm^2	J_{kc} A/cm^2	J_{ks} A/cm^2	$\|J_k\|$ A/cm^2
V_2 = -0.10							
	0	660.17	-670.54	940.98	600.85	-664.21	895.65
	1	220.36	-16.02	220.94	189.93	-27.51	191.92
	2	42.20	-667.26	668.59	-12.73	-633.94	634.06
	3	630.87	-53.08	633.10	600.79	-51.65	603.01
	4	49.29	-925.22	926.53	-15.63	-891.91	892.05
	5	706.72	-67.33	709.92	681.48	-59.39	684.06
	6	43.80	-1000.00	1000.96	-21.09	-969.73	969.96
	7	641.10	-68.38	644.74	621.78	-58.46	624.52
	8	32.34	-931.91	932.47	-25.27	-906.67	907.01
	9	507.74	-60.10	511.28	494.15	-50.96	496.77
V_1 = 0.001							
V_2 =-0.01							
	0	267.08	-267.10	377.72	244.28	-265.68	360.91
	1	13.09	-891.00	13.12	11.31	-1.58	11.42
	2	2.52	-39.62	40.41	-0.75	-37.73	37.74
	3	37.45	-2.79	37.55	35.76	-2.72	35.86
	4	3.21	-54.91	54.99	-0.64	-53.08	53.08
	5	41.93	-3.39	42.07	40.53	-2.92	40.64
	6	3.19	-59.29	59.38	-0.65	-57.67	57.68
	7	38.01	-3.32	38.15	36.95	-2.73	37.05
	8	2.74	-55.19	55.25	-0.66	-53.88	53.88
	9	30.07	-2.83	30.20	29.33	-2.28	29.42
V_1 = 0.0001							
V_2 = -0.001							
	0	264.11	-264.07	373.42	241.57	-262.68	356.87
	1	1.30	-0.88	13.03	1.12	-0.16	1.14
	2	0.25	-3.94	4.02	-0.08	-3.75	3.75
	3	3.72	-0.28	3.82	3.55	-0.27	3.56
	4	0.32	-5.46	5.54	-0.07	-5.28	5.28
	5	4.17	-0.33	4.30	4.03	-0.29	4.04
	6	0.31	-5.89	5.97	-0.68	-5.73	5.73
	7	3.78	-0.33	3.94	3.67	-0.27	3.68
	8	0.27	-5.48	5.54	-0.07	-5.35	5.35
	9	2.99	-0.28	3.13	2.92	-0.23	2.92

Table 5.2. Exact calculation of the current densities

		Abrupt Junction			Graded Junction		
$V_1 = 0.01$	k	J_{kc} A/cm^2	J_{ks} A/cm^2	$\|J_k\|$ A/cm^2	J_{kc} A/cm^2	J_{ks} A/cm^2	$\|J_k\|$ A/cm^2
$V_2 = -0.1$							
	0	-0.26	-941.00	941.00	-0.16	-895.65	895.65
	1	1.64	-1.68	2.34	1.03	-1.58	1.89
	2	-142.30	-1.40	142.30	-134.66	-0.88	134.67
	3	2.52	-1.73	3.05	1.41	-1.09	1.78
	4	-29.52	-0.42	29.52	-18.61	-0.24	18.61
	5	0.78	-0.48	0.92	0.41	-0.27	0.49
	6	-6.61	-0.10	6.61	-3.70	-0.05	3.70
	7	0.20	-0.12	0.23	0.10	-0.06	0.12
	8	-1.45	-0.02	1.45	-0.76	-0.01	0.76
	9	0.04	-0.03	0.05	0.02	-0.01	0.02
$V_1 = 0.001$							
$V_2 = -0.01$							
	0	0.00	-377.50	377.50	0.00	-360.91	360.91
	1	0.07	-0.07	0.09	0.42	-0.64	0.08
	2	-5.71	-0.06	5.71	-5.43	-0.04	5.43
	3	0.10	-0.07	0.12	0.05	-0.04	0.07
	4	-1.18	-0.02	1.18	-0.75	-0.01	0.75
	5	0.03	-0.02	0.04	0.02	-0.01	0.02
	6	-0.26	0.00	0.26	-0.15	0.00	0.15
	7	0.01	0.00	0.01	0.00	0.00	0.00
	8	-0.06	0.00	0.06	0.03	0.00	0.03
	9	0.00	0.00	0.00	0.00	0.00	0.00
$V_1 = 0.0001$							
$V_2 = -0.001$							
	0	0.00	-374.00	374.00	0.00	-356.87	356.87
	1	0.01	-0.01	0.01	0.00	-0.01	0.01
	2	-0.56	-0.01	0.56	-0.53	0.00	0.53
	3	0.01	-0.01	0.01	0.00	0.00	0.01
	4	-0.12	0.00	0.00	-0.07	0.00	0.07
	5	0.00	0.00	0.00	0.00	0.00	0.00
	6	-0.03	0.00	0.03	-0.01	0.00	0.01
	7	0.00	0.00	0.00	0.00	0.00	0.00
	8	-0.01	0.00	0.01	0.00	0.00	0.00
	9	0.00	0.00	0.00	0.00	0.00	0.00

Table 5.3. Current densities caused only by nonlinear depletion capacitance when normalized to give the same pump current $|J_0|$ as the diffusion current

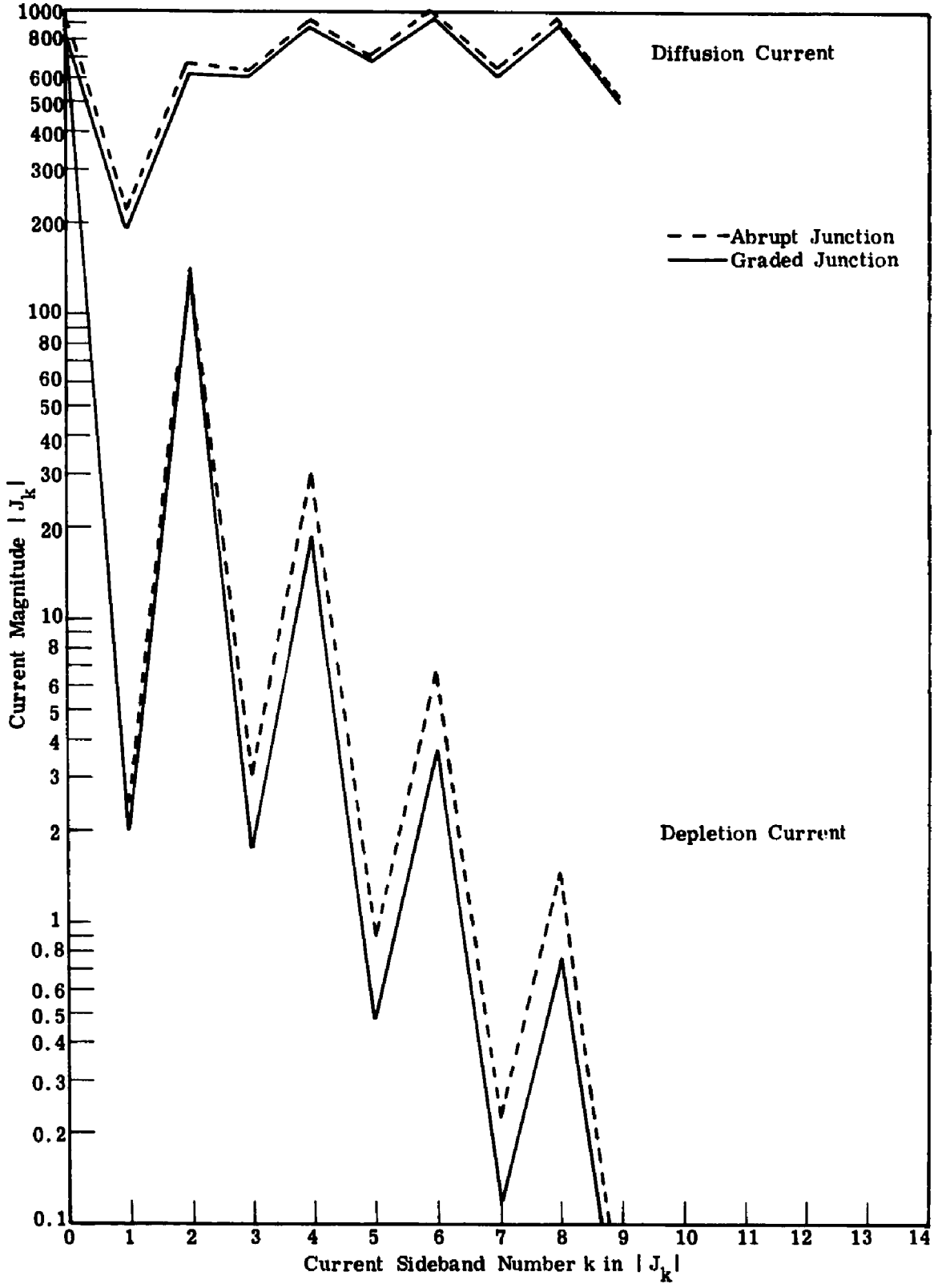


Fig. 5.15. A comparison of the sideband currents generated by the nonlinear diffusion admittance and the nonlinear depletion capacitance when $V_1 = 0.01$ V and $V_2 = -0.1$ V.

A comparison will be made between the current values determined by this method and by the exact method to determine the applicability of the small signal method.

If V_1, $V_2 << V_0$, then

$$e^{\alpha V(t)} \simeq e^{\alpha(V_b + V_0 \cos \omega_0 t)} \left[1 + \alpha \sum_{i=1}^{2} V_i \cos(\omega_i t + \psi_i)\right] .$$

Using Sonine's expansion this becomes

$$e^{\alpha V(t)} \simeq e^{\alpha V_b} \left[I_0(\alpha V_0) + 2 \sum_{r=1}^{\infty} I_r(\alpha V_0) \cos(r\omega_0 t)\right]$$

$$\cdot \left[1 + \alpha \sum_{i=1}^{2} V_i \cos(\omega_i t + \psi_i)\right]$$

where $I_r(\alpha V_0)$ is a modified Bessel function of order r. When this is substituted into (5. 20) and (5. 21) an integrand is obtained with three factors each containing terms harmonically related to the fundamental frequency. Using the orthogonality of the trigonometric functions these integrals can be easily simplified and evaluated. Thus (5. 20) becomes

$$J_{mc} = \frac{qD_p p_n(W) e^{\alpha V_b}}{W\pi} \left\{ \int_0^{2\pi} \left[I_0(\alpha V_0) + 2 \sum_{r=1}^{\infty} I_r(\alpha V_0) \cos(r\omega_0 t)\right] \right.$$

$$\cdot [\alpha_m \cos m\omega t + \beta_m \sin m\omega t] \, d\omega t + \int_0^{2\pi} \left[I_0(\alpha V_0) + 2 \sum_{r=1}^{\infty} I_r(\alpha V_0) \cos(r\omega_0 t)\right]$$

$$\left. \cdot \left[\alpha \sum_{i=1}^{2} V_i \cos(\omega_i t + \psi_i)\right] \quad [\alpha_m \cos m\omega t + \beta_m \sin m\omega t \,] \, d\omega t \right\}$$

After some straightforward but lengthy calculations, this reduces to

$$J_{mc} = \frac{qD_p p_n(W)}{W} e^{\alpha V_b} \Big[2I_r(\alpha V_0)\alpha_m \delta_{m,\, rm_0}$$

$$+ \delta_{m,\, rm_0 - m_1} \alpha V_1 I_r(\alpha V_0) (\alpha_m \cos \psi_1 + \beta_m \sin \psi_1)$$

$$+ \delta_{m,\, rm_0 + m_1} \alpha V_1 I_r(\alpha V_0) (\alpha_m \cos \psi_1 - \beta_m \sin \psi_1)$$

$$+ \delta_{m,\, rm_0 - m_2} \alpha V_2 I_r(\alpha V_0) (\alpha_m \cos \psi_2 + \beta_m \sin \psi_2)$$

$$+ \delta_{m,\, rm_0 + m_2} \alpha V_2 I_r(\alpha V_0) (\alpha_m \cos \psi_2 - \beta_m \sin \psi_2) \Big] \qquad (5.30)$$

where $\delta_{m,\, n}$ is the Kronecker delta function and r is the harmonic number of the pump frequency. In similar fashion the sine component of the current density is

$$J_{ms} = \frac{qD_p p_n(W)}{W} e^{\alpha V_b} \Big[-2I_r(\alpha V_0)\beta_m \delta_{m,\, rm_0}$$

$$+ \delta_{m,\, rm_0 - m_1} \alpha V_1 I_r(\alpha V_0) (\alpha_m \sin \psi_1 - \beta_m \cos \psi_1)$$

$$- \delta_{m,\, rm_0 + m_1} \alpha V_1 I_r(\alpha V_0) (\alpha_m \sin \psi_1 + \beta_m \cos \psi_1)$$

$$+ \delta_{m,\, rm_0 - m_2} \alpha V_2 I_r(\alpha V_0) (\alpha_m \sin \psi_2 - \beta_m \cos \psi_2)$$

$$- \delta_{m,\, rm_0 + m_2} \alpha V_2 I_r(\alpha V_0) (\alpha_m \sin \psi_2 + \beta_m \cos \psi_2) \Big] \qquad (5.31)$$

It should be noted that (5.31) can be obtained from (5.30) by substituting $-\beta_m$ for $+\alpha_m$, and $+\alpha_m$ for $+\beta_m$, and all the unsubscripted m's above have an implicit subscript k in accordance with definitions (5.26) and (5.28).

Table 5.4 shows the results of the calculations based on the small signal assumption for the abrupt and graded junction. The program used to generate Table 5.4 is program E in Appendix A. As might be expected a comparison between the small signal and exact method of Table 5.2 when V_2 is comparable in magnitude to V_0 indicates an

		Abrupt Junction			Graded Junction		
$V_1 = 0.01$	k	J_{kc} A/cm^2	J_{ks} A/cm^2	$\|J_k\|$ A/cm^2	J_{kc} A/cm^2	J_{ks} A/cm^2	$\|J_k\|$ A/cm^2
$V_2 = -0.1$							
	0	264.08	-264.04	373.43	241.54	-262.65	356.83
	1	130.11	-8.86	130.41	112.46	-15.74	113.56
	2	25.05	-393.93	394.73	-7.41	-375.18	375.25
	3	372.40	-27.76	373.44	355.54	-27.01	356.57
	4	31.97	-545.94	546.87	-6.35	-527.77	527.81
	5	416.92	-33.65	418.28	403.01	-29.01	404.05
	6	31.84	-589.53	590.39	-6.39	-573.47	573.50
	7	377.84	-32.93	379.27	367.33	-27.08	368.32
	8	27.37	-548.64	549.32	-6.47	-535.63	535.67
	9	298.88	-28.06	300.19	291.56	-22.64	292.44
$V_1 = 0.001$							
$V_2 = -0.01$							
	0	264.08	-264.04	373.43	241.54	-262.65	356.83
	1	13.01	-0.86	1.30	11.25	-1.57	11.36
	2	2.51	-39.39	39.47	-0.74	-37.52	37.53
	3	37.24	2.78	37.34	35.55	-2.70	35.66
	4	3.20	-54.59	54.69	-0.64	-52.78	52.78
	5	41.69	-3.37	41.83	40.30	-2.90	40.41
	6	3.18	-58.95	59.04	-0.64	-57.35	57.35
	7	37.78	-3.29	37.93	36.73	-2.71	36.83
	8	2.74	-54.86	54.93	-0.65	-53.56	53.57
	9	29.89	-2.81	30.02	29.16	-2.26	29.24
$V_1 = 0.0001$							
$V_2 = -0.001$							
	0	264.08	-264.04	373.43	241.54	-262.65	356.83
	1	1.30	-0.09	1.30	1.12	-0.16	1.14
	2	0.25	-3.94	3.95	-0.07	-3.75	3.75
	3	3.72	-0.28	3.73	3.56	-0.27	3.57
	4	0.32	-5.46	5.47	-0.06	-5.28	5.28
	5	4.17	-0.34	4.18	4.03	-0.29	4.04
	6	0.32	-5.90	5.90	-0.06	-5.74	5.74
	7	3.78	-0.33	3.79	3.67	-0.27	3.68
	8	0.27	-5.49	5.49	-0.06	-5.36	5.36
	9	2.99	-0.28	3.00	2.92	-0.23	2.92

Table 5.4. Small signal method for calculating the current densities

unacceptable error for the small signal method. However, when V_1 and V_2 are at least one order of magnitude lower than V_0, the small signal method gives quite accurate results all the way to $4\omega_p + \omega_s$.

Recalling that the total current density is $J_k = J_{kc} - jJ_{ks}$, the signal and lower sideband currents are

$$i_1 = \kappa \Big\{ I_0(\alpha V_0) \left[(\alpha_1 + j\beta_1) \cos \psi_1 + j(\alpha_1 + j\beta_1) \sin \psi_1 \right] V_1$$

$$+ I_1(\alpha V_0) \left[(\alpha_1 + j\beta_1) \cos \psi_2 - j(\alpha_1 + j\beta_1) \sin \psi_2 \right] V_2 \Big\}$$

$$i_2 = \kappa \Big\{ I_1(\alpha V_0) \left[(\alpha_2 + j\beta_2) \cos \psi_1 - j(\alpha_2 + j\beta_2) \sin \psi_1 \right] V_1$$

$$+ I_0(\alpha V_0) \left[(\alpha_2 + j\beta_2) \cos \psi_2 + j(\alpha_2 + j\beta_2) \sin \psi_2 \right] V_2 \Big\}$$

where $\kappa = \dfrac{AqD_p p_n(W)\alpha}{W} e^{\alpha V_b}$, and A is the diode area. The subscripts are particular values of k rather than m, and therefore designate the sideband number according to definition (5.26). The 2 x 2 admittance matrix is then

$$\begin{bmatrix} i_1 \\ i_2^* \end{bmatrix} = \begin{bmatrix} \kappa I_0(\alpha V_0)\ (\alpha_1 + j\beta_1) & \kappa I_1(\alpha V_0)\ (\alpha_1 + j\beta_1) \\ \kappa I_1(\alpha V_0)\ (\alpha_2 - j\beta_2) & \kappa I_0(\alpha V_0)\ (\alpha_2 - j\beta_2) \end{bmatrix} \begin{bmatrix} V_1 e^{j\psi_1} \\ (V_2 e^{j\psi_2})^* \end{bmatrix} \tag{5.32}$$

The gain of a LSUC is

$$G_{21} = 4|Z_{21}|^2 G_\ell G_g \tag{5.33}$$

where Z_{21} is the (2, 1) element of the inverse of the admittance matrix

$$\begin{bmatrix} Y_{11} & Y_{12} \\ Y_{21} & Y_{22} \end{bmatrix} .$$

The symbol G_g is the generator conductance at signal frequency, and G_ℓ is the load conductance at the lower sideband frequency. If the current is the forcing function, then $i_2 = 0$ and

$$Z_{21} = -\frac{Y_{21}}{Y_{11}Y_{22} - Y_{12}Y_{21}}$$

Therefore the gain for the diffusion matrix is

$$G_{21} = \frac{4\kappa^2 I_1^2(\alpha_2^2 + \beta_2^2)G_\ell G_g}{\left|(\kappa I_0\alpha_1 + G_g + j\kappa I_0\beta_1)(\kappa I_0\alpha_2 + G_\ell - j\kappa I_0\beta_2) - \kappa^2 I_1^2(\alpha_1 + j\beta_1)(\alpha_2 - j\beta_2)\right|^2} \quad (5.34)$$

where the argument of the modified Bessel functions is understood to be αV_0. If the input and output circuits are resonated by additional reactive circuit elements, the gain simplifies to

$$G_{21} = \frac{4\kappa^2 I_1^2(\alpha_2^2 + \beta_2^2)\, G_\ell G_g}{\left[(\kappa I_0\alpha_1 + G_g)(\kappa I_0\alpha_2 + G_\ell) - \kappa^2 I_1^2(\alpha_1\alpha_2 + \beta_1\beta_2)\right]^2 + \kappa^4 I_1^4(\beta_1\alpha_2 - \beta_2\alpha_1)^2} \quad (5.35)$$

The last term in the denominator does not have an analogous term in the usual reverse bias LSUC gain expression. This term is due to the real part in the off diagonal terms of (5.32). Equation (5.35) clearly shows how losses in the diffusion admittance can degrade LSUC gain and indicates the necessity for a high ratio of β_k/α_k.

The actual amount of additional circuit susceptance needed to tune the diffusion susceptance of the diode depends not only on the diode parameters and frequencies, but also on the bias and pump voltages. A list of these susceptance values is found below in Table 5.5 which is based on the diode parameters given in Section 5.3.5 when it is biased at 0.7 volts. As the bias voltage decreases, these susceptance values decrease until at 0 volts, the susceptance is negligible.

	Diode Profile		
	$\gamma = 1/2$	$\gamma = 1/3$	$\gamma = 1/5$
$f_{10} = 1.000$ GHz	-0.324	-0.139	-0.0356
$f_{20} = 8.500$ GHz	-1.328	-0.835	-0.296

Table 5.5. Susceptance values in mhos needed to tune the diffusion susceptance of the diode when it is biased at 0.7 V

5.4.3 The LSUC with the Total Varactor Diode Model. The admittance matrix for the LSUC when both depletion capacitance and diffusion admittance are considered is the following simple modification of (5.32)

$$[Y] = \begin{bmatrix} \kappa I_0\alpha_1 + j(\omega_1 C_0 + \kappa I_0\beta_1) & \kappa I_1\alpha_1 + j(\omega_1 C_1 + \kappa I_1\beta_1) \\ \kappa I_1\alpha_2 + j(\omega_2 C_{-1} + \kappa I_1\beta_2) & \kappa I_0\alpha_2 - j(\omega_2 C_0 + \kappa I_0\beta_2) \end{bmatrix} \tag{5.36}$$

where C_0 and $C_{\pm 1}$ are the average and first harmonic depletion layer capacitances. The impedance matrix for the total diode model of Fig. 5.10 is obtained by inverting the Y matrix of (5.36) and adding terms resulting from the series bulk resistance. The inversion is a lengthy but straightforward process, and the result is

$$[Z] = \frac{\begin{bmatrix} \kappa I_0\alpha_2 - j(\omega_2 C_0 + \kappa I_0\beta_2) & -\kappa I_1\alpha_1 - j(\omega_1 C_1 + \kappa I_1\beta_1) \\ -\kappa I_1\alpha_2 + j(\omega_2 C_{-1} + \kappa I_1\beta_2) & \kappa I_0\alpha_1 + j(\omega_1 C_0 + \kappa I_0\beta_1) \end{bmatrix}}{\Delta} + \begin{bmatrix} R_s & 0 \\ 0 & R_s \end{bmatrix} \tag{5.37}$$

where Δ is the determinant of the Y matrix. The gain for the LSUC then is obtained by resonating the reactance terms on the diagonal of (5.37) and substituting Y_{21}, the row 2 column 1 element of the inverse of the resulting matrix, in

$$G_{21} = 4 \left| Y_{21} \right|^2 R_\ell R_g \quad . \tag{5.38}$$

To display the effects of diffusion capacitance effectively, the gain and noise figure should be found as a function of bias or pump voltage. However if the voltage changes, then so does the depletion layer capacitance together with the relative magnitudes of the pumped elastance harmonics. In order not to mask the effects of diffusion admittance with the changes in depletion capacitance, the following numerical calculations of gain and noise figure were performed with a fixed value of S_1, the first harmonic of the nonlinear depletion layer elastance. To insure the circuit is tuned at midband the average varactor elastance and modulation coefficient are allowed to vary. This procedure means that if only depletion layer capacitance were considered, the midband gain would remain

constant for any bias or pump voltage, although the bandwidth would vary because of the different tuning reactances.

However there are still two problems that must be resolved: (1) the circuit is described in terms of depletion layer capacitance rather than elastance, and (2) the bias and pump voltages give a dynamic capacitance different from the static capacitance. The first problem is easily resolved since the inverse of the 2 x 2 capacitance matrix is an elastance matrix where

$$S_0 = \frac{C_0}{C_0^2(1 - C_1^2/C_0^2)} = \frac{1}{C_0(1 - m_s^2)} \tag{5.39}$$

$$S_1 = - \frac{C_1}{C_0^2(1 - m_s^2)} = \frac{m_s}{C_0(1 - m_s^2)} \tag{5.40}$$

and the modulation coefficient $m_s = S_1/S_0 = - C_1/C_0$. When the rank of the matrix is larger than two however, the relationship between the elastance and capacitance matrices is not simple (Ref. 15, pp. 54-64).

The second problem arises because the nonlinear depletion capacitance when expanded into a Fourier series will have an average capacitance different from the dc capacitance. The depletion layer capacitance is

$$C(t) = \frac{C_b}{[1 - V(t)/\phi_v]^\gamma} \tag{5.41}$$

where C_b is the static dc capacitance and $V(t) = V_b + V_0 \cos(\omega_p t)$. The Fourier series expansion of C(t) was carried out by Oliver (Ref. 15, Appendix B) and is shown below:

$$H_\ell(a_v) = \sum_{k=0}^{\infty} \frac{(-1)^\ell a_v^{(2k+\ell)} \Gamma(2k+\ell+\gamma) \cos(\ell\omega_p t)}{\Gamma(\gamma)\, 2^{(\ell+2k-1)} \Gamma(\ell+k+1)\Gamma(k+1)} \tag{5.42}$$

where

$$a_v \triangleq \frac{V_0}{V_b - \phi_v}$$

and Γ is the well known gamma function. Therefore the dynamic average capacitance is

$$C_0 = \frac{C_b H_0(a_v)}{(1 - V_b/\varphi_v)^\gamma} \quad , \tag{5.43}$$

the modulation coefficient is

$$m_s = \frac{H_1(a_v)}{H_0(a_v)} \quad , \tag{5.44}$$

and the desired first harmonic capacitance is

$$C_1 = - m_s C_0 \quad . \tag{5.45}$$

Thus when the diode built-in potential φ_v, the doping profile γ, the desired elastance S_1, and the applied voltage are known, m_s is found from (5.44), C_0 from (5.40), and C_1 from (5.45). These values of C_0 and C_1 can be used in (5.35) to find the LSUC gain and noise figure.

The numerical calculations of gain and noise figure were performed using program F in Appendix A, and the results are shown in Figs. 5.16 to 5.19. The diode model had the same properties listed in Section 5.3.4 with the additional property that the first harmonic of depletion elastance is $S_1 = 2.20 \times 10^{11}\ F^{-1}$, and the diode area was not used explicitly. The circuit properties were chosen as follows:

pump frequency $f_p = 9.500$ GHz

signal frequency $f_s = 1.000$ GHz

generator resistance $R_g = 100$ ohms

load resistance $R_\ell = 1.3$ ohms .

The maximum gain (not midband gain) and the minimum noise figure were calculated as a function of bias and pump voltage. If only the depletion layer capacitance were involved the transducer power gain would be 19.12 dB and the noise figure would be 1.1410 for all voltages. The graphs in Figs. 5.16 to 5.19 show the deviation from the depletion layer calculations for the LSUC. The diffusion admittance is deleterious to the operation of this LSUC when an abrupt or graded junction diode is used. However when $\gamma = 1/5$

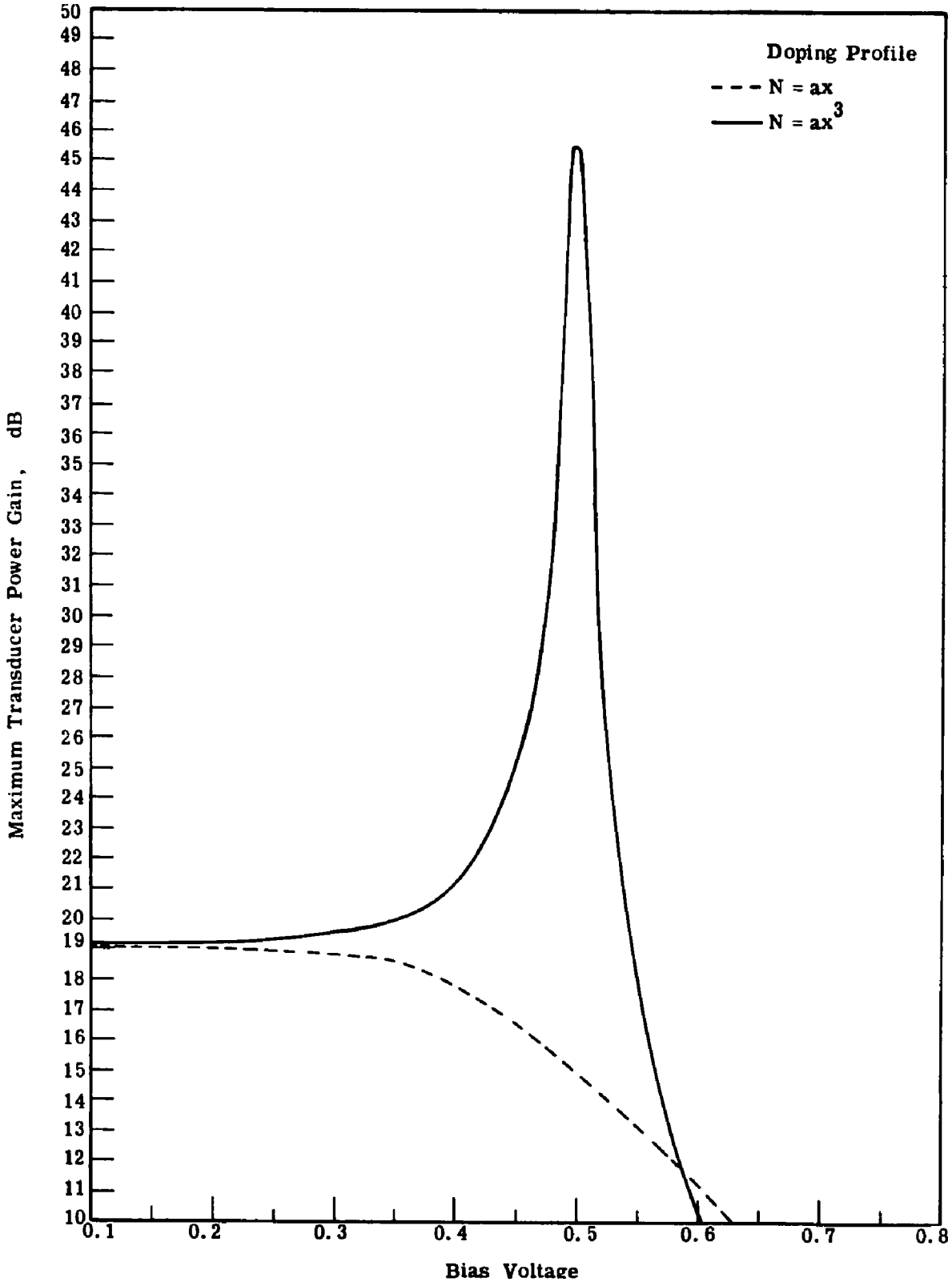


Fig. 5.16. Maximum gain as a function of bias voltage with pump voltage = 0.1 V when the optimum lifetime is used for both doping profiles. In each case ϕ_v = 0.9 V, $S_1 = 2.20 \times 10^{11}$ F^{-1}, W/L = 0.1, and $p_n(W) = 10^{10}$ cm^{-3}

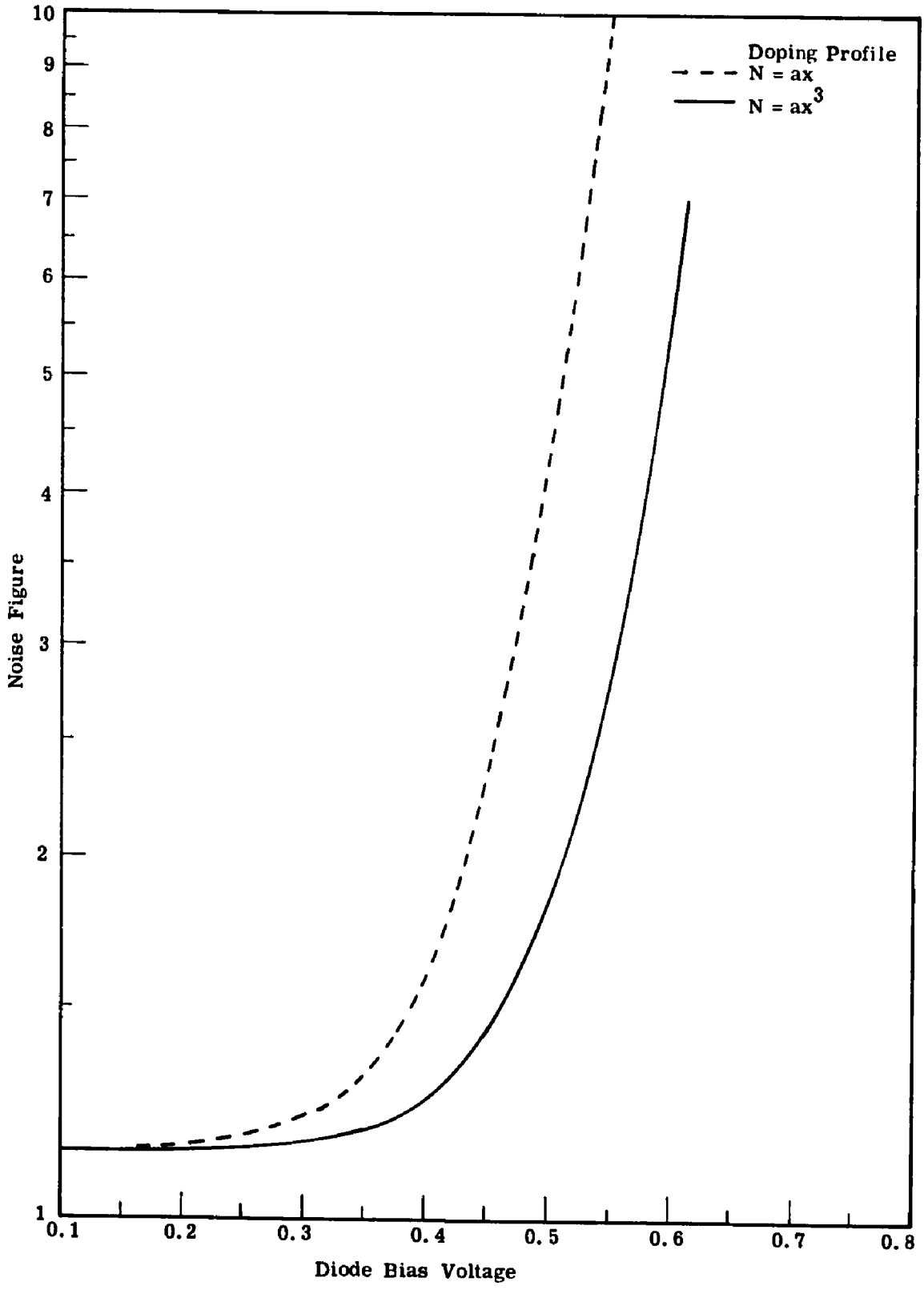


Fig. 5.17. Noise figure as a function of bias voltage with pump voltage = 0.1 V when the optimum lifetime is used for both doping profiles. In each case $\phi_v = 0.9$ V, $S_1 = 2.20 \times 10^{11}$ F^{-1}, W/L = 0.1, and $p_n(W) = 10^{10}$ cm^{-3}

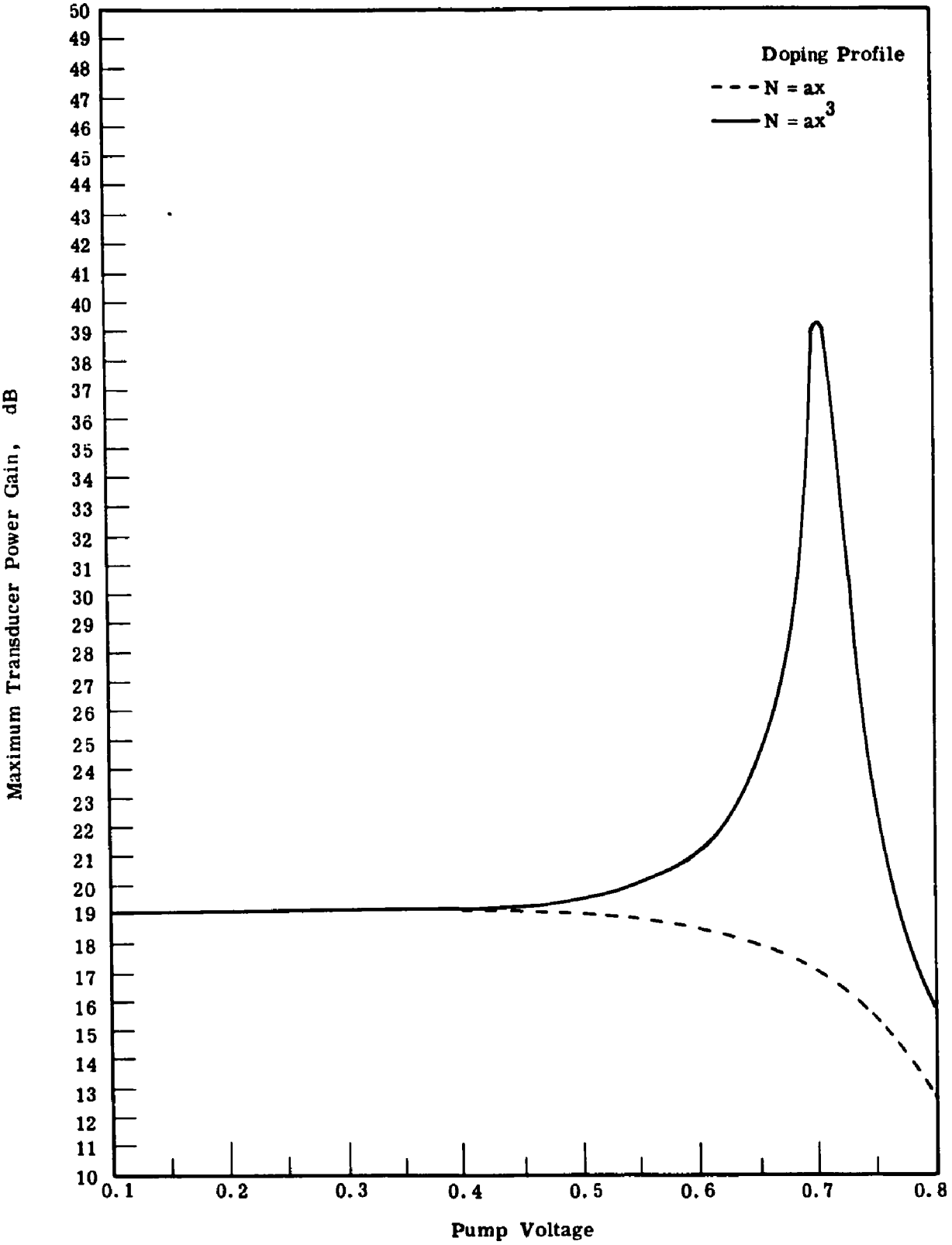


Fig. 5.18. Maximum gain as a function of pump voltage at zero bias voltage when the optimum lifetime is used for both doping profiles. In each case $\phi_v = 0.9$ V, $S_1 = 2.20 \times 10^{11}$ F^{-1}, $W/L = 0.1$, and $p_n(W) = 10^{10}$ cm^{-3}

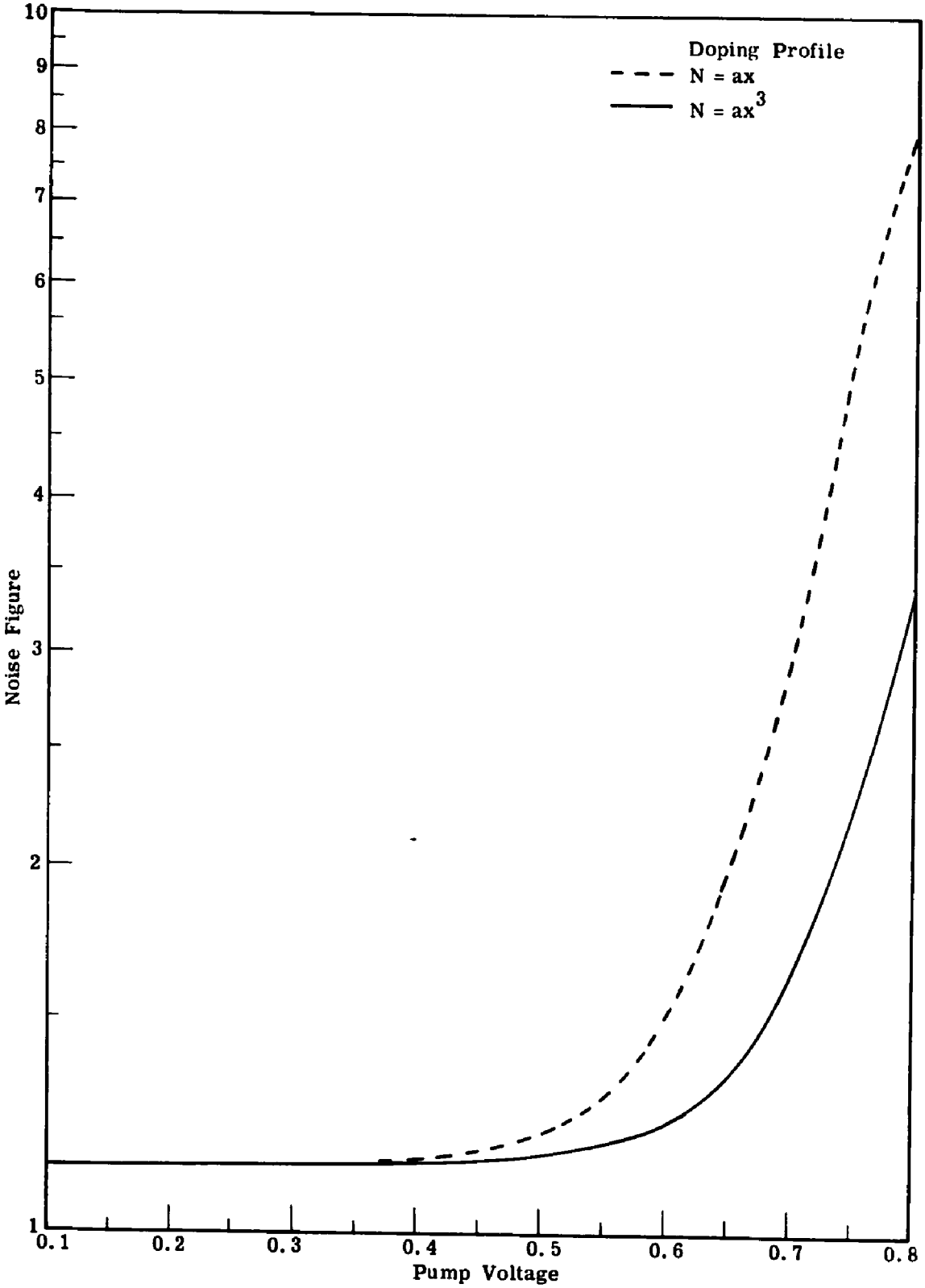


Fig. 5.19. Noise figure as a function of pump voltage at zero bias voltage when the optimum lifetime is used for both doping profiles. In each case $\phi_v = 0.9$ V, $S_1 = 2.20 \times 10^{11}$ F^{-1}, W/L = 0.1, and $p_n(W) = 10^{10}$ cm^{-3}

the diffusion admittance can substantially increase the gain or alternatively the bandwidth. The diffusion admittance increases the noise figure above that which would occur for the depletion capacitance, but noise figure improves as γ decreases. Low loss diffusion admittance is a prerequisite for improved LSUC performance when the diode is forward biased. The general trends expressed in Table 5. 1 can therefore be used in judging how a varactor ought to be chosen if its diffusion admittance is to be utilized.

The experimental existence of the optimum bias voltage for maximum LSUC gain shown in Fig. 5. 16 was observed in an empirically tuned LSUC (Fig. 5. 20). This circuit consisted of a silicon varactor diode series mounted in a length of 14 mm coaxial line, together with several standard filters and double-stub tuners. The input pump and signal frequencies (f_p = 9. 1 GHz and f_s = 0. 975 GHz) were combined through a coaxial wye junction and transmitted to the mounted diode. The output lower sideband frequency was observed at the opposite end of the diode mount. The bias voltage was applied through a General Radio 874-FBL bias insertion unit and monitered with a VTVM and a microampere meter. The variable tuning elements were needed to compensate for changes in diode capacitance when the bias voltage changed. Throughout the measurement procedure, the pump power remained constant, while the tuners were changed to achieve maximum gain at each bias voltage. Either because of parasitic circuit losses or lack of sufficient pump power, this LSUC did not oscillate when retuned for maximum gain. In both the theoretical and experimental curves the gain falls very quickly after achieving a maximum. This comparison together with the correlation of the diffusion susceptance curve in Fig. 5. 13 with the previously observed "inductive effect" adds to the confidence that can be placed in the diffusion admittance theory presented here.

The present model provides more accurate description of the varactor diode than the model described in Section 5. 2 where the diffusion admittance was neglected. However a direct comparison cannot be made between the large signal USUC analysis reviewed there and the LSUC presented subsequently, since in the USUC power handling capability and efficiency are the primary parameters of concern, while in the LSUC gain by means of generating negative resistance is of primary concern. However, the additional diffusion admittance discussed here would affect the optimum drive level in the USUC since the additional capacitance would be helpful only as long as the diffusion conductance losses

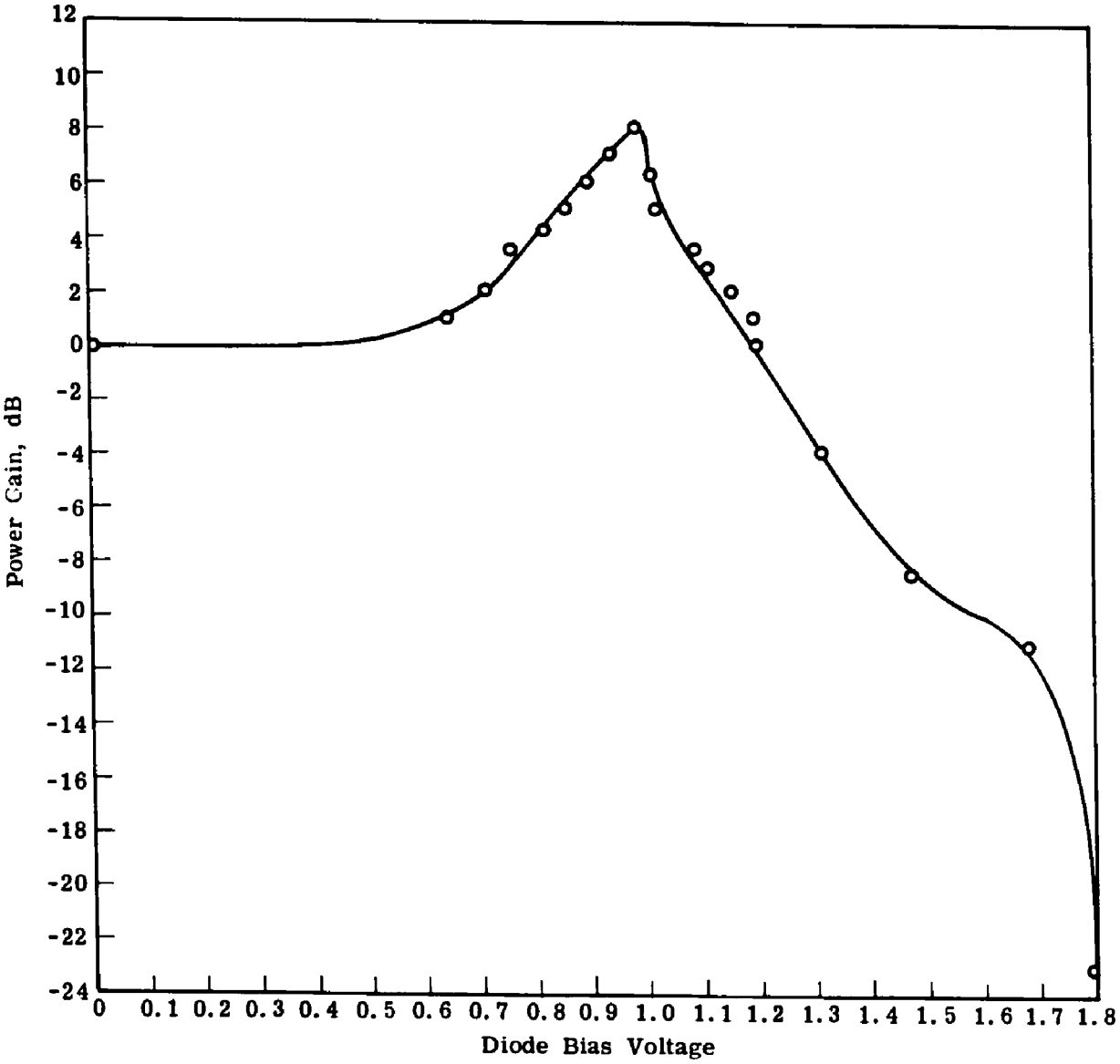


Fig. 5.20. Experimental gain of a LSUC as a function of bias voltage on the varactor

were sufficiently small. There appears to be no analytical discussion in the literature of the effects of forward bias on either the RPA or the small signal upconverter. The diffusion capacitance calculations here show why the capacitance-voltage curve has a maximum and how this can be utilized in a LSUC and presumably in other varactor devices.

5. 5 Conclusions

Calculations of the diffusion admittance showed that when the impurity distribution is $N(x) = ax^b$, increasing b, optimizing the minority carrier lifetime τ_p, and decreasing the depletion layer width W decrease the losses in an overdriven diode. The current densities in the LSUC were calculated using the diffusion admittance theory. The small signal method is sufficiently accurate at all frequencies when the larger of the signal and lower sideband voltage is at least one order of magnitude lower than the pump voltage. Therefore this assumption was used to find an admittance matrix from which the gain and noise figure were obtained. The existence of an optimum bias where the gain is maximized was experimentally and theoretically verified.

CHAPTER VI

CONCLUSIONS AND SUGGESTIONS FOR FUTURE RESEARCH

6.1 Introduction

In the preceding chapters, the analysis of a LSUC was extended, and a design technique was developed and experimentally verified. The analysis consisted of both an investigation of the effect of the circuit and the effect of a forward biased diode in a LSUC. The synthesis made use of an improved design of coaxial filters and some high frequency properties of a coaxial tee junction. The original contribution of the previous chapters are summarized in Section 6.2, and several suggestions for related future research are given in Section 6.3.

6.2 Summary of Original Contributions

6.2.1 Distributed Design of Coaxial Filters. In Chapter II, two methods for designing coaxial band-pass filters were compared: the lumped method and the distributed method. In both cases a set of impedance inverters, each separated by a half wavelength of coaxial transmission line, have to be synthesized. In the lumped method, a capacitor is approximated by a disk whose size gives the correct capacitance at low frequencies. However, when the disk lengths in the filter are $\gtrsim 0.08\lambda$, as often occurs when the bandwidth $\lesssim 10$ percent, the filter characteristic is seriously distorted. On the other hand, the distributed method which was derived here, gives much improved filter characteristics and is applicable to filter bandwidths down to 1 percent of the center frequency.

6.2.2 Discontinuity Capacitance Compensation. Three methods of accommodating the disk discontinuity capacitance associated with an abrupt change in the characteristic impedance of a transmission line were compared. Although all these methods were known, their relative strengths and weaknesses had not been analyzed previously. This comparison was made here when these three methods were applied to the coaxial filter design, in Section 2.6.

6.2.3 Effect of Higher Order Sidebands in the LSUC. The design of a LSUC is based on the assumption that only the signal and lower sideband frequencies exist, although in reality energy at many other sidebands often exists near the diode. The effects of as many as seven higher order sidebands were investigated in several LSUC designs. However, when the gain and noise figure were calculated, little change was observed between the approximation using four frequency sidebands and higher order approximations. Explicit expressions for the LSUC gain, gain sensitivity, gain-bandwidth product, noise figure, and noise measure were derived, which included the effects of the impedance at the upper sideband frequency as well as the second harmonic of the pumped elastance. These expressions show that a small impedance at the upper sideband frequency can seriously degrade the LSUC performance. Thus, while a LSUC can be synthesized using only impedances at the signal and lower sideband frequencies, an analysis including higher order sideband frequencies should be performed to insure the desired characteristics will be obtained.

6.2.4 A Noniterative Design Algorithm for a LSUC. A practical design for a LSUC which required neither trial and error nor iterative methods is described and experimentally verified. The design was accomplished by isolating each port of the amplifier from the out-of-band frequencies, thus making it possible to synthesize impedance transformers by a straightforward application of the coaxial filter theory. The nonideal characteristic of the coaxial tee junction was used advantageously to help isolate the different frequencies from the signal port.

6.2.5 Verification of Noise Figure Dependence on Gain. Most analyses of the noise figure of a LSUC show that noise figure is independent of amplifier gain. However the theory reviewed here showed that, in most cases, noise figure decreased with increasing gain (Ref. 11). The experimental measurement of noise figure clearly shows the relationship between noise figure and gain which this latter theory describes.

6.2.6 Application of Diffusion Admittance to a LSUC. The theory for the diffusion admittance exhibited by a forward biased diode was developed by Maneshin and Parygin (Ref. 80). It was shown here with this theory that the diffusion admittance could explain the "inductive effect" observed by many workers. The diffusion admittance can improve

the bandwidth or gain of a LSUC when the impruity doping profile and depletion layer width W are appropriately chosen. However, some sacrifice in thermal noise figure must be made when diffusion admittance is used. In general a diode having small γ and small W was found to give the best results.

6.2.7 Modified Bessel Functions. In the course of the work on diffusion admittance, numerical evaluation of the K modified Bessel function with complex argument z was required. The computer program which is developed here is based on economization of power series. It yields accurate values of the K Bessel functions for almost all values of z; the accuracy diminishes somewhat for $|z| > 1$, $\arg(z) \approx 180^{o}$.

6.3 Suggestions for Future Research

In the course of the studies presented here, several related problems arose which would be fruitful areas of future research.

6.3.1 Stripline Filters. The theory developed in Chapter II on coaxial filters can be applied to synthesis of stripline and possibly microstrip band-pass filters. However, the range of characteristic impedances in stripline is more restricted than in coaxial line with the result that narrow bandwidth filters cannot presently be built in stripline.

6.3.2 A LSUC Made in Stripline. The filters described above could be used to design and build a LSUC in stripline. Some of the techniques used in the coaxial LSUC would not be applicable, however, since the nonideal tee junction and diode mount would be different in this case.

6.3.3 Double Sideband Operation. The theory for the LSUC described here can be extended readily to include a port at the upper sideband frequency as well as the lower sideband frequency. In this way a LSUC can be made more stable, and an upper sideband upconverter can be made to have higher gain. The resulting amplifier would provide output from both parts, but would differ from the phase-shift amplifier in having unequal loading at the two ports.

6.3.4 The Coaxial Tee Junction. The 7 mm coaxial tee junction is shown in Chapter IV to act as an ideal power splitter only below 4 GHz. No thorough analysis has been made of a coaxial tee junction above this limiting frequency, although it is a widely used circuit element. R. W. P. King (Ref. 61, pp. 389-397) has derived an equivalent circuit

for the two wire transmission line tee junction, and as a first approximation his technique could be applied to a coaxial tee.

There are at least two other junctions which could be more useful than the standard coaxial tee: the coaxial wye and the stripline tee. A preliminary investigation of the first was performed by terminating two ports of a 7 mm coaxial wye junction with 50 ohm loads and measuring the input impedance of the third port referenced at the junction as a function of frequency. Instead of deteriorating above 4 GHz, the wye junction impedance stayed between 25 and 21 - j3 ohms up through 12 GHz and within $25 \pm (4 \pm j5)$ ohms from 12 to 17 GHz. The symmetrical power splitting capabilities of the wye junction stand in sharp contrast to the tee junction.

The coaxial tee characteristics arise from its asymmetrical geometry, which results in a complicated electric field pattern in the neighborhood of the junction. However, in a stripline tee the electric field (to a first approximation) is always perpendicular to the center and outer conductors; consequently the high frequency characteristics of the stripline tee ought to be better than the coaxial tee. Further improvement would be expected from a stripline wye junction.

6.3.5 Measurement of Diffusion Admittance. There has been no direct experimental verification of the theory presented in Chapter V on the diffusion admittance. To make such a correlation, the minority carrier lifetime, the depletion layer width, the diffusion length, the doping profile, and the minority carrier lifetime would have to be known. Measurement of the diode impedance as a function of applied bias voltage could then be compared to the theoretical prediction. The diode parasitic elements would of course have to be determined by a separate measurement.

6.3.6 A LSUC with a Step Recovery Diode. Step recovery diodes are characterized by their long minority carrier lifetimes and their ability to generate a large number of frequency harmonics. Since the lifetimes of commercial step recovery diodes are between 20 and 400 ns, the curves showing minimum loss for diffusion admittance would indicate these diodes are only useful in the lower microwave frequency range. However if one of these diodes were used in a LSUC, a large number of frequency sidebands would be generated. A detailed study of the step recovery diode used in a LSUC could yield

beneficial results with regard to either or both the minority carrier lifetime and the large number of frequency sidebands.

6.4 Conclusion

The theory and experimental verification for the design of a parametric LSUC has been presented, together with a study of diffusion capacitance which could greatly improve the amplifier bandwidth. In this study several contributions to LSUC design have been presented; there also remain several topics which merit further investigation.

APPENDIX A

PROGRAM LISTINGS

The major programs and subroutines used in this report are listed here. There are six main programs A - F and seven subroutines which which are used in the main programs. These programs are summarized below and listed in full subsequently. The symbol SSP used below stands for IBM's scientific subroutine package.

Main Programs

Program	Description	Subroutines Required	Referred From
A	Filter design and analysis	DESIGN IMPST IMPM	Sec. 2.6
B	Design and analysis of LSUC3 with coaxial filters	TGAIN GAINST PROTOG DESIGN IMPST IMPM TRNR	Sec. 3.5.4
C	Diode diffusion admittance	BESI (in IBM SSP) BESKC	Sec. 5.3.4
D	Large signal currents with short circuit assumptions in a LSUC using diffusion admittance	DQG12 (in IBM SSP) BESKC DFT FC1 FC2	Sec. 5.4.1.3
E	Currents in a LSUC by small signal method and Laplace asymptotic method	BESI (in IBM SSP) BESKC	Sec. 5.4.2 Appendix D
F	Gain of LSUC using combined diffusion and depletion admittance diode model	BESI (in IBM SSP) GAMMA (in IBM SSP) BESKC CMINV	Sec. 5.4.3

Subroutines

Name	Entries	Other Subroutines Called
TGAIN	GAINST	IMPST
		IMPM
		TRNR
		CMINV
TRNR	TRNS	
IMPST	IMPM	TRNR
DESIGN		
PROTOG		
CMINV	MPRD	
BESKC		

```
001   PROGRAM A
002
003   C     THIS PROGRAM SYNTHESIZES AND ANALYZES COAXIAL BAND-PASS FILTERS.
004
005   C     SUBROUTINES USED ARE DESIGN,IMPST,IMPM.
006         DIMENSION G(10),K(10),LNTH(10),ANG(10),C(10),Z(42),FR(21),GAMA(22)
007         DIMENSION DI(10) ,FPS(10), LD(10),DIST(10),CD(10) ,ZOC(10)
008         REAL K,LNTH,LL,LD
009         INTEGER N,TEST,J ,JJ ,LIMIT,TESTI
010         DATA EPS/10*17.97362/
011         FPS(1)=0.854
012         FPS(4)=0.854
013         TPI=6.2831853
014         ZI=50.
015         VC=2.997925 ER
016         R=20
017         DELTA=1.
018         TL=.5
019   1     FORMAT (I1,6E11.5/(7E11.5))
020   2     FORMAT ('1DATA IS N,F,W,QA  ',I11,3E13.5/(' G'7E13.5))
021         READ (5,1) LIMIT,STEP
022   40    CONTINUE
023         READ (5,1) N,F,W,QA   ,(G(J),J=1,N,1)
024         G(N+1)=1.
025         NN=N+1
026         WRITE(6,2) N,F,W,QA,  (G(J),J=1,NN,1)
027         TEST=0
028         CALL DESIGN (R*G(N+1),F,DI,W,DELTA,N,G,K,ANG,C,LNTH,EPS,TEST)
029         IF (TEST.EQ.1)  GO TO 46
030         TEST1=3
031         CALL IMPST (DI,LNTH,FPS,N,TEST1,LD,CD,ZOC,F*1.E-9)
032   92    FORMAT (' DISCONTINUITY CAP = '4(5X,E14.6))
033         WRITE (6,92) (CD(J),J=1,4,1)
034         DO 100 J=1,N,1
035   C     DISTANCE AND LENGTH (FR) IN INCHES
036         IF (J.EQ.1) GO TO 47
037         DIST(J)=((ANG(J-1)+ANG(J))/(2.*TPI)+TL)*VC /(1+.0254)
038   47    CONTINUE
039         FR(J)= LD(J)/.0254
040         IF (FR(J).LT. 0.)GO TO 45
041   100   CONTINUE
042         DIST(1)=0.
043   90    FORMAT (' THIS FILTER CANNOT BE BUILT')
044   30    FORMAT ('0F= 'E11.5,' O= ' E11.5,/' K INVERTER VALUES = '
045        14(5X,E15.6)/' ANGLE PHI IN RADIANS = '4(5X,E13.6)/
046        2'  CAPACITANCE IN PICO FARADS = ' 4(5X,E15.6)/' LENGTH IN METERS
047        3NEGLECTING DISCONTINUITY CAPACITANCE ' 4(3X,E15.6)/' DISK DIAMETER
048        4S ARE ' 4(5X,E15.9)/' DISTANCE BETWEEN DISKS IN INCHES '4(3X,
049        5E15.9)/' LENGTH IN INCHES OF DISK WITH DISC. CAP ' 4(3X,E15.4))
050         WRITE (6,30) F,QA,(K(J),J=1,4,1),(ANG(J),J=1,4,1), (C(J),J=1,4,1),
051        1(LNTH(J),J=1,4,1),(DI(J),J=1,4,1) ,(DIST(J),J=1,4,1),(FR(J),
052        2J=1,4,1)
053         DO 48 J=1,N,1
054         DIST(J)=DIST(J)*.0254
055   48    CONTINUE
056   4     FORMAT (' ',3('F IN GC',' GAMA    R',13X,'+JX',10X))
057         WRITE (6,4)
058         JJ=0
059         R=F*1.E-9-STEP*LIMIT*10.
060   11    CONTINUE
061         JJ=JJ+1
062         DO 10 J=1,20,1
063         FV=R+(J-1)*STEP
064         CALL IMPM (FV,N,LD,DIST,CD,ZOC,Z0,0.,ROUT,XOUT)
065         Z(J*2-1)=ROUT
066         Z(J*2)=XOUT
067         FR(J)=FV
068         GAMA(J)=((ROUT-R )**2+XOUT*XOUT)/((ROUT+R )**2+XOUT*XOUT)
069   10    CONTINUE
070   5     FORMAT (' '/(' ',3(E4.3,2X,F6.4,2X,E12.5,2X,E12.5,1X)))
071         WRITE (6,5)(FR(J),GAMA(J),Z(J*2-1),Z(J*2),J=1,20,1)
072         IF (JJ.GE.LIMIT) GO TO 40
073         R=R+STEP*20.
074         GO TO 11
075   46    CONTINUE
076         WRITE (6,90)
077         GO TO 40
078   45    WRITE (6,91) J
079   91    FORMAT(' DISCONTINUITY CAPACITANCE EXCEEDS DISTRIBUTED CAPACITANCE
080        1 OF DISK ' I5)
081         GO TO 40
082         END
```

```
001   PROGRAM A
002
003   C       THIS PROGRAM DESIGNS A LSUC WITH DIODE IN LOWER SIDEBAND PORT.
004
005   C       THIS PROGRAM CALLS TGAIN,GAINST,PROTOG,DESIGN,IMPST,IMPM,TRNR.
006   C       INPUT DATA CONSISTS OF DIODE PARAMETERS, OPERATING FREQUENCIES,
007   C       DIELECTRIC CONSTANTS AROUND DISKS IN FILTERS, AND SOME AUXILIARY
008   C       INFORMATION.
009   C       PRT=1 MEANS NO PRINT: PRT=0 MEANS PRINT
010   C       LDISC DETERMINES METHOD FOR ACCOMODATING DISC. CAP. IN IMPST.
011   C       TESTS,TEST1,TESTP CHECKS FOR UNREALIZABILITY  IN DESIGN PROG.
012   C       PRTT=0 MEANS PRINT FULL GAIN CURVE IN TGAIN. PRTT=1 MEANS PRINT
013   C       ONLY CENTER FREQUENCY GAIN.
014   C       IF THE INPUT QA'S ARE 0. THEN PROGRAM FINDS QA.
015   C       PRT=0 MEANS PRINT DIAGNOSTIC INFORMATION
016           REAL LL,LP ,LR,K(10),LNTH(10)
017           INTEGER PRT,TESTS,PRTT,TEST,TESTP,TEST1
018           DIMENSION G(20),C(10),DIAS(10),DIA1(10),DIAP(10),ANG(10),S(10),
019          1EPS(10),DISTS(10),DIST1(10),DISTP(10),DLNTS(10),DLNT1(10),
020          2DLNTP(10),ZOC(10),DIST(10),DIA(10),DLNT(10),ES(4),F1(4),FP(4)
021           DIMENSION AREA(10)
022           TPI=6.2831853
023           VC=2.997925E8
024   9       FORMAT(7E11/(7E11))
025   10      FORMAT(7E11.5)
026           ZO=50.
027   21      CONTINUE
028           READ (5,9) LDISC,FIRST,NUM,PRTT, PRT,N,NN ,NPTEST
029           READ (5,10) STEP,QAS,QA1,QAP
030           READ (5,10) FS,FP,RG,RL,RS,LL,SP,SO,(S(J),J=1,NN,1),WS,WI,WP
031          1,(ES(J),J=1,N,1),(E1(J),J=1,N,1),(EP(J),J=1,N,1)
032   20      FORMAT (' DATA IS LDISC,FIRST,NUM,PRTT,N,NN,FS,FP,RG,RL,RS,LL,
033          1SP,SO'/A(3X,I6)/A(3X,E13.6)/' WS,WI,WP ='3(3X,E13.6)/
034          2' S(1)...S(N),ES(1)...ES(N),E1(1)...E1(N),EP(1)...EP(N)'/
035          3(A(3X,E13.6)))
036           WRITE (6,20) LDISC,FIRST,NUM,PRTT,N,NN,FS,FP,RG,RL,RS,LL,SP,SO,
037          1WS,WI,WP,(S(J),J=1,NN,1),(ES(J),J=1,N,1),(E1(J),J=1,N,1),
038          2(EP(J),J=1,N,1)
039   C       .05<DELTA<2.0
040   C       MULTIPLY THE MATCHING RESISTANCE BY G(N+1) TO GET RIGHT MATCH
041   C       PUMP PORT
042           F=FP
043           F1=FP-FS
044   C       PUMP RESISTANCE ARBITRARILY SET TO 1. OHM.
045           RM=1.
046           KEY=4
047           LP=SP/(TPI*FP*TPI*FP)
048   C       GET DIODE Z AND RESONATED Q, QA
049           GO TO 72
050   76      CONTINUE
051           IF ( ABS(QAP).LT.1.E-10) QAP=QA
052           DELTA=1./(WP*QAP)
053           CALL PROTOG (N,DELTA,TEST,G)
054   31      FORMAT (' F = 'E13.6,' DELTA = 'E13.6,'G(1)...G(N)'/4(3X,E13.6))
055           JJ=N+1
056           IF (PRT.EQ.0) WRITE (6,31) F,DELTA,(G(J),J=1,JJ,1)
057           IF (TEST.EQ.1) GO TO 21
058           TESTP=0
059           CALL DESIGN (G(N+1),FP,DIAP,WP,DELTA,N,G,K,ANG,C,LNTH,FP,TESTP)
060           IF (TESTP.EQ.1) WRITE (6,403)
061   403     FORMAT (' PUMP CIRCUIT CANNOT BE BUILT')
062           CALL IMPST (DIAP,LNTH,FP,N,LDISC,DLNTP,C,ZOC,FP*1.E-9)
063           DO 100 J=1,N,1
064           IF (J.EQ.1) GO TO 47
065           DISTP(J)=((ANG (J-1)+ANG (J))/(2.*TPI)+.5)*VC/FP
066   47      CONTINUE
067           IF (DLNTP(J).LT.0.) GO TO 45
068   100     CONTINUE
069           DISTP(1)=ANG(1)/(2.*TPI*FP)*VC
070   C       DISTP(1) WILL BE MODIFIED BELOW
071   C       LOWER SIDEBAND PORT
072           F=F1
073           LP=0.
074           RM=RL
075           KEY=5
076           GO TO 72
077   77      CONTINUE
078           RF1=DR
079           XF1=DX
080           IF (ABS(QA1) .LT.1.E-2) QA1=QA
081           DELTA = 1./(WI*QA1)
082           CALL PROTOG (N,DELTA,TEST,G)
083           IF (PRT.EQ.0) WRITE (6,31) F,DELTA,(G(J),J=1,JJ,1)
084           IF (TEST.EQ.1) GO TO 21
085           TEST1=0
086           CALL DESIGN (RF1*G(N+1),F1,DIA1,WI,DELTA,N,G,K,ANG,C,LNTH,F1,TEST1
087          1)
088   401     FORMAT (' IDLER CIRCUIT CANNOT BE BUILT')
089           IF (TEST1.EQ.1) WRITE (6,401)
090   29      FORMAT (' RESONATE VARACTOR SERIES REACTANCE WITH ELASTANCE = '
091          1E12.5,' INDUCTANCE = 'E12.5)
092           IF (PRT.EQ.0) WRITE (6,29) SR,LR
093           CALL IMPST (DIA1,LNTH,F1,N,LDISC,DLNT1,C,ZOC,F1*1.E-9)
094           DO 102 J=1,N,1
095           IF (J.EQ.1) GO TO 103
096           DIST1(J)=((ANG(J-1)+ANG(J))/(2.*TPI)+.5)*VC/F1
097   103     CONTINUE
098           IF (DLNT1(J).LT.0.) GO TO 45
099   102     CONTINUE
100           DIST1(1)=ANG(1)*VC/(2.*TPI*F1)
101   C       SIGNAL CIRCUIT
102           F=FS
103           RM=RG
104           LP=0.
105           KEY=3
106           GO TO 72
107   75      CONTINUE
108           RU=DR
109           XU=DX
110           KEY=2
111           GO TO 48
112   52      CONTINUE
113           RFS=RF
114           THSM=RL*VC/(FS*TPI)
115           IF (ABS(QAS).GT.1.E-10) GO TO 80
116   C       CALCULATE QAS
117           F=1.01*FS
118           KEY=1
119           GO TO 72
120   73      R1=DR
```

```
      X1=DX
      F=.99*FS
      KEY=2
      GO TO 72
74    CONTINUE
      CALL TRNR (Z0,1.01*RL/TPI,R1,X1,RU,XU)
      CALL TRNR (Z0,.99*RL/TPI,DR,DX,RL,XL)
      QAS=FS*ABS(XU-XL)/((RU-RL)*(.02*FS))
      IF (PRT.EQ.0)
     1WRITE (6,12) RU,XU,RL,XL,QAS
12    FORMAT (' RU = 'E13.5,' XU = 'E13.5,' RL = 'E13.5,' XL = 'E13.5,
     1' QA = ' E13.5)
80    DELTA=1./(WS*QAS)
      CALL PRDTDG (N,DELTA,TESTS,G)
      IF (TESTS.EQ.0) GO TO 6
13    FORMAT (' NO G VALUES FOR THIS W AND QA ')
      WRITE (6,13)
6     CONTINUE
      IF (PRT.EQ.0) WRITE (6,31) F,DELTA,(G(J),J=1,JJ,1)
C     J INVERTER MEANS THAT TESTS=2..     THIS WILL BE CHANGED TO 0
      TESTS=2
      CALL DESIGN (RFS*G(N+1),FS,DIAS,WS,DELTA,N,G,K,ANG,C,LNTH,ES,
     1TESTS)
      VA=C(2)
404   FORMAT (' SIGNAL CIRCUIT CANNOT BE BUILT')
      IF (TESTS.EQ.1) WRITE (6,404)
      IF (TESTS.EQ.1.OR.TESTI.EQ.1.OR.TESTP.EQ.1) GO TO 21
      CALL IMPST (DIAS,LNTH ,ES, N,LDISC,DLNTS,C ,ZOC,FS*1.E-9)
      DLNTS(2)=VA
      DLNTS(1)=DLNTS(1)/.0254
      DLNTS(3)=DLNTS(3)/.0254
      TL=.25
      DO 101 J=2,N,1
101   DISTS(J)=(( ANG(J-1)+ ANG(J))/(2.*TPI)+TL)*VC/(FS*.0254)
      DISTS(1)=( ANG(1)*VC/(FS*TPI*2.)+THSM1)/.0254
      WRITE (6,34) FS,(DISTS(J),J=1,N,1),(DLNTS(J),J=1,N,1),(DIAS(J)
     1,J=1,N,1)
      DLNTS(1)=DLNTS(1)*.0254
      DLNTS(3)=DLNTS(3)*.0254
      DO 19 J=1,N,1
      DISTS(J)=DISTS(J)*.0254
      DIST(J)=DISTS(J)
19    CONTINUE
C     AT THIS POINT DISTP(1), TDDSTS,TDDSTI ARE NOT KNOWN.
      DIST(1)=VC/F1
C     FIND INPUT IMPEDANCE OF SIGNAL CIRCUIT.
      KJ=N
      VA=ZO
      VB=0.
C     GET DISCONTINUITY CAPACITANCE
      CALL IMPST (DIAS,DLNTS,ES,N ,LDISC,DLNT,C ,ZOC,FS*1.E-9)
      F=F1
400   CONTINUE
      XD=-1.E12/(TPI*F    *C  JKJ))
      WAVE=DLNTS(KJ)*F    *SQRT(ES(KJ) /A.854)/VC
      BOT=VA*VA+(VB+XD)*(VB+XD)
      RC=VA
      VA=RC*XD*XD/BOT
      VB=(XD*(RC*RC+VB*VB)+VB*XD*XD)/BOT
      CALL TRNR (ZOC (KJ),WAVE,VA,VB,RC,XC)
      BOT=RC*RC+(XC+XD)*(XC+XD)
      VA=RC
      RC=RC*XD*XD/BOT
      XC=(XD*(VA*VA+XC*XC)+XC*XD*XD)/BOT
      WAVE=DIST (KJ)*F    /VC
      CALL TRNR (Z0,WAVE,RC,XC,VA,VB)
      IF (KJ.LE.1) GO TO 300
C     LNTHS(EVEN)=SERIES CAPACITANCE OF J INVERTER.
      VB=VB-1.E12/(TPI*F    *DLNTS(KJ-1))
      WAVE=DIST (KJ-1)*F    /VC
      CALL TRNR (Z0,WAVE,VA,VB,RC,XC)
      VA=RC
      VB=XC
      KJ=KJ-2
      GO TO 400
300   CONTINUE
      RSC=VA
      XSC=VB
C     FIND DISTANCE TO GET ZS(F1)=INFINITY. THIS COMES FROM:
C     J*INF = J*Z0*(XL+Z0*TAN(PHI))/(Z0-XL*TAN(PHI))
      TDDSTS=VC*ATAN(Z0/XSC)/(TPI*F1)+DIST(1)
      TDDSTI=DISTS(1)-TDDSTS
C     NOW FIND DISTP(1) TO RESONATE DIODE AT F1. GET C,ZOC.
      CALL IMPST (DIAP,DLNTP,EP,N,LDISC,LNTH,C,ZOC,FP*1.E-9)
      CALL IMPM (F1*1.E-9,N,DLNTP,DISTP,C,ZOC,Z0,0.,VA,VB)
      WAVE=TDDSTI*F1/VC
      CALL TRNR(Z0,WAVE,VA,VB,RU,XU)
C     X=Z0*(XL+Z0*TAN(PHI))/(Z0-XL*TAN(PHI)),
C     THEN  TAN(PHI) = Z0*(X-XL)/(Z0**2+X*XL). ASSUME RU=0.
      THPM=TPI*VC/( F1*4.)
      BOT = (Z0*Z0-XU*XF1)
      IF (ABS(BOT).GT.1.E-3) THPM=VC*ATAN(Z0*(-XF1        -XU)/BOT)/(F1
     1*TPI)
      DISTP(1)=THPM+DISTP(1)
      DO 110 J=1,N,1
      DIST(J)=DIST(J)/.0254
      DISTP(J)=DISTP(J)/.0254
      DLNT(J)=DLNT(J)/.0254
110   DLNTP(J)=DLNTP(J)/.0254
34    FORMAT (' F = ',E11.5/ ' DISTANCE BETWEEN DISKS IN INCHES'
     13(3X,E11.5)/' LENGTH OF DISK IN INCHES WITH DISC. CAP. '
     23(3X,E11.5)/' DISK DIAMETERS ' 3(3X,E11.5))
      WRITE (6,34) F1,(DIST(J),J=1,N,1),(DLNT(J),J=1,N,1), (
     1DIA(J),J=1,N,1)
      WRITE (6,34) FP,(DISTP(J),J=1,N,1),(DLNTP(J),J=1,N,1)
     1,(DIAP(J),J=1,3,1)
      DO 18 J=1,N,1
      DIST(J)=DIST(J)*.0254
      DISTP(J)=DISTP(J)*.0254
      DLNT(J)=DLNT(J)*.0254
      DLNTP(J)=DLNTP(J)*.0254
18    CONTINUE
35    FORMAT (' SIGNAL DISK TO JUNCTION DIST. = 'E13.5,' IDLER DISK TO J
     1UNCTION DIST. = 'E13.5)
      VA=TDDSTS/.0254
      VB=TDDSTI/.0254
      WRITE (6,35) VA,VB
C     CALCULATE DISTANCE OF COAX TO WAVEGUIDE ADAPTER FROM FILTERS.
      KEY=1
      DO 176 J=1,N,1
```

```
      DIA(N-J+1)=DIA(J)
      DLNT(N-J+1)=DLNT(J)
      EPS(N-J+1)=EP(J)
      IF (J.EQ.N) GO TO 177
174   DIST(N+1-J)=DIST(J+1)
177   DIST(1)=0.
      WAVE = DIST(1)*FS/VC
      CALL TRNR (ZO,WAVE,0.,0.,RC,XC)
180   CONTINUE
      CALL IMPST (DIA,DLNT,EPS,N,LDISC,LNTH,C,ZOC,F1*1.E-9)
      CALL IMPM (FS*1.E-9,N,DLNT,DIST,C ,ZOC,RC,XC,XOUT,XOUT)
C     ZOUT IS THE CONJUGATE OF THE IMPEDANCE LOOKING AWAY FROM VARACTOR.
      VA=TPI/4.
      IF (ABS(XOUT).GT.1.E-3) VA = ATAN(ZO/XOUT)
      IF (VA.LT.0.) VA=VA+TPI/2.
      GO TO (174,175),KEY
174   CONTINUE
      RSIDST=VA*VC/(TPI*FS)
C     NOW FOR PUMP CITCUIT.
      DO 178 J=1,N,1
      DIA(N-J+1)=DIAP(J)
      DLNT(N-J+1)=DLNTP(J)
      EPS(N-J+1)=EP(J)
      IF (J.EQ.N) GO TO 179
178   DIST(N+1-J)=DISTP(J+1)
179   DIST(1)=0.
      WAVE = DISTP(1)*FS/VC
      CALL TRNR (ZO,WAVE,0.,1.E15,RC,XC)
      KEY=2
      GO TO 180
175   RSPDST=VA*VC/(TPI*FS)
43    FORMAT (' DISTANCE TO WAVEGUIDE IN LSB FILTER= 'E13.6,' METERS.
     1DISTANCE IN PUMP FILTER= 'E13.6,' METERS')
      WRITE (6,43) RSIDST,RSPDST
      SWT=0
C     AREA USED FOR TGAIN.
      AREA(1)=RSIDST
      AREA(2)=RSPDST
      AREA(3)=TDDSTS
      AREA(4)=TDDSTI
352   CONTINUE
      IF (SWT.EQ.1) CALL GAINST (41,2,NUM,STEP,0,NPTEST)
      IF (SWT.EQ.0) CALL GAINST (1,2,NUM,STEP,1,NPTEST)
      CALL TGAIN (N,FS,FP,DLNTS,DLNTI,DLNTP,DISTS,DISTI,DISTP,DIAS,
     1DIAI,DIAP,ES,EI,EP,AREA,RS,LL,SP,SO,S,GAIN)
      IF (GAIN.LT.0.) WRITE (6,420)
420   FORMAT (' ' AMPLIFIER OSCILLATES')
      IF (SWT.EQ.1) GO TO 21
40    FORMAT (' GAIN CONVERGED TO ' E13.6)
      WRITE (6,40) GAIN
      IF (PRTT.EQ.1) GO TO 21
      SWT=1
      GO TO 352
48    CONTINUE
C     GIVEN ZL, FIND RF AND PHI WHERE
C     RF = ZO*(ZL+J*ZO*TAN(PHI))/(ZO+J*ZL*TAN(PHI))
      IF (ABS(XU).GT..5E-3) GO TO 26
      BL=0.
      GO TO 23
26    VA=(ZO*ZO-RU*RU-XU*XU)/(2.*ZO*XU)
      BL1=ATAN(VA+SQRT(VA*VA+1.))
      BL2=ATAN(VA-SQRT(VA*VA+1.))
      IF (BL1.LT.0.)   BL1=BL1+TPI/2.
      IF (BL2.LT.0.) BL2=BL2+TPI/2.
      IF (BL1-BL2) 121,122,122
121   BL=BL1
      GO TO 23
122   BL=BL2
23    CONTINUE
      TN=TAN(BL)
.     RF=ZO*ZO*RU*(1.+TN*TN)/((ZO-XU*TN)**2+(TN*RU)**2)
      IF (RF.GT.ZO) GO TO 60
      GO TO 62
60    CONTINUE
      IF (BL.GE.TPI/4.) GO TO 62
      BL=BL+TPI/4.
      GO TO 23
62    CONTINUE
      BL=BL-TPI/4.
      GO TO 23
C     GET Z AND Q OF DIODE. LP IS AN EXTRA INDUCTANCE IN PARALLEL WITH
C     SP.
77    CONTINUE
      OMEGA=TPI*F
      VA=OMEGA*LL-SO/OMEGA
      IF (LP.LT.1.E-17) GO TO 70
      VB=OMEGA/SP-1./(OMEGA*LP)
71    CONTINUE
      ROT=( 1.-VA*VB)**2+(VB*RM)**2
      DR=RM/ROT
      DX=(VA*(1.-VB*VA)-RM*RM*VB)/ROT
      SR=0.
      LR=0.
      IF (DX.LT.0.) LR=-DX/OMEGA
      IF (DX.GE.0.) SR=DX*OMEGA
      VB=SP/OMEGA
      VD=VA-VB
      VE=OMEGA*LL+SO/OMEGA
      ROTT = VB*VB*ROT
      QA=ABS((VB/OMEGA)*((VA*VD+RM*RM-VE*VD-VA*(VE*VB))/ROTT+
     1(VA*VD+RM*RM)*2.*VD*VD/(ROTT**2))+LR-SR/(OMEGA*OMEGA))
      QA=QA*OMEGA/(2.*DR)
      GO TO (73,74,75,76,77),KEY
70    CONTINUE
      VB=OMEGA/SP
      GO TO 71
45    WRITE (6,91) J
91    FORMAT (' ' DISCONTINUITY CAPACITANCE EXCEEDS DISTRIBUTED CAPACITAN
     1E OF DISK ' I5)
      GO TO 21
      END
```

```
001   SUBROUTINE TGAIN, ENTRY GAINST
002
003   C     TGAIN AND ENTRY GAINST FINDS GAIN AND NOISE FIGURE OF LSUC
004   C     WITH DIODE IN LOWER SIDEBAND PORT.
005
006   C     THIS PROGRAM CALLS IMPST,IMPM,TRNR,CMINV.
007         SUBROUTINE TGAIN (NI,FS,FP,DLNTS,DLNTI,DLNTP,DISTS,DISTI,DISTP,
008        1DIAS,DIAI,DIAP,ES,EI,EP,AREA,RS,LL,SP,SO,S,GAIN)
009   C     PRT=0 MEANS PRINT.  PRT=1 MEANS DO NOT PRINT
010   C     WAVEGUIDE USED IN PUMP AND LSB CIRCUITS TO STOP SIGNAL FREQUENCY.
011   C     NFTEST  =0  DO NOT FIND NOISE FIGURE. NFTEST=1 FIND NF.
012   C     FREQUENCY FS,FP IS IN CYCLES/SEC.
013   C     LENGTHS DLNTS,..DISTP RSIDST,RSPDST ARE ALL IN METERS
014   C     DIAMETERS DIAS,DIAI,DIAP ARE IN INCHES
015   C     ES,EI,EP,IS DIELECTRIC CONSTANT IN PF/M.
016   C     RS IN OHMS, ELASTANCES SP,S ARE IN DARAFS
017   C     RSIDST AND RSPDST ARE THE DISTANCES TO WAVEGUIDE ADAPTERS IN METER
018   C     NI IS THE NUMBER OF DISKS IN HAND-PASS FILTERS. NN IN LP FILTER
019         DIMENSION CZRP(8),CZIP(8),CZRS(8),CZIS(8)
020         DIMENSION DISTS(10),DISTI(10),DISTP(10)
021         DIMENSION DIAS(10),DIAI(10),DIAP(10),DLNTS(10),DLNTI(10),DLNTP(10)
022         DIMENSION S(10),F(10),ZR(8,8),ZI(8,8) ,YR(8,8),YI(8,8)
023         DIMENSION ES(4),EI(4),EP(4),CD(10),DLNT(10),ZUC(10)
024         DOUBLE PRECISION DZR(8,8),DZI(8,8),DYR(8,8),DYI(8,8),DSA(8,8)
025         DOUBLE PRECISION DSB(8,8),DSC(8,8)
026         DIMENSION IPERM(16)
027         DIMENSION AREA(10)
028         REAL NF,LL,LR
029         INTEGER J,NUM,LAST,K,M,N,L,TEST ,FIRST,ND,MM,PRT
030         RPARAL (VVA,VVB,VVC,VVD)=(VVA*VVC*(VVB+VVD)+VVB*VVD*VVC+
031        1VVD*VVD *VVA)/((VVA+VVC)**2+(VVB+VVD)**2)
032         XPARAL (VVA,VVB,VVC,VVD)=(VVB*VVD*(VVB+VVD)+VVC*VVC*VVB+
033        1VVD*VVA *VVA)/((VVA+VVC)**2+(VVB+VVD)**2)
034         RSIDST=AREA(1)
035         RSPDST=AREA(2)
036         TDDSTS=AREA(3)
037         TDDSTI=AREA(4)
038         IF (TEST.EQ.1) GO TO 15
039         ND=41
040         FIRST=2
041         STEP=1.E7
042         NUM=5
043         PRT=0
044         NFTEST=0
045   15    CONTINUE
046   C     LDISC = 1 TO AVOID CHANGING FILTER DISK DIAMETERS IN IMPST.
047         LDISC=1
048         C=2.997925E8
049   11    FORMAT ('0')
050         TPI=6.2831853
051         FI=FP-FS
052         ZO=50.
053         DO 10 J=1,ND,1
054         IF (PRT.EQ.0) WRITE (6,11)
055         F(1)=FS+ STEP*(J-(ND+1)/2)
056         F(2)=FP-F(1)
057         F(3)=FP+F(1)
058         F(4)=2.*FP-F(1)
059         F(5)=2.*FP+F(1)
060         F(6)=3.*FP-F(1)
061         F(7)=3.*FP+F(1)
062         F(8)=4.*FP-F(1)
063         DO 20 K=1,NUM,1
064         IF (K.GT.2) GO TO 301
065   C     FIND INPUT IMPEDANCE OF SIGNAL CIRCUIT.
066         KJ=NI
067         VA=ZO
068         VB=0.
069   C     GET DISCONTINUITY CAPACITANCE
070         CALL IMPST (DIAS,DLNTS,ES,NI,LDISC,DLNT,CD,ZUC,FS*1.E-9)
071   C     STORE DISTS(1) AND TRANSLATE TO JUNCTION
072         RS1=DISTS(1)
073         DISTS(1)=TDDSTS
074   400   CONTINUE
075         XD=-1.E12/(TPI*F(K)*CD (KJ))
076         WAVE=DLNTS(KJ)*F(K)*SQRT(ES(KJ) /A,A54)/C
077         ROT=VA*VA+(VB+XD)*(VB+XD)
078         RC=VA
079         VA=RC*XD*XD/ROT
080         VB=(XD*(RC*RC+VB*VB)+VB*XD*XD)/ROT
081         CALL TRNR (ZUC (KJ),WAVE,VA,VB,RC,XC)
082         ROT=RC*RC+(XC+XD)*(XC+XD)
083         VA=RC
084         RC=RC*XD*XD/ROT
085         XC=(XD*(VA*VA+XC*XC)+XC*XD*XD))/ROT
086         WAVE=DISTS(KJ)*F(K)/C
087         CALL TRNR (ZO,WAVE,RC,XC,VA,VB)
088         IF (KJ.LE.1) GO TO 300
089   C     LNTHS(EVEN)=SERIES CAPACITANCE OF J INVERTER.
090         VB=VB-1.E12/(TPI*F(K)*DLNTS(KJ-1))
091         WAVE=DISTS(KJ-1)*F(K)/C
092         CALL TRNR (ZO,WAVE,VA,VB,RC,XC)
093         VA=RC
094         VB=XC
095         KJ=KJ-2
096         GO TO 400
097   300   CONTINUE
098         DISTS(1)=RS1
099         RS1=VA
100         XS1=VB
101         IF (K.EQ.1) GO TO 149
102   301   RINI=ZO
103         XINI=0.
104         RINP=ZO
105         XINP=0.
106         GO TO 148
107   149   CONTINUE
108         RINI=0.
109         XINI=-ZO/TAN(RSIDST*TPI*F(K)/C)
110         RINP=0.
111         XINP=-ZO/TAN(RSPDST*TPI*F(K)/C)
112   148   CONTINUE
113         CALL IMPST (DIAI,DLNTI,FI,NI,LDISC,DLNT,CD,ZUC,FI*1.E-9)
114         CALL IMPM (F(K)*1.E-9,NI,DLNTI,DISTI,CD ,ZUC,RINI,XINI,RII,XII)
115         CALL IMPST (DIAP,DLNTP,FP,NI,LDISC,DLNT,CD,ZUC,FP*1.E-9)
116         CALL IMPM(F(K)*1.E-9,NI,DLNTP,DISTP,CD ,ZUC,XINP,XINP,RP1,XP1)
117   12    FORMAT(' THE SIGNAL, IDLER, AND PUMP ARE '/(' FILTER OUTPUT = '
118        1E12.5,' + J 'E12.5))
119         IF (PRT.EQ.1) WRITE (6,12) RS1,XS1,RII,XII,RP1,XP1
120         IF (K.NE.1) GO TO 150
```

```
      VA=RPARAL (RS1,XS1,RP1,XP1)
      VB=XPARAL (RS1,XS1,RP1,XP1)
151   CONTINUE
      CALL TRNR (ZO,TODST)*F(K)/C,VA,VB,RC,XC)
      RCI=RPARAL (RC+RI),XC+XI),0.,-SP/(TPI*F(K)))
      XCI=XPARAL (RC+RI),XC+XI),0.,-SP/(TPI*F(K)))
      ZR(K,K)=RS+RCI
      ZI(K,K)=TPI*F(K)*LL-SO/(TPI*F(K))+XCI
C     TAKE CONJUGATE OF EVEN NUMBERED Z'S
      IF (2*(K/2).EQ.K)  ZI(K,K)=-ZI(K,K)
      IF (J.EQ.1) WRITE (6,12) VA,VB,RS1,XS1,RC1,XCI,ZR(K,K),ZI(K,K)
20    CONTINUE
      DO 31 M=1,NUM,1
      DO 30 N=1,NUM,1
      IF (N.EQ.M)  GO TO 30
C     SEE DAVE OLIVER, P.49.
      L=    (((-1)**N)*(2*N-1)+1)/4-(((-1)**M)*(2*M-1)+1)/4
      IF (L)  23,24,21
23    CONTINUE
      L=-L
      GO TO 21
24    ZI(M,N)=((-1)**N)*SO  /(TPI*F(N))
      GO TO 22
21    ZI(M,N)=((-1)**N)*S(L)/(TPI*F(N))
22    CONTINUE
      ZR(M,N)=0.
30    CONTINUE
31    CONTINUE
40    FORMAT ('0DEGREE OF MATRIX = '14)
41    FORMAT ('0ZR MATRIX '/('0',8(3X,E13.6)))
42    FORMAT ('0ZI MATRIX '/('0',8(3X,E13.6)))
      IF (J.NE.(NO+1)/2) GO TO 50
      IF (PRT.EQ.1) GO TO 50
      WRITE (6,40) NUM
      WRITE (6,41) ((ZR(M,N),N=1,8  ,1),M=1,8  ,1)
      WRITE (6,42) ((ZI(M,N),N=1,8  ,1),M=1,8  ,1)
50    CONTINUE
C     MATRIX TRIANGULARIZATION.  UPPER RIGHT HAND SIDE MADE ZERO.
      IF (NFTEST.EQ.0) GO TO 202
      DO 203 M=1,NUM,1
      DO 203 I=1,NUM,1
      DZR(I,M)=DALE(ZR(I,M) )
      DZI(I,M)=DALE(ZI(I,M))
203   CONTINUE
202   CONTINUE
      DO 120 LAST=FIRST,NUM,1
      RLAST=ZR(LAST,LAST)
      XLAST=ZI(LAST,LAST)
      MM=LAST-1
      DO 61 M=1,MM,1
      RM=ZR(M,LAST)
      XM=ZI(M,LAST)
      DO 60 N=1,LAST,1
      YR(M,N)=ZR(M,N)-((RM *ZR(LAST,N)-XM*ZI(LAST,N))
     1*RLAST+(RM*ZI(LAST,N)+XM*ZR(LAST,N))
     2*XLAST)/(RLAST*RLAST+XLAST*XLAST)
      YI(M,N)=ZI(M,N)-((XM*ZI(LAST,N)-RM*ZR(LAST,N)
     1)*XLAST+(RM*ZR(LAST,N)+XM*ZR(LAST,N)
     2)*RLAST)/ (RLAST*RLAST+XLAST*XLAST )
      YR(LAST,N)=ZR(LAST,N)
      YI(LAST,N)=ZI(LAST,N)
60    CONTINUE
61    CONTINUE
      L=LAST-1
70    CONTINUE
      IF (L-2) 100,80,80
80    CONTINUE
      RLAST=YR(L,L)
      XLAST=YI(L,L)
      MM=L-1
      DO 91 M=1,MM,1
      RM=YR(M,L)
      XM=YI(M,L)
      DO 90 N=1,L,1
      YR(M,N)=YR(M,N)-((RM*YR(L,N)-XM*YI(L,N))*RLAST+
     1(RM*YI(L,N)+XM*YR(L,N))*XLAST)/(RLAST*RLAST+XLAST*XLAST )
      YI(M,N)=YI(M,N)-((XM*YI(L,N)-RM*YR(L,N))*XLAST+(
     1RM*YI(L,N)+XM*YR( L,N))*RLAST)/(RLAST*RLAST+XLAST*XLAST )
90    CONTINUE
91    CONTINUE
      L=L-1
      GO TO 70
100   CONTINUE
      BOTR=YR(1,1)*YR(2,2)-YI(1,1)*YI(2,2)
      BOTI=YR(1,1)*YI(2,2)+YI(1,1)*YR(2,2)
C     AMPLIFIER  OSCILLATES IF DENOMINATOR IS <0.  IT OSCILLATES AT
C     FREQUENCY WHERE REACTANCE IS ZERO.
      IF (BOTR.GT.1.E-5.OR.ABS(BOTI).GT.1.) GO TO 93
      GAIN=-1.
      GO TO 94
93    CONTINUE
      VA=ZR(1,1)-RS
      VB=ZR(2,2)-RS
      GAIN=4.*VA*VB*(YR(2,1)**2+YI(2,1)**2)/(BOTR*BOTR+BOTI*BOTI)
C     GAIN IS ABS(Y21)**2*4.*VA*VB WHERE Y21=721/1222=Z11)
C     THAT IS THE VARIABLES YR AND YI ARE REALLY IMPEDANCES.
      IF (NFTEST.EQ.0) GO TO 94
      CALL CMINV (LAST,A,DZR,DZI,IPERM,DYR,DYI,DSA,DSB,DSC)
      DO 204 M=1,LAST,1
      DO 204 I=1,LAST,1
      YR(I,M)=SNGL(DYR(I,M))
      YI(I,M)=SNGL (DYI(I,M))
204   CONTINUE
94    CONTINUE
      VA=0.
      DO 201 I=1,LAST,1
201   VA=(YR(2,I)**2+YI(2,I)**2)*ZR(I,I)+VA
      NF=(4.*VB*(VA-VB*(YR(2,2)**2+YI(2,2)**2))
     1+(1.-2.*VB*YR(2,2))**2+4.*(VB*YI(2,2))**2)/GAIN
110   FORMAT (' THE GAIN FOR THE  '11,' BY '11,' MATRIX IS 'F12.2,
     15X,' WITH SIGNAL FREQUENCY ' E12.5 ,' NOISE FIGURE IS 'E12.5)
      IF (PRT.EQ.1) GO TO 120
      WRITE (6,110) LAST,LAST,GAIN,F(1),NF
120   CONTINUE
10    CONTINUE
      RETURN
150   VA=RP1
      VB=XP1
      GO TO 151
      ENTRY GAINST (NO,FIRST,NUM,STEP,PRT,NFTEST)
```

```
C     NO IS THE NUMBER OF ITERATIONS. FIRST IS THE SMALLEST MATRIX
C     APPROXIMATION AND FIRST >1.  PRT=1 FOR NO PRINT OUT.
C     STEP IS THE FREQUENCY INCREASE/ITERATION IN CPS.
C     IF NFTEST=0, NO NOISE FIGURE: IF NFTEST=1 FIND NOISE FIGURE.
      DATA TEST/0/
      TEST=1
      RETURN
      END
```

```
001   PROGRAM C
002
003   C     THIS PROGRAM FINDS DIFFUSION DIODE IMPEDANCE WHEN APPLIED VOLTAGE
004   C     IS KNOWN.
005
006   C     THIS PROGRAM USES BESKC AND BESI WHICH IS AN IBM SSP PROGRAM.
007         REAL L,MU
008         DIMENSION Q(10),YC(10),YS(10)  ,YCGO(10),YSGO(10)
009         INTEGER N
010         COMPLEX Z,BKO,BK1,ZA
011         AREA=4.41E-5
012         EPS=11.8*8.854E-14
013         PHI=.9
014         RS=1.
015         N=2
016   C     ELECTRONIC CHARGE
017         QE=1.60210E-19
018   C     QE/KT =40.
019         ALPH=20.
020         SQR2=1.41421356
021         TPI=6.28318531
022   1     FORMAT (111,6E11.5/17E11.5)
023         READ(5,1) LIMIT,STEP
024         MU=401.
025         DP=MU/40.1
026   C     PNW=PN/ IN CM**-3   SEE WAYSON P 107
027   25    CONTINUE
028         READ (5,1) R,VO,V1,TAU,WL,PNW
029         GAM=1./(R+2.)
030         J=0
031   50    FORMAT('0DIODE N= X**'I2,          ' VO = 'E11.5,' V1 = 'E11.5,
032        1' HOLE LIFETIME = 'E11.5,' BASE WIDTH/DIFFUSION LENGTH='E11.5 /
033        1' ADMITTANCE IS IN MHOS/CM**2',' PN(W) = 'E11.5)
034   C     N=X**R, TAU=LIFETIME IN P MATERIAL,F=FREQ.,V=VOLTAGE WL=W/L RATIO
035         WRITE (6,50) R,  VO,V1,TAU,WL,PNW
036         L=SQRT(DP*TAU)
037         W=L*WL
038         P=QE*DP*PNW*2.*EXP(ALPH*VO)/W
039   26    J=J+1
040         OMEGA=(J-1)*STEP
041         DO 200 I=1,N,1
042         K=I-1
043         ALPHA=SQRT(1.+SQRT(1.+(K*OMEGA*TAU)**2))*WL/SQR2
044         BETA=SQRT(-1.+SQRT(1.+(K*OMEGA*TAU)**2))*WL/SQR2
045         Z=CMPLX(ALPHA,BETA)
046         IF (R.EQ.0) GO TO 30
047         NU=(R-1)/2
048         CALL BESKC(Z,NU,BKO,IER)
049         GO TO (40,42,46,48),IER
050         CALL BESKC (Z,NU+1,BK1,IER)
051         GO TO (40,42,46,48), IER
052         ZA=Z*BKO/BK1
053   31    CONTINUE
054         VA=ALPH*V1
055         CALL BESI(VA,K,BI,IER)
056         GO TO (40,42,44,46),IER
057         VA=REAL(ZA)
058         VB=AIMAG(ZA)
059         IF (K.GT.0) GO TO 201
060   C     D.C. TERM NEEDS FACTOR OF 1/2
061         VA=VA/2.
062         RCO=VA*P*BI*ALPH
063         RSO=VB*P*BI*ALPH
064         OO=VB/VA
065         GO TO 200
066   201   CONTINUE
067         YC(K)=VA*P*BI*ALPH
068         YS(K)= VB*P*BI*ALPH
069   C     IS(K)=-VB*P*BI*ALPH,  BUT COS(A+90)=-SIN(A) MEANS CURRENT LEADS
070   C     VOLTAGE.  HENCE CAPACITANCE AND POSITIVE SUSCEPTANCE.
071         YCGO(K)=YC(K)/RCO
072         YSGO(K)=YS(K)/RCO
073         Q(K)=VB/VA
074   200   CONTINUE
075         FV=OMEGA/TPI
076         K=0
077   51    FORMAT (' FREQUENCY = 'E11.5,' FOURIER COMPONENTS OF ADMITTANCE
078        1AND Q ARE '/( ' J= 'I2,' G = ' E11.5,' B = ' E11.5,' Q = ' E11.5,
079        2' G/GO = 'E11.5,' B/GO = 'E11.5))
080         VA=1.
081         VB=RSO/RCO
082         NN=N-1
083         WRITE (6,51) FV,K,RCO,RSO,OO,VA,VB,(K,YC(K),YS(K),Q(K),YCGO(K),
084        1YSGO(K),K=1,NN,1)
085         GO=RCO*AREA
086         RO=RSO*AREA
087         G1=YC(1)*AREA
088         B1=YS(1)*AREA
089         BDEP=OMEGA*EPS*AREA/(W*(1.-V0/PHI)**GAM)
090         BOT=G1*G1+(B1+BDEP)**2
091         RD=RS+G1/BOT
092         XD=-(B1+BDEP)/BOT
093   55    FORMAT ('0YDIF = 'E13.5,' +J 'E13.5,' BDEP = 'E13.5,' ZDIODE = '
094        1E13.5,' +J 'E13.5)
095         WRITE (6,55) G1,B1,BDEP,RD,XD
096         BOT=RD*RD+XD*XD
097         GD=RD/BOT
098         BD=-XD/ BOT
099         WRITE (6,56) GD,BD
100   56    FORMAT (' DIODE Y = 'E13.6,' +J 'E13.6)
101   100   CONTINUE
102         IF (J .GE.LIMIT) GO TO 25
103         GO TO 26
104   39    FORMAT (' NEGATIVE ORDER FOR BESSEL FUNCTION')
105   40    WRITE (6,39)
106         GO TO 25
107   41    FORMAT (' NEGATIVE ARGUMENT')
108   42    WRITE (6,41)
109         GO TO 25
110   43    FORMAT (' RESULT <1.E-69')
111   44    WRITE (6,43)
112         GO TO 25
113   45    FORMAT (' ARGUMENT>170.')
114   46    WRITE (6,45)
115         GO TO 25
116   47    FORMAT (' RESULT>1.E70')
117   48    WRITE (6,47)
118         GO TO 25
119   30    CONTINUE
120         ZA=Z
121         GO TO 31
122         END
```

```
001   PROGRAM D
002
003   C     THIS PROGRAM CALCULATES THE LARGE SIGNAL CURRENTS DEVELOPED IN A
004   C     LSUC WHEN DIFFUSION ADMITTANCE IS USED.
005
006   C     THIS PROGRAM CALLS BESKC.  IT ALSO CALLS DQG12 WHICH IN TURN
007   C     USES THE EXTERNAL FUNCTION DFT WITH ENTRIES FC1, FC2.
008   C     DQG12 IS AN IBM SSP ROUTINE WHICH IS A GUASSIAN QUADRATURE
009   C     INTEGRATION PROGRAM.
010         IMPLICIT REAL*8 (D)
011         REAL*8 FC1,FC2
012         EXTERNAL DFT
013         H1(THET)=-VP*VARO*SIN(THET*VARO)-VAR1*V1*SIN(THET*VAR1+PHI1)
014        1-VAR2*V2*SIN(THET*VAR2+PHI2)
015         H11(THET)=-VP*VARO*VARO*COS(THET*VARO)-VAR1*VAR1*COS(THET*VAR1
016        1+PHI1)*V1-VAR2*VAR2*V2*COS(THET*VAR2+PHI2)
017         REAL*4 DP
018         REAL L,MU
019         REAL JS(10),JC(10)
020         DIMENSION D(10),ALPHAV(10),THETA(60)
021         INTEGER R
022         COMPLEX Z,AKO,AK1,ZA
023         N=10
024   C     ELECTRONIC CHARGE
025         QE=1.60210E-19
026   C     QE/KT =40.
027   C     ALPHA/N WHERE N,NE, 1 IMPLIES TRAPS IN FORBIDDEN BAND
028         ALPH=20.
029         SQR2=1.41421356
030         TPI=6.2831853
031   1     FORMAT (I11,6E11.5/(7E11.5))
032         MU=401.
033         DP=MU/40.1
034   C     PNW=PN/ IN CM**-3   SEE WATSON P 107
035         PNW=1.E17
036         EPS=1.E-4
037   25    CONTINUE
038   50    FORMAT('1DIODE N= ',I2,' VO = 'E11.5,' VP = ' E11.5,' V1 = '
039        1E11.5,' V2 = 'E11.5, /' HOLE LIFETIME = 'E11.5,' BASE WIDTH/DIFFUS
040        2ION LENGTH = 'E11.5/' FUNDAMENTAL FREQ '  E11.5,' FS ='E11.5,
041        4' FP = '   E11.5,' PHIO = 0  PHI1 = 'E11.5)
042         READ (5,1) R,VO,VP,V1,V2,TAU,WL,F,FS,FP ,PHI1
043         WRITE (6,50) R,VO,VP,V1,V2,TAU,WL,F,FS,FP ,PHI1
044   C     N=X**B, TAU=LIFETIME IN P MATERIAL,F=FREQ.,V=VOLTAGE WL=W/L RATIO
045         L=SQRT(DP*TAU)
046         W=L*WL
047         PP=QE*DP*PNW*2./(W*SQRT(TPI))
048         PSS=QE*DP*PNW*EXP(ALPH*VO)/W
049   C     CHANGE FROM DEGREES TO RADIANS
050         PHI1=PHI1*TPI/360.
051         DO 200 I=1,N,1
052         K=I-1
053         OMEGA=TPI*((K/2)*FP-FS*(-1)**K)
054         IF (K.EQ.0) OMEGA=TPI*FP
055         AV=SQRT(1.+SQRT(1.+(OMEGA*TAU)**2))*WL/SQR2
056         BV=SQRT(-1.+SQRT(1.+(OMEGA*TAU)**2))*WL/SQR2
057         Z=CMPLX(AV,BV)
058         IF (R.EQ.0) GO TO 30
059         NU=(R-1)/2
060         CALL BESKC(Z,NU,AKO,IER)
061         GO TO (40,42,46,48),IER
062         CALL BESKC (Z,NU+1,AK1,IER)
063         GO TO (40,42,46,48), IER
064         ZA=Z*AKO/AK1
065   31    CONTINUE
066         ALPHA=REAL(ZA)
067         BETA=AIMAG(ZA)
068         D(I)=  BETA/ALPHA
069         ALPHAV(I)=ALPHA
070   200   CONTINUE
071         PHI2=ATAN(D(1))-PHI1-TPI/2.
072   C     THIS PHASE CONDITION USED SMALL SIGNAL ASSUMPTION
073         VARO=FP/F
074         VAR1=FS/F
075         VAR2=VARO-VAR1
076         DALPH=DALE(ALPH)
077         DVP=DALE(VP)
078         DV1=DALE(V1)
079         DV2=DALE(V2)
080         DVARO=DALE(VARO)
081         DVAR1=DALE(VAR1)
082         DVAR2=DALE(VAR2)
083         DPHI1=DALE(PHI1)
084         DPHI2=DALE (PHI2)
085   C     NEWTON METHOD
086         IMAX=0.
087         AH1=H1(0.)
088         M=0
089         VA=0.
090         J=1
091         THETA(1)=0.
092   211   CONTINUE
093   C     FIND BOTH MINIMUM AND MAXIMUM OF H1
094         M=M+1
095         VA=M*TPI*F/(FP*6.)
096         VC=H1(VA)
097         IF (VC*AH1.LE.0.) GO TO 217
098         AH1=VC
099         VA=VA
100         GO TO 211
101   217   CONTINUE
102   C     TRIAL THETA VALUE.  LINEAR INTERPOLATION
103         THETB=VA+(VA-VA)*AH1/(VC-AH1)
104         AH1=VC
105         VA=VA
106         II=0
107   218   CONTINUE
108         FCT=H1(THETB)
109         THET1=THETB-FCT/H11(THETB)
110         TOL=EPS
111         IF (ABS(THET1)-1.) 4,4,3
112   C     SEE SSP UNDER NEWTON METHOD
113   3     TOL=TOL*ABS(THET1)
114   4     IF(ABS(THET1-THETB)-TOL) 5,5,6
115   5     IF (ABS(FCT)-100.*EPS) 7,7,6
116   6     CONTINUE
117         THETB=THET1
118         II=II+1
119         IF (II.GT.10) GO TO 220
120         GO TO 218
```

```
      IF ((THET1-TMAX),GT.1.E-4) GO TO 8
      GO TO 211
8     CONTINUE
      IF (THET1 .GE.TPI) GO TO 221
      VH11=H11(THET1)
      TMAX=THET1
      J=J+1
      THETA(J)=THET1
      GO TO 211
220   CONTINUE
56    FORMAT (' FUNCTION = 'E11.5,' DERIVATIVE = 'E11.5,' THETA = 'F11.5
     1)
      VH11=H11(THET1)
      FCT=H1(THET1)
      WRITE (6,56) FCT,VH11,THET1
      GO TO 7
221   CONTINUF
57    FORMAT (' THETA(J)= '/(' '8(E11.5,3X)))
      WRITE (6,57) (THETA(JJ),JJ=1,J,1  )
      THETA(J+1)=TPI
      DO 210 I=1,N,1
      JC(I)=0.
      JS(I)=0.
      K=I-1
      AM=((K/2)*FP-(-1)**K*FS)/F
      IF (K.EQ.0) AM=FP/F
      DAM=DBLE(AM)
      DO=DBLE(O(I))
      DV=  FC1(DAM,DO,DALPH,DVP,DV1,DV2,DVARO,DVAR1,DVAR2,DPHI1,DPHI2)
      VA=ALPHAV(I)*PSS*2./TPI
      DO 226 JJ=1,J,1
      DXL=DBLE(THETA(JJ))
      DXH=DBLE(THETA(JJ+1))
      DV=  FC2(I)
      CALL DOG12 (DXL,DXH,DFT,DJC)
      DV=  FC2(2)
      CALL DOG12 (DXL,DXH,DFT,DJS)
      JC(I)=VA*SNGL(DJC)+JC(I)
      JS(I)=VA*SNGL(DJS)+JS(I)
226   CONTINUE
210   CONTINUE
53    FORMAT(' PHI1= 'E11.5,' PHI2 = 'E11.5)
52    FORMAT (' O(',I2,') = 'E11.5,' JC('I2,') = 'E11.5,' JS('I2,
     1') = 'E11.5,' J('I2,') = 'E11.5)
      WRITE (6,53) PHI1,PHI2
      DO 216 I=1,N,1
      K=I-1
      VA=SQRT(JC(I)**2+JS(I)**2)
      WRITE (6,52) K,O(I),K,JC(I),K,JS(I),K,VA
216   CONTINUE
      GO TO 25
39    FORMAT (' NEGATIVE ORDER FOR BESSEL FUNCTION')
40    WRITE (6,39)
      GO TO 25
41    FORMAT (' NEGATIVE ARGUMENT')
42    WRITE (6,41)
      GO TO 25
43    FORMAT (' RESULT <1.E-69')
44    WRITE (6,43)
      GO TO 25
45    FORMAT (' ARGUMENT>170.')
46    WRITE (6,45)
      GO TO 25
47    FORMAT (' RESULT>1.E70')
48    WRITE (6,47)
      GO TO 25
30    CONTINUE
      ZA=Z
      GO TO 31
      END
      REAL FUNCTION DFT*8(THET)
      IMPLICIT REAL*8 (A-H,O-Z,$),INTEGER(I-N)
C     FOR USE WITH SSP GUASSIAN QUADRATURE.  CALL FC1,FC2 BEFORE  FCT.
      GO TO (11,12),I
      RETURN
11    VA=DCOS(AM*THET)+O*DSIN(AM*THET)
      GO TO 13
12    VA=DSIN(AM*THET)-O*DCOS(AM*THET)
13    CONTINUE
      DFT=VA*DEXP(ALPH*(VP*DCOS(THET*VARO)+V1*DCOS(VAR1*THET+PHI1)+
     1V2*DCOS(VAR2*THET+PHI2)))
      RETURN
      ENTRY FC1 (AM,O,ALPH,VP,V1,V2,VARO,VAR1,VAR2,PHI1,PHI2)
      FC1=1.
      RETURN
      ENTRY FC2(I)
      FC2=1.
      RETURN
      END
```

```
001  PROGRAM E
002
003  C     THIS PROGRAM CALCULATES THE CURRENTS DEVELPED IN A LSIC WHEN
004  C     DIFFUSION ADMITTANCE IS USED BY MEANS OF THE LAPLACE METHOD AND
005  C     SMALL SIGNAL METHOD.
006
007  C     THIS PROGRAM CALLS ON BESKC AND BESI, THE LATER BEING AN IBM
008  C     SSP SUBROUTINE.
009        H1(THET)=-VP*VARO*SIN(THET*VARO)-VAR1*V1*SIN(THET*VAR1+PHI1)
010       1-VAR2*V2*SIN(THET*VAR2+PHI2)
011        H11(THET)=-VP*VARO*VARO*COS(THET*VARO)-VAR1*VAR1*COS(THET*VAR1
012       1+PHI1)*V1-VAR2*VAR2*V2*COS(THET*VAR2+PHI2)
013        REAL*4 DP
014        REAL L,MU
015        REAL JS(10),JC(10)
016        DIMENSION  O(10),ALPHAV(10),THETA(30)
017        INTEGER B
018        COMPLEX Z,BKO,BK1,ZA
019        N=10
020  C     ELECTRONIC CHARGE
021        QE=1.60210E-19
022  C     QE/KT =40.
023  C     ALPHA/N WHERE N,NE. 1 IMPLIES TRAPS IN FORBIDDEN BAND
024        ALPH=20.
025        SQR2=1.41421356
026        TPI=6.2831853
027  1     FORMAT (I11,6E11.5/(7E11.5))
028        MU=401.
029        DP=MU/40.1
030  C     PNW=PN/ IN CM**-3   SEE WATSON P 107
031        PNW=1.E17
032        EPS=1.E-4
033  25    CONTINUE
034  50    FORMAT('1DIODE N= X**'I2,' VO = 'E11.5,' VP = ' E11.5,' V1 = '
035       1E11.5,' V2 = 'E11.5, /' HOLE LIFETIME = 'E11.5,' BASE WIDTH/DIFFUS
036       2ION LENGTH = 'E11.5/' FUNDAMENTAL FREQ '  E11.5,' FS ='E11.5,
037       4' FP = '   E11.5,' PHI0 = 0  PHI1 = 'E11.5)
038        READ (5,1) B,VO,VP,V1,V2,TAU,WL,F,FS,FP ,PHI1
039        WRITE (6,50) B,VO,VP,V1,V2,TAU,WL,F,FS,FP ,PHI1
040  C     N=X**B, TAU=LIFETIME IN P MATERIAL,F=FREQ.,V=VOLTAGE WL=W/L RATIO
041        L=SQRT(DP*TAU)
042        W=L*WL
043        PP=QE*DP*PNW*2./(W*SQRT(TPI))
044        PSS=QE*DP*PNW*EXP(ALPH*VO)/W
045  C     CHANGE FROM DEGREES TO RADIANS
046        PHI1=PHI1*TPI/360.
047        DO 200 I=1,N,1
048        K=I-1
049        OMEGA=TPI*((K/2)*FP-FS*(-1)**K)
050        IF (K.EQ.0) OMEGA=TPI*FP
051        AV=SQRT(1.+SQRT(1.+(OMEGA*TAU)**2))*WL/SQR2
052        BV=SQRT(-1.+SQRT(1.+(OMEGA*TAU)**2))*WL/SQR2
053        Z=CMPLX(AV,BV)
054        IF (B.EQ.0) GO TO 30
055        NU=(B-1)/2
056        CALL BESKC(Z,NU,BKO,IER)
057        GO TO (40,42,46,48),IER
058        CALL BESKC (Z,NU+1,BK1,IER)
059        GO TO (40,42,46,48), IER
060        ZA=Z*BKO/BK1
061  31    CONTINUE
062        ALPHA=REAL(ZA)
063        BETA=AIMAG(ZA)
064        O(I)=  BETA/ALPHA
065        ALPHAV(I)=ALPHA
066  200   CONTINUE
067        PHI2=ATAN(O(1))-PHI1-TPI/2.
068  C     THIS PHASE CONDITION USED SMALL SIGNAL ASSUMPTION
069        VARO=FP/F
070        VAR1=FS/F
071        VAR2=VARO-VAR1
072  C     NEWTON METHOD
073        TMAX=0.
074        BH1=H1(0.)
075        M=0
076        VB=0.
077        J=0
078  211   CONTINUE
079        M=M+1
080        VA=M*TPI*F/(FP*4.)
081        VC=H1(VA)
082        IF (VC*BH1.LE.0.) GO TO 217
083        BH1=VC
084        VB=VA
085        GO TO 211
086  217   CONTINUE
087  C     TRIAL THETA VALUE.  LINEAR INTERPOLATION
088        THETB=VB+(VB-VA)*BH1/(VC-BH1)
089        BH1=VC
090        VB=VA
091        II=0
092  218   CONTINUE
093        FCT=H1(THETB)
094        THET1=THETB-FCT/H11(THETB)
095        TOL=EPS
096        IF (ABS(THET1)-1.) 4,4,3
097  C     SEE SSP UNDER NEWTON METHOD
098  3     TOL=TOL*ABS(THET1)
099  4     IF(ABS(THET1-THETB)-TOL) 5,5,6
100  5     IF (ABS(FCT)-100.*EPS) 7,7,6
101  6     CONTINUE
102        THETB=THET1
103        II=II+1
104        IF (II.GT.10) GO TO 220
105        GO TO 218
106  7     IF ((THET1-TMAX).GT.1.E-4) GO TO 8
107        GO TO 211
108  8     CONTINUE
109        IF (THET1 .GE.TPI) GO TO 221
110        VH11=H11(THET1)
111        IF (VH11 .GT.0.) GO TO 211
112        TMAX=THET1
113        J=J+1
114        THETA(J)=THET1
115        GO TO 211
116  220   CONTINUE
117  56    FORMAT (' FUNCTION = 'E11.5,' DERIVATIVE = 'E11.5,' THETA = 'E11.5
118       1)
119        VH11=H11(THET1)
120        IF (VH11.GT.0.) GO TO 211
```

```
      FCT=H1(THET1)
      WRITE (6,56) FCT,VH11,THET1
      GO TO 7
221   CONTINUE
57    FORMAT (' THETA(J)= '/(' 'R(E11.5,3X)))
5A    FORMAT ('OLAPLACE ASYMPTOTIC METHOD' )
59    FORMAT ('OSMALL SIGNAL METHOD' )
      WRITE (6,5A)
      WRITE (6,57) (THETA(JJ),JJ=1,J,1   )
      DO 210 I=1,N,1
      JC(I)=0.
      JS(I)=0.
      K=I-1
      FK=((K/2)*FP-FS*(-1)**K)
      IF (K.EQ.0) FK=FP
      DO 222 JJ=1,J,1
      VA=ALPHAV(I)*PP*EXP(ALPH*(V0+VP*COS(THETA(JJ)*VAR0)+V1*COS(
     1THETA(JJ)*VAR1+PHI1)+V2*COS(THETA(JJ)*VAR2+PHI2)))/SQRT(-H11(
     2)HETA(JJ))*ALPH)
      JC(I)=VA*(COS(THETA(JJ)*FK/F     )+Q(I)*SIN(THETA(JJ)*FK/F     ))+
     1JC(I)
      JS(I)=VA*(SIN(THETA(JJ)*FK/F     )-Q(I)*COS(THETA(JJ)*FK/F     ))
     1+JS(I)
222   CONTINUE
210   CONTINUE
53    FORMAT(' PHI1= 'E11.5,' PHI2 = 'E11.5)
52    FORMAT (' Q('I2,') = 'E11.5,' JC('I2,') = 'E11.5,' JS('I2,
     1') = 'E11.5,' J('I2,') = 'E11.5)
      WRITE (6,53) PHI1,PHI2
      DO 21A I=1,N,1
      K=I-1
      VA=SQRT(JC(I)**2+JS(I)**2)
      WRITE (6,52) K,Q(I),K,JC(I),K,JS(I),K,VA
21A   CONTINUE
C     SMALL SIGNAL , NONDEGENERATE CASE
      WRITE (6,59)
      VA=ALPH*VP
      CS1=COS(PHI1)
      SN1=SIN(PHI1)
      CS2=COS(PHI2)
      SN2=SIN(PHI2)
      CALL BESI(VA,1,BR1,IER)
      GO TO (40,42,44,46),IER
      JC(1)=PSS*BR1*ALPHAV(1)*2.
      JS(1)=-JC(1)*Q(1)
      CALL BESI (VA,0,BR2,IER)
      GO TO (40,42,44,46),IER
      IN=0
      DO 300 I=2,N,1
      IF ((I/2)*2.EQ.I) GO TO 301
      KD1=1
      KD2=0
      KD3=0
      KD4=1
302   CONTINUE
      JC(I)=PSS*ALPHAV(I)*ALPH*(KD1*V1*BR2*(CS1+Q(I)*SN1)
     1+KD2*V1*BR1*(CS1-Q(I)*SN1)
     1+KD3*V2*BR2*(CS2+Q(I)*SN2)
     1+KD4*V2*BR1*(CS2-Q(I)*SN2))
      JS(I)=PSS*ALPHAV(I)*ALPH*(KD1*V1*BR2*(SN1-Q(I)*CS1)
     1-KD2*V1*BR1*(SN1+Q(I)*CS1)
     1+KD3*V2*BR2*(SN2-Q(I)*CS2)
     4-KD4*V2*BR1*(SN2+Q(I)*CS2))
300   CONTINUE
      DO 303 I=1,N,1
      K=I-1
60    FORMAT (' JC('I2,') = 'E11.5,' JS('I2,') = 'E11.5,' J('I2,
     1') = 'E11.5,' PHI('I2,') = 'E11.5)
      CJ=JC(I)
      SJ=JS(I)
      VA=SQRT(CJ*CJ+SJ*SJ)
      IF (ABS(SJ).LT..001) GO TO 305
      PHI=ATAN(CJ/SJ)*360./TPI
      GO TO 306
305   PHI=90.
306   CONTINUE
      WRITE (6,60) K,CJ,K,SJ,K,VA,K,PHI
303   CONTINUE
      GO TO 25
39    FORMAT (' NEGATIVE ORDER FOR BESSEL FUNCTION')
40    WRITE (6,39)
      GO TO 25
41    FORMAT (' NEGATIVE ARGUMENT')
42    WRITE (6,41)
      GO TO 25
43    FORMAT (' RESULT <1.E-69')
44    WRITE (6,43)
      GO TO 25
45    FORMAT (' ARGUMENT>170.')
46    WRITE (6,45)
      GO TO 25
47    FORMAT (' RESULT>1.E70')
48    WRITE (6,47)
      GO TO 25
301   CONTINUE
      KD1=0
      KD2=1
      KD3=1
      KD4=0
      IN=IN+1
      BR1=BR2
      CALL BESI (VA,IN,BR2,IER)
      GO TO (40,42,44,46),IER
      GO TO 302
30    CONTINUE
      ZA=Z
      GO TO 31
      END
```

```
001   PROGRAM F
002
003   C     LSUC GAIN AND NOISE FIGURE USING DEPLETION AND DIFFUSION
004   C     ADMITTANCE IS CALCULATED HERE.
005
006   C     THIS PROGRAM USES BESKC,CMINV, AS WELL AS BESI AND GAMMA
007   C     WHICH ARE SSP ROUTINES.
008         REAL L,MU,LR1,LR2,NF ,NFO
009         DIMENSION IPERM(6),YR(2,2),YI(2,2),ZR(2,2),ZI(2,2),ALPHA(3),
010        1BETA(3) ,F(8),C(8)
011         DOUBLE PRECISION DYR(2,2),DYI(2,2),          DZI(2,2),DSA(2,2),DSA(2
012        1,2),DSC(2,2),DRS,DZR(2,2)
013         COMPLEX  Z,BKO,BK1,ZA
014         TPI = 6.2831853
015         INTEGER N
016         EPS = 11.8*8.854 E-14
017   C     QE = ELECTRONIC CHARGE
018         QE=1.6021QE-19
019         ALPH=20.
020         SQR2=1.4142135
021         N=2
022   10    FORMAT(2111,5E11.5/(7E11.5))
023         READ (5,10) NO,J,STEP
024         MU=401.
025         DP=    MU/40.1
026   C     PNW=PN IN CM**-3   SEE WATSON P. 107
027   C     PHI = BUILT-IN POTENTIAL
028         PHI=.9
029   75    CONTINUE
030   C     OLIVER P.54 CO=SO/(SO*SO-S1*S1). IF SO=6.2853E11, THEN CO=1.80798
031   C     TAU=LIFETIME, WL=DEPLETION WIDTH/DIFFUSION LENGTH,
032   C     VR=BIAS VOLTAGE, VO=PUMP VOLTAGE,
033         READ (5,10) B,NN,FS,FP,RS,RG,RL,TAU,WL,PNW,VB,VO,S1
034         WRITE (6,3) B,NN,FS,FP,RS,RG,RL,TAU,WL,PNW,VB,VO,S1
035   3     FORMAT (' N = X**'I2,'  N = ' I2,'FS,FP,RS,RG,RL,TAU,WL,PNW,VR,VO
036        1,S1  =  ' /(8(3X,E13.5)))
037         GAM=1./(B+2)
038         A=VO/(VR-PHI)
039         DENG=GAMMA(GAM)
040         DO 223 MM=1,2,1
041         VA=0.
042         M=MM-1
043         DO 220 JJ=1,20,1
044         J=JJ-1
045         IF (J.GT.0.OR. M.GT.0) GO TO 225
046         VC=1.
047         GO TO 224
048   225   VC=GAMMA(2*J+M+GAM)/DENG
049   224   CONTINUE
050         VD=VA
051         TWO = 2.**(M+2*J-1)
052   C     SEE DAVE OLIVER APPENDIX A EQ. A.11
053         VA=A**(2*J+M)*(-1)**M*VC/(TWO*GAMMA(M+J+1.)*GAMMA(J+1.))+VA
054         IF (J.LE.0) GO TO 220
055         VC=ABS((VD-VA)/VD)
056         IF (VC.LT..0001) GO TO (221,222),MM
057   220   CONTINUE
058   13    FORMAT (' PERCENT CHANGE  = 'F13.5)
059         WRITE (6,13) VC
060         GO TO (221,222),MM
061   221   VKSAO=VA
062         JO=JJ
063         GO TO 223
064   222   VKSA1=VA
065         J1=JJ
066   223   CONTINUE
067         VM=VKSA1/VKSAO
068         CO=VM/(S1*(1.-VM*VM))
069         C(1)=VM*CO
070         COS=CO*(1.-VB/PHI)**GAM/VKSAO
071         CR=CO/VKSAO
072         WRITE (6,55) CO,JO,C(1),J1,VM,COS,CR
073   55    FORMAT (' CO = 'F13.5,' ITERATIONS = 'I3,' C1 = 'E13.5,' ITERATION
074        1S = 'I3,' M = 'E13.5,' COS = 'E13.5,' CR = 'E13.5)
075         IF (TAU .GT. 0.) GO TO 216
076         DO 217 J=1,N,1
077         ALPHA(J)=0.
078         BETA(J)=0.
079   217   CONTINUE
080         PSS=0.
081         RR1=0.
082         RRO=0.
083         GO TO 218
084   216   CONTINUE
085         L=SQRT(DP*TAU)
086         W=L*WL
087         AREA = CO*W/EPS
088         PSS=QE*DP*PNW*EXP(ALPH*VR)/W*AREA*ALPH
089         VA=ALPH*VO
090         CALL BESI(VA,1,RR1,IER)
091         GO TO (40,42,44,46),IER
092         CALL BESI (VA,0,RRO,IER)
093         GO TO (40,42,44,46),IER
094   218   CONTINUE
095         JL=0
096         ITEST=1
097         F(1)=FS
098   211   CONTINUE
099         F(2)=FP-F(1)
100         IF (TAU .LE.0.) GO TO 219
101         DO 200 K=1,N,1
102         OMEGA = TPI*F(K)
103         AV   =SQRT(1.+SQRT(1.+(  OMEGA*TAU)**2))*WL/SQR2
104         AV   =SQRT(-1.+SQRT(1.+(  OMEGA*TAU)**2))*WL/SQR2
105         Z=CMPLX(AV,BV)
106         IF (B.EQ.0) GO TO 30
107         NU=(B-1)/2
108         CALL BESKC(Z,NU,BKO,IER)
109         GO TO (40,42,46,48),IER
110         CALL BESKC (Z,NU+1,BK1,IER)
111         GO TO (40,42,44,48), IER
112         ZA=Z*BKO/BK1
113   31    CONTINUE
114         ALPHA(K)=REAL(ZA)
115   200   BETA(K)=AIMAG(ZA)
116   219   CONTINUE
117         DO 201 J=1,N,1
118         DYR(J,J)=DBLE(PSS*RRO*ALPHA(J))
119   201   DYI(J,J)=  DBLE((PSS*RRO*BETA(J)+CO*TPI*F(J))*(-1)**(J+1))
120         DYR(1,2)=DBLE(PSS*RR1*ALPHA(1))
```

```
      DYI(1,2)=DBLE(PSS*RR1*BETA(1)+TPI*F(1)*C(1))
      DYR(2,1)=DBLE(PSS*RR1*ALPHA(2))
      DYI(2,1)=-DBLE(PSS*RR1*BETA(2)+TPI*F(2)*C(1))
      IF (JL.GT.0) GO TO 215
      DO 214 J=1,N,1
      DO 214 K=1,N,1
      YR(J,K)=SNGL(DYR(J,K))
      YI(J,K)=SNGL(DYI(J,K))
214   CONTINUE
      WRITE (6,51) ((YR(M,J),J=1,2  ,1),M=1,2  ,1)
      WRITE (6,52) ((YI(M,J),J=1,2  ,1),M=1,2  ,1)
      RDIF1 =PSS*RRO*BETA(1)
      RDIF2=PSS*RRO*BETA(2)
      RDFP1=CO*TPI*F(1)
      RDFP2=CO*TPI*F(2)
      RDIF12=PSS*RR1*BETA(1)
      RDFP12=TPI*F(1)*C(1)
      WRITE (6,53) F(1),RDFP1,RDIF1,F(2),RDFP2,RDIF2,F(1),RDFP12,RDIF12
53    FORMAT (' F = 'E13.5,' RDFP = '     E13.5,' EDIF = 'E13.5)
215   CONTINUE
      CALL CMINV (N,2,DYR,DYI,IPERM,DZR,DZI,DSA,DSb,DSC)
      IF (IPERM(2*N-1).NE.0) GO TO 230
      DOUBLE PRECISION DZIE(4)
      EQUIVALENCE (DZIE(1),DZI(1,1))
      CALL CMINV (N,2,DYI,DYR,IPERM,DZI,DZR,DSA,DSb,DSC)
      IF (IPERM(2*N-1) .EQ.0) GO TO 25
      M=2*N
      DO 231 J=1,M,1
      DZIE(J)=-DZIE(J)
231   CONTINUE
230   CONTINUE
      IF (ITEST.EQ.1) GO TO 207
208   CONTINUE
      DRS=DBLE(RS)
      DZR(1,1)=DZR(1,1)+DRS+DBLE(RG)
      DZR(2,2)=DZR(2,2)+DRS+DBLE(RL)
      DZI(1,1)=DZI(1,1)+DBLE(F(1)*TPI*LR1-SR1/(F(1)*TPI))
      DZI(2,2)=DZI(2,2)-DBLE(F(2)*TPI*LR2-SR2/(F(2)*TPI))
      CALL CMINV (N,2,DZR,DZI,IPERM,DYR,DYI,DSA,DSb,DSC)
      DO 203 J=1,N,1
      DO 202 K=1,N,1
      ZR(J,K)=SNGL(DZR(J,K))
      ZI(J,K)=SNGL(DZI(J,K))
      YR(J,K)=SNGL(DYR(J,K))
      YI(J,K)=SNGL(DYI(J,K))
202   CONTINUE
203   CONTINUE
      IF (JL.GT.0) GO TO 212
51    FORMAT ('0ZR MATRIX '/('0',2(3X,E13.6)))
52    FORMAT ('0ZI MATRIX '/('0',2(3X,E13.6)))
      WRITE (6,51) ((ZR(M,J),J=1,2  ,1),M=1,2  ,1)
      WRITE (6,52) ((ZI(M,J),J=1,2  ,1),M=1,2  ,1)
      WRITE (6,51) ((YR(M,J),J=1,2  ,1),M=1,2  ,1)
      WRITE (6,52) ((YI(M,J),J=1,2  ,1),M=1,2  ,1)
212     CONTINUE
      GAIN=4.*RG*RL*(YR(2,1)**2+YI(2,1)**2)
      VC=ZR(2,2)-RS
      VA=0.
      DO 206 I=1,N,1
206   VA=(YR(2,1)**2+YI(2,1)**2)*ZR(1,1)+VA
      NF=(4.*VC*(VA-VC*(YR(2,2)**2+YI(2,2)**2))
     1*(1.-2.*VC*YR(2,2))**2+4.*(VC*YI(2,2))**2)/GAIN
      IF (ITEST.EQ.1) GO TO 209
213   WRITE (6,4) N,N,GAIN,F(1),NF
4     FORMAT (' THE GAIN FOR THE  'I1,' BY 'I1,' MATRIX IS 'F12.2,
     15X,' WITH SIGNAL FREQUENCY ' E12.5,5X,' NOISE FIGURE = 'E12.5)
210   CONTINUE
      JL=JL+1
      F(1)=FS+STEP*(JL-(NO+1)/2)
      IF (JL.GT.NO) GO TO 25
      IF (JL.NE.( NO+1)/2) GO TO 211
      NF=NFO
      GAIN=GAINO
      GO TO 213
207   CONTINUE
      LR1=0.
      SR1=LR1
      LR2=LR1
      SR2=LR1
      VA=SNGL(DZI(1,1)  )
      IF (VA.LT.0.)  LR1=-VA/(TPI*FS)
      IF (VA.GT.0.)  SR1=VA*TPI*FS
      VA =-SNGL (DZI(2,2))
      IF (VA.LT.0.)  LR2=-VA/(TPI*F(2))
      IF (VA.GT.0.)  SR2=VA*TPI*F(2)
      WRITE (6,5) LR1,SR1,LR2,SR2
5     FORMAT (' DIODE RESONATED WITH LR1= 'E13.5,' SR1 = ' E13.5,' LR2
     1= 'E13.5,' SR2 = ' E13.5)
      GO TO 208
209   CONTINUE
      GAINO = GAIN
      NFO=NF
      ITEST=0
      GO TO 210
39    FORMAT (' NEGATIVE ORDER FOR BESSEL FUNCTION')
40    WRITE (6,39)
      GO TO 25
41    FORMAT (' NEGATIVE ARGUMENT')
42    WRITE (6,41)
      GO TO 25
43    FORMAT (' RESULT <1.E-69')
44    WRITE (6,43)
      GO TO 25
45    FORMAT (' ARGUMENT>170.')
46    WRITE (6,45)
      GO TO 25
47    FORMAT (' RESULT>1.E70')
48    WRITE (6,47)
      GO TO 25
30    CONTINUE
      ZA=Z
      GO TO 31
      END
```

```
001   SUBROUTINE TRNR
002
003   C     TRNR TRANSLATES RECEIVING END IMMITTANCE TOWARD GENERATOR.
004   C     ENTRY TRNS TRANSLATES AWAY FROM GENERATOR.
005
006         SUBROUTINE TRNR (YO,D,GR,BR,GS,BS)
007   C     Z = (ZR+J*ZO*TAN(PHI))/(ZO+J*ZR*TAN(PHI))
008   C     D IS DISTNACE TRANSLATED IN NUMBER OF WAVELENGTHS
009   C     GR IS THE REAL PART OF THE RECEIVING ADMITTANCE
010   C     BR IS THE IMAGINARY PART OF THE RECEIVING ADMITTANCE
011   C     THIS FUNCTION RETURNS SENDING END ADMITTANCE GS AND BS
012   C     THE CHARACTERISTIC ADMITTANCE IS YO MHOS
013         THETA=6.2831853*D
014   10    CONTINUE
015         BOT=(YO*COS(THETA)-BR*SIN(THETA))**2+(GR*SIN(THETA))**2
016         IF (ABS(BOT).GT.1.E-20) GO TO 20
017         GS=0.
018         BS=1.E20
019   C     TWO CASES
020   C     YO*BR*TAN(THETA) AND GR*SIN(THETA)  THEREFORE GR=0
021   C     OR GR=0 AND BR = 0
022         RETURN
023   20    CONTINUE
024         GS=YO*YO*GR/BOT
025         BS=YO*(BR*YO*(1.-2.*SIN(THETA)*SIN(THETA))+(YO*YO-BR*BR
026        1-GR*GR)*SIN(THETA)*COS(THETA))/BOT
027         RETURN
028   C     Z=(ZS-ZO*TANH(A))/(ZO-ZS*TANH(A))
029         ENTRY TRNS(YO,D,GR,BR,GS,BS)
030         THETA=-6.2831853*D
031         GO TO 10
032         END
```

```
001   SUBROUTINE IMPST, ENTRY IMPM
002
003   C     IMPST FINDS CHARACTERISTIC IMPEDANCES AND ACCOUNTS FOR
004   C     DISCONTINUITY CAPACITANCES OF DISKS IN COAXIAL FILTER.
005   C     ENTRY IMPM FINDS INPUT IMPEDANCE OF FILTER WHEN FILTER TERMINATION
006   C     IS KNOWN.
007
008   C     THIS PROGRAM USES TRNR.   IMPST MUST BE CALLED FIRST TO SET
009   C     VARIOUS PARAMETERS IN IMPM.
010         SUBROUTINE IMPST (DIA,LNTH,EPS,N,TEST,SIZE,CD,ZOC,FN)
011         RPARAL (VVA,VVB,VVC,VVD)=((VVA*VVA+VVB*VVB)*VVC+(VVC*VVC+
012        1VVD*VVD)*VVA)/((VVA+VVC)**2+(VVB+VVD)**2)
013         XPARAL(VVA,VVB,VVC,VVD)=((VVA*VVA+VVB*VVB)*VVD+(VVC*VVC+
014        1VVD*VVD)*VVB)/((VVA+VVC)**2+(VVB+VVD)**2)
015         INTEGER J ,N,TEST ,TEST1,NV
016         REAL LNTH,LN
017         DIMENSION LNTH(10),DIA(10),DIST(10),LN(10),CD(10),ZOC(10),
018        1SIZE(10),EPS(10)
019         DIMENSION CDO(10)
020   C     LNTH IS THE LENGTH SIZE OF THE DISK IN METERS
021   C     DIST IS THE DISTANCE BETWEEN DISKS IN METERS
022   C     F IS THE FREQUENCY IN GC/S
023   C     DO IS DIAMETER OF OUTER CONDUCTOR OF G R LINE
024   C     DIST(J) IS DISTANCE BETWEEN DISK(J-1) AND DISK (J)
025   C     SIZE IS THE MODIFIED DISK LENGTH IN METERS
026   C     CD IS THE DISCONTINUITY CAPACITANCE IN PF
027   C     TEST=1 SEE REF. MATTHAEI MTT AUG. 1964 PP.372-383
028   C     TEST=2 MODIFY MATTHAEI'S METHOD BY USING DISTRIBUTED CAPACITANCE
029   C     TEST=3 SEE REF. LEVY & ROZZI, MIT MARCH 1968, PP.142-147.
030   C     TEST=4,5,6 CORRESPOND TO TEST =1,2,3 RESPECTIVELY BUT WITH
031   C     LOW-PASS MATCHING NETWORK.  SEE MATTHAEI, AUG. 1964 PROC. IEEE.
032         TPI=6.2831853
033         TEST1=0
034         IF (TEST.LE.3) GO TO 21
035         TEST1=1
036         TEST=TEST-3
037   21    CONTINUE
038         DO=.5625
039         ZO=50.
040         CN=.2997925
041         BETA=TPI*FN/CN
042         JJ=0
043         KEY=0
044   C     JJ COUNTS ITERATIONS FOR TEST=3. KEY IS USED FOR CONDITIONAL BRANCH
045         DO 11 J=1,N,1
046         CDO(J)=0.
047   11    SIZE(J)=LNTH(J)
048         ZOC(N+1)=0.
049         IF (TEST1.EQ.0) GO TO 14
050         LN(1) =ALOG(DO/DIA(1))
051         ZOC(N+1)=100.*LN(1)*SQRT(20./(TPI*8.854))
052   14    CONTINUE
053   12    CONTINUE
054         DO 10 J=1,N,1
055         THETA=BETA*SIZE(J)
056         ALPHA =(DO-DIA(J) )/(DO-.24425)
057         TAU=DO/.24425
058         IF (TEST1.EQ.0) GO TO 13
059         ALPHA=(DO-DIA(2*J))/(DO-DIA(1))
060         TAU=DO/DIA(1)
```

```
      C     DIA(1)=.0319A INCHES OR #20 WIRE.
   13 CONTINUE
      C     .24425 IS DIAMETER IN INCHES OF INNER CONDUCTOR OF GR LINE
      C     CD IS THE DISCONTINUITY CAPACITANCE
      C     REF. P. 1. SOMLO  MTT-15,NO. 1  P.48
            CD(J)=A.A54*DD*.0254*((((ALPHA *ALPHA+1.)/ALPHA)*ALOG(((1.+ALPHA)
           1/(1.-ALPHA))-2.*ALOG(4.*ALPHA/(1.-ALPHA*ALPHA)))      *.111*
           2(1.-ALPHA)*(DD/.24425-1.)  *TPI*DD/2. *.0254
            IF (KEY.EQ.1) GO TO 10
            LN(J)=ALOG(DD/DIA (ITEST1+1)*J))
            ZOC(J)=100.*LN(J)*SQRT (20./(TPI*EPS(J)))
            GO TO (41,42,43), TEST
   41 CONTINUE
            SIZE(J)=LNTH(J)-2.*CD(J)*LN(J)/(TPI*EPS(J))
            GO TO 10
   42 CONTINUE
            SIZE(J)=2.*ATAN(TAN(THETA/2.)-ZOC(J)*CD(J)*TPI*FN*1.E-3)/BETA
            GO TO 10
   43 CONTINUE
            VA=COS(THETA)+TPI*FN*(CD(J)-CDO(J))*ZOC(J)*SIN(THETA)*1.E-3
            IF (ABS(VA).GT.1.) GO TO 44
            SIZE(J)=ARCOS(VA)/BETA
            ZOC(JJ)=ZOC(J)*SIN(THETA)/SIN(BETA*SIZE(J))
            DIA(J)=DD*EXP(-ZOC(J)*.01*SQRT(TPI*EPS(J)/20.))
            IF (JJ.EQ.0) CDO(J)=CD(J)
   10 CONTINUE
            IF (TEST.NE.3) RETURN
            IF (KEY.EQ.1) RETURN
            JJ=JJ+1
      C     AT LEAST TWO ITERATIONS REQUIRED.
            IF (JJ.EQ.1) GO TO 12
            VA=(CD(1)-CDO(1))/CDO(1)
   31 FORMAT (' PERCENT CHANGE = 'E13.6,' JJ= 'I11)
            WRITE (6,31) VA,JJ
            IF (ABS(VA).LT..01.OR.JJ.GT.10)  GO TO 46
            DO 45 J=1,N,1
   45 CDO(J)=CD(J)
            GO TO 12
   44 SIZE(J)=-1.
            KEY=1
            GO TO 10
   46 KEY=1
            GO TO 12
            ENTRY IMPM (F,N,SIZE,DIST,CD,ZOC,RIN,XIN,ROUT,XOUT)
            R1=RIN
            X1=XIN
            J=N
            ZC=Z0
            IF (ZOC(N+1).GT.Z0) ZC=ZOC(N+1)
   20 CONTINUE
            IF (J-1) 30,40,40
   40 CONTINUE
            XD=-1.E3/(TPI*F*CD(J))
            WAVE=SIZE(J)*F**SQRT(EPS(J)/A.A54)/CN
            RA=R1
            XA=X1
      C     EPS(5) = FACTOR TO VARY DISCONTINUITY LOSS
            R1=RPARAL(RA,XA,-XD*EPS(5),XD)
            X1=XPARAL(RA,XA,-XD*EPS(5),XD)
            CALL TRNR (ZOC(J),WAVE,R1,X1,R2,X2)
            RA=R2
            XA=X2
            R2=RPARAL (RA,XA,-XD*EPS(5),XD)
            X2=XPARAL (RA,XA,-XD*EPS(5),XD)
            WAVE=DIST(J)*F/CN
            CALL TRNR (ZC,WAVE,R2,X2,R1,X1)
            J=J-1
            GO TO 20
   30 CONTINUE
            ROUT=R1
            XOUT=X1
            RETURN
            END
```

```
001   SUBROUTINE DESIGN, ENTRY LUMP
002
003   C     DESIGN SYNTHESIZES COAXIAL BAND-PASS FILTERS USING DISTRIBUTED
004   C     METHOD.  ENTRY LUMP USES THE INFERIOR LUMPED METHOD.
005
006   C     NOTATION USED FOLLOWS COOLEY TECH. MEMO. 100, BUT IS EQUIVALENT
007   C     TO NOTATION USED IN CHAPTER 2 HERE. NUMBERS IN THIS PROGRAM
008   C     ARE FOR 14 MM LINE.  FOR DIFFERENT LINE DO,DI(J), AND POSSIBLY
009   C     ZO WOULD HAVE TO BE CHANGED.
010         SUBROUTINE DESIGN (R,F,DI,W,DELTA,N,G,K,ANG,C,LNTH,EPS,TESTI)
011         REAL K,LN,LNTH,LL,J2
012         DIMENSION G(10),K(10),C(10),LNTH(10),ANG(10),X(10),DI(10)
013         DIMENSION EPS(10)
014   C     F IS IN CPS
015   C     TESTI=0 OUTPUT MEANS GOOD DESIGN; TESTI=1 MEANS DESIGN WAS NOT
016   C     POSSIBLE SINCE V.1 WHICH MEANS THAT K IS PROBABLY LESS THAN ZOC
017   C     IF TESTI=2 IS PUT IN THIS PROGRAM, THE MIDDLE INVERTER IS A J
018   C     INVERTER AND THE J INVERTER IS A SERIES CAPACITOR.
019   C     IF TESTI =3, THE INVERTER IS A SERIES INDUCTOR (DISTRIBUTED DESN.)
020   C     W IS FRACTIONAL BANDWIDTH
021   C     G ARE THE PROTOTYPE G VALUES
022   C     LNTH ARE THE DISK LENGTHS AND ANG ARE THE K INVERTER LENGTHS
023         INTEGER J,N,NN,I
024         INTEGER TESTI ,JINV
025          JINV=0
026         IF(TESTI.GE.2) JINV=TESTI-1
027         TESTI=0
028         TPI=6.2831853
029         ZO=50.
030         VC=2.997925 E8
031         OMEGAN=TPI*F*1.E-9
032   C     REACTANCE SLOPE PARAMETER FOR 1/2 WAVE K INVERTER IS ZO*PI/2
033         K(1)=SQRT(W*R*TPI*ZO/(G(1)*G(2)*4.*DELTA))
034         NN=N-1
035         DO 31 J=2,NN,1
036   31    K(J)=(TPI*ZO/4.)/(SQRT(G(J)*G(J+1)))*W
037         K(N)=SQRT(ZO*ZO*TPI*W/(G(N)*G(N+1)*4.))
038   C     OUTSIDE DIAMETER OF COAXIAL LINE IN INCHES
039         DO=.5625
040         IF (JINV.EQ.0) GO TO 25
041         K(1)=K(1)/1.41421356
042         K(3)=K(3)/1.41421356
043   25    CONTINUE
044         DO 33 J=1,N,1
045         DI(J)=.502
046   C     X IS REACTANCE, C IS CAPACITANCE
047         X(J)=K(J)*ZO*ZO/(ZO*ZO-K(J)*K(J))
048         C(J)=1.E3/(X(J)*OMEGAN)
049   C     LENGTH OF PHI OF INVERTER IN RADIANS
050         I=0
051   21    CONTINUE
052         I=I+1
053         LN=ALOG(DO/DI(J))
054         ZOC=100.*LN*SQRT(20./(TPI*EPS(J)))
055         P=(ZO*ZO-ZOC*ZOC)/(ZO*ZO-K(J)*K(J))
056         V=K(J)*P/ZOC
057   C     IF V<1. THEN INCREASE DIAMETER.
058         IF (ABS(V),LT,1, ) GO TO (41,42,43,44,45),I
059   20    CONTINUE
060         VO=V-SQRT(V*V-1)
061         VR=ATAN(VO)
062         LNTH(J)=2.*VC/(TPI*F*SQRT(EPS(J)/R.454))*VR
063         ANG(J)=2.*ATAN(ZO*(K(J)-ZOC*VO)/(ZO*ZO*K(J)*ZOC*VO))
064   33    CONTINUE
065         IF (JINV.GE.1) GO TO 35
066         RETURN
067   41    DI(J)=.532
068         GO TO 21
069   42    DI(J)=.542
070         GO TO 21
071   43    DI(J)=.552
072         GO TO 21
073   44    DI(J)=.554
074         GO TO 21
075   45    TESTI=1
076         IF (JINV.GE.1.AND.J.EQ.2) TESTI=0
077         GO TO 33
078   35    CONTINUE
079         REAL J2
080   C     J INVERTER IS 1/4 WAVE LENGTH FROM K INVERTERS
081         J2=W*TPI/(ZO*R.*SQRT(G(2)*G(3)))
082         K(2)=1./J2
083         A2=J2/(1.-ZO*ZO*J2*J2)
084         C(2)=1.E3*A2/OMEGAN
085         IF (JINV.EQ.2) GO TO 50
086         ANG(2)=-ATAN(2.*A2*ZO)
087         LNTH(2)=EPS(2)*TPI*(1.24625*.0254)**2/(R.*C(2))
088         RETURN
089         ENTRY LUMP (C)
090         DO 34 J=1,N,1
091         ANG(J)=ATAN(2.*X(J)/ZO)
092         LN=ALOG(DO/DI(J))
093         LNTH(J)=C(J)*LN/(TPI*EPS(J))
094   34    CONTINUE
095         RETURN
096   50    CONTINUE
097   C     ASSUME #20 WIRE (31.96 MIL DIAMETER) FOR J INVERTER
098         LN=ALOG(DO/.0319A)
099         YOC=.01*SQRT(TPI*8.454/20.)/LN
100         YO=1./ZO
101         P=(YO*YO-YOC*YOC)/(YO*YO-J2*J2)
102         V=J2*P/YOC
103         IF (ABS(V),LT,1, ) GO TO 51
104         VO=V-SQRT(V*V-1.)
105         VR=ATAN(VO)
106         LNTH(2)=2.*VC*VR/(TPI*F)
107         ANG(2)=2.*ATAN(YO*(J2-YOC*VO)/(YO*YO+J2*YOC*VO))
108         GO TO 34
109   51    TESTI=1
110         GO TO 34
111         END
```

```
001   SUBROUTINE PROTOG
002
003   C     PROTOG FINDS G VALUES FOR THE LUMPED LOW-PASS PROTOTYPE CIRCUIT.
004
005   C     THE NUMBERS HERE ARE FOR A 3 POLE CHEBYSHEV MATCHING CIRCUIT
006   C     WHERE THE VALUES ARE OBTAINED FROM INTERPOLATION OF GRAPHS
007   C     IN MATTHAEI, YOUNG, AND JONES  P.128.
008         SUBROUTINE PROTOG (N,DELTA,K,G)
009         DIMENSION G (20) ,GG(40)
010         INTEGER N,K,I
011         K=0
012         I=0
013         IF (N.NE.3 .OR.DELTA.LT..05) GO TO 90
014         IF (DELTA .GT..1) GO TO 310
015         DEL1=.05
016         DEL2=.1
017         GG(I+1)=20.
018         GG(I+2)=.10
019         GG(I+3)=12.2
020         GG(I+4)=.0715
021         I=I+4
022         IF (I.GE.2*N+2) GO TO 91
023         GO TO 311
024   310   CONTINUE
025         IF (DELTA .GT..2) GO TO 320
026         DEL1=.1
027         DEL2=.2
028   311   GG(I+1)=10.
029         GG(I+2)=.182
030         GG(I+3)=6.3
031         GG(I+4)=.14
032         I=I+4
033         IF (I.GE.2*N+2) GO TO 91
034         GO TO 321
035   320   CONTINUE
036         IF (DELTA .GT..3) GO TO 330
037         DEL1=.2
038         DEL2=.3
039   321   GG(I+1)=5.
040         GG(I+2)=.360
041         GG(I+3)=3.2
042         GG(I+4)=.272
043         I=I+4
044         IF (I.GE.2*N+2) GO TO 91
045         GO TO 331
046   330   CONTINUE
047         IF (DELTA .GT..4) GO TO 340
048         DEL1=.3
049         DEL2=.4
050   331   GG(I+1)=3.3
051         GG(I+2)=.52
052         GG(I+3)=2.1
053         GG(I+4)=.40
054         I=I+4
055         IF (I.GE.2*N+2) GO TO 91
056         GO TO 341
057   340   CONTINUE
058         IF (DELTA .GT..5) GO TO 350
059         DEL1=.4
060         DEL2=.5
061   341   GG(I+1)=2.5
062         GG(I+2)=.65
063         GG(I+3)=1.62
064         GG(I+4)=.6
065         I=I+4
066         IF (I.GE.2*N+2) GO TO 91
067         GO TO 351
068   350   CONTINUE
069         IF (DELTA .GT..70) GO TO 370
070         DEL1=.5
071         DEL2=.7
072   351   GG(I+1)=2.0
073         GG(I+2)=.76
074         GG(I+3)=1.35
075         GG(I+4)=.60
076         I=I+4
077         IF (I.GE.2*N+2) GO TO 91
078         GO TO 371
079   370   CONTINUE
080         IF (DELTA .GT.1.00) GO TO 3100
081         DEL1=.7
082         DEL2=1.00
083   371   GG(I+1)=1.4
084         GG(I+2)=.90
085         GG(I+3)=1.0
086         GG(I+4)=.74
087         I=I+4
088         IF (I.GE.2*N+2) GO TO 91
089         GO TO 3101
090   3100  CONTINUE
091         IF (DELTA .GT. 1.50) GO TO 3150
092         DEL1=1.00
093         DEL2=1.50
094   3101  GG(I+1)=1.0
095         GG(I+2)=.965
096         GG(I+3)=.765
097         GG(I+4)=.865
098         I=I+4
099         IF (I.GE.2*N+2) GO TO 91
100         GO TO 3151
101   3150  CONTINUE
102         IF (DELTA .GT. 2.0  ) GO TO 90
103         DEL1=1.50
104         DEL2=2.00
105   3151  GG(I+1)=.66
106         GG(I+2)=.90
107         GG(I+3)=.55
108         GG(I+4)=.95
109         I=I+4
110         IF (I.GE.2*N+2) GO TO 91
111         GG(I+1)=.51
112         GG(I+2)=.79
113         GG(I+3)=.44
114         GG(I+4)=.98
115   91    CONTINUE
116         NN=N+1
117         DO 92 I=1,NN,1
118   92    G(I)=(DELTA-DEL1)/(DEL2-DEL1)*(GG(N+I+1)-GG(I))+GG(I)
119         RETURN
120   C     NO G VALUES FOR THIS DATA
121   90    K=1
122         RETURN
123         END
```

```
001   SUBROUTINE CMINV, ENTRY MPRD
002
003   C     CMINV INVERTS COMPLEX MATRICES, AND ENTRY MPRD MULTIPLIES REAL
004   C     MATRICES.
005
006   C     CMINV CALLS MPRD AND INV.  INV INVERTS REAL MATRICES AND IS
007   C     AVAILABLE IN THE U. OF M. LIBRARY.
008         SUBROUTINE CMINV(N,LEN,A,B,IPERM,CR,CI,R,AA,BB)
009   C     A + J B = INPUT MATRIX.   CR + J CI = OUTPUT INVERTED MATRIX
010   C     IPERM IS INTEGER VECTOR OF LENGTH 2*N
011   C     LEN X LEN IS DIMENSION OF MATRICES
012   C     N X N IS THE NUMBER OF ELEMENTS IN THE MATRICES.
013   C     R,AA,BB,I ARE SCRATCH MATRICES.
014   C     REF.  C.LANCZOS, APPLIED ANALYSIS, P. 137.
015   C     A' MEANS INVERSE OF A
016   C     IF C = A + J*B, AND D = (A + B*A'*B)', THEN C' = D -J*D*B*A'
017         IMPLICIT REAL*8(A-H,O-Z,$),INTEGER (I-N)
018         DIMENSION A(1),B(1),CR(1),CI(1),R(1),AA(1),BB(1),      IPERM(1)
019          CALL INV (N,LEN,A,IPERM,LEN,BB)
020   C     RETURN IF MATRIX IS SINGULAR, HENCE THIS PROGRAM WILL NOT WORK FOR
021   C     PURE IMAGINARY MATRICES.
022         IF (IPERM(2*N-1) .EQ.0) RETURN
023         LEN2=LEN*LEN
024         DO 100 I=1,LEN2,1
025   100   AA(I)=B(I)
026         KEY=1
027         GO TO 20
028   31    CONTINUE
029         DO 110 I=1,LEN2,1
030         CI(I)=R(I)
031         AA(I)=B(I)
032         BB(I)=R(I)
033   110   CONTINUE
034         KEY=2
035         GO TO 20
036   32    CONTINUE
037         DO 120 I=1,LEN2,1
038         AA(I)=A(I)*R(I)
039   120   CONTINUE
040         CALL INV (N,LEN,AA,IPERM,LEN,CR)
041         IF (IPERM(2*N-1) .EQ.0)  RETURN
042         DO 130  I=1,LEN2,1
043         AA(I)=CR(I)
044         BB(I)=CI(I)
045   130   CONTINUE
046         KEY=3
047         GO TO 20
048   33    CONTINUE
049         DO 140 I=1,LEN2,1
050         CI(I)=-R(I)
051   140   CONTINUE
052         RETURN
053         ENTRY MPRD(AA,BB,R,N,LEN)
054   C     AA*BB=R
055   C     SUBROUTINE BASED ON GMPRD ON PAGE 99 OF SSP.
056         KEY=0
057   20    CONTINUE
058         IK=-LEN
059         DO 10 K=1,N,1
060         IK=IK+LEN
061         IR=IK
062   C     THIS GETS A PARTICULAR COLUMN.
063         DO 10 J=1,N,1
064         IR=IR+1
065         JI=J-LEN
066         IB=IK
067         R(IR)=0.
068         DO 10 I=1,N,1
069         JI=JI+LEN
070         IB=IB+1
071   10    R(IR)=R(IR)+AA(JI)*BB(IB)
072         GO TO (31,32,33),KEY
073         RETURN
074         END
```

```
001   SUBROUTINE BESKC
002
003   C     BESKC FINDS THE K BESSEL FUNCTION OF COMPLEX ARGUMENT.
004
005         SUBROUTINE BESKC(Z,N,BK,IER)
006   C     COMPUTE THE K BESSEL FUNCTION FOR A GIVEN ARGUMENT AND ORDER
007   C     USAGE IS  CALL BESKC(Z,N,BK,IER)
008   C     Z = THE ARGUMENT OF THE K BESSEL FUNCTION DESIRED
009   C     N = INTEGER ORDER OF THE K BESSEL FUNCTION DESIRED
010   C     BK = THE RESULTANT K BESSEL FUNCTION
011   C     IER = RESULTANT ERROR CODE WHERE
012   C     IER=0 MEANS NO ERROR, IER=1  N IS NEGATIVE, IER=2  X IS 0 OR <0
013   C     IER=3 Z .GT. 170, MACHINE RANGE EXCEEDED     , IER=4  BK .GT.10**70
014   C     N MUST BE >0 AND NO OTHER SUBROUTINES ARE REQUIRED
015   C     THE METHOD INVOLVES COMPUTING THE ZERO ORDER AND FIRST ORDER
016   C     BESSEL FUNCTIONS USING SERIES APPROXIMATIONS AND THEN COMPUTES N
017   C     ORDER FUNCTION USING RECURRENCE RELATION.
018         COMPLEX Z ,A,B,C,T,GO,G1,GJ,BK,Z2J ,GON,GOD
019         DIMENSION T(13)
020         BK=(0.,0.)
021         PI=3.1415927
022         SPI=SQRT(PI/2.)
023         IF (N) 10,11,11
024   10    IER=1
025         RETURN
026   11    CONTINUE
027   20    IF(CABS(Z)-170.)22,22,21
028   21    IER=3
029         RETURN
030   22    IER=0
031         VA=REAL(Z)
032         VB=AIMAG(Z)
033         IF (CABS(Z)-1.) 36,36,25
034   25    A=CEXP(-Z)
035         C=1./CSQRT(Z)
036         T(1)=Z
037         DO 26 L=2,13
038   26    T(L)=T(L-1)*Z
039         IF (N-1) 27,29,27
040   C     COMPUTE KO USING POLYNOMIAL APPROXIMATION
041   27    CONTINUE
042         GON=A*C*SPI*(.93444970E3*T(1)+.74419710E5*T(2)+.13370803E7*T(3)
043        1+.85699270E7*T(4)+.24927645E8*T(5)+.37746865E8*T(6)+.32310445E8*
044        1T(7)
045        2+.16404092E8*T(8)+.50516268E7*T(9)+.96154163E6*T(10)+.10265537E6
046        3*T(11)+.59648092E4*T(12)+.14137062E3*T(13)  )
047         GOD=    .2704E4*T(1)+.13459911E6*T(2)+.18951595E7*T(3)
048        1+.10608451E8*T(4)+.28498751E8*T(5)+.41110144E8*T(6)+.34130589E8
049        2*T(7)+ .16989449E8*T(8)+.51640362E7*T(9)+.95405550E6*T(10)+
050        1.10339324E6*T(11)+.59824805E4*T(12)+.14137061?E3*T(13)
051         GO=GON/GOD
052         IF (N) 20,28,29
053   28    BK=GO
054         RETURN
055   C     COMPUTE K1 USING POLYNOMIAL APPROXIMATION
056   29    CONTINUE
057         GON=A*C*SPI*(.9191825E4*T(1)+.3155701AE6*T(2)+.3256B246E7*T(3)
058        1+.14642396E8*T(4)+.33952021E8*T(5)+.4449327EE8*T(6)+.3473A231E8
059        2*T(7)+ .16631127E8*T(8)+ .49336335E7*T(9)+.89796245E6*T(10)+
060        3.96451139E5*T(11)+.5552961?E4*T(12)+.130B9872E3*T(13)   )
061         GOD=    .90133333E3*T(1)+.807594A7E5*T(2)+.13536A25E7*T(3)+
062        1.A2510171E7*T(4)+.23317599E8*T(5)+.34785507E8*T(6)+
063        2.29579A43E8*T(7)+.14990B9E8*T(8)+.4620A536E7*T(9)+.863193076E6*
064        31(10)+.94402523E5*T(11)+.5503A821E4*T(12)+.130B9872E3*T(13)
065         G1=GON/GOD
066         IF (N-1) 20,30,31
067   30    BK=G1
068         RETURN
069   C     FROM KO,K1 COMPUTE KN USING RECURRENCE RELATION
070   31    DO 35 J=2,N
071         GJ=2.*(FLOAT(J)-1.)*G1/Z+GO
072         IF (CABS(GJ)-1.E70) 33,33,32
073   32    IER=4
074         GO TO 34
075   33    GO=G1
076   35    G1=GJ
077   34    BK=GJ
078         RETURN
079   36    CONTINUE
080         VA=REAL (Z)
081         VB=AIMAG(Z)
082         Z=CMPLX(VA,VB)
083         B=Z/2.
084         A=.5772156B+CLOG(B)
085         C=A*B
086         IF (N-1) 37,43,37
087   C     COMPUTE KO USING SERIES EXPANSION
088   37    GO=-A
089         Z2J=(1.,0.)
090         FACT=1.
091         HJ=0.
092         DO 40 J=1,6
093         RJ=1./FLOAT(J)
094         Z2J=Z2J*C
095         FACT=FACT*RJ*RJ
096         HJ=HJ+RJ
097   40    GO=GO+Z2J*FACT*(HJ-A)
098         IF(N) 43,42,43
099   42    BK=GO
100         RETURN
101   C     COMPUTE K1 USING SERIES EXPANSION
102   43    Z2J=B
103         FACT=1.
104         HJ=1.
105         G1=1./Z+Z2J*(.5+A-HJ)
106         DO 50 J=2,B
107         Z2J=Z2J*C
108         RJ=1./FLOAT(J)
109         FACT=FACT*RJ*RJ
110         HJ=HJ+RJ
111   50    G1=G1+Z2J*FACT*(.5+(A-HJ)*FLOAT(J))
112         IF (N-1)31,52,31
113   52    BK=G1
114         RETURN
115         END
```

APPENDIX B

DETERMINATION OF PARAMETRIC CONVERTER CIRCUIT IMPEDANCES

B.1 Introduction

The optimum load and generator impedance levels for a lower sideband upconverter were found in Chapter II. However, the actual impedances of the signal and lower sideband circuits are far different, because the diode parasitic elements and the characteristics of the out-of-band ports modify these impedances. First the impedance of the diode parasitics plus circuit are found for signal and all sideband frequencies. Then the signal and lower sideband port impedances are found which give the desired impedance level at the diode chip.

The various impedances at terminal A-B are found in terms of the unknown Z_t and Z_i, after which the Z_t at ω_{10} and Z_i at ω_{20} are found. In all cases the circuit impedances Z_s, Z_p, and Z_{p-s} at out-of-band frequencies are assumed to be purely reactive. In the computer calculations using this analysis, it was generally assumed that these reactances were in the form of short circuited quarter wave transmission lines so that, for example, $X_s = X_s(\omega_k) = Z_o \tan\left(\frac{\omega_k \pi}{\omega_{10} 2}\right)$ $k = 1, 2, 3, \ldots$ for out-of-band frequencies. However, in this analysis these reactances are left in terms of X_s, X_p, and X_{p-s} so that any reactance function desired may be used.

B.2 LSUC1

All three ports are in parallel in an ideal tee junction or wye junction if the diode is mounted between the center and the outer conductors. The diode and circuit can be modeled as shown in Fig. B.1.

The input impedance Z_{11} at terminal A-B at frequency ω_1 is obtained in the following manner.

$$Z_{11} = R_s + j(\omega_1 L - S_0/\omega_1) + \frac{1}{j\left(\frac{\omega_1}{S_p} - \frac{1}{X_p} - \frac{1}{X_{p-s}}\right) + \frac{1}{Z_t}} \qquad (B.1)$$

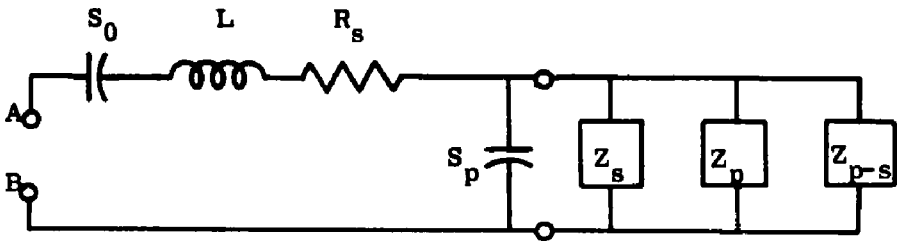


Fig. B.1. Equivalent circuit when all ports are in parallel

If

$$M_g \triangleq \frac{R_t}{R_t^2 + X_t^2} \tag{B.2}$$

and

$$M_b \triangleq \frac{\omega_1}{S_p} - \frac{1}{X_p} - \frac{1}{X_{p-s}} - \frac{X_t}{R_t^2 + X_t^2} \tag{B.3}$$

then

$$Z_{11} = R_s + \frac{M_g}{M_g^2 + M_b^2} + j\left(\omega_1 L - S_0/\omega_1 - \frac{M_b}{M_g^2 + M_b^2}\right) \tag{B.4}$$

Z_{22} is obtained in the same way except that X_s replaces X_{p-s}, Z_i replaces Z_t and ω_2 replaces ω_1. For higher order sidebands

$$Z_{kk} = R_s + j\left[\omega_k L - S_0/\omega_k - \left(\frac{\omega_k}{S_p} - \frac{1}{X_p} - \frac{1}{X_{p-s}} - \frac{1}{X_s}\right)^{-1}\right]. \tag{B.5}$$

The desired impedance at signal frequency is $Z_{11} = R_g + R_s$. If this is substituted into (B.1), the desired value for Z_t can be found.

$$R_g + R_s = R_s + j(\omega_{10} L - S_0/\omega_{10}) + \left[j\left(\frac{\omega_{10}}{S_p} - \frac{1}{X_p} - \frac{1}{X_{p-s}}\right) + \frac{1}{Z_t}\right]^{-1} \tag{B.6}$$

$$\frac{1}{Z_t} = [R_g - j(\omega_{10} - S_0/\omega_{10})]^{-1} - j\left(\frac{\omega_{10}}{S_p} - \frac{1}{X_p} - \frac{1}{X_{p-s}}\right) \tag{B.7}$$

$$Z_t = \frac{R_g - j(\omega_{10}L - S_0/\omega_{10})}{1 - (\omega_{10}L - S_0/\omega_{10})\left(\frac{\omega_{10}}{S_p} - \frac{1}{X_p} - \frac{1}{X_{p-s}}\right) - j\,R_g\left(\frac{\omega_{10}}{S_p} - \frac{1}{X_p} - \frac{1}{X_{p-s}}\right)} \tag{B.8}$$

If

$$M_r \triangleq 1 - (\omega_{10}L - S_0/\omega_{10})\left(\frac{\omega_{10}}{S_p} - \frac{1}{X_p} - \frac{1}{X_{p-s}}\right) \tag{B.9}$$

$$M_x \triangleq - R_g\left(\frac{\omega_{10}}{S_p} - \frac{1}{X_p} - \frac{1}{X_{p-s}}\right) \tag{B.10}$$

then

$$Z_t = \frac{R_g}{M_r^2 + M_x^2} - j\,\frac{M_x R_g + M_r(\omega_{10}L - S_0/\omega_{10})}{M_r^2 + M_x^2} \tag{B.11}$$

Similarly the lower sideband impedance Z_i can be found at $\omega_{20} = \omega_p - \omega_{10}$ which gives the desired impedance $Z_{22} = R_\ell + R_s$. The result is the same as (B.11) except R_ℓ replaces R_g, X_s replaces X_{p-s}, and ω_{20} replaces ω_{10}.

B.3 LSUC2

This circuit is obtained when the diode is mounted in a tee junction with one end in the signal port and the other between the pump and lower sideband ports. The input impedance Z_{11} of the circuit of Fig. B.2 at terminals A-B is found below.

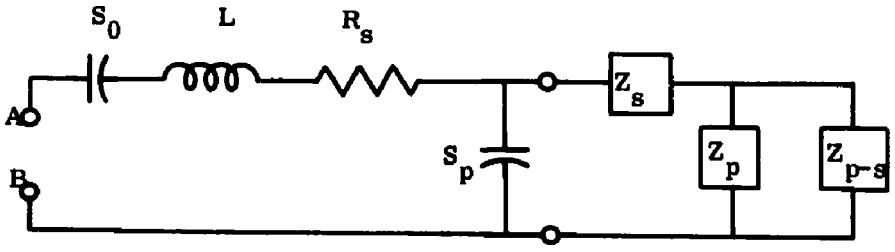


Fig. B. 2. Equivalent circuit when Z_s is in series with $Z_p \| Z_{p-s}$

$$Z_{11} = R_s + j\left(\omega_1 L - \frac{S_0}{\omega_1}\right) + \frac{\left[(jX_t + R_t) + jX_p \| X_{p-s}\right]\left(\frac{-jS_p}{\omega_1}\right)}{R_t + j\left(X_t + X_p \| X_{p-s} - \frac{S_p}{\omega_1}\right)} \tag{B.12}$$

$$Z_{11} = R_s + \frac{R_t\left(\frac{S_p}{\omega_{10}}\right)^2}{R_t^2 + (X_t + X_p \| X_{p-s} - S_p/\omega_1)^2}$$

$$+ j\left\{\left(\omega_1 L - \frac{S_0}{\omega_1}\right) - \frac{S_p}{\omega_1}\left[R_t^2 + X_t^2 + X_t\left(X_p \| X_{p-s} - \frac{S_p}{\omega_1}\right)\right.\right.$$

$$\left.\left. + X_p \| X_{p-s}\left(X_t + X_p \| X_{p-s} - \frac{S_p}{\omega_1}\right)\right] \Big/ \right.$$

$$\left.\left[R_t^2 + \left(X_t + X_p \| X_{p-s} - \frac{S_p}{\omega_1}\right)^2\right]\right\} \tag{B.13}$$

The impedance Z_{22} is found by setting $Z_{p-s}(\omega_{20}) = R_i + jX_i$.

$$Z_{22} = R_s + j\left(\omega_2 L - \frac{S_0}{\omega_2}\right) + \frac{[jX_s + jX_p \| (R_i + jX_i)]\ \frac{-jS_p}{\omega_2}}{jX_s + jX_p \| (jX_i + R_i) - j\frac{S_p}{\omega_2}}$$

If

$$R_a + jX_a \triangleq \frac{jX_p(R_i + jX_i)}{R_i + j(X_p + X_i)}$$

$$R_a + jX_a = \frac{R_i X_p^2}{R_i^2 + (X_p + X_i)^2} + j\,\frac{X_p R_i^2 + X_p X_i (X_p + X_i)}{R_i^2 + (X_p + X_i)^2}$$

then

$$Z_{22} = R_s + j\left(\omega_2 L - \frac{S_0}{\omega_2}\right) + \frac{[R_a + j(X_s + X_a)]\ \frac{-jS_p}{\omega_2}}{R_a + j\left(X_s - \frac{S_p}{\omega_2} + X_a\right)}$$

$$Z_{22} = R_s + \frac{\left(\frac{S_p}{\omega_2}\right)^2 R_a}{R_a^2 + \left(X_s - \frac{S_p}{\omega_2} + X_a\right)^2} + j\left[\left(\omega_2 L - \frac{S_0}{\omega_2}\right) - \frac{R_a^2 \frac{S_p}{\omega_2} + \frac{S_p}{\omega_2}(X_s + X_a)\left(X_s - \frac{S_p}{\omega_2} + X_a\right)}{R_a^2 + \left(X_s - \frac{S_p}{\omega_2} + X_a\right)^2}\right] \tag{B.14}$$

and for $k > 2$

$$Z_{kk} = R_s + j\left\{\left(\omega_k L - \frac{S_0}{\omega_k}\right) - \frac{\left(X_s + X_p \| X_{p-s}\right)\frac{S_p}{\omega_k}}{X_s + X_p \| X_{p-s} - \frac{S_p}{\omega_k}}\right\} . \tag{B.15}$$

For the simpler diode model when $C_p = 0$, the above equations apply by simply taking the limit as $S_p \to \infty$. The results of doing this are shown below.

$$Z_{11} = R_s + R_t + j\left(X_t - \frac{S_0}{\omega_1} + \omega_1 L + X_p \| X_{p-s}\right) \tag{B.16}$$

$$Z_{22} = R_s + \frac{R_i X_p^2}{R_i^2 + (X_p + X_i)^2} + j\left[X_s + \omega_2 L - \frac{S_0}{\omega_2} + \frac{R_i^2 X_p + X_p X_i (X_p + X_i)}{R_i^2 + (X_p + X_i)^2}\right] \tag{B.17}$$

$$Z_{kk} = R_s + j(\omega_k L - S_0/\omega_k + X_s + X_p \| X_{p-s}) \qquad k > 2 \tag{B.18}$$

In all cases X_s, X_p, and X_{p-s} are evaluated at the frequency of interest. For example in the Z_{11} term, $X_p = X_p(\omega_1)$ and $X_{p-s} = X_{p-s}(\omega_1)$. The impedance, Z_t, is found by setting $Z_{11} = R_g + R_s$ and solving for Z_t (Fig. B.3) at ω_{10}.

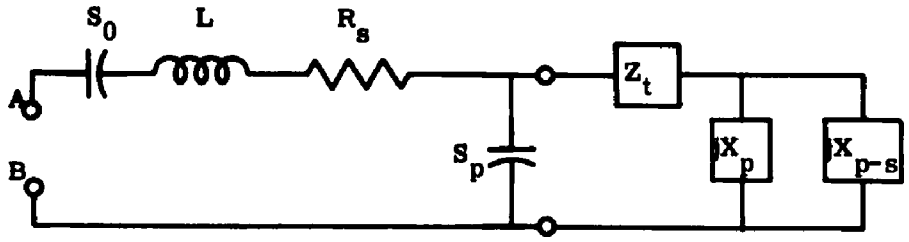


Fig. B.3. Circuit used for the determination of the signal impedance Z_t

$$Z_{11} = R_g + R_s = R_s + j\left(\omega_{10}L - \frac{S_0}{\omega_{10}}\right) + (Z_t + jX_p \| X_{p-s}) \left\| \frac{-jS_p}{\omega_{10}} \right.$$

$$\frac{1}{R_g - j\left(\omega_{10}L - \frac{S_0}{\omega_{10}}\right)} = \frac{1}{Z_t + jX_p \| X_{p-s}} + j\frac{\omega_{10}}{S_p}$$

$$Z_t + jX_p \| X_{p-s} = \frac{1}{[R_g - j(\omega_{10}L - S_0/\omega_{10})]^{-1} - j\frac{\omega_{10}}{S_p}}$$

$$= \frac{\frac{S_p}{\omega_{10}}\left[R_g - j\left(\omega_{10}L - \frac{S_0}{\omega_{10}}\right)\right]}{(S_p + S_0)/\omega_{10} - \omega_{10}L - jR_g}$$

$$Z_t = \frac{R_g\left(\frac{S_p}{\omega_{10}}\right)^2}{R_g^2 + [\omega_{10}L - (S_0 + S_p)/\omega_{10}]^2} + j\frac{S_p}{\omega_{10}} \frac{R_g^2 + \left(\omega_{10}L - \frac{S_p}{\omega_{10}}\right)\left(\omega_{10}L - \frac{S_0+S_p}{\omega_{10}}\right)}{R_g^2 + [\omega_{10}L - (S_0 + S_p)/\omega_{10}]^2}$$

$$- j X_p \| X_{p-s} \qquad \text{(B.19)}$$

Similarly Z_i is found by setting $Z_{22} = R_\ell + R_s$ and solving for Z_i (Fig. B.4) at $\omega_{20} = \omega_p - \omega_{10}$.

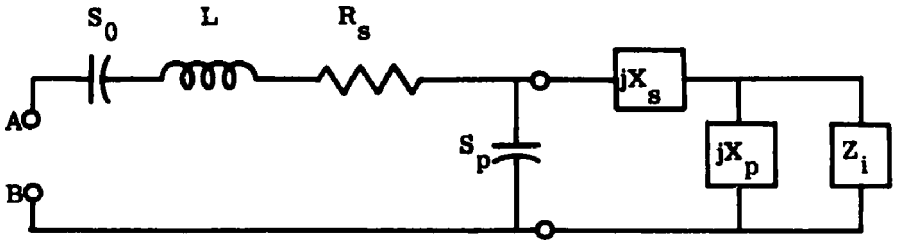


Fig. B.4. Circuit used for the determination of the lower sideband impedance Z_i

$$Z_{22} = R_\ell + R_s = R_s + j\left(\omega_{20}L - \frac{S_0}{\omega_{20}}\right) - j\frac{S_p}{\omega_{20}} \| (jX_s + jX_p \| Z_i)$$

If

$$X_b \triangleq \omega_{20}L - \frac{S_0 + S_p}{\omega_{20}} \quad \text{and} \quad X_c \triangleq \omega_{20}L - \frac{S_0}{\omega_{20}}, \quad \text{then}$$

$$\frac{1}{R_\ell - jX_c} - j\frac{\omega_{20}}{S_p} = \frac{1}{jX_s + jX_p \| Z_i}$$

$$jX_p \| Z_i = -jX_s + \frac{j\frac{S_p}{\omega_{20}}(R_\ell - jX_c)}{R_\ell - jX_b}$$

$$\frac{1}{Z_i} = \frac{1}{-jX_p} + \frac{R_\ell - jX_b}{j\frac{S_p}{\omega_{20}}(R_\ell - jX_c) - jX_s(R_\ell - jX_b)}$$

$$\frac{1}{Z_i} = \frac{-jX_p(R_\ell - jX_b) + j\frac{S_p}{\omega_{20}}(R_\ell - jX_c) - jX_s(R_\ell - jX_b)}{\frac{S_pX_p}{\omega_{20}}(R_\ell - jX_c) - X_sX_p(R_\ell - jX_b)}$$

$$Z_i = \frac{R_\ell X_p\left(\frac{S_p}{\omega_{20}} - X_s\right) + jX_p\left(X_sX_b - \frac{S_p}{\omega_{20}}X_c\right)}{\frac{S_pX_c}{\omega_{20}} - X_b(X_p + X_s) + jR_\ell\left(\frac{S_p}{\omega_{20}} - X_p - X_s\right)} \qquad \text{(B.20)}$$

Now if M_d is defined as the magnitude squared of the denominator,

$$M_d \triangleq \left[\frac{S_p X_c}{\omega_{20}} - X_b(X_p + X_s)\right]^2 + R_\ell^2 \left(\frac{S_p}{\omega_{20}} - X_p - X_s\right)^2 \tag{B.21}$$

then

$$R_i = \left(\frac{S_p}{\omega_{20}}\right)^2 \frac{R_\ell X_p^2}{M_d} \tag{B.22}$$

$$X_i = \frac{X_p R_\ell^2 \left(\frac{S_p}{\omega_{20}} - X_s\right)\left(X_p + X_s - \frac{S_p}{\omega_{20}}\right) + X_p\left(X_s X_b - \frac{S_p}{\omega_{20}} X_c\right)\left(\frac{S_p}{\omega_{20}} X_c - X_b X_p - X_b X_s\right)}{M_d} . \tag{B.23}$$

Again for the diode model with $C_p = 0$, the impedances at the signal and lower sideband ports at their respective pass-band frequencies are obtained by letting $S_p \to \infty$. The results are shown below.

$$Z_t = R_g - j\left(\omega_{10}L - \frac{S_0}{\omega_{10}} + X_p \| X_{p-s}\right) \tag{B.24}$$

$$R_i = \frac{R_L X_p^2}{R_L^2 + \left(X_p + X_s + \omega_{20}L - \frac{S_0}{\omega_{20}}\right)^2} \tag{B.25}$$

$$X_i = -X_p \frac{R_L^2 + \left(X_s + \omega_{20}L - \frac{S_0}{\omega_{20}}\right)\left(X_p + X_s + \omega_{20}L - \frac{S_0}{\omega_{20}}\right)}{R_L^2 + \left(X_p + X_s + \omega_{20}L - \frac{S_0}{\omega_{20}}\right)^2} \tag{B.26}$$

B.4 LSUC3

The equivalent circuit when the diode is mounted in the lower sideband port (Fig. B.5) is similar to the previous circuit (Fig. B.2) except that Z_s and Z_{p-s} are interchanged.

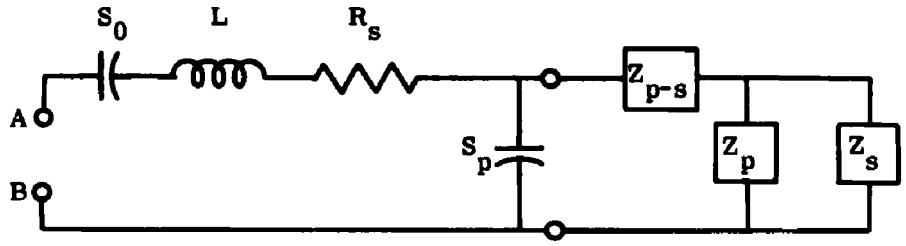


Fig. B.5. Equivalent circuit when diode is in the lower sideband port

The difference in these two situations is not evident from a comparison of the two circuits in Figs. B.2 and B.5 since now the tee junction is assumed to be nonideal. In Fig. B.5 at all frequencies above the signal frequency Z_s is an open circuit.

Making use of the similarities of these two circuits Z_{11} is given by the Z_{22} term in (B.14) of the previous section except ω_1 replaces ω_2, X_{p-s} replaces X_s, and Z_t replaces Z_i. Also, Z_{22} is given by the Z_{11} expression (B.13) of the previous section except ω_2 replaces ω_1, X_p replaces $X_p \| X_{p-s}$ and Z_i replaces Z_t.

For higher order sidebands ($k > 2$):

$$Z_{kk} = R_s + j\left[(\omega_k L - S_0/\omega_k) - \frac{(X_{p-s} + X_p)\frac{S_p}{\omega_k}}{X_{p-s} + X_p - \frac{S_p}{\omega_k}}\right] \qquad \text{(B.27)}$$

The values for Z_t and Z_i can also be found from the previous section by the appropriate substitutions. The impedance Z_t is given by (B.22) and (B.23) when ω_{10} replaces ω_{20}, X_{p-s} replaces X_s, and R_g replaces R_ℓ, while Z_i is given by (B.19) when ω_{20} replaces ω_{10}, X_p replaces $X_p \| X_{p-s}$, and R_ℓ replaces R_g.

APPENDIX C

CALCULATION OF $K_\nu(z)$ BESSEL FUNCTIONS WITH COMPLEX ARGUMENT

The general method for calculating the $K_\nu(z)$ Bessel function[1] is first to find $K_0(z)$ and $K_1(z)$ and use the recurrence formulas to find $K_\nu(z)$. Values for the Bessel functions when $|z| \leq 1$ can be found by straightforward substitution into the power series expansion. When $|z| > 1$, an expansion of the Bessel function in Chebyshev polynomials is needed to insure reasonably fast convergence, although care must be taken when $1 < |z| < 5$ and $170^\circ < \arg z < 190^\circ$ (i.e., near negative real axis for not large z) since the Chebyshev approximation is poor in this region. Following is a detailed description of the method of economization of power series due to Lanczos (Refs. 44 and 87), and its specific application to $K_\nu(z)$.

The Chebyshev polynomials are a special case of the ultraspherical polynomials with the important property that an expansion of a function into Chebyshev polynomials has the smallest error of any of the other ultraspherical polynomials. Expansion by Taylor series yields the slowest convergence while expansion in the Chebyshev functions, $T_n(x)$, yields the fastest convergence. The Chebyshev polynomial of the first kind is

$$T_n(x) = \cos (n \arccos x)$$

where $|T_n(x)| \leq 1$ for x in the range $[-1, 1]$. However for many problems a more appropriate range for the argument is $[0, 1]$. One example where this is useful occurs when a function is evaluated for large values of x by taking powers of the reciprocal of x. This will be the case for the evaluation of $K_\nu(z)$ for large argument. The new shifted Chebyshev polynomial is

$$T_n^*(x) = T_n(2x-1)$$

---

[1] The normalization used by Macdonald is assumed here.

which will be used for the remainder of this discussion. In addition the range of x may be normalized to x/Ψ to extend the polynomials over the range $[0,\Psi]$.

The formal solution of a differential equation about an ordinary point of the equation is

$$u = \sum_{k=0}^{\infty} a_k x^k \quad . \tag{C.1}$$

This formal solution is substituted into the given differential equation to give in general an $m+1$ term recurrence relation:

$$A_k^1 a_k + A_{k+1}^2 a_{k+1} + \ldots + A_{k+m}^{m+1} a_{k+m} = 0 \quad . \tag{C.2}$$

However, the final numerical solution of the equation will involve a finite number of terms, so a finite expansion, $u_n(x)$, will be used which approximates u.

$$u_n = \sum_{k=0}^{n} b_k x^k \tag{C.3}$$

If u_n is substituted back into the given differential equation, there will be m more equations than unknowns. A sacrifice in accuracy must be made somewhere, and this can be accomplished best by putting an appropriate error term on the right side of the differential equation. One procedure is to use some fraction of the next term in the power series

$$\epsilon_e(x) = \tau x^{n+1} \tag{C.4}$$

as the error term, which when $m=1$, makes the power series in b_k uniquely determinate. However any polynomial of order $n+1$ will also work as an error term, and using

$$\epsilon_e(x) = \tau T_{n+1}^*\left(\frac{x}{\Psi}\right) \qquad 0 \leq x \leq \Psi \tag{C.5}$$

the error will be distributed more evenly throughout the interval.

If the coefficients of the shifted polynomials are $T_n^{*(k)}$, then

$$T_n^*(x) = \sum_{k=0}^{n} T_n^{*(k)} \; x^k \quad . \tag{C.6}$$

Suppose the given differential equation is

$$\mathscr{L}u = \tau T^*_{n+1}\left(\frac{x}{\Psi}\right) \tag{C.7}$$

where $\mathscr{L}$ is the differential operator, and the recurrence formula for the finite term solution is

$$A^1_k b_k + A^2_{k+1} b_{k+1} + \cdots + A^{m+1}_{k+m} b_{k+m} = \frac{\tau T^{*(k+1)}_{n+1}}{\Psi^{k+1}} \quad . \tag{C.8}$$

If the degree of approximation n is changed, the coefficients of $T^*_{n+1}(x)$ are also changed, and for successive recursions, an entirely new set of coefficients are needed for each n. To avoid having to recalculate all the coefficients when n is changed, a fixed set of canonical polynomials, $Q_j(x)$, are found based on the solution of

$$\mathscr{L}u = x^{j+1} \qquad j = 0, 1, 2, \ldots n \quad . \tag{C.9}$$

These polynomials are generated by replacing the right side of (C.8) by δ_{kj}, the Kronecker delta function.

$$\sum_{i=0}^{m} A^{i+1}_{k+i} b_{k+i} = \delta_{kj} \tag{C.10}$$

These equations are solved by successive recurrences starting with the last term

$$b_j = \frac{1}{A^1_j}$$

(since all b's with higher subscript are zero) and working backward toward b_0. These b_k coefficients define the canonical polynomial

$$Q_j(x) = b_0 + b_1 x + b_2 x^2 + \cdots + b_j x^j$$

which is the approximate solution of $\mathscr{L}u = x^{j+1}$. To obtain the solution to

$$\mathscr{L}u = \tau \sum_{j=0}^{n} \frac{T^{*(j+1)}_{n+1}}{\Psi^{j+1}} x^{j+1} \tag{C.11}$$

the linear superposition principle is used. The solution is

$$u_n(x) = \tau \sum_{k=0}^{n}{}' \frac{T^{*(k+1)}_{n+1}}{\Psi^{k+1}} Q_k(x) \qquad (C.12)$$

Still needed are the m initial conditions to make the problem determinate. One τ term is not enough, so an error term of the form

$$\epsilon_e(x) = \tau_1 T_{n+1}(x/\Psi) + \tau_2 T_{n+2}(x/\Psi) + \ldots + \tau_m T_{n+m}(x/\Psi)$$

is needed which gives the final solution

$$u'_{n+m-1}(x) = y_n(x) + y_{n+1}(x) + \ldots + y_{n+m}(x) .$$

The undetermined τ factors are found by satisfying the m initial conditions. For many physical problems m = 1, as will be found for the case $K_\nu(z)$, and a two term recurrence relation is obtained. In this special case

$$Q_j(x) = \frac{U_j(x)}{A^1_j a_j} \qquad (C.13)$$

where $U_j(x)$ is the partial sum

$$U_j(x) = \sum_{k=0}^{j}{}' a_k x^k .$$

The proof of this follows.

The infinite series solution gives the two term recurrence relation

$$A^1_k a_k + A^2_{k+1} a_{k+1} = 0 \qquad k = 0, 1, 2 \ldots \qquad (C.14)$$

If $a_0 = 1$, the a_k's are

$$a_1 = -\frac{A_0^1}{A_1^2}$$

$$a_2 = \frac{A_0^1 A_1^1}{A_1^2 A_2^2}$$

$$\vdots$$

$$a_n = (-1)^n \frac{A_0^1 \cdots A_{n-1}^1}{A_1^2 \cdots A_n^2} \quad .$$

For the corresponding truncated solution, the recurrence relation

$$A_k^1 b_k + A_{k+1}^2 b_{k+1} = \delta_{kn} \tag{C.15}$$

yields the following polynomial coefficients.

$$b_n = \frac{1}{A_n^1}$$

$$b_{n-1} = -\frac{A_n^2}{A_n^1 A_{n-1}^1}$$

$$b_{n-2} = \frac{A_n^2 A_{n-1}^2}{A_n^1 A_{n-1}^1 A_{n-2}^1}$$

$$\vdots$$

$$b_0 = (-1)^n \frac{A_n^2 \cdots A_1^2}{A_n^1 \cdots A_0^1}$$

Using these factors, the expression (C.13) is proved.

$$A_n^1 a_n Q_n(x) = (-1)^n \frac{A_0^1 \cdots A_n^1}{A_1^2 \cdots A_n^2} (b_0 + b_1 x + b_2 x^2 + \ldots + b_n x^n)$$

$$= 1 - \frac{A_0^1}{A_1^2} x + \frac{A_0^1 A_1^1}{A_1^2 A_2^2} x^2 + \ldots + (-1)^n \frac{A_0^1 \cdots A_{n-1}^1}{A_1^2 \cdots A_n^2} x^n$$

$$= 1 + a_1 x + a_2 x^2 + \ldots + a_n x^n$$

$$= U_n(x) \qquad \text{QED}$$

If the weight factors are defined as

$$w_k \triangleq - \frac{T_{n+1}^{*(k+1)}}{\Psi^{k+1}} \frac{1}{A_{k+1}^2 a_{k+1}}$$

$$= \frac{T_{n+1}^{*(k+1)}}{\Psi^{k+1}} \frac{1}{A_k^1 a_k} \qquad (k = 0, \ldots n) \qquad \text{(C.16)}$$

$$w_0' \triangleq - T_{n+1}^{*(0)}$$

the solution for the two term recurrence relation is obtained from (C.12), (C.13) and (C.16).

$$u_n(x) = \tau \sum_{k=0}^{n} w_k U_k(x)$$

If the given differential equation is homogeneous, τ can be found by using the boundary condition, $u(0) = 1$, which implies $U_k(0) = 1$.

$$u_n(0) = 1 = \tau \sum_{k=0}^{n} w_k$$

For an inhomogeneous equation, where the right side is 1 and $a_0 = 1$,

$$b_0 = 1 + \tau T_{n+1}^{*(0)} = 1 - \tau w_0'$$

$$U_k(0) = a_0 = 1$$

$$u_n(0) = b_0 = \tau \sum_{k=0}^{n} w_k$$

$$\tau = \frac{1}{w_0' + \sum_{k=0}^{n} w_k} .$$

Therefore the solution of the differential equation with the two term recurrence formula is

$$u_n(x) = \frac{\sum_{k=0}^{n} w_k U_k(x)}{w_0' + \sum_{k=0}^{n} w_k} \tag{C.17}$$

where $w_0' = 0$ for the homogeneous case.

When the solution of an equation is complex, the above theory must be modified. The parameter Ψ in this case can be adjusted to make possible approximations to arbitrary complex values of z. However, now instead of having a polynomial in x, rational functions of z are obtained.

If the given differential equation is solved along the ray $[0, z']$, then Ψ can be set to z', and the Chebyshev polynomials of the form $T_n^*(\frac{z}{z'})$ can be used. To avoid stretching the range of convergence further than necessary and thereby increasing the error, set $z = \Psi$. Then z can assume any complex value in which $u(z)$ is analytic along the ray that connects the origin to z, and the range parameter Ψ is absorbed in z. Thus the modified solution when $m = 1$ is

$$u_n(z) = \frac{\sum_{k=0}^{n} w_k U_k(z) z^{-1-k}}{w_0' + \sum_{k=0}^{n} w_k z^{-k-1}} \tag{C.18}$$

where here $w_k = T_{n+1}^{*(k+1)}/(A_k^1 a_k)$. Since most asymptotic series are expanded in descending powers, it is often more convenient to give the solution as

$$u_n(\tfrac{1}{z}) = \frac{\sum_{k=0}^{n} w_k z^{k+1} U_k(\frac{1}{z})}{w_0' + \sum_{k=0}^{n} w_k z^{k+1}} \tag{C.19}$$

where as before $w_0' = 0$ for the homogeneous equation.

The evaluation of $K_\nu(z)$ is now done by using the above theory. An asymptotic form of the Bessel function is

$$K_\nu(z) = \frac{\pi}{2z}\, e^{-z}\, u(\tfrac{1}{z}) ,$$

which when substituted into the modified Bessel equation gives

$$z^2 \frac{d^2u}{dz^2} - 2z^2 \frac{du}{dz} - (\nu^2 + 1/4)\, u = 0 .$$

If $z_r = 1/z$, then this equation is transformed into

$$z_r^{\,2} \frac{d^2u}{dz_r^2} + 2(1+z_r) \frac{du}{dz_r} - (\nu^2 - 1/4)\, u = 0 .$$

The recurrence formula for this last equation is

$$[(k+1/2)^2 - \nu^2]\, a_k + 2(k+1)\, a_{k+1} = 0 \qquad \text{(C.20)}$$

and the resulting solution for $u(\frac{1}{z})$ can be written as

$$u(\tfrac{1}{z}) = \sum_{k=0}^{\infty} \frac{\Gamma(k+\nu+\frac{1}{2})}{\Gamma(\nu-k+\frac{1}{2})\, 2^k k!\, z^k} \qquad (|\arg z| < \tfrac{3\pi}{2}) . \qquad \text{(C.21)}$$

The weight factor then becomes

$$w_k = - \frac{T^{*(k+1)}_{n+1}}{(k+1)a_{k+1}}$$

$$= - \frac{T^{*(k+1)}_{n+1} k!\, 2^{k+1}\, \Gamma(\nu-k-1/2)}{\Gamma(3/2+\nu+k)}$$

$$w_0' = 0$$

and the solution for the nth approximation is found from (C.19). The numerator of (C.19), designated by M_a, can be expressed as polynomial in z.

$$M_a \triangleq \sum_{k=1}^{n+1} c_k z^k = \sum_{k=0}^{n} w_k U_k(\tfrac{1}{z})\, z^{k+1}$$

$$M_a = zw_0a_0 + z^2w_1(a_0 + a_1z^{-1}) + z^3w_2(a_0 + a_1z^{-1} + a_2z^{-2}) + \ldots$$

$$+ z^{n+1}w_n(a_0 + a_1z^{-1} + \ldots + a_nz^{-n})$$

$$M_a = z(w_0a_0 + w_1a_1 + \ldots + w_na_n) + z^2(w_1a_0 + w_2a_1 + \ldots + w_na_{n-1}) + \ldots + z^{n+1}w_na_0$$

The series in c_k is therefore

$$c_1 = \sum_{k=0}^{n} a_k w_k$$

$$c_2 = \sum_{k=0}^{n-1} a_k w_{k+1}$$

$$\vdots$$

$$c_{m+1} = \sum_{k=0}^{n-m} a_k w_{k+m} \qquad 0 \le m \le n$$

or

$$c_m = \sum_{k=0}^{n-m+1} a_k w_{k+m-1} \qquad 1 \le m \le n+1 \quad . \tag{C.22}$$

The final solution for the K Bessel function is therefore given by

$$K_\nu(z) = \sqrt{\frac{\pi}{2z}}\, e^{-z}\, \frac{\sum_{k=1}^{n+1} c_k z^k}{\sum_{k=0}^{n} w_k z^{k+1}} \tag{C.23}$$

This was evaluated for $n=12$, $\nu = 0, 1$ where values for $T_{13}^{*(k+1)}$ were obtained from Ref. 87. The coefficients of the two polynomials in (C.23) are listed below.

$\nu=0$	k	c_k	w_k
	0	0	$-2.7040000\ 000000\ 10^{3}$
	1	$-9.3444970\ 446304\ 10^{2}$	$-1.3459911\ 111111\ 10^{5}$
	2	$-7.4419709\ 831272\ 10^{4}$	$-1.8951554\ 844444\ 10^{6}$
	3	$-1.3370803\ 316846\ 10^{6}$	$-1.0608450\ 525170\ 10^{7}$
	4	$-8.5699270\ 111211\ 10^{6}$	$-2.8498751\ 040457\ 10^{7}$
	5	$-2.4927644\ 878595\ 10^{7}$	$-4.1110144\ 250697\ 10^{7}$
	6	$-3.7746864\ 595237\ 10^{7}$	$-3.4130588\ 581370\ 10^{7}$
	7	$-3.2310444\ 731793\ 10^{7}$	$-1.6989448\ 538282\ 10^{7}$
	8	$-1.6404092\ 135688\ 10^{7}$	$-5.1640361\ 931952\ 10^{6}$
	9	$-5.0516267\ 780907\ 10^{6}$	$-9.5405549\ 847164\ 10^{5}$
	10	$-9.4154163\ 240077\ 10^{5}$	$-1.0339323\ 951985\ 10^{5}$
	11	$-1.0265536\ 957496\ 10^{5}$	$-5.9824805\ 311068\ 10^{3}$
	12	$-5.9648092\ 039995\ 10^{3}$	$-1.4137061\ 685815\ 10^{2}$
	13	$-1.4137061\ 685815\ 10^{2}$	0
$\nu=1$	0	0	$+9.0133333\ 333333\ 10^{2}$
	1	$+9.1918251\ 276379\ 10^{3}$	$+8.0759466\ 666667\ 10^{4}$
	2	$+3.1557018\ 013485\ 10^{5}$	$+1.3536824\ 888889\ 10^{6}$
	3	$+3.2568245\ 707891\ 10^{6}$	$+8.2510170\ 751323\ 10^{6}$
	4	$+1.4642396\ 054591\ 10^{7}$	$+2.3317159\ 942192\ 10^{7}$
	5	$+3.3952020\ 559774\ 10^{7}$	$+3.4785506\ 673666\ 10^{7}$
	6	$+4.4493275\ 831754\ 10^{7}$	$+2.9579843\ 437188\ 10^{7}$
	7	$+3.4736230\ 524404\ 10^{7}$	$+1.4990689\ 886720\ 10^{7}$
	8	$+1.6631127\ 132600\ 10^{7}$	$+4.6204534\ 360167\ 10^{6}$
	9	$+4.9336335\ 295110\ 10^{6}$	$+8.6319307\ 004577\ 10^{5}$
	10	$+8.9796245\ 223542\ 10^{5}$	$+9.4402523\ 039865\ 10^{4}$
	11	$+9.6451139\ 129428\ 10^{4}$	$+5.5038820\ 886182\ 10^{3}$
	12	$+5.5529691\ 083607\ 10^{3}$	$+1.3089871\ 931311\ 10^{2}$
	13	$+1.3089871\ 931311\ 10^{2}$	0

APPENDIX D

LAPLACE ASYMPTOTIC METHOD OF INTEGRATION

Numerical integration of (5.20) and (5.21) by means of a Gaussian quadrature formula is described in Section 5.4.2. A much faster integration method, though less accurate, is the Laplace asymptotic method which is really a special case of the saddle-point method. This method is well suited for this kind of integral and has been found to be approximately 15 times faster than the Gaussian quadrature method. If the integral to be solved is

$$F(t) = \int_{-\infty}^{\infty} u(x)\, e^{th(x)}\, dx \qquad \text{large } t > 0 \tag{D.1}$$

the solution is approximately (Ref. 88, p. 65)

$$F(t) \cong \sqrt{2\pi}\, \frac{u(x_{max})}{\sqrt{-th''(x_{max})}}\, e^{th(x_{max})} \tag{D.2}$$

where x_{max} is the value of x where h(x) is maximum, i.e., $h'(x_{max}) = 0$ and $h''(x_{max}) < 0$. This is valid when there is only one maximum of h(x), so to apply this technique to (5.20) and (5.24), the contributions from each maximum in the integration interval have to be added together. If $\theta = \omega t$ are the values of ωt where $V(t) = h(\omega t)$ are maximum, then the solutions to (5.20) and (5.21) are

$$J_{kc} = \frac{qD_p p_n(W)\sqrt{2\pi}}{\pi W} \cdot \sum_{\substack{0<\theta<2\pi \\ \max V(\theta)}} \frac{\exp\left\{\alpha\left[V_b + V_0 \cos\left(\theta \frac{\omega_0}{\omega_f}\right) + V_1 \cos\left(\theta \frac{\omega_1}{\omega_f} + \psi_1\right) + V_2 \cos\left(\theta \frac{\omega_2}{\omega_f} + \psi_2\right)\right]\right\}}{\sqrt{\alpha\left[V_0\left(\frac{\omega_0}{\omega_f}\right)^2 \cos\left(\theta \frac{\omega_0}{\omega_f}\right) + V_1\left(\frac{\omega_1}{\omega_f}\right)^2 \cos\left(\theta \frac{\omega_1}{\omega_f} + \psi_1\right) + V_2\left(\frac{\omega_2}{\omega_f}\right)^2 \cos\left(\theta \frac{\omega_2}{\omega_f} + \psi_2\right)\right]}}$$

$$\cdot \left[\alpha_{m_k} \cos(m_k\theta) + \beta_{m_k} \sin(m_k\theta)\right] \tag{D.3}$$

and $$J_{ks} = \frac{qD_p p_n(W)\sqrt{2\pi}}{\pi W} \quad .$$

$$\sum_{\substack{0<\theta<2\pi \\ \max V(\theta)}} \frac{\left| \exp\left\{\alpha \left[V_b + V_0 \cos\left(\theta \frac{\omega_0}{\omega_f}\right) + V_1 \cos\left(\theta \frac{\omega_1}{\omega_f} + \psi_1\right) + V_2 \cos\left(\theta \frac{\omega_2}{\omega_f} + \psi_2\right)\right]\right\} \right|}{\sqrt{\alpha \left[V_0\left(\frac{\omega_0}{\omega_f}\right)^2 \cos\left(\theta \frac{\omega_0}{\omega_f}\right) + V_1\left(\frac{\omega_1}{\omega_f}\right)^2 \cos\left(\theta \frac{\omega_1}{\omega_f} + \psi_1\right) + V_2\left(\frac{\omega_2}{\omega_f}\right)^2 \cos\left(\theta \frac{\omega_2}{\omega_f} + \psi_2\right)\right]}}$$

$$\cdot \left[\alpha_{m_k} \sin(m_k\theta) - \beta_{m_k} \cos(m_k\theta)\right] \qquad \text{(D.4)}$$

The results of using the above formulas are shown in Table D.1 for both the abrupt and graded junctions for various voltage levels in the diode. The calculations show fairly close agreement with the Gaussian quadrature method summarized in Table 5.2 up to about J_6, $3f_p - f_s$, and at the highest frequency calculated, $4f_p + f_s$, this method gives currents less than twice the correct value. If $V_1 = V_2 = 0$, all currents for $k \geq 1$ should be zero, whereas the Laplace asymptotic method gives values of $|J_k|$ as high as 42 A/cm^2.

		Abrupt Junction			Graded Junction		
$V_1 = 0.01$ $V_2 = -0.1$	k	J_{kc} A/cm^2	J_{ks} A/cm^2	$\|J_k\|$ A/cm^2	J_{kc} A/cm^2	J_{ks} A/cm^2	$\|J_k\|$ A/cm^2
	0	680.32	-690.89	969.62	619.19	-684.37	922.91
	1	218.41	-15.87	218.98	188.25	-27.26	190.22
	2	43.22	-681.44	695.01	-12.87	-647.42	647.54
	3	655.30	-55.20	673.35	624.06	-53.72	626.37
	4	56.72	-1052.20	1053.73	-17.10	-1014.40	1014.50
	5	829.30	-79.70	833.11	799.67	-70.40	802.76
	6	61.45	-1369.00	1370.38	-27.37	-1327.60	1327.90
	7	913.70	-99.79	919.13	886.20	-85.66	890.30
	8	60.13	-1658.60	1659.69	-42.32	-1613.80	1614.40
	9	941.96	-116.72	949.16	916.70	-99.77	922.20
$V_1 = 0.001$ $V_2 = -0.01$							
	0	275.95	-275.96	390.26	252.40	-274.50	372.90
	1	12.96	-0.88	12.96	11.20	-1.57	11.31
	2	2.58	-40.50	41.32	-0.76	-38.57	38.58
	3	88.98	-2.92	40.06	37.22	-2.84	37.33
	4	3.71	62.89	63.00	-0.70	-60.80	60.80
	5	49.64	-4.06	51.35	47.98	-3.51	48.10
	6	4.55	-82.61	82.74	-0.81	-80.37	80.38
	7	55.22	-4.97	55.45	53.67	-4.14	53.83
	8	5.23	-101.50	101.59	-1.04	-99.05	99.05
	9	57.67	5.77	57.95	56.25	-4.75	56.45
$V_1 = 0.0001$ $V_2 = -0.001$							
	0	272.88	-272.83	385.86	249.60	-271.40	368.70
	1	1.29	-0.09	1.29	1.11	-0.16	1.13
	2	0.26	-4.03	4.04	-0.08	-3.84	3.84
	3	3.88	-0.29	3.88	3.70	-0.28	3.71
	4	0.37	-6.25	6.35	-0.07	-6.04	6.05
	5	4.94	-0.41	4.95	4.77	-0.35	4.78
	6	0.46	-8.23	8.24	-0.08	-8.01	8.01
	7	5.49	-0.50	5.53	5.33	-0.40	5.34
	8	0.52	-10.09	10.10	-0.09	-9.87	9.87
	9	5.74	-0.57	5.77	5.61	-0.47	5.62

Table D.1. Laplace asymptotic method for calculating the current densities

REFERENCES

1. L. Cuccia, W. J. Gill, and L. Wilson, "Sensitivity of Microwave Earth Stations for Analog and Digital Communications," Microwave Journal, Vol. 11, January 1968, p. 53.

2. J. A. Storman, "Some Performance Data on an Operational 4.2°K Parametric Amplifier," Proc. IEEE, Vol. 54, October 1966, pp. 1500-1501.

3. P. J. Khan, Design of Parametric Lower-Sideband Upconverters using Semiconductor Diodes, Ph.D. Thesis, University of Sydney, October 1963.

4. H. C. Torrey and C. A. Whitmer, Crystal Rectifiers. MIT Radiation Laboratory Series, Vol. 15, New York, N.Y.: McGraw-Hill, 1948.

5. A. van der Ziel, "On the Mixing Properties of Non-linear Condensers," Journal of Applied Physics, Vol. 19, November 1948, pp. 999-1006.

6. J. M. Manley and H. E. Rowe, "Some General Properties of Nonlinear Elements: Part I - General Energy Relations," Proc. IRE, Vol. 44, July 1956, pp. 904-913.

7. A. E. Bakanawski, N. G. Cranna, and A. Uhlir, Jr., "Diffused Silicon Nonlinear Capacitors," IRE Trans. Electron Devices, Vol. ED-6, October 1959, pp. 384-390.

8. W. W. Mumford, "Some Notes on the History of Parametric Transducers," Proc. IRE, Vol. 48, May 1960, pp. 848-853.

9. H. E. Rowe, "Some General Properties of Nonlinear Elements: Part II - Small Signal Theory," Proc. IRE, Vol. 46, May 1958, pp. 850-860.

10. K. Kurokawa and M. Uenohara, "Minimum Noise Figure of the Variable-Capacitance Amplifier," Bell System Technical Journal, Vol. XL, May 1961, pp. 695-722.

11. P. J. Khan, "Optimum Design of Low-Noise Lower-Sideband Parametric Up-Converters," to be published in IEEE Trans. Electron Devices, Vol. ED-18, October 1971.

12. M. Uenohara and H. Seidel, "961-mc Lower-Sideband Up-Converter for Satellite Tracking Radar," Bell System Technical Journal, Vol. XL, July 1961, pp. 1183-1205.

13. H. A. Watson, Microwave Semiconductor Devices and Their Circuit Applications. New York, N.Y.: McGraw-Hill, 1969.

14. D. P. Howson and R. B. Smith, Parametric Amplifiers. London, New York: McGraw-Hill, 1970.

15. D. E. Oliver, Impedance Characteristics of Pumped Varactors, Report No. 7695-189, prepared for USAEL Contract No. DA28-043-AMC-01870(E), Cooley Electronics Laboratory, The University of Michigan, Ann Arbor, Michigan, November 1967.

16. G. L. Matthaei, L. Young, and E. M. T. Jones, Microwave Filters, Impedance-Matching Networks, and Coupling Structures. New York: McGraw-Hill, 1965.

17. F. F. Kuo, Network Analysis and Synthesis. New York: John Wiley and Sons, 1962.

REFERENCES (Cont.)

18. R. E. Collin, Foundations for Microwave Engineering. New York: McGraw-Hill, 1966.

19. W. A. Davis, "Coaxial Microwave Bandpass Filters," (Technical Memorandum No. 100), ECOM-0318-5, prepared for USAEL, Fort Monmouth, New Jersey, Contract No. DAAB 07-68-C-0138, Cooley Electronics Laboratory, The University of Michigan, Ann Arbor, May 1969.

20. S. B. Cohn, "Direct Coupled Resonator Filters," Proc. IRE, Vol. 45, February 1957, pp. 187-196.

21. S. B. Cohn, "Principles of Transmission Line Filter Design," Very High Frequency Techniques. Vol. II, New York: McGraw-Hill, 1947, Ch. 26.

22. J. R. Whinnery and H. W. Jamieson, "Equivalent Circuits for Discontinuities, Proc. IRE, Vol. 32, February 1944, pp. 98-114.

23. J. R. Whinnery, H. W. Jamieson and T. E. Robbins, "Coaxial-line Discontinuities," Proc. IRE, Vol. 32, November 1944, pp. 695-709.

24. P. I. Somlo, "The Computation of Coaxial Line Step Capacitances," IEEE Trans. Microwave Theory Tech., Vol. MTT-15, January 1967, pp. 48-53.

25. S. B. Cohn, "Design of Transmission-line Filters," Very High Frequency Techniques. Vol. II, New York: McGraw-Hill, 1947.

26. G. L. Matthaei, "Short-step Chebyshev Impedance Transformers," IEEE Trans. Microwave Theory Tech., Vol. MTT-14, August 1966, pp. 372-383.

27. R. Levy and T. E. Rozzi, "Precise Design of Coaxial Low-pass Filters," IEEE Trans. Microwave Theory Tech., Vol. MTT-16, March 1968, pp. 142-147.

28. S. B. Cohn, "Confusion and Misconceptions in Microwave Engineering," Microwave Journal, Vol. 11, September 1968, p. 20.

29. B. D. O. Anderson, "When do the Manley-Rowe Relations Really Hold?," Proc. IEE Vol. 113, April 1966, pp. 585-587.

30. A. P. Bolle, "Application of Complex Symbolism to Linear Variable Networks," IRE Trans. on Circuit Theory, Vol. CT-2, March 1955, pp. 32-35.

31. D. B. Leeson, "Capacitance and Charge Coefficients for Varactor Diodes," Proc. IRE, Vol. 50, August 1962, p. 1854.

32. H. A. Haus and R. B. Adler, "An Extension of the Noise Figure Definition," Proc. IRE, Vol. 45, May 1957, pp. 690-691.

33. P. J. Khan, "Parametric Amplifier Nonresonant Gain Maximum," Proc. IEEE, Vol. 56, January 1968, pp. 99-100.

34. P. J. Khan, "Determination of Parametric-Amplifier Nonresonant Gain Maximum," IEEE J. Solid State Circuits, Vol. SC-5, April 1970, pp. 79-81.

35. P. J. Khan, Private communication.

36. B. J. Robinson, "Theory of Variable-Capacitance Parametric Amplifiers," Proc. IEE, Monograph No. 480E, November 1961, pp. 1-11.

REFERENCES (Cont.)

37. A. Uhlir, "High-Frequency Shot Noise in P-N Junctions," Proc. IRE, Vol. 44, April 1956, pp. 557-558.

38. A. Uhlir, "Shot Noise in p-n Junction Frequency Converters," Bell System Technical Journal, Vol. 37, July 1958, pp. 951-988.

39. J. G. Josenhans, "Forward Bias Shot Noise in Varactor Diodes," in Microwave Diode Research Report No. 16, Seventh Quarterly Progress Report, Contract DA 36-039 SC-89205, Bell Telephone Laboratory, 1964.

40. K. Kurokawa, "Actual Noise Measure of Linear Amplifiers," Proc. IRE, Vol. 49, September 1961, pp. 1391-1397.

41. M. Uenohara, "Noise Consideration of the Variable Capacitance Parametric Amplifier," Proc. IRE, Vol. 48, February 1960, pp. 169-179.

42. K. Siegel, "Anomalous Reverse Current in Varactor Diodes," Proc. IRE, Vol. 48, June 1960, pp. 1159-1160.

43. J. Lindmayer and C. Wrigley, "A New Aspect of the Semiconductor Diode," Journal of Electronics and Control, Vol. 14, March 1963, pp. 289-301.

44. C. Lanczos, Applied Analysis. Englewood Cliffs, N. J.: Prentice Hall, 1956.

45. B. S. Perlman and B. B. Bossard, "Efficient High Level Parametric Frequency Converters," 1963 IEEE International Convention Record Part 3 - Electron Devices; Microwave Theory and Techniques, March 25-28, 1963.

46. G. L. Matthaei, "Tables of Chebyshev Impedance-Transforming Networks of Low-pass Filter Form," Proc. IRE, Vol. 52, August 1964, pp. 939-963.

47. J. C. Irvin, T. P. Lee, and D. R. Decker, "Varactor Diodes," Microwave Semiconductor Devices and Their Circuit Applications, ed. by H. A. Watson, New York: McGraw-Hill, 1969, p. 159.

48. P. Penfield, Jr. and R. P. Rafuse, Varactor Applications. Cambridge, Massachusetts: M.I.T. Press, 1962.

49. D. AE. Roberts and K. Wilson, "Evaluation of High Quality Varactor Diodes," The Radio and Electronic Engineer. Vol. 31, May 1965, pp. 277-285.

50. D. E. Crook, "A Simplified Technique for Measuring High Quality Varactor Parameters," Solid State Design, Vol. 6, August 1965, pp. 31-33.

51. N. Houlding, "Measurements of Varactor Quality," Microwave Journal, Vol. 3, January 1960, pp. 40-45.

52. R. Harrison, "Parametric Diode Q Measurements," Microwave Journal, Vol. 3, May 1960, pp. 43-46.

53. R. Mavaddat, "Varactor Diode Q-factor Measurements," Journal of Electronics and Control, Vol. 15, July 1963, pp. 51-54.

54. F. J. Hyde and R. B. Smith, "Effect of Losses in Varactor-diode Impedance Measurements," Proc. IEE, Vol. 111, March 1964, pp. 471-480.

55. E. W. Sard, "A New Procedure for Calculating Varactor Q from Impedance versus Bias Measurements," IEEE Trans. Microwave Theory Tech., Vol. MTT-16, October 1968, pp. 849-960.

REFERENCES (Cont.)

56. B. C. DeLoach, "A New Microwave Measurement Technique to Characterize Diodes and an 800 Gc Cutoff Frequency Varactor at Zero Volts Bias," IEEE Trans. Microwave Theory Tech., Vol. MTT-12, January 1964, pp. 15-20.

57. N. Houlding, "Varactor Measurements and Equivalent Circuits," IEEE Trans. Microwave Theory Tech., Vol. MTT-13, November 1965, pp. 872-873.

58. D. A. E. Roberts, "Measurements of Varactor Diode Impedance," IEEE Trans. Microwave Theory Tech., Vol. MTT-12, July 1964, pp. 471-475.

59. J. W. Bandler, "Precision Microwave Measurement of the Internal Parasitics of Tunnel-Diodes," IEEE Trans. on Electron Devices, Vol. ED-15, May 1968, pp. 275-282.

60. R. J. Wenzel, "Compact Multiplexing Networks for L-band through K_u-band," Digest of the 1970 G-MTT International Symposium, May 11-14, pp. 85-89.

61. R. W. P. King, Transmission-line Theory. New York: Dover Publications, Inc., 1955.

62. 59 IRE 20.S1, "IRE Standards on Methods of Measuring Noise in Linear Two Ports, 1959," Proc. IRE, Vol. 48, January 1960, pp. 60-68.

63. R. D. Lending, "New Criteria for Microwave Component Surfaces," Proc. of the National Electronics Conference, Vol. 11, 1955, pp. 391-401.

64. R. J. Josenhans, "Noise Spectra of Read Diode and Gunn Oscillators," Proc. IEEE, Vol. 54, October 1966, pp. 1478-1479.

65. W. M. Gray, L. Kikushima, N. P. Morenc, and R. J. Wagner, "Applying IMPATT Power Sources to Modern Microwave Systems," IEEE J. Solid State Circuits, Vol. SC-4, December 1969, pp. 409-413.

66. K. Garbrecht, "Lower Limit of Paramp Noise due to Pump Heating," Digest of Technical Papers: 1965 International Solid-State Circuits Conference, 1965, pp. 22-23.

67. J. A. Morrison, "Maximization of the Fundamental Power in Nonlinear Capacitance Diodes," Bell System Technical Journal, Vol. 41, March 1962, pp. 677-721.

68. J. A. Davis, "The Forward-driven Varactor Frequency Doubler," M.S. Thesis, Dept. of Electrical Engineering, M.I.T., Cambridge, Massachusetts, May 1963.

69. C. B. Burckhardt, "Analysis of Varactor Frequency Multipliers for Arbitrary Capacitance Variation and Drive Level," Bell System Technical Journal, Vol. 44, April 1965, pp. 675-692.

70. J. I. Smith, "Practical Analysis of the Overdriven Varactor Multiplier with a Single Idler," Proc. IEEE, Vol. 55, April 1967, pp. 575-576.

71. S. W. Conning, "An Analysis of the High-power Varactor Upconverter," Proc. IREE Australia, Vol. 27, July 1966, pp. 163-173.

72. A. I. Grayzel, "The Overdriven Varactor Upper Sideband Upconverter," IEEE Trans. Microwave Theory Tech., Vol. MTT-15, October 1967, pp. 561-565.

73. J. W. Gewartowski and R. H. Minetti, "Large-Signal Calculations for the Overdriven Varactor Upper-Sideband Upconverter Operating at Maximum Power Output," Bell System Technical Journal, Vol. 46, July-August 1967, pp. 1223-1242.

REFERENCES (Cont.)

74. C. E. Nelson, "A Note on the Large-Signal Varactor Upper-Sideband Upconverter," Proc. IEEE, Vol. 54, July 1966, pp. 1013-1014.

75. C. E. Nelson, "The Theoretical Approximate Maximum Output Power of Varactor Upper-sideband Upconverters," General Electric Co., Syracuse, N.Y., Internal Report TIS R66ELS-46, June 1966.

76. J. L. Moll, Physics of Semiconductors. New York: McGraw-Hill, 1964.

77. S. M. Sze, Physics of Semiconductor Devices. New York: Wiley-Interscience, 1969.

78. T. P. Lee, "p-n Junction Theory," Microwave Semiconductor Devices and Their Circuit Applications, ed. H. A. Watson. New York: McGraw-Hill, 1969, Ch. 5.

79. V. A. Shpirt, "The Properties of p-n Junctions Under the Influence of a Sinusoidal Voltage of Arbitrary Amplitude (Low Injection Level)," Radio Engineering and Electronic Physics, Vol. 11, December 1966, pp. 1947-1953.

80. V. N. Parygin and N. K. Maneshin, "Frequency Multiplication Using the Diffusion Capacitance," Radio Engineering and Electronic Physics, Vol. 11, July 1966, pp. 1111-1118.

81. R. M. Romanova, "Equivalent Circuit of a Turned-on Varactor," Radio Engineering, Vol. 23, October 1968, pp. 111-115.

82. C. T. Sah, "Effects of Electrons and Holes on the Transition Layer Characteristics of Linearly Graded P-N Junctions," Proc. IRE, Vol. 49, March 1961, pp. 603-618.

83. C. T. Sah, "Effect of Surface Recombination and Channel on P-N Junction and Transistor Characteristics," IRE Trans. Electron Devices, Vol. ED-9, January 1962, pp. 94-108.

84. C. C. Wang, "Space-Charge-Layer Width and Capacitance of Symmetrical Step Junctions," Proc. IRE, Vol. 50, August 1962, pp. 1838-1839.

85. W. F. O'Hearn and Y. F. Chang, "An Analysis of the Frequency Dependence of the Capacitance of Abrupt P-N Junction Semiconductor Devices," Solid-State Electronics, Vol. 13, April 1970, pp. 473-483.

86. D. B. Anderson and J. C. Aukland, "Transmission-Phase Relations of Four-Frequency Parametric Devices," IRE Trans. Microwave Theory Tech., Vol. MTT-9, November 1961, pp. 491-498.

87. C. Lanczos, Tables of Chebyshev Polynomials $S_n(x)$ and $C_n(x)$. Washington, D.C.: U.S. Department of Commerce, National Bureau of Standards, 1952, pp. V-XXIX.

88. N. G. DeBruijn, Asymptotic Methods in Analysis. New York: Wiley-Interscience, 1961.